EXCERPTA

98 Intradiploic Epidermoid Cyst Compressing the Transverse Sinus in an Adolescent With Papilledema: A Rare Mimic of IIH

Jedediah Bondy B.S[1], Sammy Khalouf B.S[1], Mansi Shah B.S[2], Fahim Bachu[1], Paul Dobria M.D[3], Mozhan Hagigatian[1], Helly Patel[4], Aminah Ahmed[1], Malak Shah M.D[5], Meha Patel MD[6], Eric Spitzer M.D[3], Manuel Rodriguez M.D[3]

[1]Lake Erie College of Osteopathic Medicine (LECOM), Erie, PA, USA. [2]Thomas Jefferson University Sidney Kimmel Medical College (SKMC), Philadelphia, PA, USA. [3]Rochester Regional Health, Rochester, NY, USA. [4]University of Michigan, Ann Arbor, Michigan, USA. [5]University at Buffalo (UB) Radiology Department, Buffalo, NY, USA. [6]Mount Sinai West, New York, NY, USA

Clinical History

A 16-year-old female with obesity, hypertension, and pre-diabetes presented with a two-month history of daily headaches accompanied by eye pain, photophobia, pulsatile tinnitus, and intermittent blurred vision. Ophthalmologic exam demonstrated bilateral grade III papilledema with preserved visual acuity. Initial evaluation presumed migraine; however, symptom progression led to neuroimaging. MRI of the brain revealed an intradiploic epidermoid inclusion cyst in the right occipital bone compressing the dominant right transverse sinus. The left transverse sinus was diminutive, further limiting venous drainage. Findings indicated secondary intracranial hypertension due to venous outflow obstruction. She was started on acetazolamide, with planned lumbar puncture and MR venography.

Imaging Findings

Non-contrast head CT showed a 1.8 cm lucent lesion in the right occipital bone with thinning of the inner table, raising concern for a bony lesion. MRI demonstrated a 1.6 × 1.0 cm T2-hyperintense, non-enhancing lesion with marked diffusion restriction, consistent with an intradiploic epidermoid cyst. The lesion compressed the dominant right transverse sinus, while the left transverse sinus appeared hypoplastic. These findings explained venous outflow obstruction and elevated intracranial pressure.

Discussion

Although idiopathic intracranial hypertension (IIH) is common in young obese females, secondary causes must be excluded. Transverse sinus stenosis can impair cerebral venous drainage and CSF absorption, raising intracranial pressure. While most stenosis in IIH is intrinsic, extrinsic compression from calvarial lesions is rare, particularly in pediatric patients. Intradiploic epidermoid cysts arise from ectodermal remnants and may erode bone and compress adjacent venous sinuses. Failure to recognize a structural cause risks delayed treatment and permanent vision loss. MRI with MR venography is essential when papilledema is present to assess venous sinus patency.

Teaching Point

In patients with papilledema and IIH-like symptoms—especially adolescents—secondary causes should be excluded. MRI with MR venography is crucial to detect venous outflow obstruction from structural lesions such as intradiploic epidermoid cysts, enabling timely intervention and vision preservation.

References

1. Friedman DI, Liu GT, Digre KB. *Neurology*. 2013;81(13):1159–65.
2. Wall M. *Neurol Clin*. 2010;28(3):593–617.
3. Farb RI, et al. *Neurology*. 2003;60(9):1418–24.
4. Rohr A, et al. *AJNR Am J Neuroradiol*. 2007;28(1):e20.
5. Bono F, et al. *Cephalalgia*. 2006;26(3):253–7.

Images/Tables

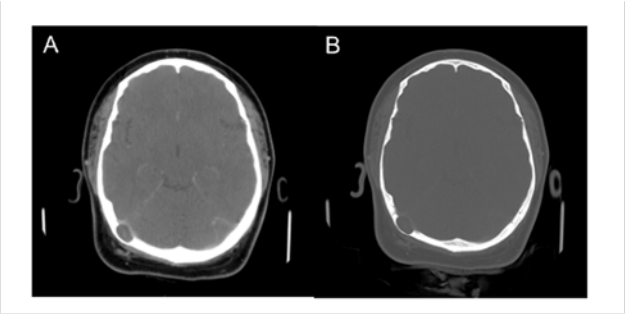

Figure 1: Soft tissue (A) and bone (B) algorithm axial slice contrast enhanced CT head demonstrates a 1.8 cm intradiploic lucent lesion which right occipital calvarium which markedly thins the inner table (B) and exerts mass effect upon the transverse sinus (A).

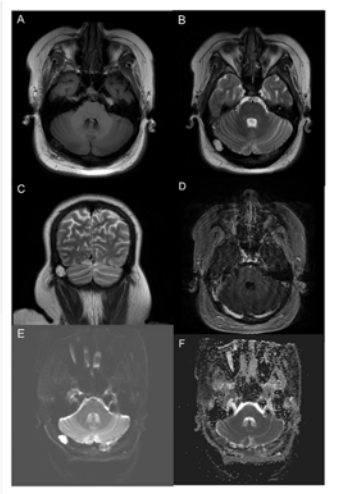

Figure 2: Subsequent contrast enhanced MRI of the brain reveals a 1.6 x 1.0 cm low T1, high T2 (A, B & C) nonenhancing (D), intensely diffusion restricting (E, F) lesion within the right parietal calvarium. This markedly thins the inner and outer tables (B, C) and narrows the right transverse sinus (D). This appearance is consistent with an intradiploic epidermoid inclusion cyst.

104 Monomelic Amyotrophy, a Rare Cause of Asymmetric Upper Extremity Weakness

Jason Schick DO[1], Brian Glowski[2], Saad Umar[3], Muhammad Farooq MD[1], Alex Dombrowski MD[4]
[1]Trinity Health Grand Rapids, Hauenstein Neurosciences, Grand Rapids, Michigan, USA. [2]Michigan State University College of Osteopathic Medicine, East Lansing, Michigan, USA. [3]University of Michigan Ross School of Business, Ann Arbor, Michigan, USA. [4]Trinity Health Grand Rapids, Grand Rapids, Michigan, USA

Clinical History

A 20-year-old male presented with a 3-month history of progressive right-hand weakness. His neurologic exam was notable for weakness of finger abduction, finger flexion, and finger extension on the right, with atrophy of the hypothenar and intrinsic hand muscles on the right.
Broad laboratory work-up was completed for causes of neuropathy including a hereditary neuropathy panel, which was unrevealing. Right upper extremity EMG showed chronic neurogenic changes in the extensor indicis proprius, abductor pollicis brevis, and first dorsal interossei. There were also fibrillations within the abductor pollicis brevis, consistent with ongoing denervation.

Imaging Findings

Flexion-extension MR of the cervical spine was completed. In neutral position there was loss of the normal cervical lordosis with subtle right hemiatrophy of the spinal cord (arrow). In flexion position there was noted enlargement of the posterior epidural space at C5-C7 (arrowhead) with associated compression of the spinal cord at these levels.

Discussion

The combination of clinical, EMG, and MRI findings were consistent with a diagnosis of Monomelic amyotrophy (MMA), or Hirayama Disease. Patients typically present with distal upper extremity weakness and atrophy beginning in the mid 2nd to mid 3rd decades of life, with a male preponderance. The highest prevalence is typically observed in Asian populations, with less than 30 cases occurring in North America documented in the current literature. MR imaging of the cervical spine, completed in both neutral and flexion positions, is integral to diagnosis. Hallmark radiological findings include lower cervical cord atrophy, asymmetric cord flattening, enlargement of the posterior epidural space with flexion, and dynamic spinal cord compression at the levels of maximal enlargement of the epidural space. MMA is typically considered a non-progressive and self-limited disease, with first line treatment being conservative management, though surgical intervention may be indicated in severe cases or those who have progression despite conservative management.

Teaching Point

MMA is a rare cause of asymmetric upper extremity weakness and atrophy occurring in young males. Given the low prevalence, especially in North America, diagnosis can be difficult and easily missed. Diagnosis relies heavily on MR imaging of the cervical spine, specifically including both neutral and flexion positions, as neutral imaging alone may be nonspecific.

References

1. Wang H, Tian Y, Wu J, et al. Update on the Pathogenesis, Clinical Diagnosis, and Treatment of Hirayama Disease. *Front Neurol*. 2022;12:811943. Doi:10.3389/fneur.2021.811943

Images/Tables

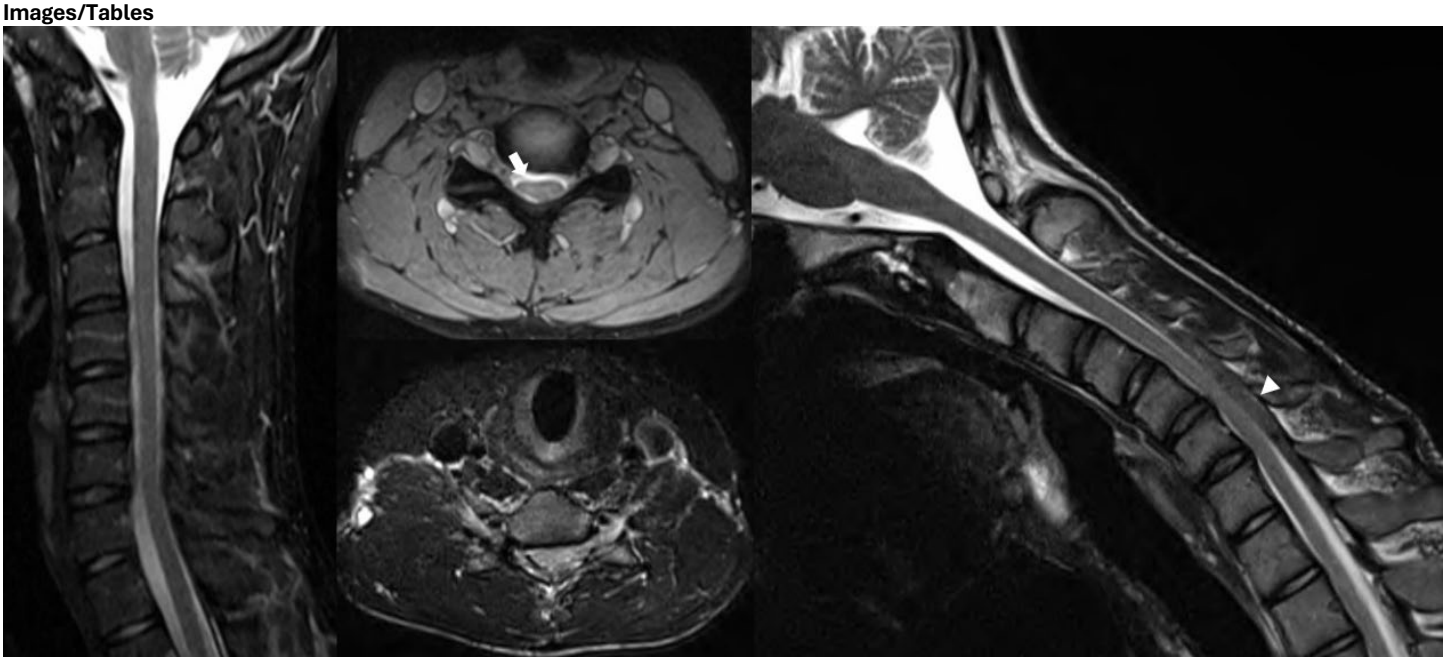

120 Beyond the Parotid: Metastasizing Pleomorphic Adenoma with Rare Intracranial Involvement

Ilkyu D Oh MD, Rahim Ismail MD, Houman Sotoudeh MD
University of Texas at Southwestern, Dallas, TX, USA

Clinical History

A 30-year-old man with a history of parotid pleomorphic adenoma, and local recurrence, status-post surgical resection and multiple radiation therapy. Surveillance MRI showed new and unexpected calvarial, dural-based enhancing lesions, and enhancing lesion in the left cavernous sinus. While these findings were suspicious for metastatic disease, the imaging pattern was atypical for pleomorphic adenoma.

Imaging Findings

Post-contrast T1-weighted images (A-D) demonstrate a dural-based enhancing mass along the anterior falx (arrow) without a dural tail or adjacent hyperostosis. Additional enhancing lesions are present within the right frontal (arrowhead) and left parietal calvarium (open arrow). A new mass-like enhancing lesion is also seen within the left cavernous sinus (circle), producing convex and bulging appearance of the cavernous sinus.

Discussion

Pleomorphic adenomas are the most common benign salivary gland tumor, consisting of 45-75% of all salivary gland tumors. They are most commonly located in the superficial lobe of the parotid gland and are comprise of variable ("pleomorphic") mucoid, myxoid, cartilaginous or hyaline material.

This patient presented with new dural, calvarial, and intracranial enhancing lesions on surveillance imaging, which were suspicious for metastatic diseases. However, the findings were perplexing because pleomorphic adenoma is histologically benign, and multifocal intracranial metastatic disease is exceedingly rare. Other more common metastatic etiologies, including mucoepidermoid carcinoma, adenoid cystic carcinoma, and carcinoma ex pleomorphic adenoma, as well as benign dural-based meningioma, could not be reliably excluded on imaging. Given the diagnostic uncertainty and to guide appropriate management, resection of the dural-based lesion along the falx was performed. Histology was consistent with intracranial metastasis from pleomorphic adenoma without evidence of malignant transformation.

The incidence of metastatic diseases in pleomorphic adenoma is exceedingly rare and is termed metastasizing pleomorphic adenoma (MPA). Most MPA metastases are thought to occur by hematogenous dissemination, potentially after prior surgical manipulations or incomplete excision, and occur more frequently in patients with prior local recurrence. Bone, lung, and cervical lymph nodes are the most commonly reported sites of metastasizing pleomorphic adenoma, but intracranial metastatic disease has been described only in a few case reports.

Radiologists play a key role in recognizing and including these unpredictable and atypical metastatic patterns of pleomorphic adenoma in the differential diagnosis. Early identification can influence clinical management by prompting systemic evaluation for additional metastases, guiding timely surgical excision or biopsy, and encouraging long-term or lifelong imaging surveillance.

Teaching Point

Pleomorphic adenoma may occasionally metastasize despite its benign histology. Intracranial involvement of the calvarium, dura, or cavernous sinus is exceptionally uncommon but should be included in the differential, particularly in patients with a history of local recurrence.

Metastasizing pleomorphic adenoma (MPA) can develop many years after the initial diagnosis, emphasizing the importance of long-term imaging surveillance, particularly in patients with a history of local recurrence.

References

Kato, H., Kanematsu, M., Mizuta, K., Ito, Y., & Hirose, Y. (2008). Carcinoma ex pleomorphic adenoma of the parotid gland: radiologic-pathologic correlation with MR imaging including diffusion-weighted imaging. AJNR. American journal of neuroradiology, 29(5), 865–867. https://doi.org/10.3174/ajnr.A0974

Knight, J., & Ratnasingham, K. (2015). Metastasising pleomorphic adenoma: Systematic review. International journal of surgery (London, England), 19, 137–145. https://doi.org/10.1016/j.ijsu.2015.04.084

Koyama, M., Terauchi, T., Koizumi, M., Tanaka, H., & Sato, Y. (2018). Metastasizing pleomorphic adenoma in the multiple organs: A case report on FDG-PET/CT imaging. Medicine, 97(23), e11077. https://doi.org/10.1097/MD.0000000000011077

McGarry, J. G., Redmond, M., Tuffy, J. B., Wilson, L., & Looby, S. (2015). Metastatic pleomorphic adenoma to the supraspinatus muscle: a case report and review of a rare aggressive clinical entity. Journal of radiology case reports, 9(10), 1–8. https://doi.org/10.3941/jrcr.v9i10.2283

Images/Tables

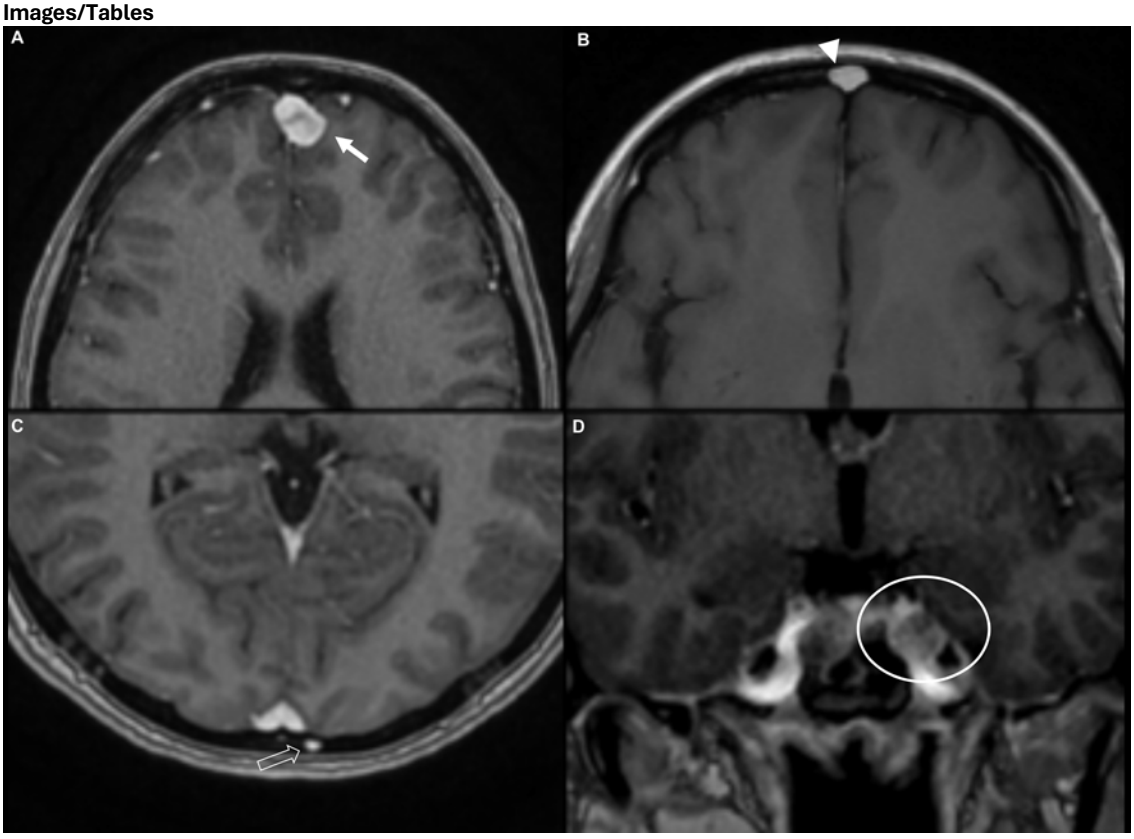

126 Pediatric Orbital Haematolymphoid Disorders: Ten Imaging Cases

Justin D Nguyen MD[1], Taylor Beal MD[1], Joshua Nichols MD[2], Lamson Tran[3], Karen Moeller MD[2], Huy D Tran MD[2]

[1]Baylor College of Medicine, Houston, TX, USA. [2]Texas Children's Hospital, Houston, TX, USA. [3]Texas A&M University, College Station, TX, USA

Clinical History

Ten patients presented with orbital masses at a tertiary care pediatric hospital. Ages of symptom onset ranged from 1–20 years. Common symptoms included proptosis, eye pain, and orbital swelling. All patients had imaging and biopsy results which confirmed diagnosis.

Imaging Findings

A. Idiopathic orbital inflammation: Ill-defined hyperdensity on CT around the right globe, especially posteriorly with moderate proptosis. On STIR, increased signal in intraconal fat surrounding the optic nerve sheath. Normal signal of the optic nerve. Facilitated diffusivity. Vivid homogenous contrast enhancement.

B. IgG4-related disease: An extraconal lesion on T1 and STIR in the superior left orbit. The lesion has intermediate to low T2 signal. Vivid homogenous contrast enhancement.

C. Post-transplant lymphoproliferative disorder: T1 intermediate signal lesion straddling the greater sphenoid wing with components in the lateral extraconal and suprazygomatic masticator spaces, infiltrating the temporalis muscle. Progressive decrease of T2 signal on follow-up imaging 3 weeks and 3 months later. Heterogeneous peripheral enhancement.

D. Anaplastic large cell lymphoma: Infiltrative intermediate density lesion in the conal and extraconal superior right orbit. Coronal T1 shows infiltration of the superior muscle complex, the lacrimal gland, and the lateral rectus. Intermediate signal on T2. Decreased diffusivity. Vivid contrast enhancement.

E. Myeloid sarcoma: T1 and STIR images show circumscribed lesions in the superior extraconal orbit bilaterally, left greater than right. Decreased diffusivity.

F. Langerhans cell histiocytosis: Lytic lesion in the right superolateral orbital rim involving the frontal bone. An exophytic soft tissue component extends into the orbit deforming the globe. The lesion is isointense to muscle on T1 and has heterogeneous intermediate signal on T2. Relatively decreased diffusivity. Heterogeneous enhancement. Small epidural extension and dural enhancement along the floor of the anterior cranial fossa.

G. Langerhans cell histiocytosis: Expansile lytic lesion along the right maxilla, zygoma and orbital floor. Intermediate T1 signal and heterogeneous T2 signal. Intermediate diffusivity. Vivid heterogeneous enhancement. Infiltration of the extraconal orbit and thickening of the lateral and inferior rectus muscles.

H. Histiocytic sarcoma: A lesion of the inferior orbital rim involves the inferior orbit, cheek, lower eyelid, and inferior muscle cone. Intermediate / increased T2 signal. Decreased diffusivity. Heterogeneous enhancement. Central nonenhancement suggests necrosis.

I. Erdheim-Chester: Reticulated lesion infiltrating the intraconal fat bilaterally on T1 with minimal infiltration of extraconal fat. Thickening of the right lateral rectus, medial rectus and inferior muscles, and mildly thickened left medial rectus muscle. Intermediate to low signal on T2. Diffuse, homogeneous contrast enhancement.

J. Rosai-Dorfman: intermediate density lesions fill the intraconal space bilaterally. Right proptosis. Intermediate STIR and T1 signal and homogeneous enhancement. Lesions surround otherwise normal optic nerves bilaterally. Not shown is enhancing lesion in right parapharyngeal space

Discussion

This series highlights orbital imaging patterns of pediatric haematolymphoid disorders. Enhancement patterns are variable. Benign processes may have facilitated diffusion, while malignant lesions may have decreased diffusivity.[1,2] Extraorbital systemic findings may help determine the etiology of an orbital mass.

Teaching Point

Pediatric orbital haematolymphoid disorders have overlapping imaging findings, and biopsy is the standard for differentiating them. However, diffusion restriction and characteristic extraorbital findings can help narrow the differential.

References

1. Cameron CA, Tong JY, Juniat V, et al. Diagnostic utility of diffusion-weighted imaging and apparent diffusion coefficient for common orbital lesions: A Review. *Ophthalmic Plastic & Reconstructive Surgery*. 2022;38(6):515-521. doi:10.1097/iop.0000000000002092
2. Ren J, Yuan Y, Wu Y, et al. Differentiation of orbital lymphoma and idiopathic orbital inflammatory pseudotumor: Combined diagnostic value of conventional MRI and histogram analysis of ADC Maps. *BMC Medical Imaging*. 2018;18 (6). doi:10.1186/s12880-018-0246-8

Images/Tables

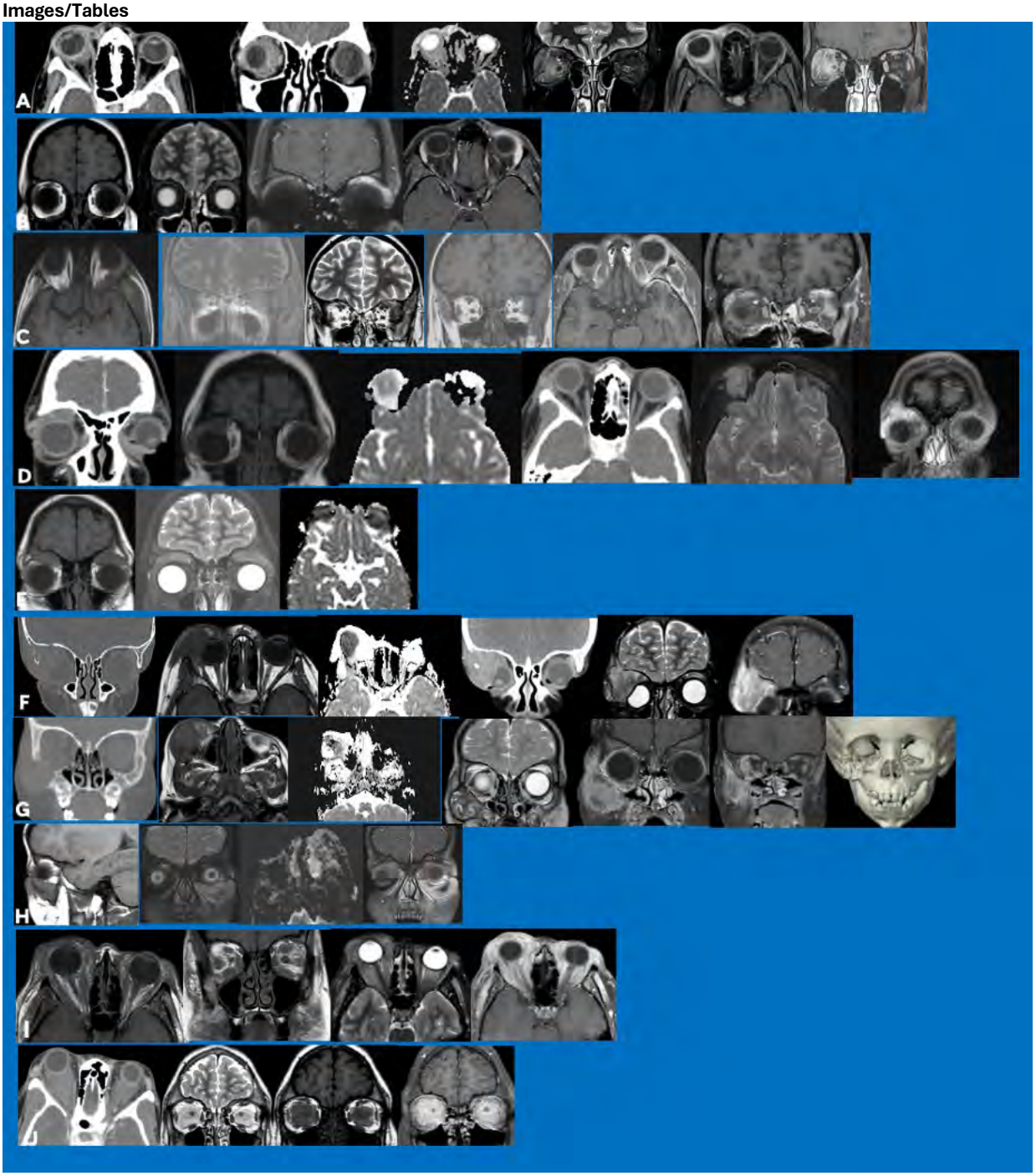

129 Hypoglossal schwannoma mimicking vestibular schwannoma

Paul Stegelmeier DO, Erika Baca MD, Uchechukwu C Ibewuike MD
University of New Mexico, Albuquerque, NM, USA

Clinical History

A 51-year-old male with a history of retrosigmoid craniotomy in 2017 for resection of a cerebellopontine (CP) angle mass, pathologically confirmed as schwannoma, presented in 2023 with intermittent dizziness, severe nausea, and vomiting. The completeness of the initial resection was unclear, and the patient discontinued follow-up MRI after several years. Recent CT imaging revealed a mass in the CP angle eroding through the hypoglossal canal and jugular foramen, raising suspicion for tumor recurrence.

Imaging Findings

CT and MRI are essential for evaluating hypoglossal schwannomas. Imaging typically demonstrates a well-defined, encapsulated mass in the CP angle, often with bone erosion or widening of the hypoglossal canal. In recurrent cases, the tumor may extend into adjacent skull base foramina, as seen here, and can present as a dumbbell-shaped lesion spanning intra- and extracranial compartments.

Discussion

Hypoglossal schwannomas are rare, accounting for less than 5% of head and neck schwannomas. Recurrence is most often associated with subtotal resection, as complete removal can be challenging due to proximity to critical neurovascular structures and risk of hypoglossal nerve palsy. Recurrent tumors may present years after initial surgery, often with new or worsening cranial neuropathies or mass effect symptoms. Surgical re-excision

remains the mainstay of treatment, but newer minimally invasive approaches, such as neuroendoscopic transnasal surgery, have shown promise in select cases, offering good tumor control with reduced morbidity. Long-term follow-up is essential due to the risk of late recurrence.

Teaching Point

Although vestibular schwannoma accounts for over 80% of tumors located at the cerebellopontine angle tumors. When evaluating a cerebellopontine angle tumor, it is crucial to examine the hypoglossal canal. This assessment is important due to the rare possibility that the tumor may originate from the hypoglossal nerve.

References

1. Hashikata H, Hayashi H, Yoshizaki W, Maki Y, Toda H. Successful treatment of recurrent extracranial hypoglossal schwannoma using the neuroendoscopic transnasal far-medial approach. Surg Neurol Int 2024;15:168.
2. Yu Z, Zhao G, Zhao Z, Li Y, Xie G. Giant recurrent dumbbell-shaped hypoglossal schwannoma in an elderly male: a case report. Oncol Lett 2015;10:3341-3346.
3. Sfar K, Jaheddine F, Maslouhi K, Chait F, Zhim M, El Kettani N, et al. Dumbbell-shaped hypoglossal schwannoma with cystic and hemorrhagic degeneration: a case report of a rare entity. Radiol Case Rep 2025;20:101234.
4. Souza VA, Bedin A, Bizzi J, Karam OR, Thibes ACM, dos Santos SC, et al. Hypoglossal nerve schwannoma: a case report in a pediatric patient. Arq Neuropsiquiatr 2024;82:e20240012.
5. Di Pascuale I, Brito N, Zerpa J, Roa C, Faria G. Hypoglossal nerve schwannoma. A case report and literature review. World Neurosurg 2019;132:282-286.

Images/Tables

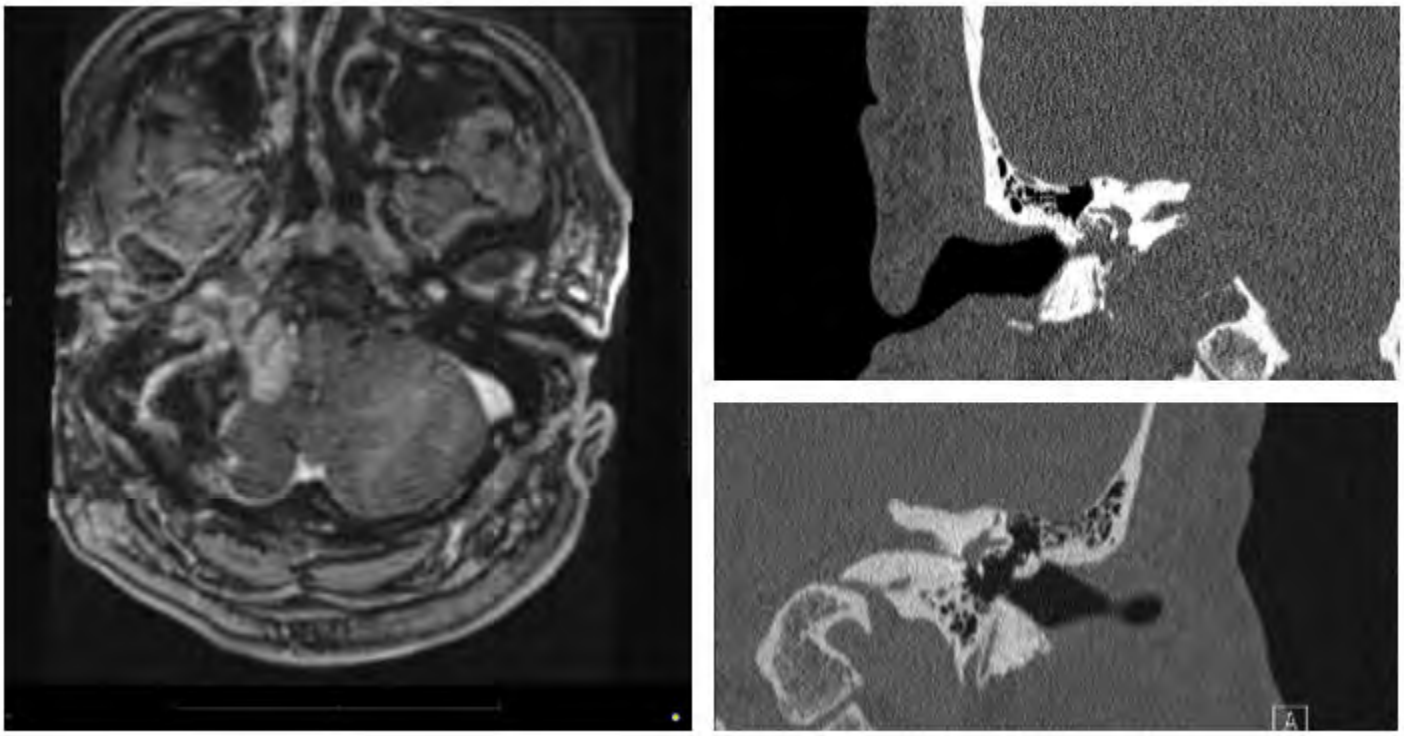

---

141 Uncovering Uncommon Presentations: A Unique Case of Neurosarcoidosis with Skull, Cranial Nerve, and Pachymeninges Involvement

Azin Aein MD, Nihanth Palivela, Abel T. Abebe MD, Aiste Baltuonyte MD, Lawrence E. Ginsberg MD

University of Texas Medical Branch (UTMB), Galveston, TX, USA

Clinical History

A 77-year-old African American female with past medical history of cardiac, pulmonary, and cutaneous biopsy-proven sarcoidosis (formerly on mycophenolate mofetil and prednisone, off therapy for possibly 2-3 years) presented to the ER with a sudden onset of expressive aphasia and dysphasia. Due to the sudden onset of symptoms and past medical history, the patient underwent stroke workups; however, no acute abnormalities were noted on NCCT or CTA studies.

Imaging Findings

CT images and subsequent non-contrast brain MRI for stroke evaluation revealed multiple well-defined, slowly progressing osteolytic lesions involving the calvarium with non-sclerotic margins (Figure 1, images A and B). Differential diagnoses at that time included multiple myeloma, metastatic disease, and, rarely, skull sarcoidosis, given the known history of sarcoidosis. Further assessment with contrast-enhanced brain MRI (Figure 1, images C, D, E, and F) demonstrated diffuse abnormal dural enhancement, most prominently involving the right frontoparietal region, falx, and tentorium, suggesting pachymeningeal neurosarcoidosis. Additionally, there were striking leptomeningeal lesions involving the left sylvian fissure, vermis, and right oculomotor nerve (CN III), consistent with leptomeningeal neurosarcoidosis (Figure 1 images C, D, E, and F).

Discussion

Sarcoidosis is a systemic, non-caseating granulomatous disease that can involve multiple organs. Pulmonary involvement occurs in approximately 90% of patients, typically presenting with hilar and mediastinal lymphadenopathy, making the lungs the most common site of disease. Less frequently affected organs include the heart, skin, nervous system, and musculoskeletal system.

Any part of the nervous system can be involved; however, central nervous system (CNS) involvement is more common than peripheral nervous system (PNS) involvement, occurring in 5-16% of cases, predominantly in systemic sarcoidosis. CNS manifestations range from intraparenchymal lesions to leptomeningeal, dural, cranial nerve, or skull involvement. Pachymeningitis is also considered a rare presentation compared to leptomeningeal disease. The facial nerve (CN VII) and the optic nerve (CN II) are most commonly affected. Cranial nerve involvement may be part of leptomeningeal disease or occur in isolation.

Bone sarcoidosis primarily affects the short bones of the appendicular skeleton, such as the hands and feet. Skeletal involvement is relatively uncommon, with an estimated prevalence of 1-13%, and lesions of the axial skeleton, including the calvarium and vertebrae, are even rarer. Bone lesions vary widely in appearance, ranging from lytic lesions with or without sclerotic margins, lace-like destruction patterns, sclerotic lesions, to mixed lytic and sclerotic lesions. Notably, most reported axial skeleton lesions are located in the lumbar spine and pelvis.

Teaching Point

Our goal is to highlight the rare imaging features of neurosarcoidosis, including involvement of the skull, pachymeninges, and oculomotor nerve (CN III), as well as more common features such as leptomeningeal disease. Recognizing both atypical and typical presentations is essential for radiologists to ensure accurate diagnosis and appropriate management.

References

1. Smith JK, Matheus MG, Castillo M. Imaging manifestations of neurosarcoidosis. AJR Am J Roentgenol. 2004 Feb;182(2):289-95. PMID: 14736648.
2. Tounsi H, Skouri W, Jlidi M, Bachrouch S, Mami H, Kaabar Y, Sbaihi S, Chaabane A, Amri R, Alaya Z. Symptomatic hypercalcemia and lytic lesions of the skull revealing sarcoidosis: A case report. Radiol Case Rep. 2024 Sep 12;19(12):5744-5749. PMID: 39308619.
3. Ginsberg LE, Williams DW 3rd, Stanton C. MRI of vertebral sarcoidosis. J Comput Assist Tomogr. 1993 Jan-Feb;17(1):158-9. PMID: 8419430.

Images/Tables

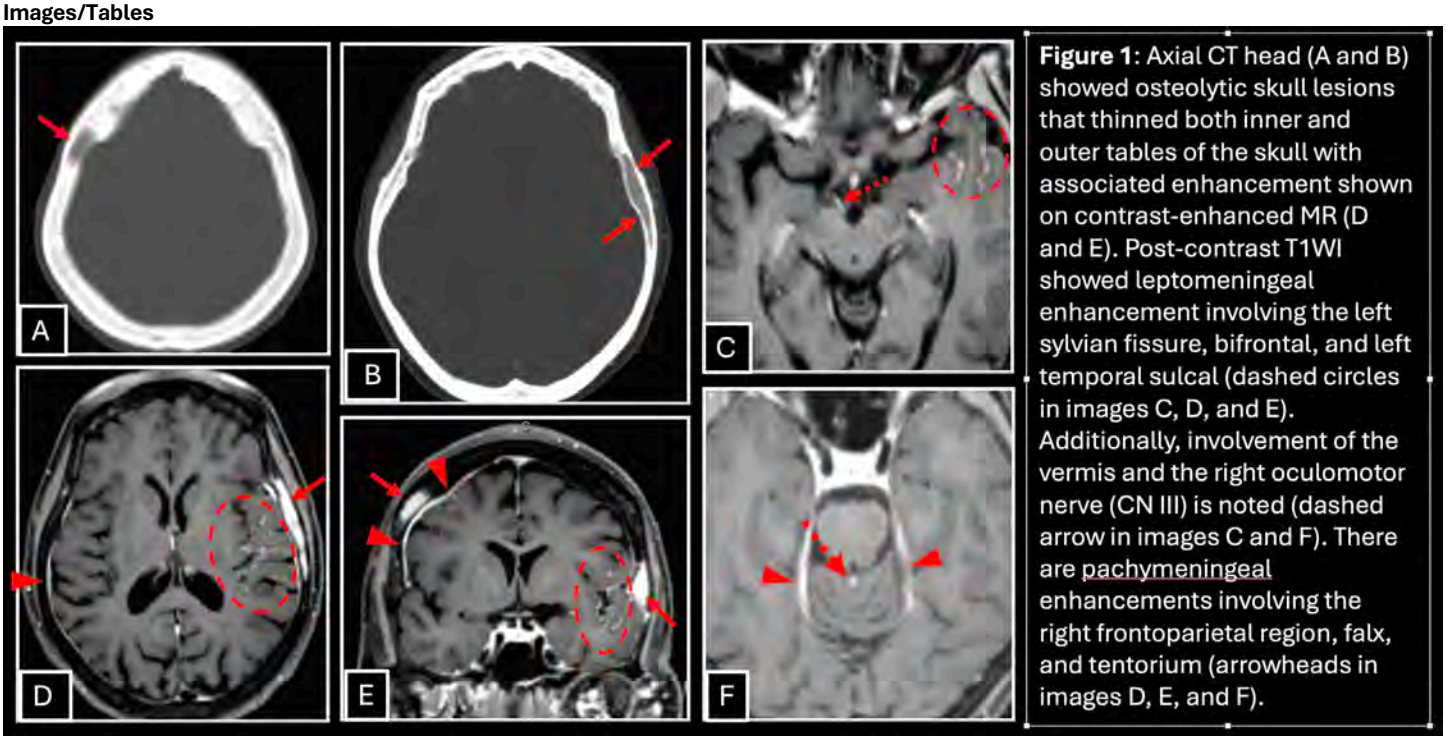

Figure 1: Axial CT head (A and B) showed osteolytic skull lesions that thinned both inner and outer tables of the skull with associated enhancement shown on contrast-enhanced MR (D and E). Post-contrast T1WI showed leptomeningeal enhancement involving the left sylvian fissure, bifrontal, and left temporal sulcal (dashed circles in images C, D, and E). Additionally, involvement of the vermis and the right oculomotor nerve (CN III) is noted (dashed arrow in images C and F). There are pachymeningeal enhancements involving the right frontoparietal region, falx, and tentorium (arrowheads in images D, E, and F).

---

144 7q36 Deletion Syndrome: Spectrum of Holoprosencephaly and Sacral Defects

Valeria Ortega M.D.[1], Mario Mahecha M.D.[2], Santiago Aristizábal M.D.[2], Andres Rodriguez M.D.[2], Maria Claudia Caldas Vasquez M.D.[2]

[1]Baylor College of Medicine, Houston, Texas, USA. [2]The University of Texas Health Science Center at Houston, Houston, Texas, USA

Clinical History

This is a 2-year-old female with developmental delay and multiple congenital anomalies. Her craniofacial and midline abnormalities include cleft palate with a single nostril and microcephaly. Fundoscopy revealed optic nerve hypoplasia. Brain and spine MRI showed holoprosencephaly, sacral agenesis, and an anterior meningocele. Additionally, she has a urogenital sinus, hydrocolpos, and endocrinologic alterations. Chromosomal microarray analysis confirmed the diagnosis of a complete 7q36 deletion involving all bands from 7q36.1 to 7q36.3.

Imaging Findings

The patient demonstrates semilobar holoprosencephaly(figure C), characterized by partial separation of the cerebral hemispheres with fused frontal lobes and thalami, while the splenium of the corpus callosum is preserved. Holoprosencephaly is defined by abnormal midline communication between gray and white matter, and MRI is the modality of choice for characterizing its three types: alobar, with complete fusion of the hemispheres and thalami and absence of the corpus callosum (figure D); semilobar, as seen in this patient; and lobar (figure B), with nearly complete hemispheric separation, fusion of the frontal lobes, and preservation of the corpus callosum body and splenium. Spinal MRI is also important to identify associated anomalies such as anterior meningocele, lipoma, cauda equina syndrome, or fused vertebrae. In this case, the patient demonstrates type II sacral

agenesis (figure E), defined by partial bilateral sacral defects in which the iliac bones articulate with S1 but the distal sacral elements fail to develop, along with an anterior meningocele (figure F, blue solid lines). Sacral agenesis is categorized into four types: type I, unilateral sacral or coccygeal agenesis; type II, partial bilateral agenesis; type III, total sacral agenesis with iliac articulation to the lowest lumbar vertebra; and type IV, total sacral agenesis with posterior fusion of the iliac bones. Additionally, patients may present with hydrocolpos, as seen in this case (figure F).

Discussion

7q36 deletion syndrome is a rare genetic disorder, with a prevalence of less than 1 in 1,000,000. It involves a distal deletion on the long arm of chromosome 7. The syndrome presents with a wide phenotypic spectrum due to the multiple genes involved. Common clinical features include facial dysmorphism, brain malformations, endocrinopathies, developmental delay, and sacral anomalies. Holoprosencephaly is a congenital malformation characterized by failure of differentiation of prosencephalon and may be linked to mutations in the SHH gene at 7q36.3, crucial for midline forebrain development. Sacral dysgenesis, ranging from partial lumbosacral agenesis to absent coccyx, is often associated with MNX1 (HLXB9) gene mutations at 7q36.3 and may occur as part of Currarino triad, characterized by anorectal malformation, sacrococcygeal defect, and presacral mass.

Teaching Point

1. Midline craniofacial defects should raise suspicion of associated intracranial and spinal anomalies.
2. Mutations in the SHH gene can cause holoprosencephaly, while MNX1 mutations are linked to sacral agenesis; both genes are located on chromosome 7q36.3.
3. Brain and spine MRI are essential for detecting underlying syndromes, guiding genetic testing, supporting multidisciplinary management, and influencing in prognosis.

References

1. Lynch SA, Bond PM, Copp AJ, Kirwan WO, Nour S, Balling R, Mariman E, Burn J, Strachan T. A gene for autosomal dominant sacral agenesis maps to the holoprosencephaly region at 7q36. Nat Genet. 1995;11:93-5. DOI: 10.1038/ng0995-93
2. Dworschak GC, Reutter HM, Ludwig M. Currarino syndrome: a comprehensive genetic review of a rare congenital disorder. Orphanet J Rare Dis. 2021;16:167. DOI: 10.1186/s13023-021-01799-0
3. Horn D, Tönnies H, Neitzel H, Wahl D, Hinkel GK, von Moers A, Bartsch O. Minimal clinical expression of the holoprosencephaly spectrum and of Currarino syndrome due to different cytogenetic rearrangements deleting the Sonic Hedgehog gene and the HLXB9 gene at 7q36.3. Am J Med Genet A. 2004;128A:85-92. DOI: 10.1002/ajmg.a.30031
4. Agrawal R, Campos A, Yap J, et al. Holoprosencephaly. https://radiopaedia.org/articles/1461(Accessed on 04 Nov 2025)
5. Winter TC, Kennedy AM, Woodward PJ. Holoprosencephaly: a survey of the entity, with embryology and fetal imaging. Radiographics. 2015;35:275-90. DOI: 10.1148/rg.351140040

Images/Tables

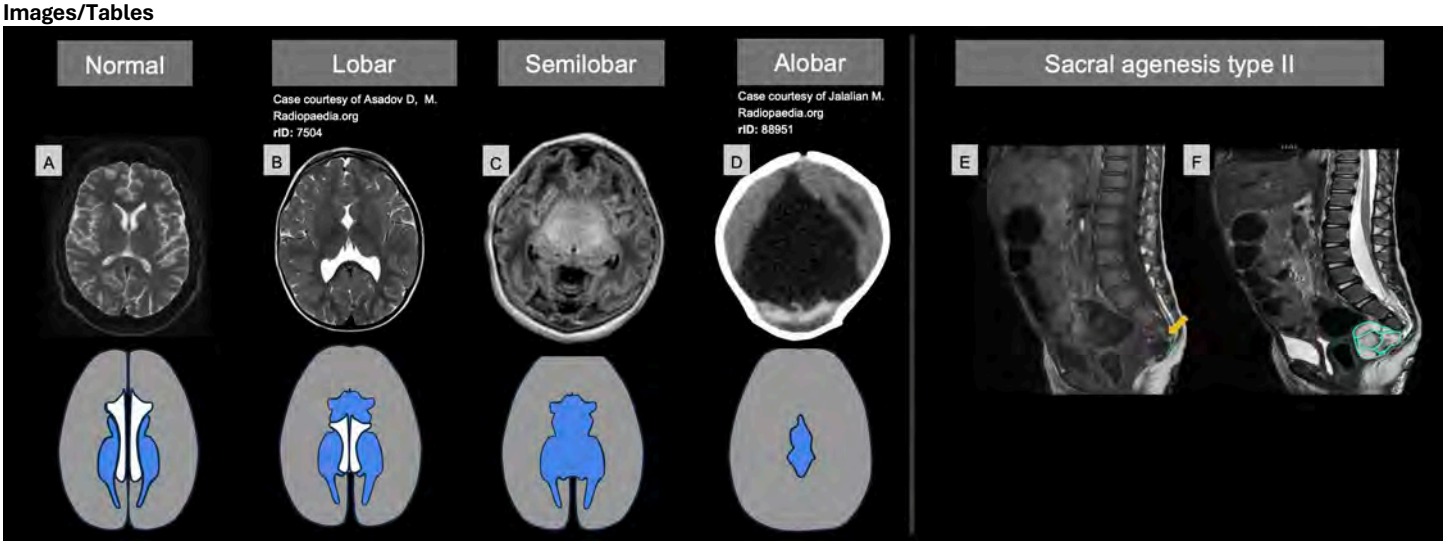

152 Expanding the the imaging spectrum of Tethered Cord-The cervical variant

Fatima Mubarak MBBS, Manahil n
Aga Khan university hospital, Karachi, Sind, Pakistan

Clinical History

A 32-year-old female with a history of spina bifida cystica presented with upper back pain, neck pain, and hand paresthesia. Magnetic resonance imaging (MRI) revealed tethering at the cervical spine, with a dermal sinus tract and dorsal meningocele. The patient underwent surgical detethering and excision of the dermal sinus tract under general anesthesia, and postoperative follow-up was conducted to assess neurological recovery. MRI confirmed cervical cord tethering, with associated abnormalities including a dermal sinus tract extending from C1 to D7, and focal syrinx formation. The patient's symptoms improved postsurgery, with no new neurological deficits observed.

Imaging Findings

MRI [Figure 1] revealed straightening of the cervical spine with loss of normal lordosis. An unfused posterior element of D1 vertebra was identified, along with a linear T2 hyperintense structure, likely representing tethered nerve roots adherent to the posterior cervical cord at C7-D1. These nerve roots extended posteriorly through a bony defect into the subcutaneous tissues, forming a dermal sinus tract with an associated dorsal meningocele and focal syrinx at C6-C7. No evidence of Chiari malformation was noted. In addition, MRI of the entire spine [Figure 2] was obtained to rule out any coexistent spinal anomalies, and no additional abnormalities were identified outside the cervical region.

Discussion

TCS is neurological disorder characterized by abnormal spinal cord attachment, resulting in excessive stretching and progressive neurological decline. Although TCS primarily affects the lumbosacral region, cervical cord tethering is exceptionally rare. Its clinical presentation varies widely, ranging from mild pain and sensory disturbances to severe motor deficits and bowel/bladder dysfunction.

In resource-limited settings, access to early diagnostic imaging and neurosurgical expertise is often restricted, leading to underreporting of such cases. In addition, it has been suggested that repetitive movements in the presence of an immobile spinal cord lead to ischemic insults and mitochondrial dysfunction, resulting in neuronal damage. South Asian populations exhibit a higher incidence of neural tube defects due to genetic predisposition, consanguinity, and nutritional deficiencies, particularly folate deficiency.

Patient presented with upper back pain radiating to the left shoulder, neck pain, and bilateral hand paresthesia without any motor deficits. This presentation contrasts with most previously reported cases, where symptoms typically include progressive motor weakness, gait disturbances, and bowel or bladder dysfunction. While most congenital cervical TCS cases present in infancy or childhood, the late onset of symptoms in our patient suggests a progressive traction on the cord or late secondary changes such as syrinx formation, as observed on MRI.

Standard treatment for TCS involves surgical detethering to prevent neurological deterioration. surgical approach in our case was more extensive due to the presence of an elongated dermal sinus extending from C1 to D7, requiring meticulous dissection to prevent cord damage. Favorable postoperative outcome highlights the effectiveness of early surgical intervention, emphasizing that even asymptomatic or mildly symptomatic cases benefit from proactive management to prevent irreversible deficits.

Teaching Point

- Cervical tethered cord with dermal sinus tract rare congenital anomaly, esp in adults.
- MRI essential for diagnosis, revealing tethering, sinus tracts, meningoceles, syrinx formation.
- Early surgical detethering can prevent neurological damage.

References

1. Irfan M, Samnani S, Mubarak F. Tethered cervical cord syndrome: A rare entity – a case report and literature review. Surg Neurol Int. 2025;16:331. doi: 10.25259/SNI_335_2025

2.Abu-Bonsrah N, Purvis TE, Rory Goodwin C, Petteys RJ, De La Garza-Ramos R, Sciubba DM. Adult cervicothoracic lipomyelomeningocele. J Clin Neurosci 2016;32:157-9.

3. Ackerman LL, Menezes AH, Follett KA. Cervical and thoracic dermal sinus tracts. A case series and review of the literature. Pediatr Neurosurg 2002;37:137-47.

4. Ackerman LL, Menezes AH. Spinal congenital dermal sinuses: A 30-year experience. Pediatrics 2003;112:641-7.

5. Ali A, Ali R, Ali G. Tethered cord syndrome in adults: Experience of 50 patients. J Popul Ther Clin Pharmacol 2023;30:337-43.

Images/Tables

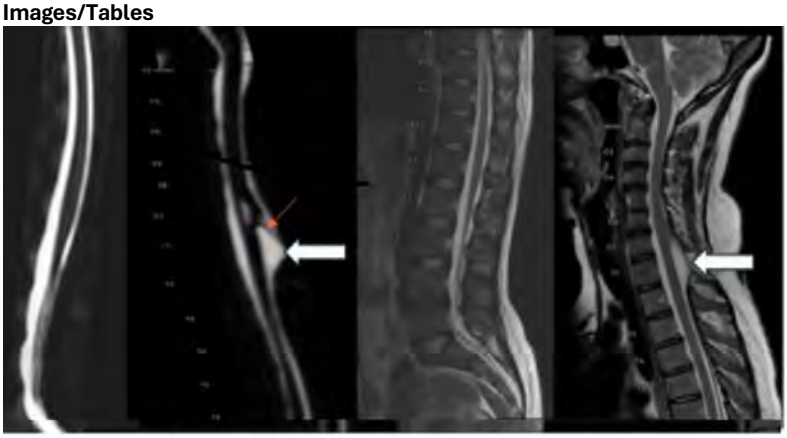

Dilated central canal (thin green arrow) with focal bony defect and a dermal sinus at C7-D1 level (thick white arrows) along with adherent nerve roots (thin orange arrow).

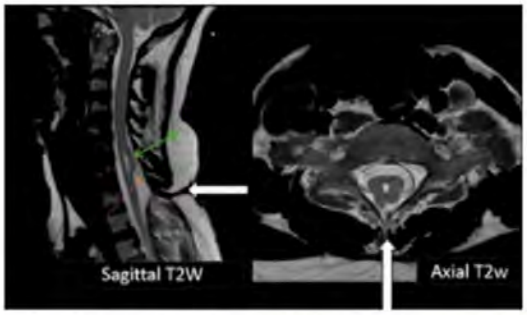

Magnetic resonance (MR) imaging of the whole spine, including MR myelogram and T2-weighted sagittal sequences, demonstrating no additional spinal anomalies beyond the cervical tethered cord (orange arrow) and dermal sinus tract(thick white arrow). The images show normal thoracic and lumbar spine anatomy, ruling out coexistent spinal anomalies that could contribute to the patient's symptoms.

---

153 Revisiting an Old Complication of Frontal Sinusitis in the Post-antibiotic Era: Pott's Puffy Tumor.

Azin Aein MD, Lawrence E. Ginsberg MD
University of Texas Medical Branch (UTMB), Galveston, TX, USA

Clinical History

A 43-year-old man with a past medical history of autoimmune hepatitis on immunosuppressive medications and recurrent frontal sinusitis (three episodes in one year) presented with rapidly progressing facial swelling and pain, as well as periorbital swelling over two weeks. Bedside drainage and incision were performed; purulent material was sent for analysis, and the patient started on broad-spectrum antibiotics. The Gram stain revealed Gram-negative bacilli without speciation, and the patient was started on IV antibiotics.

Imaging Findings

Contrast-enhanced CT sinus demonstrated an expanded, opacified frontal sinus with breakthrough of the anterior wall and extensive frontal soft tissue inflammatory changes (Figure A and B). MRI was performed and showed rim-enhancing frontal sinus infection and abscess extension into the frontal scalp compatible with Pott's Puffy Tumor (PPT) (Figure C and D). There was no definite epidural extension.

Discussion

In the antibiotic era, PPT is a rare and dangerous complication of recurrent frontal rhinosinusitis and is potentially life-threatening with relatively high morbidity and mortality (12% without treatment). Prompt surgical intervention and medical treatment are crucial to avoid complications such as epidural abscess, subdural empyema, sinovenous thrombosis, meningitis, and cerebritis.

Teaching Point

Our aim is to present a rare case of complicated sinusitis, Pott's puffy tumor, and familiarize radiologists with its appearance and potential complications.

References

1. Terui H, Numata I, Takata Y, Ogura M, Aiba S. Pott's Puffy Tumor Caused by Chronic Sinusitis Resulting in Sinocutaneous Fistula. JAMA Dermatol. 2015 Nov;151(11):1261-3. doi: 10.1001/jamadermatol.2015.0874. PMID: 26017578.
2. Rohde RL, North LM, Murray M, Khalili S, Poetker DM. Pott's puffy tumor: A comprehensive review of the literature. Am J Otolaryngol. 2022 Sep-Oct;43(5):103529. doi: 10.1016/j.amjoto.2022.103529. Epub 2022 Jun 9. PMID: 35700606.
3. Karaman E, Hacizade Y, Isildak H, Kaytaz A. Pott's puffy tumor. J Craniofac Surg. 2008 Nov;19(6):1694-7. doi: 10.1097/SCS.0b013e31818b432e. PMID: 19098585.
4. Suwan PT, Mogal S, Chaudhary S. Pott's Puffy Tumor: An Uncommon Clinical Entity. Case Rep Pediatr. 2012;2012:386104. doi: 10.1155/2012/386104. Epub 2012 Oct 4. PMID: 23091765; PMCID: PMC3471412.

Images/Tables

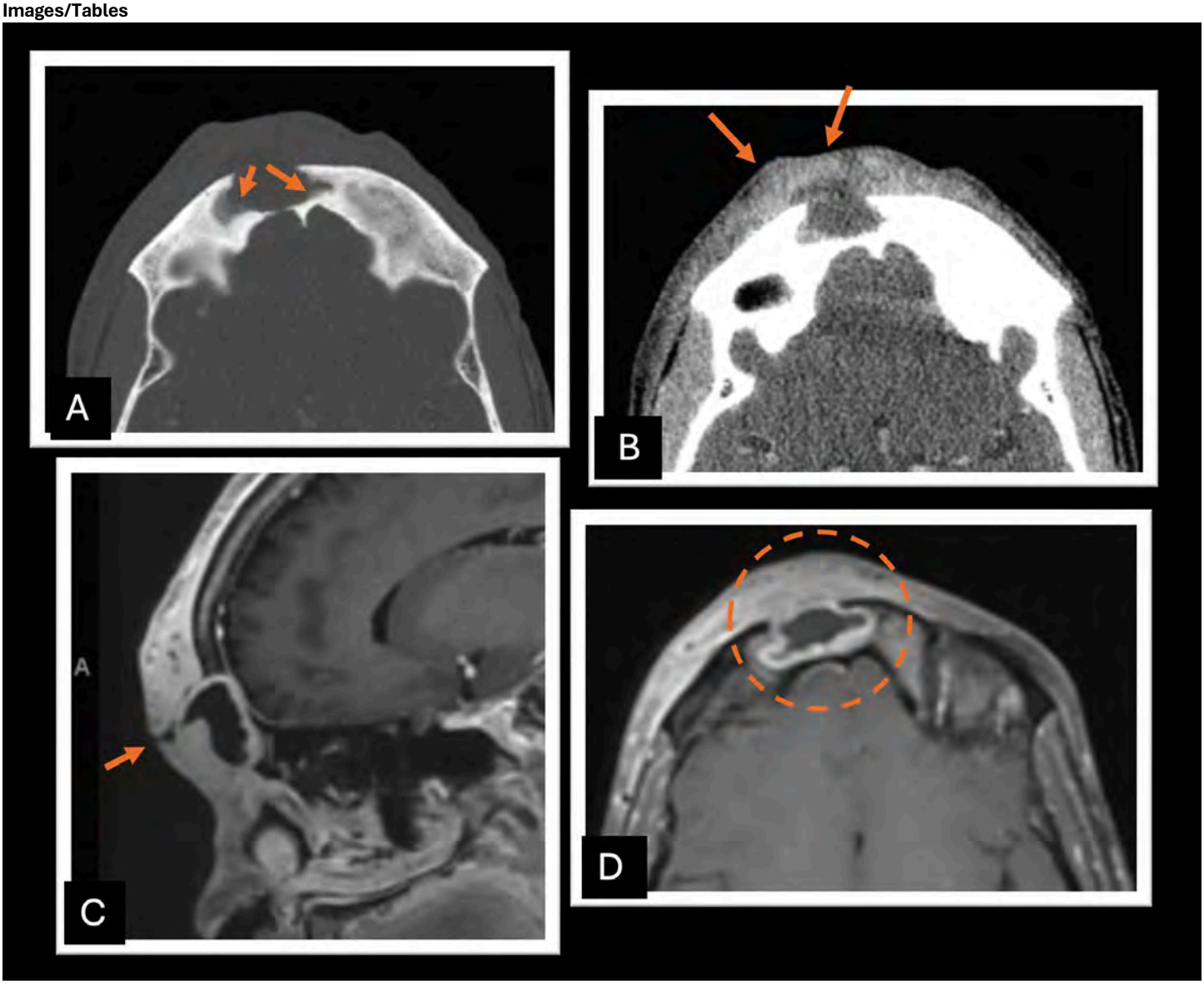

168 Beyond the Bones: Traumatic Pediatric Spine MRI

Christopher M Ruggiero MD, Bilal Battal MD

University of North Carolina- Chapel Hill, Chapel Hill, NC, USA

Clinical History

A. A 6-year-old male presented following an MVC, and his initial cervical spine CT was negative.

B. A 10-year-old female presented with right upper extremity weakness with complete left and partial right CN VI palsies following a high-speed MVC.

C. A 7-month-old male presented after a reported 3-foot fall. Bilateral retinal hemorrhages and subclinical seizures, subsequently status epilepticus, were identified clinically and raised concern for nonaccidental trauma.

D. A 4-year-old male presented immediately following an MVC as a non-restrained backseat passenger.

Imaging Findings

A. Sagittal T2-weighted cervical spine MRI demonstrates cervicothoracic cord transection and retraction (red bracket).

B. Sagittal STIR cervical spine MRI shows craniocervical junction injuries, including apical ligament disruption and anterior atlantooccipital membrane injury (green box), occiput-C1 space and C1-C2 interspinous ligament edema, and a prevertebral hematoma. A retroclival epidural hematoma (red arrow) effaces the prepontine cistern with uplifting of the tectorial membrane, likely compressing/irritating CN VI bilaterally, explaining the abducens nerve palsies.

C. Sagittal T2-weighted thoracolumbar spine MRI shows subdural hematoma from C7 through S1 (red arrows) with cord and cauda equina compression. Intracranially, bilateral infarcts, subdural hematomas, and trace subarachnoid hemorrhage were present (not shown).

D. Sagittal STIR lumbar spine MRI shows L3-L4 disco-ligamentous injury, including interspinous and posterior longitudinal ligament rupture (red arrow). Multifocal cord hyperintensities likely reflect small cord infarcts/contusions, and epidural hematoma extends from T12-L5.

Discussion

Up to 10% of spinal injuries occur in children; due to relatively weaker musculature, ligamentous laxity, and altered biomechanics, force vectors may result in severe neurologic injury with reported mortality rates as high as 59% (1). Under the age of 8, motor vehicle collisions (MVC) are more common, whereas older patients often experience falls or sports-related traumas (2). Importantly, nonaccidental trauma (NAT) must always be considered (1-2).

A higher fulcrum of motion at C2-C3 with underdeveloped facet joints and spinous processes places younger patients at increased risk for upper cervical spine injuries (2-3). Minimal osseous spine distraction may inflict cord injury, thus Spinal Cord Injury without Radiographic Abnormality (SCIWORA) is unique to pediatrics (1,3). Moreover, congenital conditions, including trisomy 21 or mucopolysaccharidosis, and inflammatory disorders, including Grisel syndrome or rheumatoid arthritis, predispose to C1-C2 subluxations and ligamentous laxity (2). Additionally, developmental variants may complicate interpretation (1-3).

While CT remains the first-line modality for assessing osseous injury, MRI is indispensable for detecting radiographically occult spinal cord, ligamentous, and extra-axial soft-tissue injuries, particularly in cases of SCIWORA. MRI provides direct visualization of cord edema, hemorrhage, transection, ligamentous disruption, and epidural or subdural hematomas. This exhibit offers a framework via examples of cord transections, ligamentous disruptions, cord/nerve compression, and extra-medullary hematomas.

Teaching Point

Radiologists should be familiar with MRI features of post-traumatic, radiographically occult pediatric spinal injuries, as timely recognition is critical for appropriate management and improved outcomes.

References

1. Mistry D, Munjal H, Ellika S, Chaturvedi A. Pediatric spine trauma: A comprehensive review. *Clin Imaging* **2022**;87:61–76. doi:10.1016/j.clinimag.2022.04.012
2. Lustrin ES, Karakas SP, Ortiz AO, et al. Pediatric cervical spine: normal anatomy, variants, and trauma. *Radiographics* **2003**;23:539–560. doi:10.1148/rg.233025121
3. Roche C, Carty H. Spinal trauma in children. *Pediatr Radiol* **2001**;31:677-700. doi:10.1007/s002470100532

Images/Tables

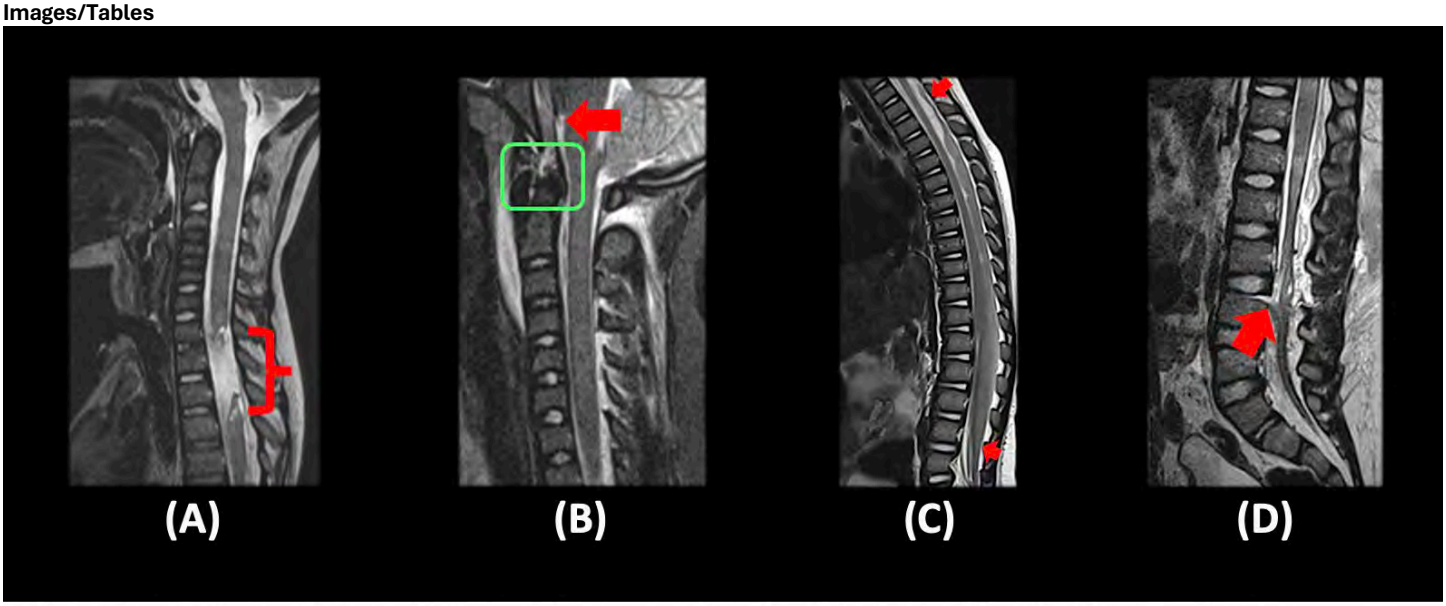

Figure 1. Overview of Non-osseous Pediatric Spinal Injuries on MRI.

---

172 CNS Lymphocytic Vasculitis Mimicking a High Grade Glioma

Alysha Vartevan DO[1], Glorirma Urbino Román MD[2], Alexa Botero[3], Osmany DeAngelo DO[2]

[1]Camelback Radiology, Scottsdale, AZ, USA. [2]Larkin Community Hospital, Miami, FL, USA. [3]Arizona State University, Phoenix, AZ, USA

Clinical History

An 18-year-old female, with a history of migraines, presented to the emergency room for progressive speech difficulties, mild right-sided weakness, and severe headaches. The initial brain CT demonstrated left anterior frontotemporal vasogenic edema with extensive mass effect and hemorrhage concerning for an underlying mass. Follow-up brain MRI showed a left frontal mass with hemorrhage, midline shift, and mass effect concerning for a

high grade glioma. The patient was treated with corticosteroids for five days before undergoing left frontal craniotomy for tumor resection. Pathology was complex, revealing cortical and subcortical infarcts, focal hemorrhage, chronic inflammatory cells, and fibrinoid necrosis, leading to a final diagnosis of CNS lymphocytic vasculitis.

Imaging Findings

Pre-operative brain MRI demonstrated focal hemorrhage in the left frontal lobe with extensive vasogenic edema extending into the genu of the corpus callosum. There was left-to-right midline shift, subfalcine herniation, and mass effect on the adjacent parenchyma and ventricles. Intrinsic T1 signal corresponded to subacute blood products without associated enhancement. Dural veins were patent, and there was restricted diffusion associated with an intra-axial hematoma. Post-operative brain MRI showed a left frontal craniotomy with resection of the previously described multi-focal mass with improvement in vasogenic edema and mass effect. Residual T2/FLAIR signal was noted within the left frontal lobe operative bed. Hemosiderin staining was visualized in the left frontal lobe. Subtle intrinsic T1 signal corresponded to an area of DWI signal. There was a peripheral rim enhancement in the left frontal operative bed without mass-like enhancement. There was interval development of ventriculomegaly.

Discussion

Primary CNS vasculitis (PCNSV) is a rare inflammatory disorder affecting small and medium-sized blood vessels of the brain, spinal cord, and meninges, accounting for 1% of all systemic vasculitides. Three histologic subtypes exist: granulomatous, necrotizing, and lymphocytic, the last being rare but seen in our case. Diagnosis is challenging due to non-specific symptoms and lack of biomarkers. The Calabrese and Mallek criteria was proposed to help clinical diagnosis. The diagnostic criteria includes the following; (1) unexplained acquired neurologic deficit, (2) evidence of CNS arteritis by angiography or biopsy, and (3) exclusion of system vasculitis or other disorders. Imaging plays a key role in the diagnostic workout, but ultimately histopathology is needed for definitive diagnosis. PCNSV typically presents in middle-aged adults, with a slight female predominance, and manifests as headaches, seizures, or focal deficits. Standard therapy includes high-dose corticosteroids and cyclophosphamide.

Teaching Point

This case highlights the importance of maintaining a broad differential diagnosis. CNS lymphocytic vasculitis can mimic high-grade glioma with vasogenic edema, mass effect, and hemorrhage. However, unlike gliomas, these lesions may lack solid enhancement and restricted diffusion. In cases with extensive edema but no true enhancement or restricted diffusion, a non-neoplastic process should be considered. Ultimately, histopathologic confirmation is essential for definitive diagnosis.

References

1. AyushAgarwal , Jyoti Sharma , M.V. Padma Srivastava, et al. Primary CNS vasculitis (PCNSV): a cohort study. 2022; 12:13494. DOI:https://www.nature.com/articles/s41598-022-17869-7
2. Sushant Agarwal, Leve Joseph Devarajan Sebastian , Shailesh Gaikwad, et al. The role of susceptibility-weighted imaging & contrast-enhanced MRI in the diagnosis of primary CNS vasculitis: a large case series. 2024; 14:4718. DOI: https://www.nature.com/articles/s41598-024-55222-2
3. Garrett M. Timmons, MD, Torge Rempe, MD, Elizabeth A. Bevins, et al. CNS Lymphocytic Vasculitis in a Young Woman With COVID-19 Infection. Neurology Neuroimmunology & Neuroinflammation. 2021; Volume 8, Number 5. DOI: https://www.neurology.org/doi/10.1212/NXI.0000000000001048

Images/Tables

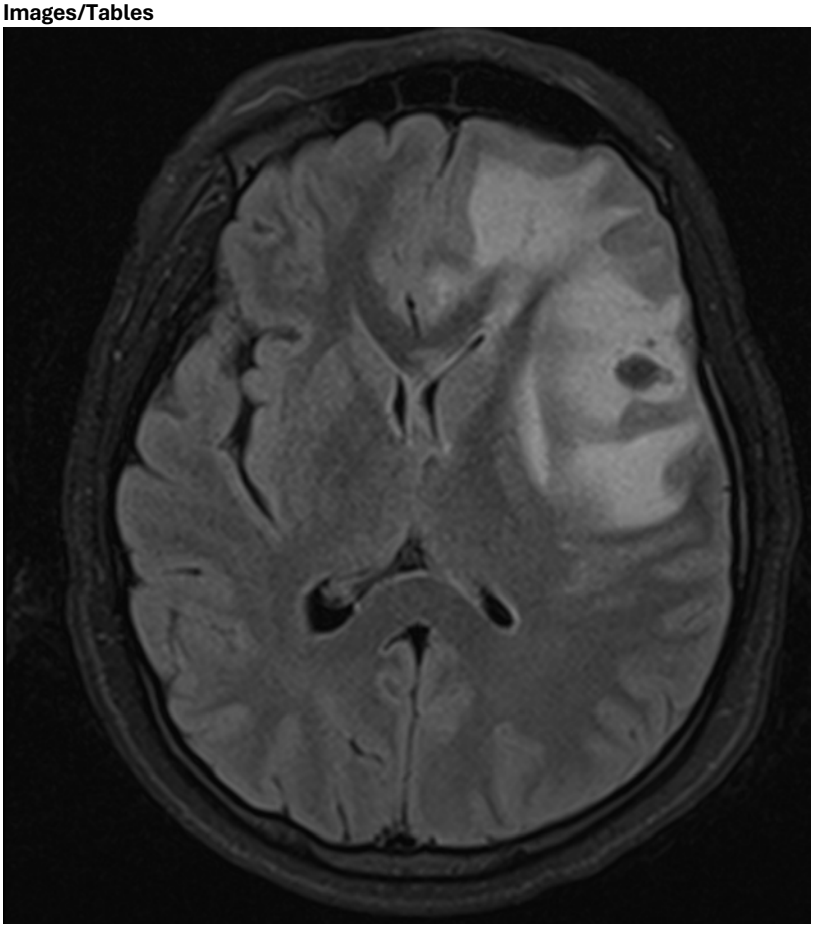

202 Chronic Sclerosing Sialadenitis of the Submandibular Gland: A Tumor Mimic

Neil B. Thackar DO, William T. Malouf MD
Wake Forest University School of Medicine, Winston-Salem, NC, USA

Clinical History

85yo male with recent episode of IgG4-related pancreatitis presenting with two months of a left neck mass. Remote history of lymphoma and colon cancer (in remission).

Imaging Findings

Ultrasound: hypoechoic, hypovascular mass in the submandibular gland with ill-defined margins.
FDG PET/CT: Low grade associated FDG uptake.
CT soft tissue neck: Mild asymmetric enlargement of the affected submandibular gland, however no well-defined mass. No cervical lymphadenopathy.

Discussion

Diagnosis: Chronic sclerosing sialadenitis
IgG4-related disease causes a wide spectrum of abnormalities in multiple organ systems. Pathologically, it is characterized by deposition of pro-inflammatory IgG4-positive plasma cells into tissues, often with elevated serum IgG4. It commonly manifests as systemic disease, classically associated with autoimmune pancreatitis. However, extra-pancreatic manifestations are well documented.
Nearly 40% of patients with known IgG4-related disease will also have involvement of the lacrimal and/or salivary glands. This can manifest in several different ways, including salivary gland swelling, enlargement, or a more focal inflammatory process that can mimic a mass.
Our case highlights a presentation in which a patient with known IgG4 autoimmune pancreatitis presented with a submandibular gland mass. Given the patient's remote history of lymphoma, a malignant entity could not be excluded on the basis of imaging alone, and thus submandibular gland resection was pursued. Final pathology result confirmed a diagnosis of chronic sclerosing sialadenitis.
Chronic sclerosing sialadenitis (also known as Küttner tumor) is a localized form of IgG4-mediated disease that can involve one or both salivary glands. Clinically, this presents as a painless lump or swelling. The imaging appearance is nonspecific, and mimics that of IgG4 related disease elsewhere. An ill-defined mass in the salivary glands can be seen, along with FDG avidity on PET/CT. MRI may show homogenous T1 and T2 hypointensity, with homogenous post-contrast enhancement and restricted diffusion. Note that these pseudotumors are often occult or poorly visualized on CT.

Teaching Point

1) Focal mass-like enlargement of the salivary glands in a patient with known diagnosis of IgG4 related systemic disease should raise concern for chronic sclerosing sialadenitis.
2) While IgG4-related disease classically involves the pancreas, extra-pancreatic manifestations may also occur. Nearly 40% of patients with known IgG4 disease will have involvement of the salivary glands.
3) Relatively large salivary gland masses may be occult on CT.

References

1) Martínez-de-Alegra A, Baleato-González S, García-Figueiras R, Bermúdez-Naveira A, Abdulkadher-Nallib I, Díaz-Peromingo JA, et al. IgG4-related disease from head to toe. *Radiographics* 2015;35:2007–2025. DOI: https://doi.org/10.1148/rg.357150066
2) Som PM, Curtin HD, eds. *Head and Neck Imaging* 5th ed. St Louis: Mosby; 2005: pp. 2496
3) Toyoda K, Oba H, Kutomi K, Furui S, Oohara A, Mori H, et al. MR imaging of IgG4-related disease in the head and neck and brain. *AJNR Am J Neuroradiol* 2012;33:2136–2139. DOI: https://doi.org/10.3174/ajnr.A3147

Images/Tables

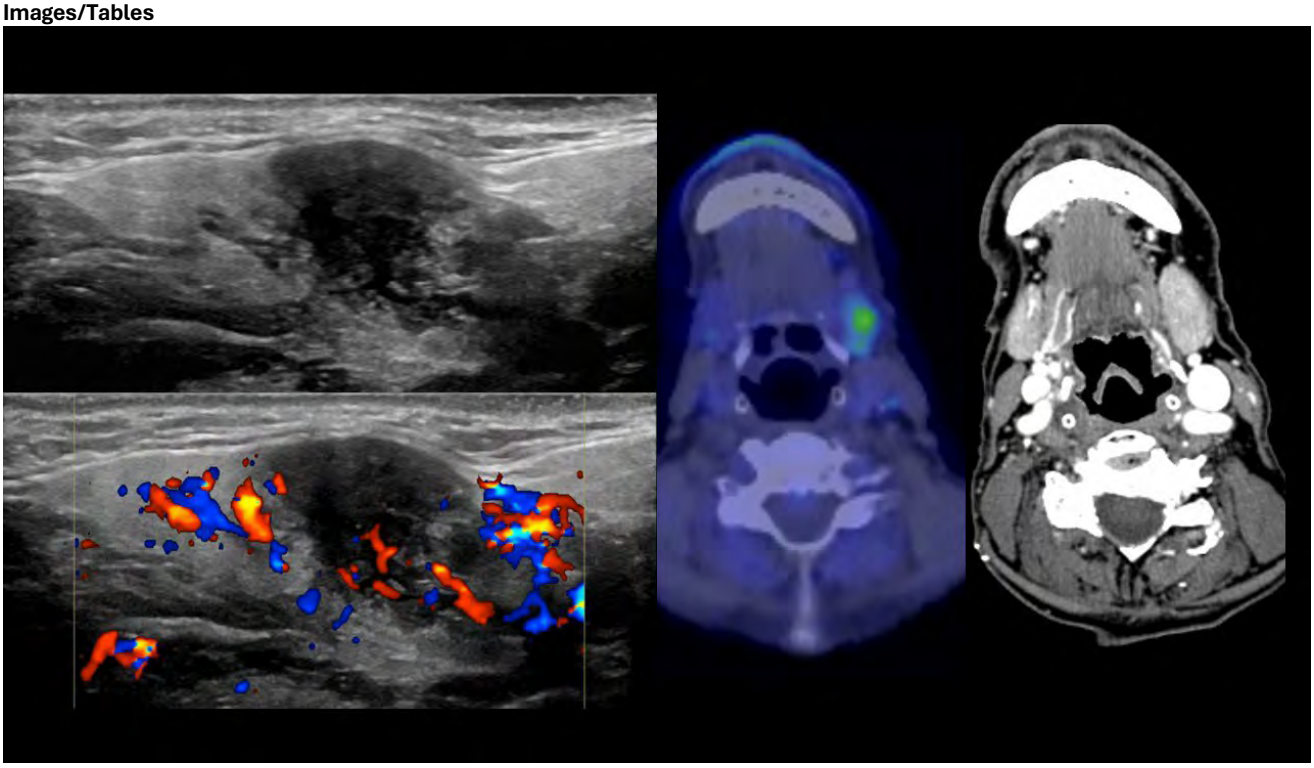

206 Metastatic Meningioma with Distant Nodal Metastasis

Anh T Nguyen DO[1], Ansley J Kunnath MD/PhD[2], Simone P Montoya MD[2]

[1]Touro College of Osteopathic Medicine, New York, NY, USA. [2]Vanderbilt University, Nashville, Tennessee, USA

Clinical History

A 32-year-old female with a history of WHO grade 2 meningioma of the right middle fossa tumor with direct locoregional extracranial extension underwent two surgical resections and radiation therapy. The patient initially underwent endoscopic endonasal subtotal resection, followed by proton therapy. Two years later, she underwent a right frontotemporal craniotomy for re-resection of progressive residual tumor, again followed by proton beam therapy. The recurrent tumor did not have malignant (grade 3) features. Following treatment, the patient experienced persistent facial pain, swelling, headaches, and progressive vision loss prompting further imaging with brain MRI to assess for recurrence/progression; this incidentally revealed an enlarged right internal jugular chain lymph node which was confirmed on dedicated neck CT. Biopsy of the lymph node demonstrated a proliferation of cells with meningothelial cytologic features. These findings confirmed the rare situation of meningioma metastasizing both locoregionally and distantly, specifically involving the right orbit, right sphenoid sinus, and a right cervical lymph node. Of note, the patient did not endorse any symptomatology readily attributable to lymphadenopathy.

Imaging Findings

The initial brain MRI shows an extra-axial, round, solid mass in the right middle cranial fossa with adjacent parenchymal edema and involving the right sphenoid bone and overlying right temporalis muscle and extending into the right orbit. The lesion is T1-hypointense with homogeneous enhancement and edema within the surrounding parenchyma. The brain MRI obtained for worsening symptomatology post-treatment reveals progression of known residual tumor with extension into the right sphenoid sinus, as well as a T2-hyperintense enhancing mass within the right carotid space. A subsequent neck CT shows an enlarged hypo-enhancing right internal jugular chain (level II/III) cervical lymph node measuring nearly 4 cm; retrospectively, this node has been abnormal on earlier imaging.

Discussion

Meningioma is the most common benign primary tumor of the brain, accounting for 33.8% of all primary brain tumors.[1] Extracranial metastasis of meningioma is rare, occurring in only 0.76% of all meningioma cases.[2] The most common sites of metastasis are the lungs, followed by bone, liver, soft tissue, and much less frequently lymph nodes.[3] This case report describes a rare case of recurrent grade 2 meningioma of the skull base with cervical nodal metastasis. By highlighting this unique presentation, we aim to emphasize the importance of considering extracranial metastasis in patients with recurrent high-grade tumor, as well as the need for further characterization of this unique patient population. A comprehensive approach to diagnosis may lead to earlier detection of distant metastases and more effective treatment planning. Furthermore, there is a continued need for research to better understand the mechanisms, risk factors, and optimal management strategies for meningioma with metastatic potential. For example, the use of PET imaging has increased, but is not yet standard of care.

Teaching Point

This case highlights the rare potential for high-grade meningioma to metastasize to extracranial sites, including the head and neck, potentially without localizing symptomatology. It underscores the importance of thorough diagnostic evaluation, including imaging of extracranial structures, for patients with high grade and aggressive recurrence following standard treatment.

References

1. Wiemels J, Wrensch M, Claus EB. Epidemiology and etiology of meningioma. *J Neuro-Oncol.* 2010;99:307–314. DOI: 10.1007/s11060-010-0386-3
2. Bender L, Lhermitte B, Carinato H, et al. Grade III meningioma with gastro-intestinal tract and brain metastases: case report and review of the literature. *World J Surg Oncol.* 2019;17:70. DOI: 10.1186/s12957-019-1596-6
3. Himič V, Burman RJ, Fountain DM, et al. Metastatic meningioma: a case series and systematic review. *Acta Neurochir.* 2023;165:2873–2883. DOI: 10.1007/s00701-023-05687-3

Images/Tables

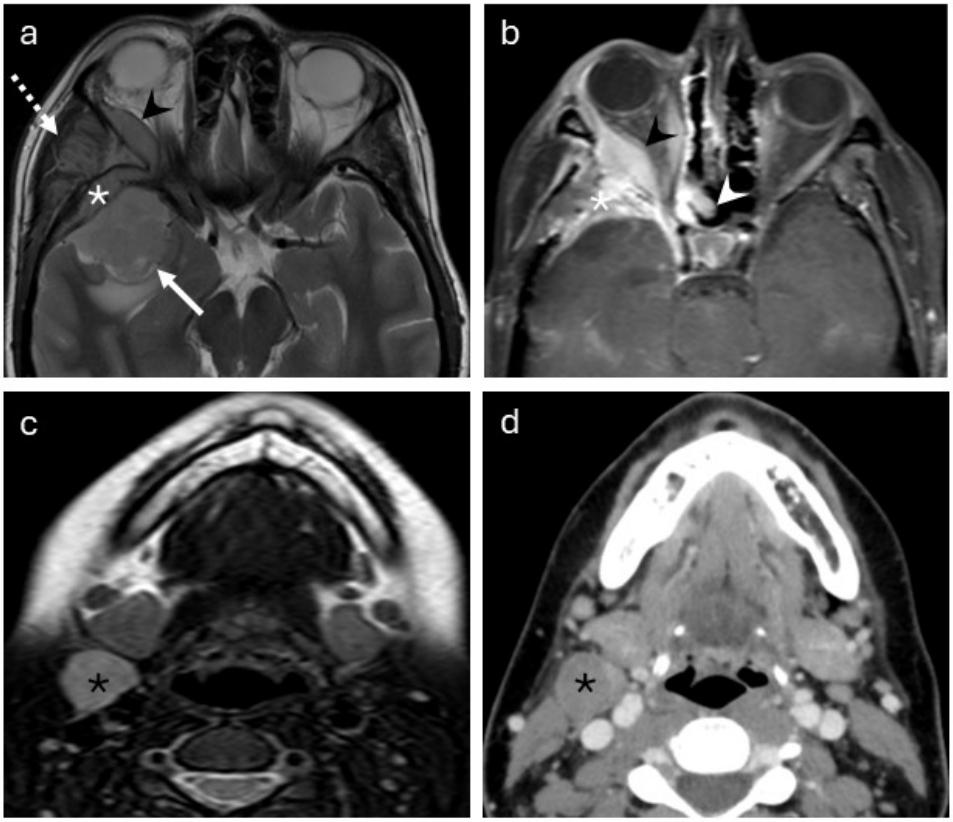

Figure 1: Meningioma with locoregional extracranial extension and distant nodal metastasis. The initial MRI (a) shows a solid extra-axial mass in the right middle cranial fossa (solid arrow) involving the right sphenoid bone (white asterisk), right temporalis muscle (dashed arrow), and right orbit (black arrowhead). MRI scans obtained post-treatment (b & c) reveal tumor progression with extension into the right sphenoid sinus (white arrowhead) and a T2-hyperintense mass within the right carotid space (black asterisk). A subsequent neck CT (d) shows an enlarged hypo-enhancing 4 cm right internal jugular chain lymph node (black asterisk); retrospectively, this node has been abnormal on earlier imaging.

---

221 **Improvement in Behavioral Variant-Frontotemporal Dementia Following Fibrin Glue Occlusion of CSF-Venous Fistula**

Richard Yu MD, Colton S Welch MD, David J Bronster MD, Brian P Rigney MD
Icahn School of Medicine at Mount Sinai, New York, New York, USA

Clinical History

A 56-year-old male with past medical history of hypertension and hyperlipidemia presented to neurology clinic for six months of progressive cognitive decline, memory loss, irritability, personality changes, involuntary tics, and difficulty with speech and swallowing. Neurological evaluation raised concern for frontotemporal dementia, and brain MRI revealed cerebellar tonsillar ectopia and brainstem sagging. CT myelogram revealed a CSF-venous fistula (CVF) at the T8-T9 level. The patient underwent CT-guided epidural fibrin glue patch targeting the right T8-T9 neural foramen and epidural space. Patient reported rebound headache as well as nausea and vomiting one day afterwards, which resolved. Approximately two weeks after the procedure, significant improvement in the patient's cognitive symptoms was noted, including improved short term memory, return to baseline personality, and decreased swallowing difficulty.

Imaging Findings

Figure 1. CT myelogram thoracic spine images at the T8-T9 level demonstrating myelographic contrast entering a right paraspinal vessel coursing towards the azygos vein, suggestive of CSF-venous fistula.

Figure 2. MRI brain (left, middle), demonstrates cerebellar tonsillar descent, brainstem sagging with decreased mamillopontine distance, decreased prepontine and suprasellar cistern caliber, and possible mildly convex margins of the right transverse sinus. MRI whole spine (right) showed meningeal diverticula, but no spinal longitudinal epidural collection (SLEC).

Figure 3. Images from CT-guided fibrin glue injection targeted at the T8-T9 right nerve root sheath demonstrate fibrin glue material mixed with contrast filling the nerve sheath. Single needle technique was used.

Discussion

Spontaneous intracranial hypotension (SIH) refers to intracranial hypotension due to non-iatrogenic CSF leaks, including from dural tears, meningeal diverticula, and CSF-venous fistulas. CSF leak results in brain sagging, which has characteristic imaging findings at MRI, and may cause symptoms including postural headache, nausea/vomiting, and neck pain/stiffness. Cognitive symptoms, including behavioral changes, are rare, reported in 2.6% of cases in one meta-analysis. Reversible behavioral-variant frontotemporal dementia (bvFTD) due to SIH was first reported in 2002 and has been termed frontotemporal brain sagging syndrome (FBSS). It is hypothesized that brain sagging may stretch frontotemporal cortices and/or connecting

pathways and may also lead to venous stagnation. A 2022 systematic review identified 70 reported cases of SIH-related bvFTD, of which 47 had complete symptom resolution following treatment.

Treatment may include epidural blood patch, surgical ligation, fibrin occlusion, or transvenous embolization, with CVF often unresponsive to blood patch. CVFs are most commonly found at the T7 to T12 levels, and do not produce SLECs, in contrast to dural tears. They are often associated with nerve root sleeve diverticula and often drain into segmental spinal veins. The underlying etiology is not currently known. Diagnosis requires careful attention with optimized myelographic imaging technique, as the findings are frequently subtle.

Teaching Point

Spontaneous intracranial hypotension is a rare cause of reversible behavioral-variant frontotemporal dementia, an entity termed frontotemporal brain sagging syndrome (FBSS). Here, we present a case of a patient with bvFTD who experienced dramatic improvement following CT-guided fibrin glue therapy of a suspected culprit CVF draining from the T8-T9 neural foramen into the azygos vein via a segmental spinal vein.

References

Callen, AL, Jones, LC, Timpone, VM, et al. Factors Predictive of treatment success in CT-Guided fibrin occlusion of CSF-Venous fistulas: a multicenter Retrospective Cross-Sectional study. *AJNR Am J Neuroradiol* 2023;44(11):1332–1338. DOI: https://doi.org/10.3174/ajnr.a8005

D'Antona, L, Merchan, MaJ, Vassiliou, A, et al. Clinical presentation, investigation findings, and treatment outcomes of spontaneous intracranial hypotension syndrome. *JAMA Neurol* 2021;78(3):329. DOI: https://doi.org/10.1001/jamaneurol.2020.4799

Kranz, PG, Gray, L, Malinzak, MD, et al. CSF–Venous fistulas: Anatomy and Diagnostic imaging. *AJR Am J Roentgenol* 2021;217(6):1418–1429. DOI: https://doi.org/10.2214/ajr.21.26182

Lashkarivand, A, & Eide, PK. Brain Sagging Dementia—Diagnosis, Treatment, and Outcome. *Neurology* 2022;98(19):798–805. DOI: https://doi.org/10.1212/wnl.0000000000200511

Schievink, WI, Maya, MM, Barnard, ZR, et al. Behavioral variant Frontotemporal dementia as a serious complication of spontaneous intracranial hypotension. *Oper Neurosurg* 2018;15(5):505–515. DOI: https://doi.org/10.1093/ons/opy029

Images/Tables

Figure 1. CT myelogram thoracic spine images at the T8-T9 level demonstrating myelographic contrast entering a right paraspinal vessel coursing towards the azygos vein, suggestive of CSF-venous fistula.

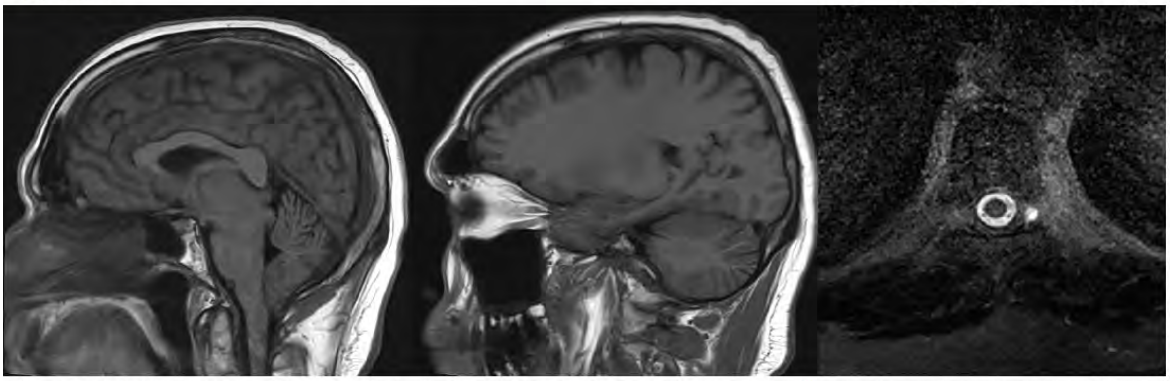

Figure 2. MRI brain (left, middle) demonstrates cerebellar tonsillar descent, and brainstem sagging with decreased mamillopontine distance, decreased prepontine and suprasellar cistern caliber, and possible mildly convex margins of the right transverse sinus. MRI whole spine (right) showed meningeal diverticula, but no spinal longitudinal epidural collection (SLEC).

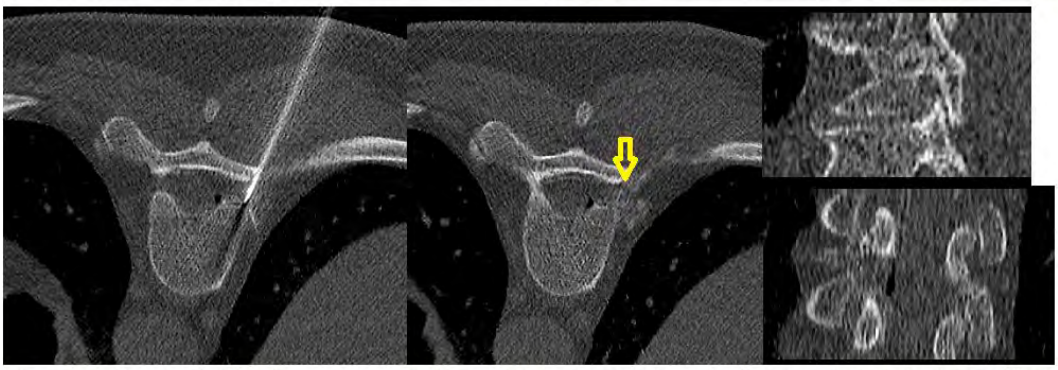

Figure 3. Images from CT-guided fibrin glue injection targeted at the T8-T9 right nerve root sheath demonstrate fibrin glue material mixed with contrast filling the nerve sheath. Single needle technique was used.

223 Iatrogenic Subarachnoid Fat Embolism Following Lumbar Drain Placement

Farhana A Ratree BS[1], Rodolfo Calderon MD[2], Vikas Agarwal MD, MBA[2], Hrishikesh A Kale MD[2]
[1]Lake Erie College of Osteopathic Medicine, Erie, PA, USA. [2]University of Pittsburgh Medical Center, Pittsburgh, PA, USA

Clinical History

A 21-year-old female with chronic headaches, initially evaluated in 2016, was found to have a non-enhancing lesion in the left medial cerebellar peduncle and roof of the fourth ventricle. Serial imaging showed slow enlargement over time raising concern for a low-grade glioma. She subsequently underwent suboccipital craniotomy and tumor resection. On postoperative day five, she developed new-onset seizures and encephalopathy. Cerebrospinal fluid (CSF) analysis on postoperative day seven revealed markedly elevated opening pressure (35 cm H2O), pleocytosis (WBC 1920), low glucose (32 mg/dL), and elevated protein (122 mg/dL), consistent with CNS infection. A lumbar drain was placed using fluoroscopic guidance for CSF diversion. Routine surveillance CT imaging following lumbar drain placement demonstrated new low-attenuation foci within the basal cisterns, consistent with subarachnoid fat deposits.

Imaging Findings

Non-contrast CT of the head before the lumbar drain placement showed expected operative changes. Specifically, no abnormalities were noted in the subarachnoid spaces. Fluoroscopic images confirmed lumbar drain insertion at the L2-L3 level. Four days later, routine surveillance non-contrast CT demonstrated new, well defined low-attenuation foci within the subarachnoid spaces and basal cisterns, (–30 to –27 HU), consistent with fat density. Lung window images excluded intracranial air, ruling out pneumocephalus.

Subsequent MRI performed to evaluate for surgical wound dehiscence revealed scattered intrinsically T1-hyperintense foci along the basal cisterns, right Sylvian fissure, and bilateral internal auditory canals that lost signal on T2 fat-saturated sequences, confirming lipid composition. These areas showed no associated restricted diffusion or enhancement. Given the temporal relationship to lumbar drain placement, the findings favored iatrogenic subarachnoid fat embolism.

Discussion

Subarachnoid fat embolism is a rare radiological finding most often seen due to a rupture of fat-containing lesion like dermoid cyst. In this case, the etiology was presumed iatrogenic, likely from minor disruption of epidural or subcutaneous fat during catheter insertion. Fat droplets can migrate cranially within CSF and accumulate in the basal cisterns.

Differential diagnosis for fat in the subarachnoid space includes ruptured intracranial dermoid, traumatic fat embolism, or postoperative introduction of fat, the last being the most plausible here. CT typically shows low-attenuation foci around (-30 HU) that may mimic air; MRI findings of T1 hyperintensity with loss of signal after fat-suppression confirms the diagnosis.

Recognizing this entity prevents misdiagnosis of pneumocephalus or infection. Whereas a ruptured dermoid may cause chemical meningitis due to inflammatory lipid reaction, iatrogenic cases are usually asymptomatic. Our patient remained clinically stable without neurologic sequalae, requiring only observation. Awareness of this pattern avoids unnecessary antibiotics and/or further surgical work-up. This underscores the importance of correlating CT attenuation with MRI fat-suppression findings to reach an accurate, noninvasive diagnosis.

Teaching Point

Subarachnoid fat embolism can occur as a rare iatrogenic complication of lumbar drain placement. Characteristic CT fat attenuation with corresponding MRI fat-suppression signal loss distinguishes it from pneumocephalus, hemorrhage, or infection, allowing for confident, conservative management.

References

1. Chaturvedi R, Williams A, Farid N, Retson T, Smitaman E. Posttraumatic subarachnoid fat embolism: Case presentation and literature review. *Clin Imaging*. 2020 Dec;68:121-123. doi: 10.1016/j.clinimag.2020.06.035. Epub 2020 Jun 20. PMID: 32592972; PMCID: PMC8898051.
2. Woo JK, Malfair D, Vertinsky T, Heran MK, Graeb D. Intracranial transthecal subarachnoid fat emboli and subarachnoid haemorrhage arising from a sacral fracture and dural tear. *Br J Radiol*. 2010 Jan;83(985):e18-21. doi: 10.1259/bjr/66268641. PMID: 20139244; PMCID: PMC3487252.
3. Polemikos M, Kiepe F, Al-Afif S, Bronzlik P, Krauss JK. When Fat Hits the Brain: Intraventricular and Subarachnoid Fat Migration Secondary to a Complex Sacropelvic Fracture-Diagnosis and Treatment. *J Neurol Surg A Cent Eur Neurosurg*. 2022 May;83(3):290-293. doi: 10.1055/s-0041-1722967. Epub 2021 Feb 22. PMID: 33618409.
4. Anandkumar D, Jakhura U, Potter K, Bhatti I. Low pressure headache and cerebral fat embolism from a sacral fracture through a Tarlov cyst: a case report. *J Med Case Rep*. 2023 Oct 7;17(1):444. doi: 10.1186/s13256-023-04142-2. PMID: 37803426; PMCID: PMC10559429.

Images/Tables

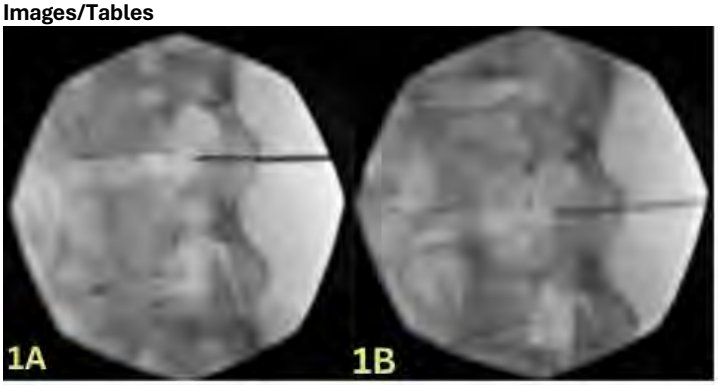

Figure 1: Lateral fluoroscopic images of the lumbar spine during lumbar drain placement show needle access (A) and subsequent lumbar drain catheter placement (B) of a lumbar drain at the L2-L3 level with catheter tracking cranial.

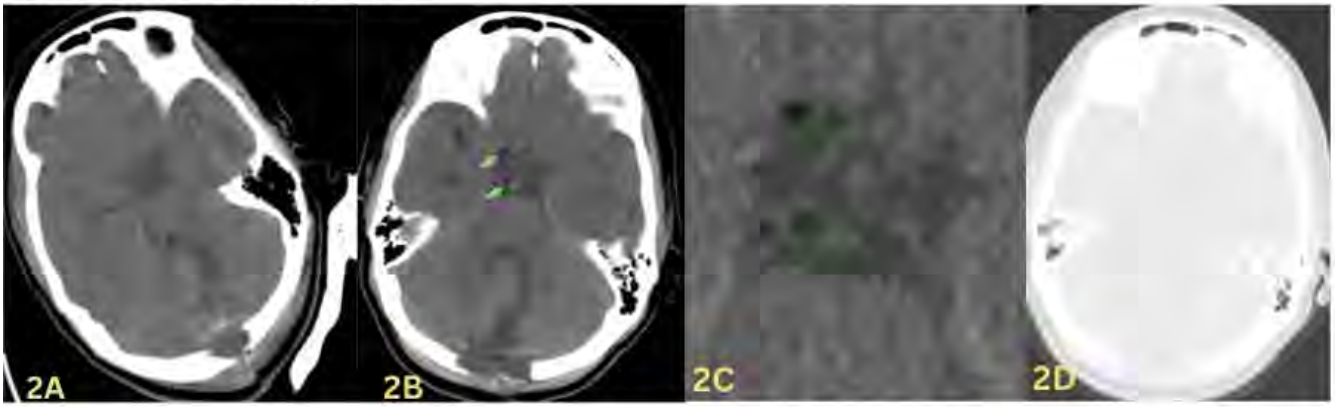

Figure 2: A) Axial noncontrast CT head obtained prior to lumbar drain placement demonstrates expected postsurgical changes from suboccipital craniectomy for left cerebellar mass resection, without low-attenuation foci along the basal cisterns, serving as the pre-lumbar drain baseline. B) Axial noncontrast CT head, windowed to accentuate fat density, obtained four days following lumbar drain placement shows new low-attenuation foci along the subarachnoid spaces and basal cisterns, consistent with fat density (green arrows). C). Magnified axial CT images from same acquisition highlight low-attenuation foci along the basal cisterns. Measured attenuation values (-38 to –25 HU) confirm the presence of fat density, consistent with subarachnoid fat deposits. D) Axial CT head, lung window, at the same level shows no intracranial air, effectively excluding pneumocephalus and suggesting that the low-attenuation foci may represent fat emboli within the subarachnoid space.

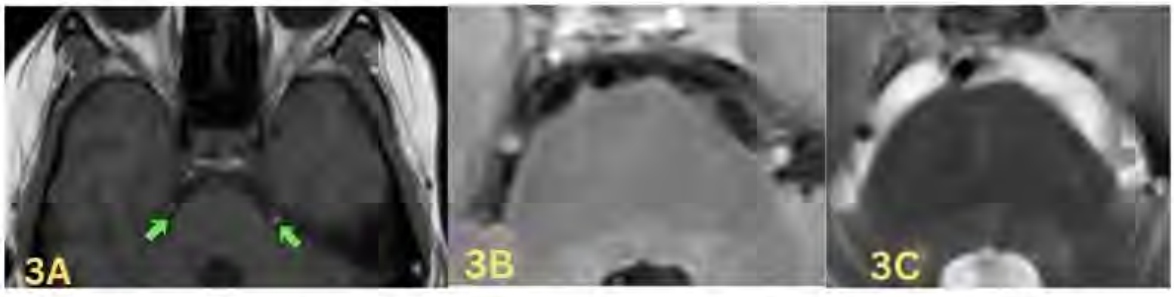

Figure 3: Axial T1-weighted MRI demonstrates scattered intrinsically T1-hyperintense foci (arrows) along the basal cisterns, consistent with subarachnoid fat deposits, likely post-procedural following lumbar drain placement. Axial T2 Flair (B) and T2- fat saturated (C) MRI demonstrated the loss of signal on fat-suppressed images (B), confirming fat composition of the subarachnoid foci along the basal cisterns (shown), with additional involvement of the right Sylvian fissure and bilateral internal auditory canals (not shown).

224 When Infection Imitates Tumor: Neurotoxoplasmosis Mimicking Central Nervous System Neoplasms

Dhanush Amin MD[1], Raman Deep MD[2]
[1]UAMS, Little Rock, AR, USA. [2]UAB, Birmingham, AL, USA

Clinical History

A 53-year-old man with a history of hypertension presented to an outside hospital with three weeks of word-finding difficulty, blurred vision, memory deficits, right-sided weakness and numbness, gait disturbance, and 30-pound unintentional weight loss. Initial laboratory studies were unremarkable, and non-contrast CT head revealed an ill-defined intra-axial mass in the left basal ganglia with marked vasogenic edema and sulcal effacement, raising concern for high-grade neoplasm. He was transferred to our centre, where he was afebrile and vitally stable; complete blood count, complete metabolic profile, and urinalysis were normal. Neurologic examination showed right inferior quadrantanopia and mild dysarthria. MRI brain demonstrated lesions in the left thalamus and left frontal lobe, concerning for high grade neoplasm with differential being lymphoma and glioblastoma multiforme (GBM). A stealth-guided parietal lobule biopsy was performed without complication, yielding frothy, blood-containing material; frozen section suggested abscess. Broad-spectrum antibiotics were initiated. Toxoplasma IgG was markedly elevated (250) with negative IgM, while cryptococcal, histoplasma, and tuberculosis testing were negative, and ophthalmologic evaluation showed no retinitis. Final pathology demonstrated necrotic abscess with positive immunohistochemical staining for toxoplasma tachyzoites, confirming cerebral toxoplasmosis. He was treated with pyrimethamine, sulfadiazine, and leucovorin. He currently reports only mild headaches under neurology follow-up, and his HIV status is now well controlled with antiretroviral therapy.

Imaging Findings

There is a heterogeneous, predominantly peripherally enhancing in the left thalamus. The mass has some central T2 hypointensity. There is minimal peripheral associated restricted diffusion. There is extensive surrounding vasogenic edema, also extending into the left midbrain/pons. There is associated mass effect on the left lateral ventricle with a minimal rightward midline shift.
There is an additional focus of incomplete peripheral enhancement in the left frontal lobe. Perfusion
images demonstrate an area of signal void associated with the lesion.

Discussion

Neurotoxoplasmosis represents the most prevalent opportunistic CNS infection among HIV/AIDS patients who have progressed to advanced disease stages when their CD4 cell count reaches below 100 cells/μL. The United States has seen a substantial decrease in its prevalence because of antiretroviral therapy (ART) adoption yet cerebral toxoplasmosis continues to be a crucial consideration for doctors evaluating focal brain lesions in immunocompromised patients. The imaging differential for Atypical neurotoxoplasmosis is primary CNS lymphoma (PCNSL) and GBM. These conditions can have overlapping imaging features.
Neurotoxoplasmosis appears as multiple ring-enhancing lesions with surrounding vasogenic edema typically in the basal ganglia and corticomedullary junction when contrast-enhanced MRI is used. They may show the "eccentric target sign" (a small eccentric nodule within a ring-enhancing lesion on post-contrast T1 MRI) or the "concentric target sign" (alternating zones of hypo- and hyperintensity on T2-weighted MRI), which are more specific for toxoplasmosis.

Teaching Point

Our case highlights the diagnostic challenge when neurotoxoplasmosis presents as a solitary lesion mimicking primary brain malignancy, even in the ART era. Integration of epidemiologic risk factors, serologic data, advanced imaging findings, and therapeutic response remains the cornerstone of differentiation. Continued clinician awareness is essential, particularly in low-incidence settings where index of suspicion may be reduced.

References

1. Elsheikha HM, Marra CM, Zhu XQ. Epidemiology, Pathophysiology, Diagnosis, and Management of Cerebral Toxoplasmosis. Clin Microbiol Rev. 2020 Nov 25;34(1):e00115-19. doi: 10.1128/CMR.00115-19.
2. Wu J, Luo X, Huang N, Li Y, Luo Y. Misdiagnosis of HIV With Toxoplasmosis Encephalopathy With Progressive Memory Loss as the Initial Symptom: A Case Report. Front Neurol. 2022 Mar 15;13:809811. doi: 10.3389/fneur.2022.809811.
3. Alves D, Sobrosa P, Morais Passos R, Silva F, Ferreira A, Corga da Silva R, Silva D. Cerebral Toxoplasmosis Mimicking a Brain Neoplasm in an Inaugural HIV-Positive Patient: The Importance of Early Decision-Making and Background Assessment in the Emergency Department. *Cureus*. 2025 Jan 5;17(1):e76936. doi: 10.7759/cureus.76936.

Images/Tables

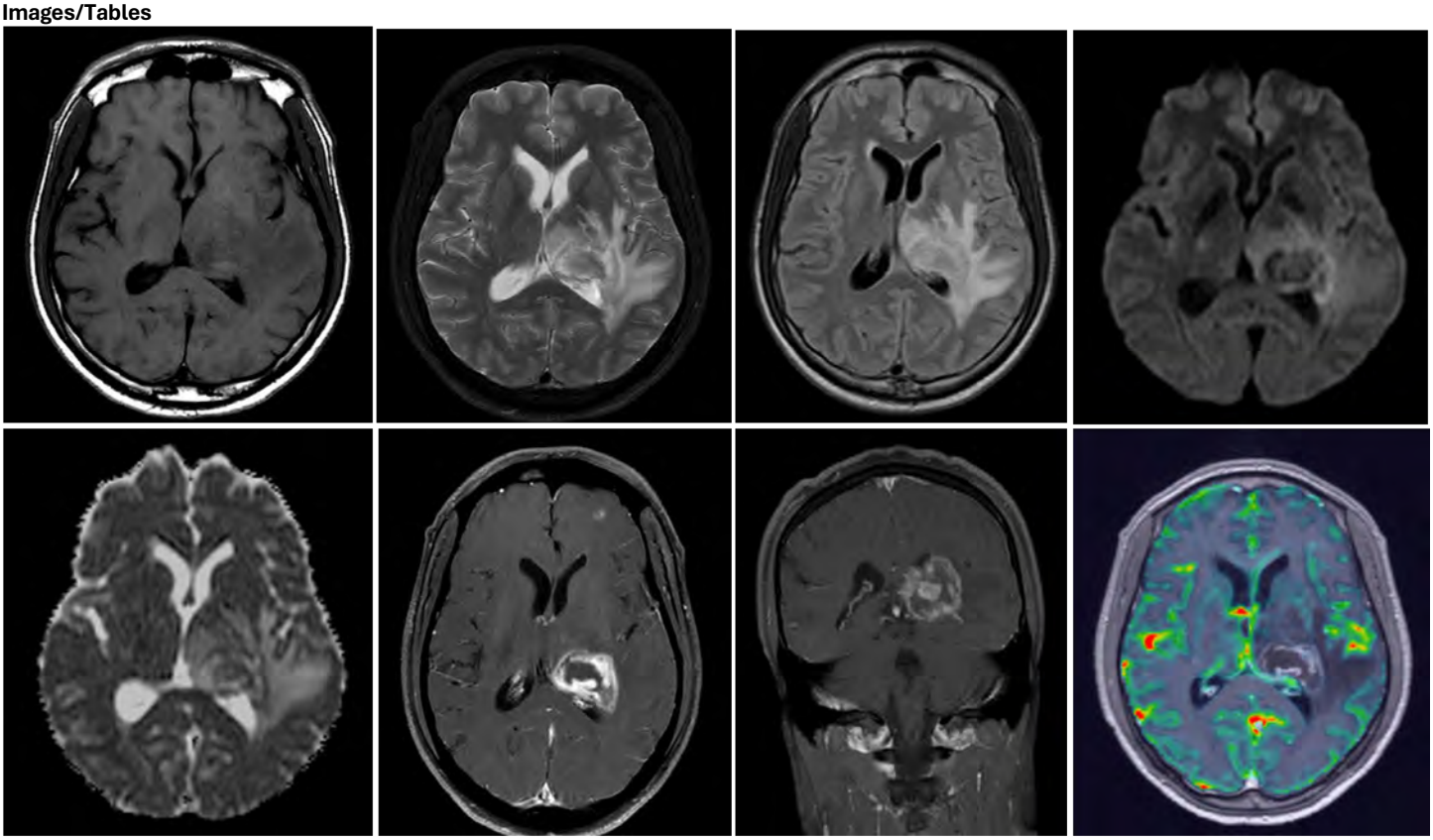

225 **Lhermitte–Duclos Disease Revealing Cowden Syndrome: Characteristic MRI Findings in a Rare Case**

Yarik Bezkor MD[1], Dhanush Amin MD[2], Marina Rodina MD[3], Lisa Godsey DO[1], Neda Wick MD[1], Desmin Milner MD[1]
[1]UAB, Birmingham, AL, USA. [2]UAMS, Little Rock, AR, USA. [3]RNIMU, Moscow, Moscow Region, Russian Federation

Clinical History

A 19-year-old Caucasian male with a past medical history of tonsillectomy presented with headache, neck and back pain, progressive gait instability, and acute vision loss, which eventually progressed to complete blindness. Physical examination was notable only for an elongated calvarium. Laboratory investigations were unremarkable, and vital signs were stable except for tachycardia. Neuroimaging revealed a posterior fossa mass with associated obstructive hydrocephalus.

The patient had a ventricular shunt placed, right sided craniotomy and successful surgical resection. The final pathology revealed dysplastic cerebellar gangliocytoma, which was also confirmed by genetic testing showing PTEN hamartoma tumor syndrome (Cowden syndrome). Patient underwent rehabilitation and physical therapy with significant improvement of symptoms.

Imaging Findings

CT of the head demonstrated thickened and irregular cerebellar folia involving the right cerebellar hemisphere, resulting in mass effect on the brainstem.

On MRI, the lesion exhibited T1 hypo-intensity, T2/FLAIR hyperintensity with thickened cerebellar folia and prominent striations. There was significant mass effect in the posterior fossa, compression of the brainstem, upward trans-tentorial herniation of the midbrain, downward herniation of the cerebellar tonsils and medulla, compression of the fourth ventricle. SWI sequence revealed prominent blood vessels. The lesion was non-diffusion restricting with T2 shine-through on ADC. On post-contrast images minimal enhancement was seen.

Discussion

Lhermitte-Duclos disease (LDD), also known as **dysplastic cerebellar gangliocytoma**, is a rare, cerebellar lesion of uncertain pathogenesis - debated to be neoplastic, malformative, or hamartomatous in nature. It carries an increased risk of malignancies, particularly of the breast, thyroid, and endometrium.

LDD is regarded as the neurologic manifestation of Cowden syndrome, and the combination of both conditions is referred to as the Cowden–Lhermitte-Duclos (COLD) syndrome.

The dysplastic hamartomatous mass grows slowly, initial treatment revolves around managing hydrocephalus. Surgical resection is the ultimate treatment of choice with only a few case reports of recurrence.

CT: Typically demonstrates a non-specific hypoattenuating cerebellar mass with striated appearance and occasional calcifications. Cystic components may be present.

MRI: LDD typically appears as a cerebellar lesion with hypo- to isointense signal on T1-weighted images, marked hyperintensity on T2/FLAIR, often demonstrating a striated, or tigroid appearance corresponding to widened cerebellar folia with preserved cortex. DWI/ADC usually shows T2 shine-through with high ADC values, indicating absence of true diffusion restriction, while SWI/T2* GRE demonstrates prominent linear veins coursing between thickened folia. On post-contrast T1, the lesion is generally non-enhancing or shows minimal enhancement along leptomeningeal or peripheral vascular structures. Perfusion MRI (PWI) may reveal increased relative cerebral blood volume (rCBV) and regional cerebral blood flow (rCBF), particularly in the molecular layer and leptomeninges, reflecting hypervascularity. MR spectroscopy (MRS) characteristically shows reduced N-acetylaspartate (NAA), choline, and myoinositol, variable lactate elevation.

Differential diagnosis includes but not limited to medulloblastoma, subacute cerebellar infarction, cerebellitis, tuberous sclerosis complex, ganglioglioma.

Teaching Point

Lhermitte–Duclos disease is a rare cerebellar lesion with striated folial enlargement on MRI, T1 hypointensity, T2 hyperintensity, minimal contrast enhancement, and characteristic folial veins on SWI/T2*. DWI, perfusion, and MRS aid in diagnosis and differentiation from other cerebellar lesions.

References

1. Klisch J, Juengling F, Spreer J et al. Lhermitte-Duclos Disease: Assessment with MR Imaging, Positron Emission Tomography, Single-Photon Emission CT, and MR Spectroscopy. AJNR Am J Neuroradiology. 2001;22(5):824-30.
2. Kulkantrakorn K, Awwad E, Levy B et al. MRI in Lhermitte-Duclos Disease. Neurology. 1997;48(3):725-31.
3. Awwad E, Levy E, Martin D, Merenda G. Atypical MR Appearance of Lhermitte-Duclos Disease with Contrast Enhancement. AJNR Am J Neuroradioly. 1995;16(8):1719-20.
4. Bayat MRH, Sarawan J. CT and MRI findings in Lhermitte-Duclos disease. (2005) SA Journal of Radiology.

Images/Tables

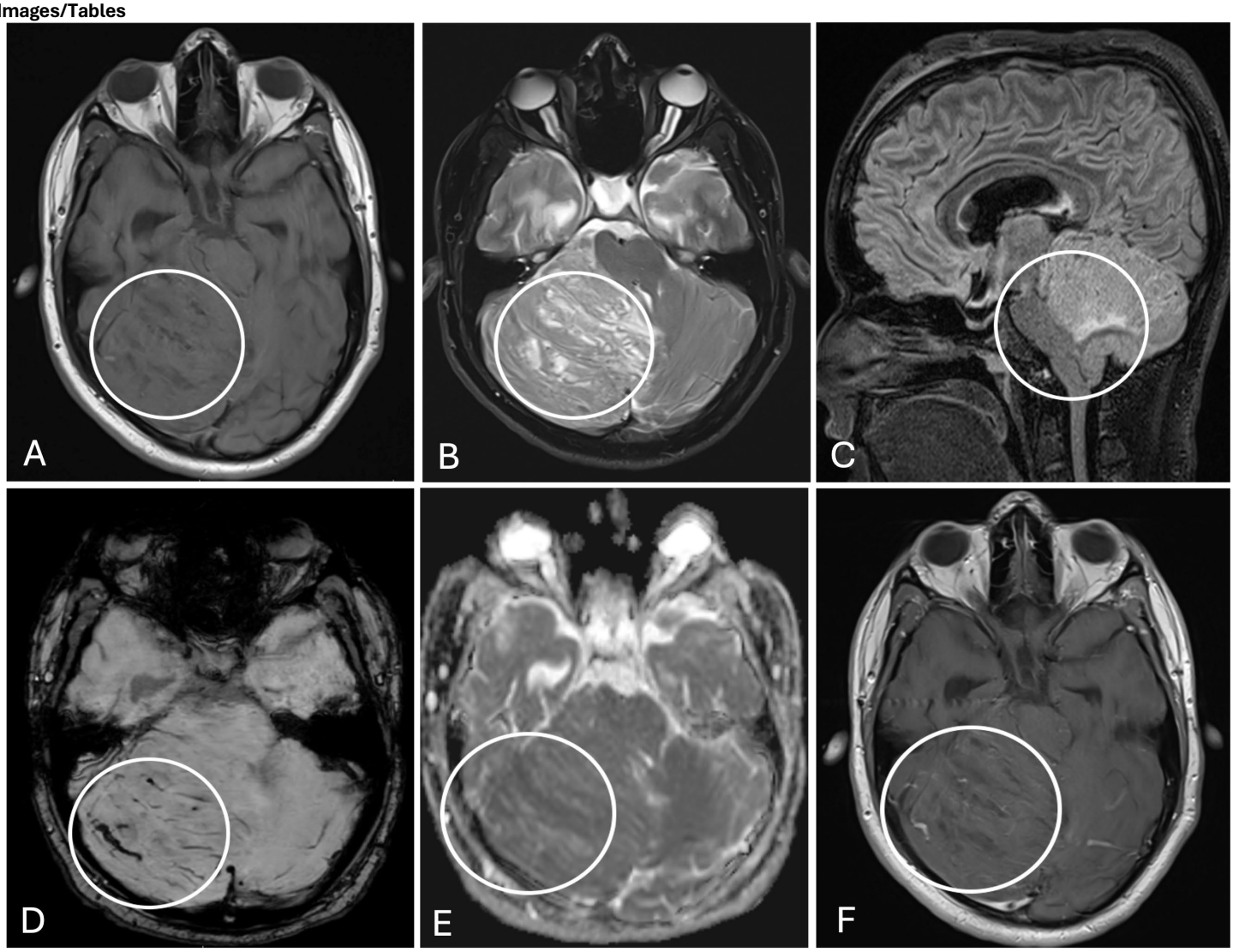

---

242 Beware of the Mimickers: Cardiac Myxoma Presenting as Cerebral Vasculopathy

Jose A. Bacalla MD[1], Jorge A. Lee Diaz MD[2]

[1]Instituto Nacional de Ciencias Neurologicas, Lima, Peru, Peru. [2]Le Bonheur Children's Hospital, Memphis, Tennesse, USA

Clinical History

A 29 -year-old female presented with 6-month history of psychiatric symptoms, right hemiparesis predominantly in the upper extremity, slurred speech and ataxia. No cardiovascular risk factors. Normal BP (110/60 mmHg). No fever or weight loss. General physical exam was unremarkable. CBC, platelets, renal function tests, liver function panel were normal. Nuclear antibodies were in the 1:80 range. ds-DNA, SS-A, SS-B, MPO and PR3 antibodies were negative. C3 complement level was normal. C Reactive protein was 2 mg/dL. Erythrocyte sedimentation rate was 36mm/hr. (N< 20 mm/hr.). Cardiolipin IgG and IgM were not reactive. Fibrinogen was in normal range. CSF Analysis was slightly xantochromic with scarce red blood fragments. Normal CSF cellularity and protein.

Imaging Findings

Fig. 1. Noncontrast CT: Loss of cortico-subcortical differentiation in the left middle, left inferior frontal gyrus and left insular cortex representing encephalomalacia.

Fig. 2. Hyperdense material in sulcal distribution in the right frontal region, most likely hemorrhagic sequela or calcium deposits.
Fig. 3. SWI demonstrated linear to nodular hemosiderin deposits following sulcal distribution in frontal, parietal and occipital lobes
Fig. 4. Axial FLAIR: Confirmed encephalomalacia in left frontal and insular lobes. Malacia in the inferior surface of the right cerebellar hemisphere. Signal alteration in the cortex adjacent to the right calcarine fissure, negative on DWI, indicative of chronic infarct
Fig. 5. DWI: Punctate foci of restricted diffusion in the right occipital lobe and left frontal lobe, likely representing acute infarction.
Fig. 6, Fig. 7 and Fig. 8. CT Angiography Head: Multiples areas of segmental narrowing followed by zones of dilated vessels (Siren tail morphology) in the frontal and parietal branches of the MCA.
Fig. 9 and Fig.10. CTA Angiography Chest: Lobulated hypodense mass in the left atrium in keeping with cardiac myxoma.

Discussion

Cardiac myxoma has been related to systemic rheumatologic symptoms and vasculitis-like phenomena in the central nervous system [1]. It is the most frequent cardiac tumor with 90% of cases presenting in the left atrium. Cardiac myxomas are linked to IL-6 production, which is related to fever, systemic symptoms and increase in the ESR [2]. It can present as connective tissue disease. Patients may present without or with cardiac symptoms (early diastolic tumor plop, mimicking mitral stenosis).

The vascular remodeling phenomena is linked to various theories including the infiltration of arterial muscular wall by myxoma cells[3]. Also, a theory states that chronic emboli lead to vascular remodeling. There have been reports of diagnosis delay for up to 1 year[4].

Teaching Point

When a patient presents unusual vascular changes in the cerebral arterial system, the work-up should be extensive including clinical examination , serological testing and vascular imaging studies, particularly echocardiography when an embolic source is suspected. Chest CT, Cardiac CT and MRI are useful but not always available. In this case, the initial diagnostic hypothesis was primary vs secondary cerebral vasculopathy. The vascular remodeling phenomena secondary to cardiac myxoma is not well understood but linked to infiltration of arterial muscular wall by myxoma cells or vascular remodeling secondary to chronic emboli.

References

1. AbuDujain NM, Alshoumar A, Alqahtani AM, Alshimemeri SA. Cardiac myxoma as a mimicker of cerebral vasculitis: a case report. Case Rep Neurol Med 2024; 2024:8675344 doi:10.1155/crnm/8675344.
2. El-Mhadi S, El Hajjaj B, Benatmane A, El Harrak M, Ahchouch S, Elktaibi A, et al. Cardiac myxoma and cerebral vasculitis: is there a link? Egypt Heart J 2024;76(1):61 doi:10.1186/s43044-024-00488-0.
3. Byrd WE, Matthews OP, Hunt RE. Left atrial myxoma presenting as a systemic vasculitis. Arthritis Rheum 1980;23(2):240–3 doi:10.1002/art.1780230216.
4. Moreno-Ariño M, Ortiz-Santamaria V, Deudero Infante A, Ayats Delgado M, Novell Teixidó F. A classic mimicker of systemic vasculitis. Reumatol Clin 2016;12(2):103–6 doi: 10.1016/j.reuma.2015.03.006.

Images/Tables

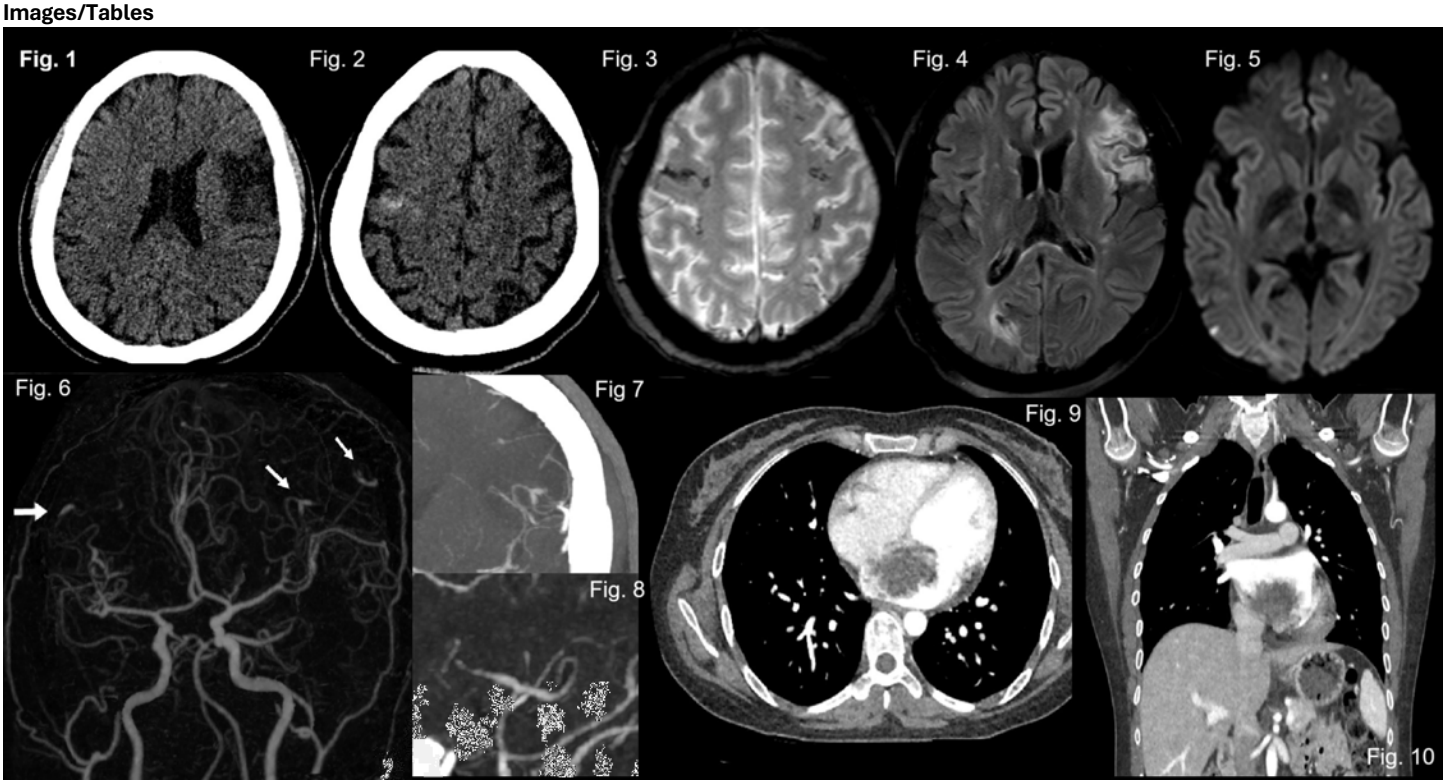

245 Rare Brachial Plexus Malignant Melanotic Nerve Sheath Tumor with Psammomatous Calcifications as the Presenting Feature of Carney Complex

Brendon Tillman MD, Daniel Boulter MD
The Ohio State University Wexner Medical Center, Columbus, OH, USA

Clinical History

A **32-year-old male** presented with a two-year history of progressive, debilitating **left shoulder and arm pain** that radiated to the elbow, wrist, and the last two fingers. Symptoms progressed to include **decreased grip strength, left arm atrophy**, left upper chest pressure, and left neck pain with

movement. The pain was worse when lying down or sitting, and movement offered mild relief. Conservative treatments provided no relief. Given the severity and progressive neurological signs, imaging was pursued, which revealed a large mass involving the cervical spine and brachial plexus.

Imaging Findings

MRI of the cervical spine demonstrates a large 7 cm cylindrical shaped well-defined, intradural extramedullary lesion centered in the left **C7-T1 neural foramen** with extension into the proximal **brachial plexus**. The lesion was notable for marked **T1-hyperintense and T2-hypointense signal** pattern, suggestive of melanin. The mass exerts mass effect on the adjacent thecal sac and compression of the exiting nerve roots. **CT of the cervical spine** confirmed smooth bony remodeling of the neural foramen and demonstrated **curvilinear and punctate laminated calcifications** within the mass. Subsequent abdominal imaging revealed a large, heterogeneously enhancing **right adrenal mass**.

Discussion

Surgical resection confirmed the diagnosis of a **malignant melanotic nerve sheath tumor (MMNST)**. Histopathological analysis demonstrated a heavily pigmented neoplasm exhibiting marked nuclear pleomorphism, nuclear pseudoinclusions, and scattered **psammomatous calcifications**. Immunohistochemical staining was positive for **Melan A, HMB45, and SOX10**, supporting the diagnosis.

The unusual presence of psammomatous calcifications within an MMNST, along with a large synchronous adrenal mass in a young patient, raised strong clinical suspicion for **Carney Complex**, which is a rare autosomal dominant syndrome associated with mutations in the **PRKAR1A** gene. MMNSTs in this context are particularly aggressive and mandate a multidisciplinary approach to management.

This case highlights the importance of early neuroimaging in cases of persistent radiculopathy, especially when accompanied by signs of muscle atrophy or progressive neurological decline.

While imaging plays a critical role in identifying lesion characteristics and guiding surgical planning, **definitive diagnosis relies on tissue biopsy and molecular profiling**. When feasible, **gross total resection** remains the cornerstone of treatment. However, due to the tumor's aggressive behavior and high rates of local recurrence and metastasis, **adjuvant therapy should be considered** in cases of subtotal resection or residual disease.

Long-term surveillance is essential, and this case reinforces the need for **increased awareness and early recognition** for MMNSTs, particularly those occurring in syndromic contexts such as Carney Complex.

Teaching Point

Malignant melanotic nerve sheath tumor (MMNST) should be included in the differential diagnosis of spinal or brachial plexus lesions demonstrating **intrinsic T1 hyperintensity and T2 hypointensity**, particularly in young patients.

The presence of a **T1 hyperintense spinal mass** with **laminated calcifications on CT**, in conjunction with lesions in other organs (e.g., an adrenal mass), is highly suggestive of **Carney Complex (CNC)**. This warrants prompt **genetic testing** and initiation of a **multidisciplinary oncologic surveillance plan**.

Radiologists play a critical role in identifying **additional features of CNC**, such as **cardiac myxomas** or **adrenal tumors** (e.g., **PPNAD**), as these findings significantly influence both **diagnosis** and **long-term management.**

References

1. Malignant Melanotic Nerve Sheath Tumor. Benson JC, Marais MD, Flanigan PM, et al. AJNR. American Journal of Neuroradiology. 2022;43(12):1696-1699. doi:10.3174/ajnr.A7691.
2. Malignant Melanotic Schwannian Tumor: A Clinicopathologic, Immunohistochemical, and Gene Expression Profiling Study of 40 Cases, With a Proposal for the Reclassification of "Melanotic Schwannoma". Torres-Mora J, Dry S, Li X, et al. The American Journal of Surgical Pathology. 2014;38(1):94-105. doi:10.1097/PAS.0b013e3182a0a150.
3. Diagnostic Pathology of Tumors of Peripheral Nerve. Belakhoua SM, Rodriguez FJ. Neurosurgery. 2021;88(3):443-456. doi:10.1093/neuros/nyab021.
4. MANAGEMENT OF ENDOCRINE DISEASE: Carney Complex: Clinical and Genetic Update 20 Years After the Identification of the CNC1 (PRKAR1A) Gene. Bouys L, Bertherat J. European Journal of Endocrinology. 2021;184(3):R99-R109. doi:10.1530/EJE-20-1120.
5. Pathology of Melanotic Schwannoma. Alexiev BA, Chou PM, Jennings LJ. Archives of Pathology & Laboratory Medicine. 2018;142(12):1517-1523. doi:10.5858/arpa.2017-0162-RA.

Images/Tables

MRI T1 Sag C-Spine

MRI STIR Sag C-Spine

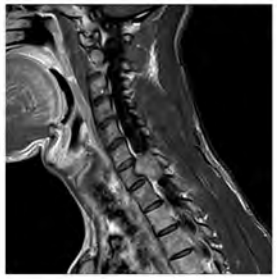

MRI T1 Post Sag C-Spine

MRI T2 Cor C-Spine

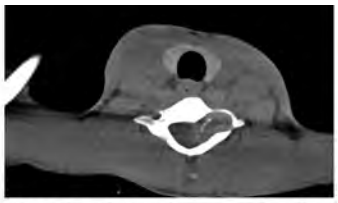

Ax CT C7 w/o – Soft Tiss

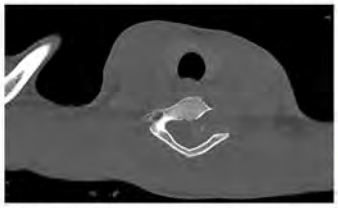

Ax CT C7 w/o – Bone

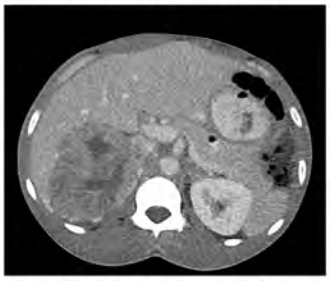

Ax CT Abdomen w/ con

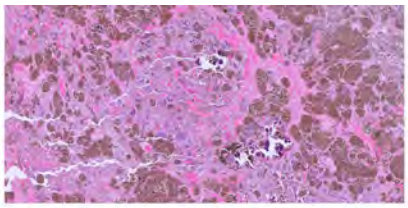

H&E IHC staining 20x

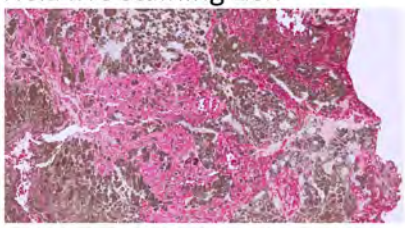

HMB45 red IHC staining 10x

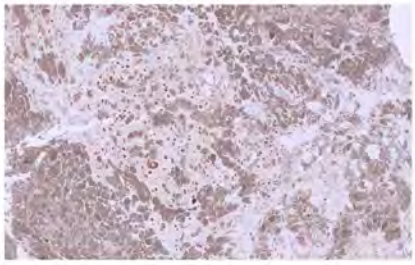

SOX10 IHC staining 10x

---

247 Recognizing Caudal Regression Syndrome in Adulthood: MRI and CT Correlation

Caleb Cummings BS[1], Katie C Bailey MD[2]

[1]USF Health Morsani College of Medicine, Tampa, FL, USA. [2]University of South Florida College of Medicine, James Haley VA Hospital, Tampa, FL, USA

Clinical History

A 36-year-old man presented with chronic low back and flank pain and no known history of trauma.

Imaging Findings

Sagittal T2-weighted MRI demonstrated a rounded, abrupt termination of the conus medullaris at the T12 vertebral level (arrow in Exhibit A and Exhibit B), rather than a typically seen tapering morphology. Sagittal CT and lateral X-ray revealed a shortened sacrum and an absent coccyx (arrow in Exhibit C and Exhibit D). A combination of these features is highly suggestive of caudal regression syndrome. No presacral mass, vertebral segmentation, open defect or posterior spinal cord protrusion were identified.

Discussion

Caudal regression syndrome is a rare congenital abnormality involving varying degrees of sacral and lower spinal agenesis in addition to a high termination of the spinal cord. The incidence of caudal regression syndrome is 1-3 of every 100,000 live births, but the risk rises dramatically in infants of diabetic mothers (1 in 350)[1]. While milder cases may rarely remain asymptomatic until adulthood, the majority of cases of caudal regression syndrome are diagnosed in infancy, often with more severe abnormalities like paraplegia, neurogenic bladder, and anorectal malformations[2]. Other potential complications include clubfeet, hip dislocations, and underdeveloped legs. Adult diagnosis, as in this case, generally reflects less extensive anatomic defects.

MRI is the imaging modality of choice for investigating spinal cord morphology and level of termination, while CT is superior for analyzing sacral and coccygeal anatomy. Differential diagnoses include Currarino syndrome, which features a presacral mass and partial sacral agenesis[3]; spinal dysraphism, typically characterized by an open neural tube defect[4]; sacrococcygeal teratoma, identified by a heterogeneous presacral mass; and VACTERL association, which includes cardiac, renal, and limb anomalies beyond the caudal spine[5]. Recognizing these imaging distinctions is essential for accurate diagnosis and guiding management.

Teaching Point

Caudal regression syndrome most commonly presents in infancy, however, milder cases rarely present in adulthood. Maternal diabetes is a significant risk factor. Imaging findings—specifically a high, rounded (rather than tapered) conus medullaris above L1 with sacral agenesis and absent coccyx—are characteristic. MRI defines neural involvement, while CT confirms bony abnormalities. Familiarity with its imaging appearance and differentiation from related congenital anomalies is vital for accurate radiologic interpretation.

References

1. Kylat RI, Bader M. Caudal Regression Syndrome. *Children (Basel)* 2020;7(11):211. DOI: https://doi.org/10.3390/children7110211
2. Jeelani Y, Mosich GM, McComb JG. Closed neural tube defects in children with caudal regression. *Childs Nerv Syst* 2013;29(9):1451-1457. https://doi.org/10.1007/s00381-013-2119-3
3. Lee SC, Chun YS, Jung SE et al. Currarino triad: anorectal malformation, sacral bony abnormality, and presacral mass--a review of 11 cases. *J Pediatr Surg* 1997;32(1):58-61. https://doi.org/10.1016/s0022-3468(97)90094-4
4. Tortori-Donati P, Rossi A, Cama A. Spinal dysraphism: a review of neuroradiological features with embryological correlations and proposal for a new classification. *Neuroradiology* 2000;42(7):471-491. https://doi.org/10.1007/s002340000325

5. Solomon BD, Patel A, Cheung SW, Pineda-Alvarez DE. VACTERL association and mitochondrial dysfunction. *Birth Defects Res A Clin Mol Teratol* 2011;91(3):192-194. https://doi.org/10.1002/bdra.20768

Images/Tables

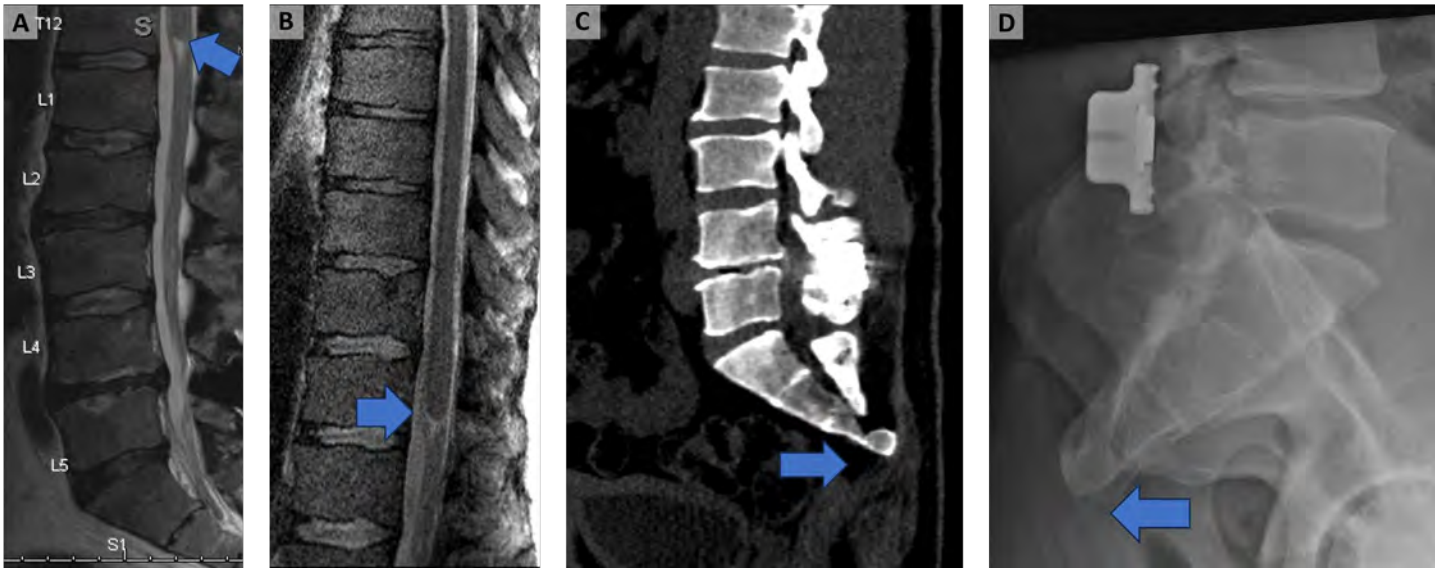

260 When the Spine Vanishes: Gorham Disease as a Rare Cause of Juvenile Levoscoliosis

Kamand Khalaj MD, MPH[1], Kasra Rahbar MD[2]

[1]UTHealth Houston, Houston, Texas, USA. [2]Baylor College of Medicine, Houston, Texas, USA

Clinical History

A 12-year-old female presented with progressive back pain and deformity. Physical examination revealed severe angular thoracolumbar levoscoliosis. There was no history of trauma, infection, or metabolic disorder. Laboratory results were within normal limits.

Imaging Findings

Radiographs and CT of the spine demonstrated severe angular kyphoscoliosis with near-complete resorption of multiple vertebral bodies and diffuse osseous rarefaction. A key finding was the absence of periosteal reaction or an associated soft-tissue mass. MRI revealed T1 and T2 hyperintense bone marrow replacement and bilateral pleural effusions. The differential based on imaging included aggressive metabolic bone disease, chronic infection (e.g., tuberculosis), and malignancy.

Discussion

Unlike the more common idiopathic dextroscoliosis, thoracolumbar levoscoliosis in a juvenile often signifies an underlying pathologic process, warranting advanced imaging. The imaging findings prompted surgical intervention for both stabilization and diagnosis. Intraoperatively, cloudy chylous fluid was encountered emanating from the spinal canal. Histopathology demonstrated numerous dilated, benign lymphovascular channels within bone, massive osteolysis, and a complete absence of osteoblastic activity, pathognomonic for Gorham disease (vanishing bone disease). This rare disorder is characterized by progressive osteolysis driven by intraosseous vascular/lymphatic proliferation and cytokine-mediated osteoclastic activity. The imaging hallmarks are progressive bone dissolution without periosteal reaction or sclerosis, as demonstrated in this case. The presence of pleural effusions and chylous leakage further supported the diagnosis.

Teaching Point

While Gorham disease is rare and spinal involvement is particularly unusual, it should be included in the differential diagnosis of progressive vertebral osteolysis, especially when imaging reveals "vanishing" bones in the absence of periosteal reaction or a soft-tissue mass. The constellation of severe levoscoliosis, pleural effusions, and chylous leakage provides highly suggestive diagnostic clues.

References

1. Sekharappa V, Arockiaraj J, Amritanand R, Krishnan V, David KS, David SG. Gorham's Disease of Spine. Asian Spine J. 2013 Sep;7(3):242-7. doi: 10.4184/asj.2013.7.3.242. Epub 2013 Sep 4. PMID: 24066223; PMCID: PMC3779779.

2. Nikolaou VS, Chytas D, Korres D, Efstathopoulos N. Vanishing bone disease (Gorham-Stout syndrome): A review of a rare entity. World J Orthop. 2014 Nov 18;5(5):694-8. doi: 10.5312/wjo.v5.i5.694. PMID: 25405099; PMCID: PMC4133478.

Images/Tables

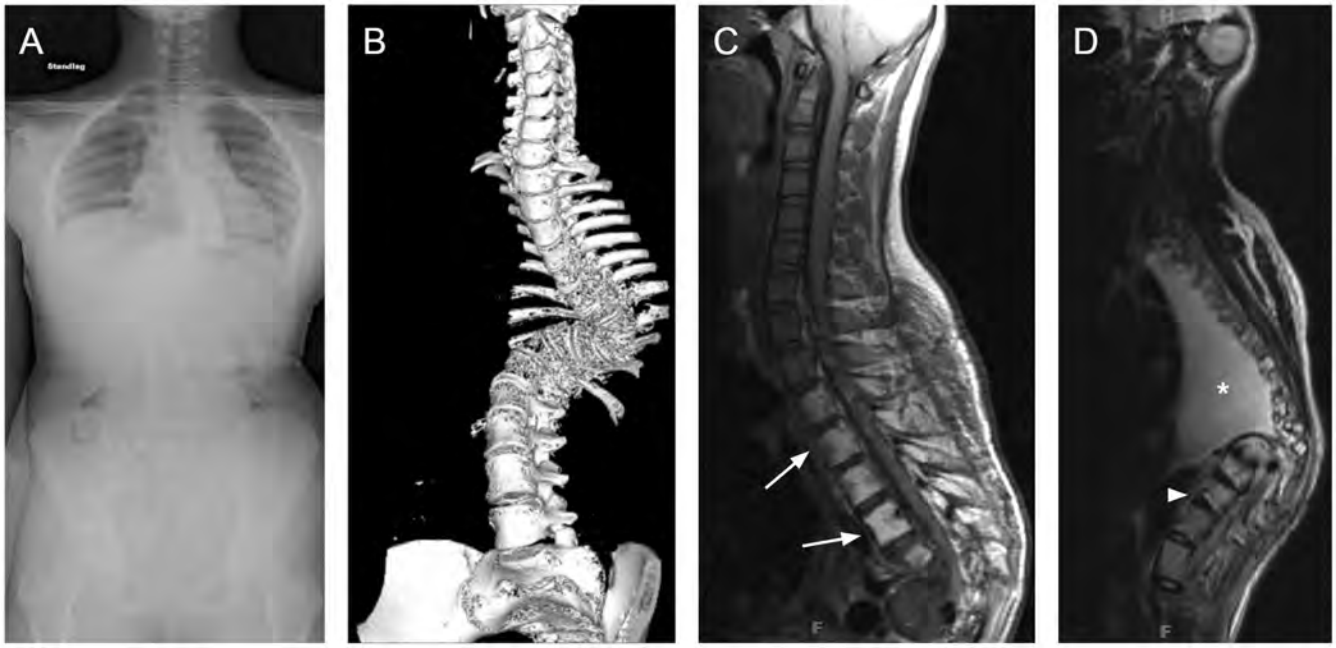

Imaging findings of Gorham disease in a 12-year-old female with progressive thoracolumbar levoscoliosis. (A) Standing AP radiograph demonstrates severe angular thoracic levoscoliosis. (B) 3D CT reconstruction reveals extensive osteolysis and near-complete resorption of vertebral bodies from T3 to L3. (C) Sagittal T1-weighted and (D) T2-weighted MR images show corresponding T1 and T2 hyperintense bone marrow replacement (arrows and arrowheads, respectively). A large pleural effusion is also noted (*).

---

266 Chondroid Synoviocytic Neoplasm

Hallie Whalen MD[1], Arzu Ozturk MD[1], Elham Tavakkol MD[1], H. Kader Karli Oguz MD[1], Lotfi Hacein-Bey MD[2], Osama Raslan MD[1]
[1]UC Davis Medical Center, Sacramento, CA, USA. [2]Stanford Medicine, Palo Alto, CA, USA

Clinical History

A 23 year old female with a history of asthma presented with left preauricular region swelling that was slowly progressive over a 2-year period. No pain or other associated symptoms were present until one week ago when she developed a clicking sound in her ear and muffled hearing.

Imaging Findings

Ultrasound showed a complex solid mass in the preauricular region. Contrast enhanced MRI demonstrated a lobulated circumscribed mass centered with the left temporal bone with enhancement and heterogenous T2 signal (including areas of marked T2 hypointensity). The mass involved the tympanic, squamosal, and mastoid portions of the temporal bone and extended into the left temporomandibular joint space and parotid gland. Erosion of the inner table of the calvarium with intracranial extension of the tumor and mass effect on the left temporal lobe was present. The mass involved the external auditory canal and abutted the middle ear cavity with a resulting left mastoid effusion. CT Temporal Bone showed osseous expansion and sclerosis of the temporal calvarium, roof of the temporomandibular joint, the external auditory canal, and the middle ear cavity. A soft tissue component extended into the superior external auditory canal and middle ear cavity, encasing the ossicles.

Discussion

Ultrasound-guided biopsy of the mass was performed, which showed a rare entity consistent with Chondroid Synioviocytic Neoplasm (CSN). CSN is a newly described, rare, and distinct synovial tumor entity, which resembles tenosynovial giant cell tumors (TGCT) but additionally is capable of forming a chondroid matrix. To the best of our knowledge, only 21 cases have been reported in the literature to date. These tumors show a mix of synoviocytes (mononuclear, eosinophilic), with other cell types (small histiocytes, macrophages, osteoclast-like giant cells), and chondroid matrix. Compared with TGCT, this tumor shows a mixed T2 signal on MRI (reflecting both cartilaginous and hemosiderin components) and patchy enhancement, rather than the predominantly low T2 signal and diffuse enhancement of TGCT. Current limited knowledge of these rare tumors reveals a median age of presentation around 50 years of age with no gender predilection. Although most of the lesions showed involvement of the TMJ (16/21 patients), these tumors appear largely centered with the adjacent temporal bone with preservation of the mandibular condyle, and therefore primary bone tumors are usually the main differential diagnosis based on imaging. Bony expansion and sclerosis can help distinguish these tumors from chondrosarcomas which shows more erosive changes. While these tumors can be locally aggressive and cause osseous destruction of the skull base and inner ear, there are no reported cases of distant metastasis.

Teaching Point

CSNs are rare, distinct, and newly described synovial tumors that are most commonly found in the temporal bone adjacent to the temporal mandibular joint, and therefore neuroradiologists should be aware of this entity. The imaging features of this tumor are distinct from other tumors which may be included in the differential diagnosis. Accurately guiding the imaging work-up of these locally aggressive tumors, which can involve the skull base, inner ear, and have intracranial extension, is an important part of the evaluation.

References

EKao EY, Ardic F, Fadra N, et al. Chondroid Synoviocytic Neoplasm: A Clinicopathologic, Immunohistochemical, and Molecular Genetic Study of a Distinctive Tumor of Synoviocytes. Modern Pathology. 2024 37(11): 100598. https://doi.org/10.1016/j.modpat.2024.100598.

Images/Tables

267 Bilateral Corticospinal Tract Signal Abnormalities in Niemann-Pick Type C: A Unique Imaging Presentation

Spencer Waldman MD, Yehuda Herman MD, Paul K. Lee MD
Department of Radiology, Zucker School of Medicine at Hofstra/Northwell, New Hyde Park, New York, USA

Clinical History

A 33-year-old woman with a past medical history of ADHD, presented with one week of progressive generalized weakness, headache, lightheadedness, and cognitive slowing.

Imaging Findings

MRI demonstrated restricted diffusion along portions of the bilateral corticospinal tracts, extending from the internal capsules to the subcortical white matter regions, with corresponding FLAIR hyperintensity and atrophy of the medial postcentral gyri. The corpus callosum splenium exhibited hyperintensity and volume loss without restricted diffusion (Figure 1). No abnormal enhancement, hemorrhage, or hydrocephalus was identified. Genetic testing confirmed Niemann-Pick disease type C.

Figure 1. Clockwise from the left: Axial DWI and ADC maps demonstrating bilateral symmetric restricted diffusion along the corticospinal tracts. Axial FLAIR depicting splenial hyperintensity and thinning of the corpus callosum. Axial FLAIR showing hyperintense white matter and atrophy of the medial postcentral gyri.

Discussion

Niemann-Pick Type C (NPC) results from NPC1 or NPC2 mutations, leading to accumulation of unesterified cholesterol and sphingolipids within neurons.[1] While brain MRI findings are usually unremarkable in the early phases of the disease, advanced stages are characterized by specific abnormalities. These include marked atrophy of the superior and anterior cerebellar vermis, thinning of the corpus callosum, and mild cerebral atrophy. Additionally, increased signal intensity in the parietal white matter, secondary to demyelination, can be seen. Recognizing this pattern enables radiologists to prompt timely metabolic and genetic testing. Given the unique imaging findings in out patient, NPC should be considered in young adults presenting with subacute encephalopathy and symmetric corticospinal tract involvement.

Teaching Point

- NPC can present with symmetric corticospinal tract diffusion restriction and FLAIR hyperintensity—an uncommon but important imaging manifestation.
- Associated MRI findings may include medial postcentral gyrus atrophy and corpus callosum splenium hyperintensity/volume loss without restricted diffusion.
- Consider NPC in young adults presenting with subacute encephalopathy and bilateral corticospinal tract involvement.
- Recognizing atypical MRI patterns can prompt timely metabolic and genetic testing and improve diagnostic yield.

References

1. Adhikari P, Jain S, Gupta S, et al. Hereditary Spastic Paraplegia Overview. In: Adam MP, Feldman J, Mirzaa GM, et al., editors. GeneReviews®. Seattle (WA): University of Washington, Seattle; 2022 Oct 20. Accessed 10/12, 2025. https://www.ncbi.nlm.nih.gov/books/NBK1296/.
2. Grau AJ, Brandt T, Weisbrod M, Niethammer R, Forsting M, Cantz M, Vanier MT, Harzer K. Adult Niemann-Pick disease type C mimicking features of multiple sclerosis. J Neurol Neurosurg Psychiatry. 1997;63:552. [PMC free article] [PubMed] [Reference list]

Images/Tables

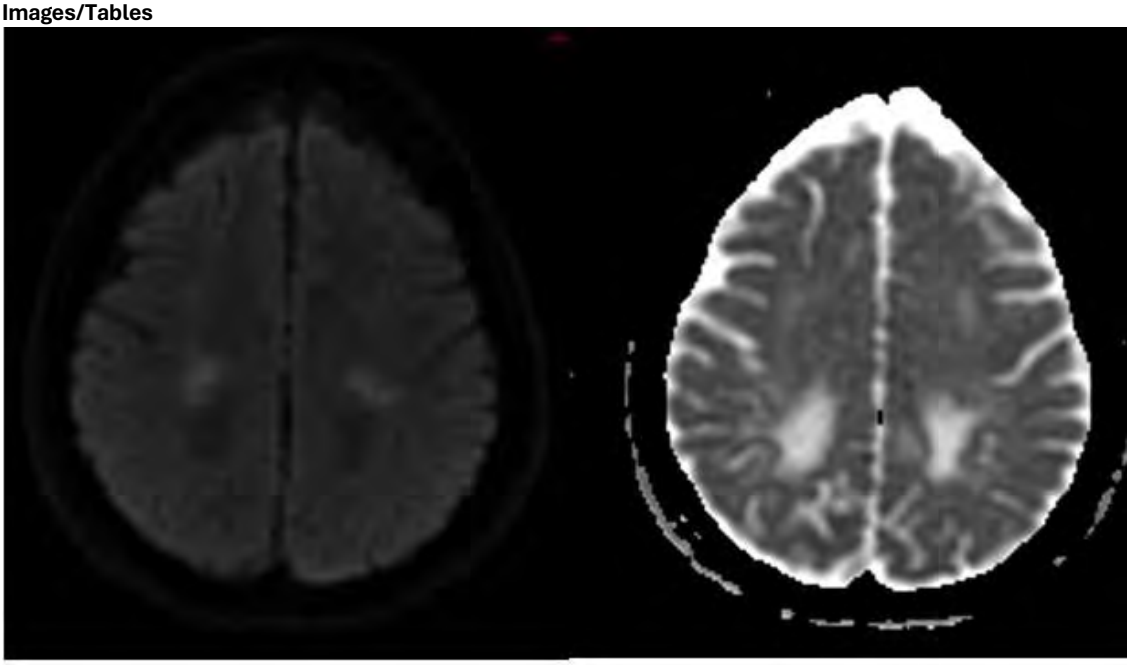

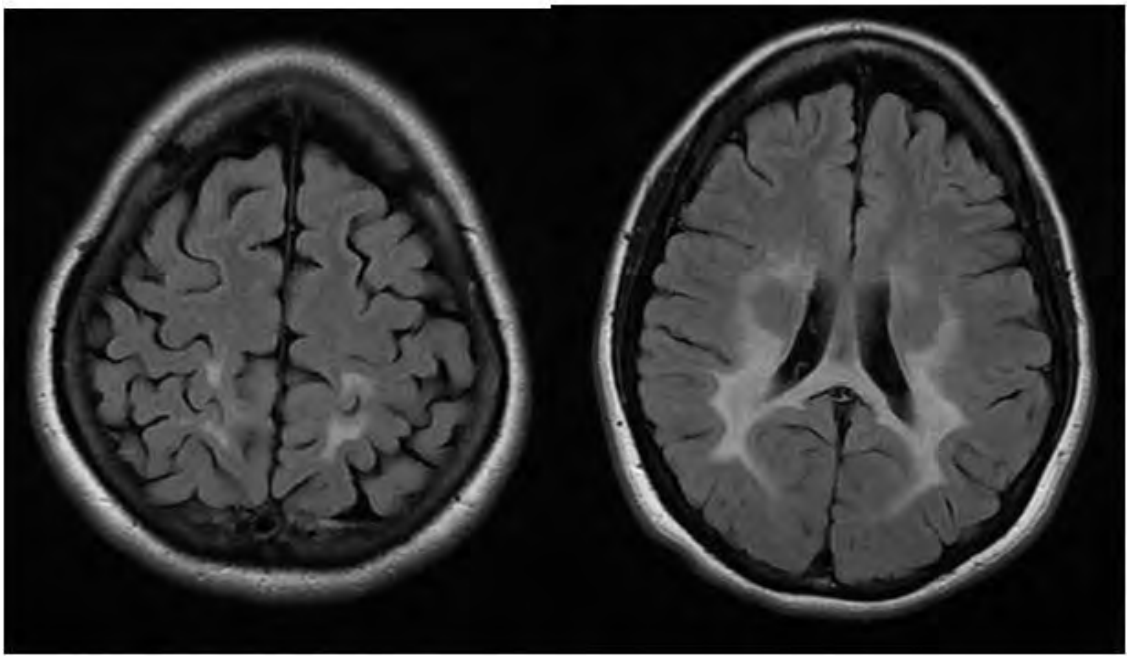

270 It's Not Un-nose-ual: The Challenging Diagnostic Journey of an Olfactory Neuroblastoma

Prerana Ramesh BS[1], Carolina Soto-Davila MD[2], Octavio Arevalo-Espejo MD[2]
[1]LSUHS SOM, Shreveport, LA, USA. [2]LSUHS, Shreveport, LA, USA

Clinical History

A 75-year-old male patient was referred to our institution for evaluation of a nasal mass that was initially identified as an allergic polyp on outside pathology. This patient presented with a 9-month history of recurrent sinus infections, nasal congestion and purulent rhinorrhea. He denied any other associated symptoms including pain, focal weakness, vision or sensory changes, headaches, unintentional weight loss, nausea or vomiting. The patient had no known history of prior malignancies or radiation exposure. Outside PET-CT and MRI images were reviewed and repeated. Repeat biopsy with rigid nasal endoscopy identified this mass as a Hyams grade 2 olfactory neuroblastoma.

Imaging Findings

Non-contrast CT (NCCT) of the paranasal sinuses showed a densely calcified mass centered at the right fovea ethmoidalis, resulting in significant mass effect upon the adjacent orbit.

MRI of the brain, face, and orbits revealed an extensive soft tissue component of the mass involving the upper nasal cavity, bilateral ethmoid air cells, and within the right orbit, along with an intracranial cystic component and associated leptomeningeal enhancement. The soft tissue component of the tumor demonstrated restricted diffusion, indicative of hypercellularity.

FDG PET-CT images showed avid radiotracer uptake within the mass as well as a metastatic lymph node located at the right lateral retropharyngeal space.

Discussion

Olfactory neuroblastomas, also called Esthesioneuroblastomas, are slow-growing intranasal malignancies that present with nonspecific sinonasal symptoms with no predisposition to age or sex. Due to their uncommon incidence, accounting for ~3-6% of reported nasal and paranasal tumors, as well as difficulty in identification based on image findings alone, the diagnosis of olfactory neuroblastomas may be delayed. As these tumors are prone to invading its surrounding structures and metastasizing to cervical lymph nodes, early detection and management are essential to ensuring good prognosis for an affected patient. Our patient will be undergoing neoadjuvant chemotherapy followed by surgery and adjuvant radiation therapy.

Teaching Point

Olfactory neuroblastomas should be included in the differentials for nasal tumors as a delay in diagnosis and the presence of distant metastases are factors that significantly affect patient prognosis. A multi-modal diagnostic and management approach is required towards this end.

References

1. Barinsky GL, Azmy MC, Kilic S et al. Comparison of open and endoscopic approaches in the resection of esthesioneuroblastoma. *Ann Otol Rhinol Laryngol* 2021; 130(2):136-141. DOI: https://doi.org/10.1177/0003489420939582
2. Fiani B, Quadri SA, Cathel A, et al. Esthesioneuroblastoma: a comprehensive review of diagnosis, management, and current treatment options. *World neurosurg* 2019; 126, 194–211. DOI: https://doi.org/10.1016/j.wneu.2019.03.014
3. Lo Casto A, Lorusso F, Palizzolo E, et al. Uncommon nasal mass presentation: a radiological case series. *J Pers Med*, 2024;14(12), 1145. DOI: https://doi.org/10.3390/jpm14121145
4. Okafor S, AlShammari S, Helou V, et al. Olfactory neuroblastoma. *Mini-invasive Surg*. 2024;8:28. DOI: http://dx.doi.org/10.20517/2574-1225.2023.128
5. Rao KR, Upadhya IB. A review on esthesioneuroblastoma. *Indian J Otolaryngol Head Neck Surg* 2022;74(Suppl 2):1584–1590. DOI: https://doi.org/10.1007/s12070-021-02726-2

Images/Tables

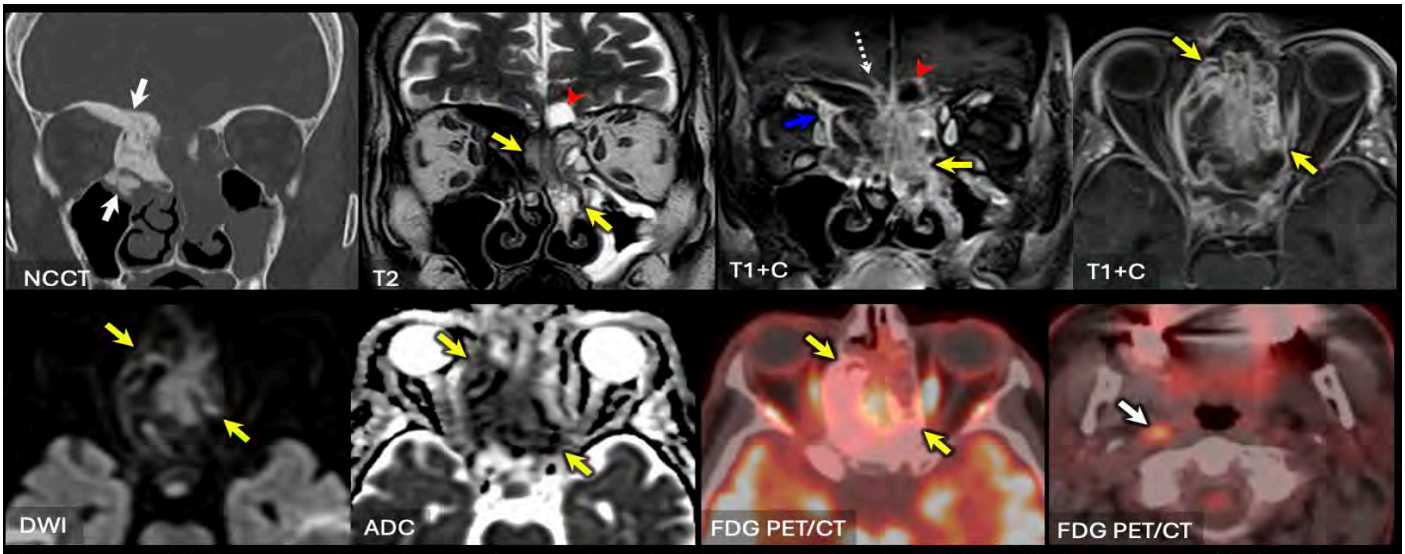

Non-contrast CT of the paranasal sinuses shows a densely calcified mass centered at the right fovea ethmoidalis with significant mass effect upon the adjacent orbit. MRI of the orbits shows extensive soft tissue component of the mass that involves the upper nasal cavity, and bilateral ethmoid air cells (yellow arrows, T2 and T1+Contrast), the soft tissue component within the right orbit (blue arrow, coronal T1+Contrast), the intracranial cystic component (red arrowhead, T2 and T1+Contrast), and associated leptomeningeal enhancement (dotted arrow, coronal T1+C). The soft tissue component of the tumor demonstrates restricted diffusion (yellow arrows, DWI and ADC). FDG PET-CT images show avid radiotracer uptake within the mass (yellow arrows) and a metastatic lymph node at the right lateral retropharyngeal space (white arrow).

---

277 Infantile Hemiconvulsion-Hemiplegia-Epilepsy Syndrome: Acute Unilateral Cerebral Edema Following a Febrile Hemiconvulsive Seizure in a Child with VP Shunt

Salim Gnabode MD, MS[1], James B Allison MD[2], Steven W Farrarher MD[2]
[1]Maine Medical Center, Portland, ME, USA. [2]Spectrum Radiology, Portland, ME, USA

Clinical History

A 5-year-old female with a history of grade III intraventricular hemorrhage and ventriculoperitoneal (VP) shunt placement presented after a 5-minute left-sided seizure during a febrile illness. Initial CT was unremarkable. MRI (Figure 1) showed some subtle findings that were initially attributed to artifact related to VP shunt/anesthesia.

Within 48 hours, she developed progressive left hemiplegia. Emergent noncontract CT (Figure 2) demonstrated massive right hemispheric edema with midline shift. The patient underwent emergent right hemicraniectomy and external ventricular drain (EVD) placement.

Postoperative MRI (Figure 3) showed diffuse right hemispheric cortical and subcortical T2 hyperintensity with restricted diffusion and no enhancement. The pattern was atypical for infarct, given relative cortical sparing and predominant subcortical diffusion restriction. Acute Rasmussen encephalitis was initially considered. Black-blood vessel-wall imaging and CTA/CTV revealed no vascular abnormality. CSF and infectious/autoimmune studies were negative. Given acute cytotoxic hemispheric edema after prolonged febrile hemiconvulsion and persistent hemiplegia, neurology diagnosed Infantile Hemiconvulsion-Hemiplegia-Epilepsy (IHHE) syndrome.

Imaging Findings

Figure 1: High b-value DWI (a) shows subtle diffuse increased signal in the right hemisphere, with shunt-related artifact in the right parietal lobe. Post-contrast 3D T1 (b) demonstrates mild sulcal vascular prominence. Axial T2 FLAIR (c) shows incomplete sulcal CSF suppression, though this was initially uncertain due to shunt artifact/exam being performed under anesthesia.

Figure 2: Axial noncontrast CT shows diffuse right hemispheric cytotoxic edema with sulcal effacement, mass effect, and 1 cm leftward midline shift. The VP shunt remains stable.

Figure 3: DWI/ADC maps demonstrate diffuse right hemispheric subcortical restricted diffusion (a, b). T2 FLAIR shows cortical edema (c). Prominent sulcal vasculature is present without parenchymal enhancement (d).

Discussion

Infantile Hemiconvulsion-Hemiplegia-Epilepsy (IHHE) is a rare postictal encephalopathy in children under 4, characterized by prolonged febrile focal seizures followed by acute ipsilateral hemiplegia. It is a diagnosis of exclusion. Acute MRI shows diffuse hemispheric cytotoxic edema with subcortical restricted diffusion not confined to a vascular territory. Over time, progressive cerebral hemiatrophy develops. Neuroimaging is key to confirming the pattern and distinguishing IHHE from conditions such as Rasmussen encephalitis.

Teaching Point

The temporal progression from febrile hemiconvulsion to delayed unilateral cytotoxic edema is characteristic of IHHE syndrome. Early recognition of this pattern is crucial, as prompt management of cerebral edema may be lifesaving. Artifact from the patient's VP shunt caused image degradation, making interpretation of the initial examination challenging. However, even without this confounding artifact, the early imaging findings were subtle.

In IHHE, unilateral hemispheric swelling during status epilepticus begins with subcortical white matter edema, followed by cortical involvement and eventual hemiatrophy. MRI typically shows diffusion restriction within a cerebral hemisphere, without vascular correlation and with normal MR angiography.

IHHE presents abruptly after a prolonged febrile seizure and is monophasic, whereas Rasmussen encephalitis evolves insidiously with progressive focal seizures and chronic inflammation-driven cortical atrophy.

References

1. Shields WD. Hemiconvulsion-hemiplegia-epilepsy syndrome. MedLink Neurology. Updated May 2025. Available at: https://www.medlink.com/articles/hemiconvulsion-hemiplegia-epilepsy-syndrome. Accessed October 27, 2025.
2. Tenney JR, Schapiro MB. Child neurology: Hemiconvulsion-hemiplegia-epilepsy syndrome. Neurology. 2012;79(1):e1–e4. doi:10.1212/WNL.0b013e31825dce5f.
3. Auvin S, Bellavoine V, Merdariu D, Delanoë C, Elmaleh-Bergés M, Gressens P, Boespflug-Tanguy O. Hemiconvulsion-hemiplegia-epilepsy syndrome: Current understandings. *Eur J Paediatr Neurol.* 2012;16(5):413-421. doi:10.1016/j.ejpn.2012.01.007.

Images/Tables

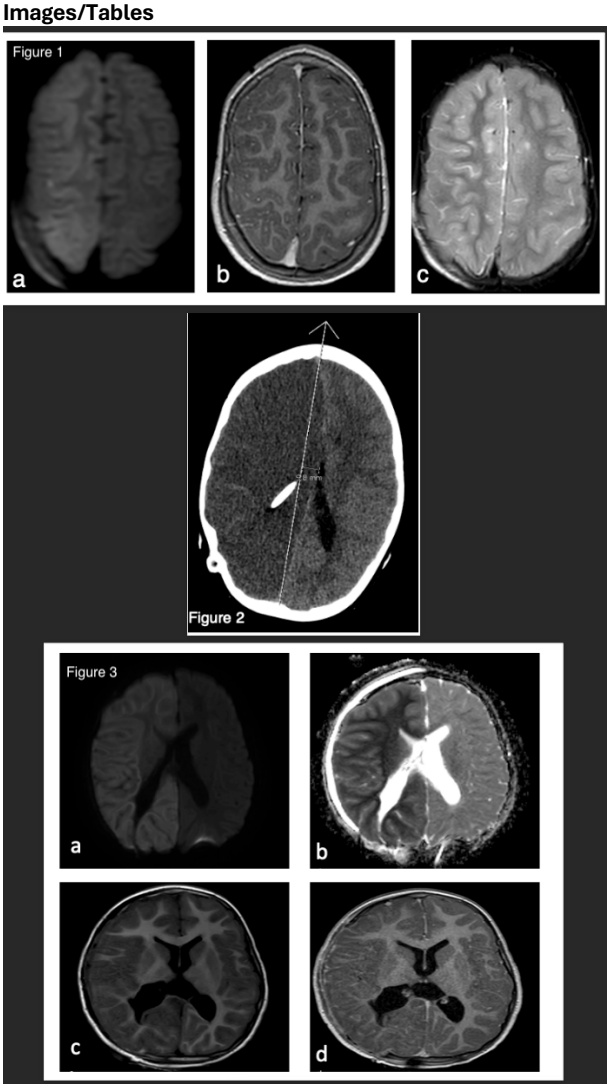

286 A diagnosis of extrusion: Presumed fibrocartilaginous embolism resulting in spinal cord infarct in 8-year-old female – A Case Report

Jay Kakadiya MD[1], Dhairya A. Lakhni MD[2], Siddhartha Gaddamanugu MD[1], Fabricio G. Goncalves MD[3], Alexander J Mullen MD[1]
[1]The University of Alabama at Birmingham, Birmingham, AL, USA. [2]West Virginia University, Morgantown, WV, USA. [3]Children's Hospital of Alabama, Birmingham, AL, USA

Clinical History

An 8-year-old previously healthy girl presented with hyperacute, progressive weakness of all four limbs following severe back pain and distal paresthesias. Symptoms began upon waking and progressed to complete inability to stand within four hours. She also developed transient urinary and fecal incontinence. There was no history of trauma, recent vaccination, or infection aside from streptococcal pharyngitis one month earlier.
Neurological examination revealed distal-predominant quadriparesis, loss of lower limb reflexes, and a T4 sensory level.
Comprehensive laboratory workup, including inflammatory markers, vitamin B12, and autoimmune and infectious panels (MOG-IgG, AQP4-IgG, viral PCR), was unremarkable. Cerebrospinal fluid analysis was normal, with no pleocytosis or oligoclonal bands.

Imaging Findings

MRI of the spine demonstrated longitudinally extensive, symmetric T2 hyperintensity involving the ventral gray matter of the spinal cord from C5 to T8 with diffusion restriction, consistent with acute ischemia. The axial T2-weighted images showed the classic "owl's eye" appearance. A small central annular tear and mild C6–C7 intervertebral disc protrusion were identified, suggesting a potential fibrocartilaginous source.
Follow-up MRI performed two weeks later revealed persistent ventral cord T2 hyperintensity with new patchy enhancement from C5 to T8 and associated C7 vertebral body marrow edema and enhancement, findings compatible with subacute ischemic evolution.

Discussion

Fibrocartilaginous embolism (FCE) is a rare cause of spinal cord infarction (SCI), resulting from migration of nucleus pulposus material into spinal vasculature, leading to occlusion—most commonly of the anterior spinal or radicular arteries. FCE accounts for approximately 5% of SCI cases but is often underdiagnosed due to overlap with inflammatory myelopathies.

The condition exhibits a bimodal age distribution—adolescents and older adults—with a slight female predominance[1,2]. Pediatric presentations, as in this case, may be associated with persistent vascular anastomoses or microtrauma during growth. Characteristic MRI findings include ventral cord T2 hyperintensity, diffusion restriction, and adjacent disc abnormalities such as Schmorl's nodes or annular tears[3]. CSF studies are typically normal, helping distinguish FCE from demyelinating or autoimmune myelitis.

Our patient was treated empirically with high-dose intravenous methylprednisolone for 5 days followed by a 4-week oral taper, along with five sessions of plasmapheresis for persistent hand weakness. She demonstrated substantial neurological recovery, regaining full lower extremity strength and near-complete upper limb function with continued rehabilitation. This favorable outcome contrasts with the generally poor prognosis reported in pediatric FCE, underscoring the value of early diagnosis and supportive management.

Teaching Point

Fibrocartilaginous embolism should be considered in children presenting with sudden-onset myelopathy and characteristic ventral cord MRI findings, particularly when inflammatory and infectious etiologies are excluded. Recognition of the radiologic pattern—longitudinally extensive ventral cord T2 hyperintensity with disc pathology—is key to diagnosis. Although histologic confirmation is rarely possible, a presumptive diagnosis based on clinical and imaging correlation can guide timely supportive therapy and improve outcomes.

References

1. Han JJ, Massagli TL, Jaffe KM. Fibrocartilaginous embolism--an uncommon cause of spinal cord infarction: a case report and review of the literature. *Arch Phys Med Rehabil*. 2004;85(1):153-157. doi:10.1016/s0003-9993(03)00289-2

2. Ahluwalia R, Hayes L, Chandra T, Maugans TA. Pediatric fibrocartilaginous embolism inducing paralysis. *Childs Nerv Syst ChNS Off J Int Soc Pediatr Neurosurg*. 2020;36(2):441-446. doi:10.1007/s00381-019-04381-z

3. Ke, W. *et al.* Clinically suspected fibrocartilaginous embolism: a case report and literature review. *Int. J. Neurosci.* **132**, 378–383 (2022).

Images/Tables

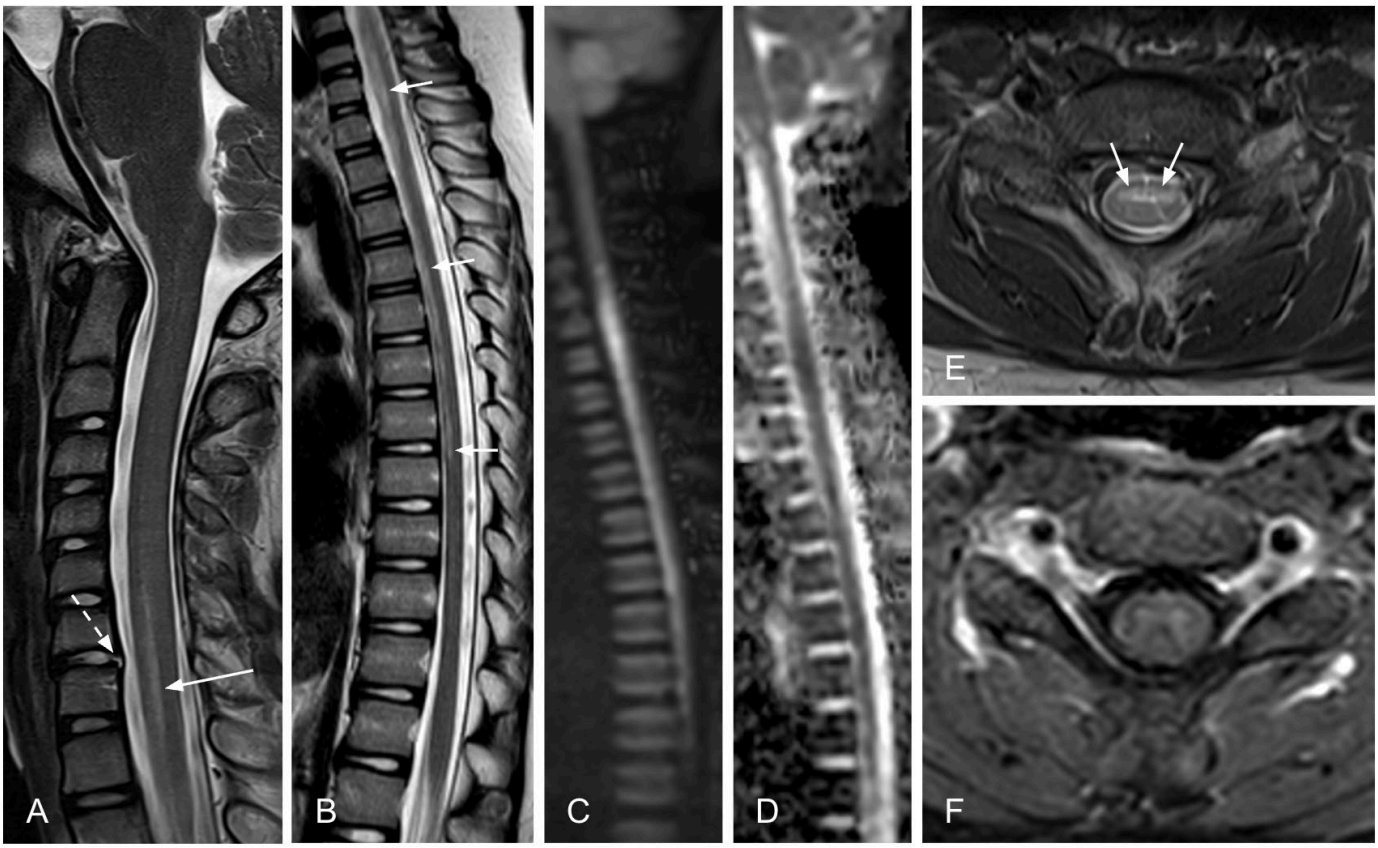

Figure 1: MRI on admission. A. Sagittal T2 of the cervical spine shows longitudinal hypersignal in the ventral cord beginning at C5 (solid arrow). A central annular fissure with small disc protrusion at C6-7 is also present (dashed arrow). B. Sagittal T2 of the thoracic spine shows extension of longitudinal hypersignal to T8. C/D. DWI/ADC images show associated diffusion restriction. E. Axial T2 at C6-7 shows hypersignal in the ventral horns ("owl's eye" sign).

F. Axial postcontrast shows questionable faint associated enhancement.

298 Imaging Findings and Endovascular Management of a Cognard Type III Dural Arteriovenous Fistula.

Arjun Ahuja M.D., Abrar Khaja M.D., Ashna Yalamanchi M.D., Parinda Shah M.D.
Advocate Illinois Masonic Medical Center, Chicago, IL, USA

Clinical History

An 88-year-old female with past medical history of HTN, DM, and dementia presented to the ED with acute onset of dizziness, increased confusion, and weakness. Stroke alert was called upon arrival, and CT head and CTA Head/Neck were immediately obtained.

Imaging Findings

CT Head demonstrated mildly expansile areas of hypoattenuation in the left cerebellum and the left temporo-occipital region, suggestive of cerebral edema.

CTA Head and Neck (Figure 1) demonstrated extensive tortuous left posterior cortical veins (red arrows) with asymmetric early enhancement of an irregular distal left transverse-sigmoid sinus (blue arrow), concerning for a dural arteriovenous fistula.

Contrast-enhanced MRI Brain demonstrated areas of mildly expansile T2/FLAIR hyperintensity in the left cerebellum, left occipital lobe, and left medial temporal lobe (Figure 2a-2b). Extensive associated magnetic susceptibility artifact consistent with chronic hemosiderin/microhemorrhage (Figure 4a-4b). No diffusion restriction to suggest acute infarction. MRV Head showed significant asymmetric irregularity of the left transverse-sigmoid sinus, with decreased caliber and extensive adjacent collaterals (Figure 3). Post-contrast MRI brain also suggested the presence of an eccentric filling defect (Figures 5a-5b, white arrows). Multiple enhancing tortuous cortical venous collaterals were present in the regions of T2/FLAIR hyperintensity (Figures 5b-5c, red arrows).

Findings were overall favored to represent remote thrombosis of the left transverse/sigmoid sinuses with subsequent development of a dural arteriovenous fistula with resultant venous congestive edema and extensive microhemorrhage.

Cerebral angiogram injection of the left ECA (Figures 6a-c) confirmed presence of a left dural arteriovenous fistula, with branches of the occipital, ascending pharyngeal, and middle meningeal arteries (red arrows) connecting with a dysplastic segment of transverse-sigmoid sinus (blue arrow). There was impaired venous drainage of this dysplastic segment, with severe venous reflux into cortical veins of the left cerebellum and temporal lobe, without any antegrade flow into the left IJV or retrograde flow into the contralateral transverse/sigmoid sinus. Thus, this is consistent with a Cognard type III dAVF.

Discussion

Intracranial dural arteriovenous fistulas (dAVFs) are pathologic vascular shunts between meningeal arteries and dural venous sinuses or cortical veins. While many are idiopathic, there have been associations with dural sinus thrombosis, previous craniotomy, and trauma. Venous drainage pattern determines the type of dAVF and correlates with the severity of symptoms and risk of hemorrhage or neurologic deficit, with cortical venous drainage conferring the highest risk.

This case demonstrates a Cognard type III dAVF, which features cortical venous drainage without venous ectasia, carrying a high risk of hemorrhage. This left transverse–sigmoid sinus dAVF was successfully treated with trans-arterial embolization using Onyx, with final angiogram confirming complete occlusion of the fistula without evidence of cortical venous reflux (Figure 6c).

Teaching Point

- Cortical venous drainage in Cognard type III dAVFs is an aggressive feature that leads to increased risk of intracranial hemorrhage and non-hemorrhagic neurologic deficit, necessitating prompt treatment.
- This case highlights the diagnostic value of noninvasive imaging with CTA and MR for diagnosis, classification, and treatment planning for dAVFs.
- Digital subtraction angiography remains the gold standard for defining venous drainage patterns and targeted endovascular therapy.

References

1. Gandhi D, Chen J, Pearl M, Huang J, Gemmete JJ, Kathuria S. Intracranial dural arteriovenous fistulas: classification, imaging findings, and treatment. *AJNR Am J Neuroradiol*. 2012;33(6):1007-1013. doi:10.3174/ajnr.A2798
2. Kwon BJ, Han MH, Kang HS, Chang KH. MR imaging findings of intracranial dural arteriovenous fistulas: relations with venous drainage patterns. *AJNR Am J Neuroradiol*. 2005;26(10):2500-2507.
3. Cognard C, Januel AC, Silva NA Jr, Tall P. Endovascular treatment of intracranial dural arteriovenous fistulas with cortical venous drainage: new management using Onyx. AJNR Am J Neuroradiol. 2008;29(2):235-241. doi:10.3174/ajnr.A0817.

Images/Tables

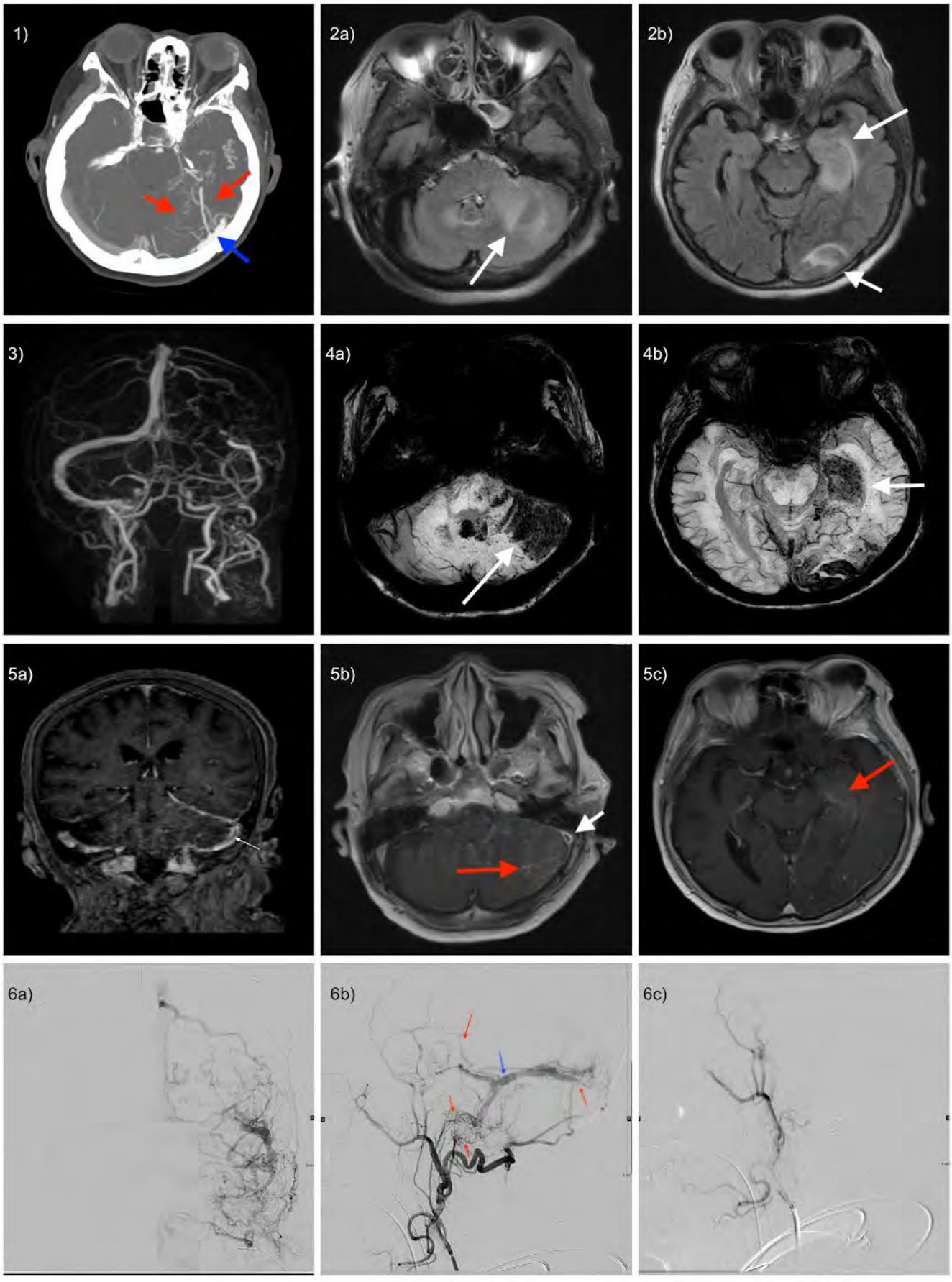

305 A Case of Rosai - Dorfman Disease: Insights from Head and Neck Imaging

SUSHMITHA PUTTAPPA SHIVAGANGE MD[1], KAVYA . MD[2], Eduardo Portela De Oliveira MD[1]
[1]University of Ottawa, Ottawa, Ontario, Canada. [2]KVG Medical college and Hospital, Sullia, Karnataka, India

Clinical History

A 50-year-old South Asian female presented with complaints of progressive diminution of vision in the left eye over the past few months, associated with ipsilateral nasal obstruction occasionally associated with mild epistaxis and postnasal drip.

Imaging Findings

CT:

Non contrast CT images of head revealed hyperdense extra axial mass lesions in the left parasellar region, left peri mesencephalic cistern and left cerebellopontine angle causing mass effect on the brainstem, no associated vasogenic edema. Hyperdense content is also seen completely opacifying the bilateral maxillary, ethmoidal sinuses, nasal cavities and nasopharynx. Associated bony changes include sclerosis and erosions involving the walls of the maxillary sinuses, bony nasal septum, ethmoidal lamellae, cribriform plates, lamina papyracea and floor of orbits bilaterally. (Figure 1a-1e)

MR:

Multifocal, extra-axial, dural based well-defined T1 isointense, T2/FLAIR hypointense mass lesions in the parasellar region, perimesencephalic cistern, Meckel's cave, temporal region, cerebellopontine angle, supravermian cistern, and retrocerebellar cistern on the left demonstrating avid, homogeneous enhancement. Associated mass effect on the brainstem without significant vasogenic edema.

Similar avidly enhancing soft tissue lesions seen completely opacifying the bilateral maxillary and ethmoidal sinuses, nasal cavities, nasopharynx and also involving left pterygoid muscles. Enhancing soft tissue is seen extending along the inferomedial aspects of bilateral orbits, also in superotemporal aspects with involvement of lacrimal glands and extending to preseptal soft tissues.. (Figure 2a-2f)

Multiple borderline enlarged bilateral level I-V cervical lymph nodes.

Discussion

Rosai Dorfman disease (RDD) - Sinus histiocytosis with massive lymphadenopathy is a rare benign idiopathic lympho-proliferative disorder of unknown etiology affecting individuals of any age with peak incidence in the 2nd-3rd decade. RDD shows a male predominance and is more frequently reported among individuals of African descent [1].

Extra nodal involvement is seen in 43% cases, commonly affecting skin, nose, sinuses, upper respiratory tracts, orbits and salivary glands. Intracranial RDD occurs in less than 5% of cases [2].

Intracranial RDD can present as solitary or multiple dura-based masses that are moderately hyperdense on CT and enhance strongly on CECT, appear isointense to grey matter on T1WI and iso to hypointense on T2WI. Theradiological similarity to meningioma, Langerhans cell histiocytosis, lymphoproliferative disorders, plasma cell granulomas, granulomatous diseases, and neurofibromatosis makes the preoperative diagnosis a challenge [3].

Histopathology showing Emperipolesis and positivity for S-100 on immunohistochemistry is diagnostic.Surgery, steroids, chemotherapy, and radiation therapy are reported treatment options [3].

Teaching Point

RDD in the head and neck often presents as multifocal avidly enhancing soft-tissue masses with or without lymphadenopathy but preserved adjacent fat planes and lack of aggressive bone destruction, features that can help distinguish it from malignancy, though correlation with clinical and pathologic findings remains essential.

References

1. Miękus A, Stefanowicz J, Kobierska-Gulida G, Adamkiewicz-Drożyńska E. Rosai-Dorfman disease as a rare cause of cervical lymphadenopathy - case report and literature review. *Cent Eur J Immunol*. 2018;43(3):341-345. doi:10.5114/ceji.2018.80055.
2. Shin M, Heo YJ, Kim D, Jeong HW, Baek JW, Park HY. Isolated Intracranial Rosai-Dorfman Disease Mimicking Meningioma: A Case Report. *Taehan Yongsang Uihakhoe Chi*. 2022;83(3):719-723. doi:10.3348/jksr.2021.0121.
3. Raslan OA, Schellingerhout D, Fuller GN, Ketonen LM. Rosai-Dorfman disease in neuroradiology: imaging findings in a series of 10 patients. *AJR Am J Roentgenol*. 2011;196(2):W187-W193. doi:10.2214/AJR.10.4778.

Images/Tables

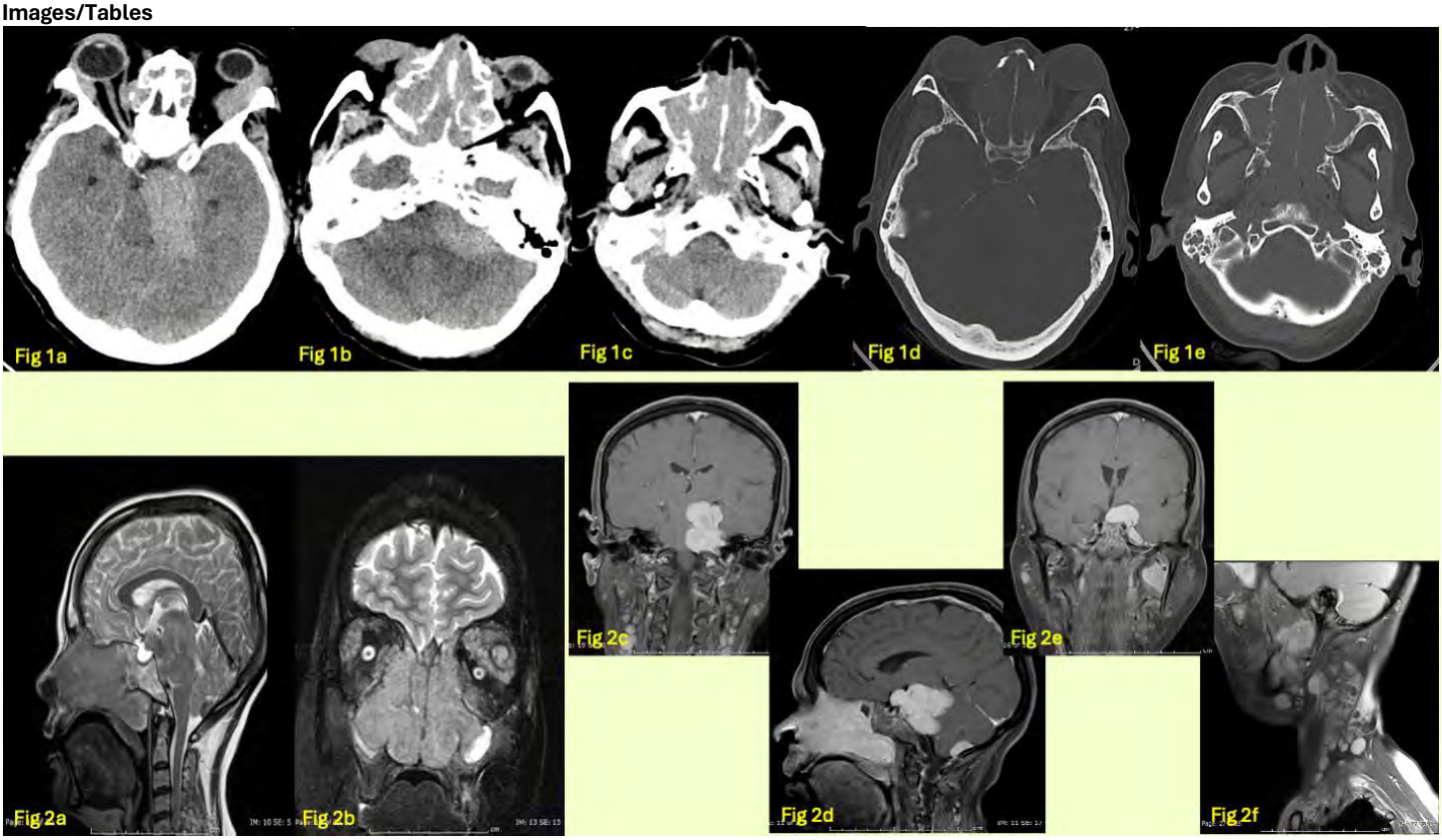

307 Unusual Case of Cervicomedullary Aneurysm With Treatment.

Arjun Ahuja M.D., Abrar Khaja M.D., Ashna Yalamanchi M.D., Parinda Shah M.D.
Advocate Illinois Masonic Medical Center, Chicago, IL, USA

Clinical History

A 65-year-old female with past medical history notable for remote tongue cancer (s/p right radical neck dissection and radiotherapy), who presented with a few days of left-sided numbness.

Imaging Findings

CTA head and neck showed a 4 mm aneurysm along the right ventral aspect of the cervical spinal cord at C1-C2 (Figure A). Of note, this was new compared to the most recent prior from 13 months ago. Additionally, there was absence of the right internal jugular vein with the sigmoid sinus draining to extensive venous collaterals in the right suboccipital region from prior neck dissection.

Subsequent MRI demonstrated a 4 mm aneurysm along the anterior cervical spinal cord at C1-C2 (Figure C). There was expansile T2 hyperintensity of the cervical spinal cord spanning C1-C6 (Figure B). In addition, there was hyperintense appearance of the C1-C6 vertebral bodies secondary to fatty marrow signal from prior radiation treatment to the neck.

Patient then underwent cerebral angiogram, which redemonstrated the aneurysm, though did not visualize any arteriovenous malformation or fistula. A couple of small arterial feeders were identified, one originating from the vertebrobasilar junction and another from the left vertebral artery (Figure D). Onyx embolization was performed, with subsequent images demonstrating resolution of contrast filling of the aneurysm.

Discussion

Post procedure, repeat imaging was notable for a small acute infarct in the left ventral medulla, and edema and trace hemorrhage around the embolization site. Overall, the expansile T2 hyperintensity of C1-C6 was felt to represent extensive spinal cord edema secondary to underlying venous congestion / venous hypertension, possibly from flow-related shunting.

Teaching Point

This case highlights the broad differential considerations for an aneurysm associated with spinal cord edema. In this patient, three main possibilities were evaluated. The initial leading consideration was a dural arteriovenous fistula, as a high-pressure shunt could cause venous congestion and result in surrounding edema. However, no definitive venous outflow channel was identified on cerebral angiography. Given the patient's history of tongue cancer and prior radiation therapy, radiation-induced myelopathy was also considered. This was deemed unlikely given that radiation had occurred more than 20 years earlier, and the diffuse, expansile nature of the edema without associated spinal cord atrophy was atypical for this diagnosis. Our final and leading diagnostic consideration was that the extensive spinal cord edema likely reflected venous hypertension, though not through a direct arterial feeder as would be seen with a fistula. The patient's history of neck dissection and the presence of extensive venous collaterals may have increased her susceptibility to venous congestion and compounded the mass effect from the aneurysm, resulting in spinal cord edema that appeared out of proportion to the size of the lesion.

References

Alkhaibary A, Alnefaie N, Alharbi A, et al. Intracranial dural arteriovenous fistula: a comprehensive review of the history, management, and future prospective. Acta Neurol Belg. 2023;123(2):359-366. doi:10.1007/s13760-022-02133-6

Bünül SD, Sarıkaya CE, Öztürk O, Sarıkaya C. A brief case series of radiation associated myelopathy. Neurosciences (Riyadh). 2021;26(4):392-395. doi:10.17712/nsj.2021.4.20210071

Deng X, Dong M, Peng C, et al. Embolizing intracranial arteriovenous malformations with Onyx: experience at a single center with 250 patients. J Interv Med. 2019;1(3):164-169. Published 2019 Apr 30. doi:10.19779/j.cnki.2096-3602.2018.03.06
Khan M, Ambady P, Kimbrough D, et al. Radiation-Induced Myelitis: Initial and Follow-Up MRI and Clinical Features in Patients at a Single Tertiary Care Institution during 20 Years. AJNR Am J Neuroradiol. 2018;39(8):1576-1581. doi:10.3174/ajnr.A5671

Images/Tables

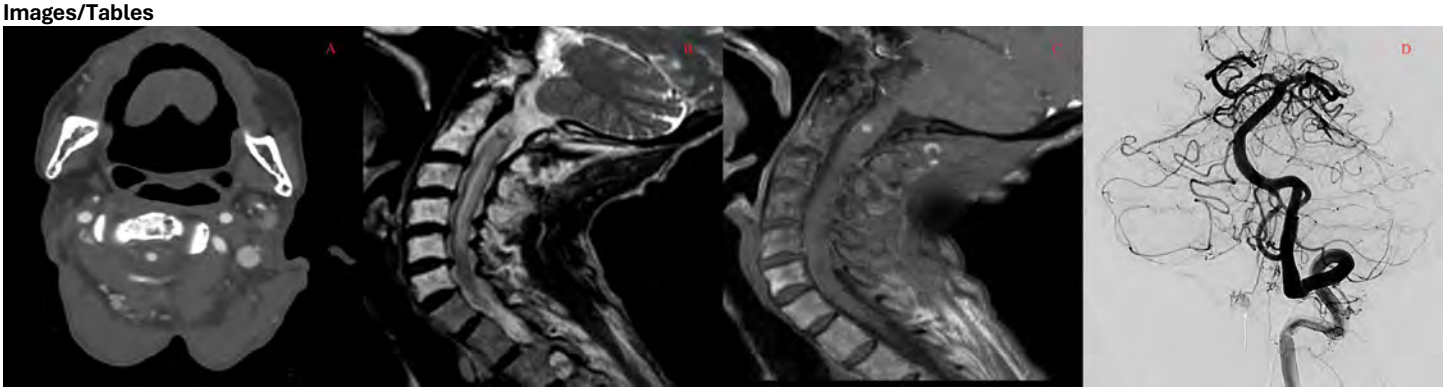

---

308 External carotid artery and salivary glands- definitive indicators of seizure laterality

Joshua Ravicz MD[1], Julia Poe MD[1], Surjith Vattoth MD[2], Tanvir Rizvi MD[1], Thomas J Eluvathingal Muttikkal MD[1]
[1]University of Virginia Health System, Charlottesville, VA, USA. [2]Rush University, Chicago, Illinois, USA

Clinical History

Case 1

A 46-year-old female presented with right upper and lower extremity weakness, sensory changes and aphasia. The patient had history of brain metastases from breast cancer and had undergone gamma knife treatment to right cerebellar metastasis a week prior to the presentation. Initial National Institute of Health Stroke Scale was 19. CTA head and neck was done to evaluate for stroke. CT scan of the head showed post treatment changes including calcified lesion in the left temporoparietal region and stable post-op changes of right cerebellar metastatectomy. There was no evidence of hemorrhage. There was diffusely increased vascularity in left cerebral hemisphere which resulted in AI-powered software misinterpreting it as large vessel occlusion in the right middle cerebral artery (MCA) territory. There was enlargement of left external carotid artery (ECA) branches, and hyperenhancement of left parotid and submandibular glands. Right sided neurological deficits and aphasia with enlargement of left MCA pointed to seizure. EEG showed left temporal epileptiform discharges and two brief runs of ictal rhythmic discharges indicating seizure focus. MRI brain done 2 days later showed restricted diffusion in left hippocampus, and pulvinar of left thalamus consistent with post ictal change. Follow up MRI showed development of mesial temporal sclerosis on the left.

Case 2, 3 and 4 had similar findings of ECA enlargement and salivary gland hyperenhancement, which will be included in the electronic poster to maintain brevity within the word limit.

Imaging Findings

Figure 1 a) Algorithm for detection of large vessel occlusion (LVO) shows false positive large vessel occlusion in the right MCA territory, due to diffusely increased vascularity in left cerebral hemisphere.

Figures 1b) Axial CTA and 1c) Coronal CTA show increased left ECA vascularity (white arrows) and hyperenhancement of left parotid and submandibular glands

Figure 1d) and 1e) Axial DWI MRI brain images show restricted diffusion in left hippocampus, and pulvinar of left thalamus

Figure 1f) Follow up MRI shows mesial temporal sclerosis on the left

Discussion

Asymmetric enlargement of ECA branches and hyperenhancement of parotid and submandibular glands are imaging signs pointing to seizure laterality and differentiating seizure from the clinically suspected stroke. This finding has not been mentioned in the literature to the best of our knowledge. Potential mechanism is parasympathetic stimulation[1]. Epilepsy can present with headache[2] and increased salivation[3], which can be explained by enlargement of middle meningeal artery and hyperactivity of salivary glands from parasympathetic stimulation, as demonstrated by enlargement of ECA branches and hyperenhancement of salivary glands.

Teaching Point

Enlargement of external carotid artery and enhancement of parotid and submandibular glands are specific indicators of seizure laterality and differentiates seizure from suspected stroke.

References

1. Taksande B, Rathi N, Kotpalliwar S. Parasympathetic overactivity: A manifestation of temporal lobe epilepsy. J Neurosci Rural Pract. 2013 Oct;4(4):479-80. doi: 10.4103/0976-3147.120200. PMID: 24347970; PMCID: PMC3858782.
2. Haki C, Akdoğan Ö, Bora İ. Headaches Associated with Seizure: A Prospective Comparative Cohort Study. Noro Psikiyatr Ars. 2019 Aug 20;58(1):48-51. doi: 10.29399/npa.23272. PMID: 33795952; PMCID: PMC7980719.
3. Shah J, Zhai H, Fuerst D, Watson C. Hypersalivation in temporal lobe epilepsy. Epilepsia. 2006 Mar;47(3):644-51. doi: 10.1111/j.1528-1167.2006.00480.x. PMID: 16529634.

Images/Tables

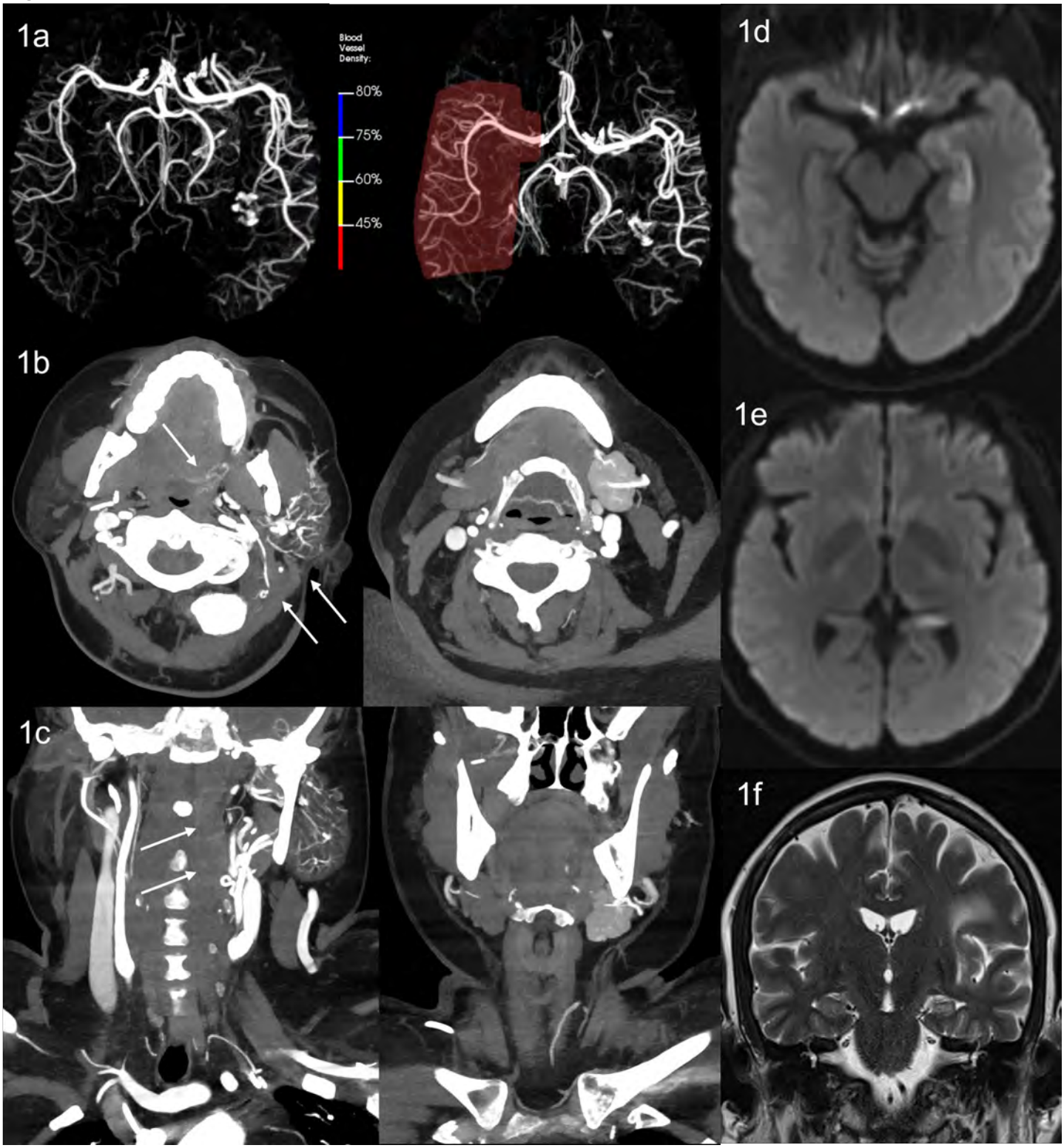

324 Unmasking the Zebras: Rare Parasitic and Fungal Infections of the Pediatric CNS—An Educational Case Series

Sawsan O Tabaza MD[1], Karen Moeller MD[2], Thierry Huisman MD[2], Nilesh Desai MD[2], Stephen Kralik MD[2], Lamson Tran[3], Huy B Tran MD[2]
[1]UTHealth Houston, Houston, Texas, USA. [2]Baylor College of Medicine, Houston, Texas, USA. [3]Texas A&M, College Station, Texas, USA

Clinical History

Eight pediatric patients presented with diverse neurological or orbital symptoms, including seizures, meningitis, encephalopathy, and visual disturbance. Each case posed an initial diagnostic challenge, frequently mimicking neoplasm or autoimmune disease. Confirmed pathogens included Angiostrongylus cantonensis, Cladophialophora bantiana, Plasmodium falciparum (cerebral malaria), Baylisascaris procyonis, Onchocerca lupi, Malassezia spp., Toxocara spp., and Naegleria fowleri. Clinical correlation and laboratory or histopathologic confirmation established the final diagnoses.

Imaging Findings

Distinctive radiologic patterns emerged:

- Baylisascaris procyonis – diffuse confluent white-matter T2/FLAIR hyperintensity with peripheral eosinophilia.
- Naegleria fowleri – fulminant, rapidly progressive meningoencephalitis with basal enhancement and diffuse edema.
- Cladophialophora bantiana – necrotic ring-enhancing abscesses and ventriculitis mimicking glioma.
- Onchocerca lupi – orbital parasitic abscess extending toward the optic nerve.
- Malassezia – shunt-associated ventriculitis.
- Other cases demonstrated variable meningeal enhancement (Angiostrongylus), microvascular injury (cerebral malaria), and ocular granulomas (Toxocara).

Discussion

These infections, though exceedingly rare, share a common diagnostic pitfall: imaging features often overlap with neoplastic or inflammatory diseases. Recognition depends on integrating imaging findings with epidemiologic clues—travel, animal exposure, immune status, or environmental contact. Global travel, migration, and increasing immunosuppression are expanding the geographic reach of these pathogens, making awareness essential even in non-endemic regions.

Teaching Point

Rare parasitic and fungal CNS infections in children can imitate more common pathologies but leave subtle, recognizable imaging fingerprints. Early recognition through correlation of radiologic features with clinical and exposure history enables accurate diagnosis and timely, often life-saving management.

References

1. White AC Jr. Parasitic infections of the nervous system. Continuum (Minneap Minn). 2022;28(5):1310-1334.
2. Revankar SG, Sutton DA. Melanized fungi in human disease (includes Cladophialophora bantiana). Clin Microbiol Rev. 2010;23(4):884-928.
3. Prohić A, Jovović Sadiković T, Krupalija-Fazlić M, et al. Malassezia species in neonatal and pediatric infections. Mycoses. 2016;59(2):79-85.
4. Chusid MJ, O'Connor M, Nylund CM. Baylisascariasis in children. Pediatr Infect Dis J. 2019;38(6):611-615.
5. Potchen MJ, Kampondeni SD, Seydel KB, et al. Brain imaging in cerebral malaria. AJNR Am J Neuroradiol. 2012;33(5):933-939.

Images/Tables

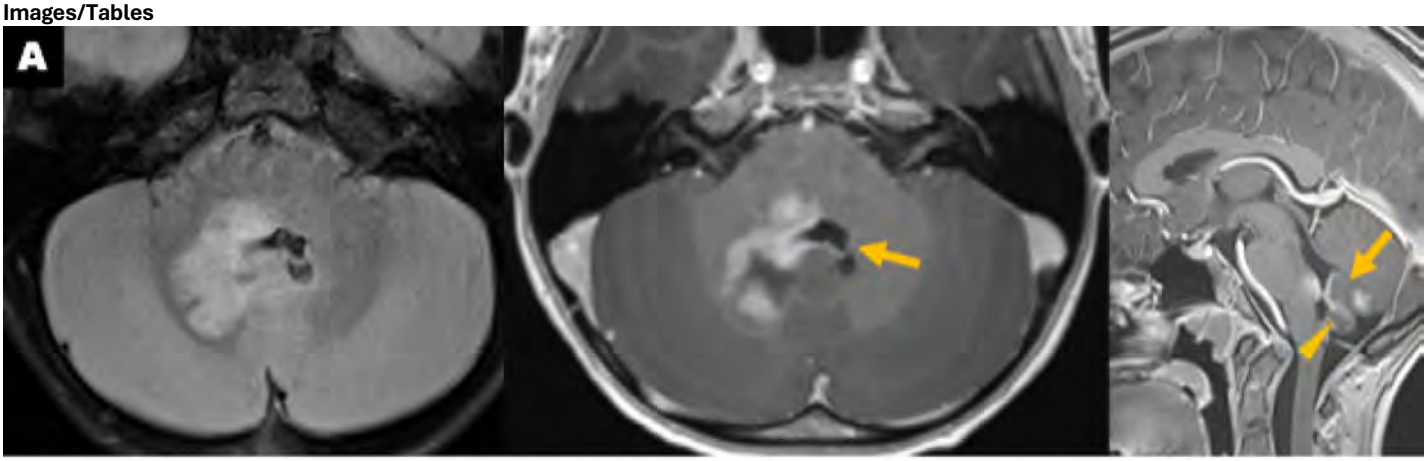

Fig 1: Cladophialophora bantiana meningoencephalitis and ventriculitis in a 9-year-old. Axial FLAIR (A), axial T1 post-contrast (B), and sagittal T1 post-contrast (C) show necrotic ring enhancement and ependymal spread.

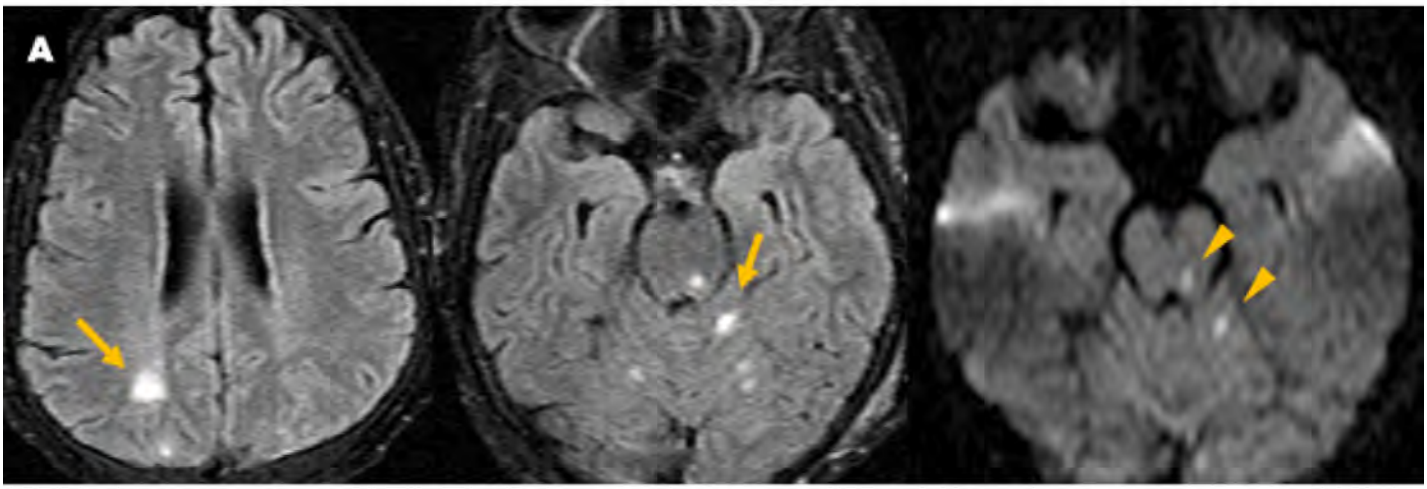

Fig 2: Invasive fungal (Malassezia) CNS infection in a 15-year-old with a history of orthotropic heart transplant. Axial FLAIR and DWI.

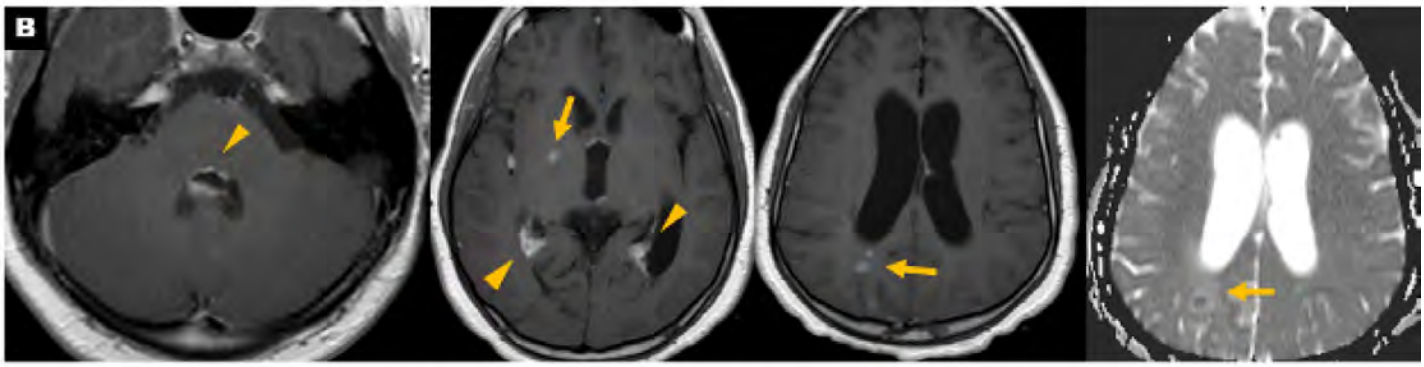

Fig 3: Invasive fungal (Malassezia) CNS infection in a 15-year-old with a history of orthotropic heart transplant. Axial T1 post contrast and ADC.

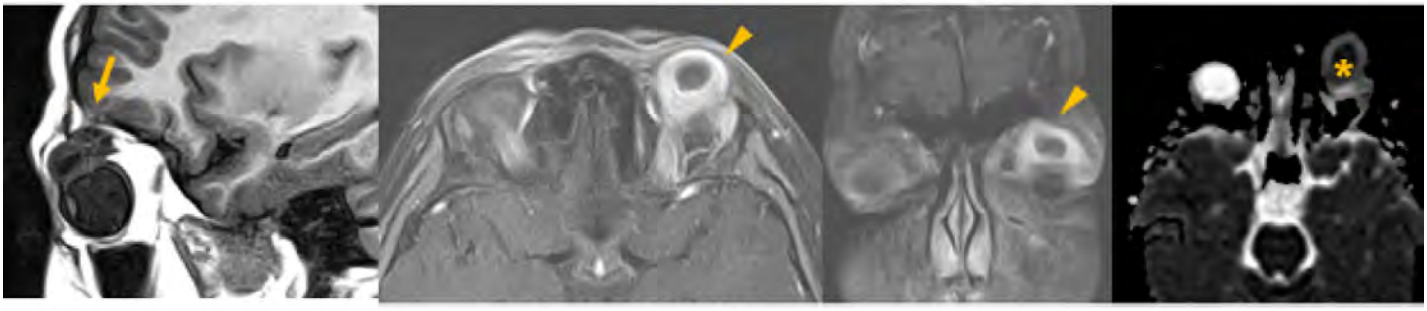

Fig 4: Onchocerca lupi (nematode) abscess of the left orbit in a 10-year-old. Sagittal T2, axial and coronal STIR and axial DWI.

329 An Iron-Stained CNS: Imaging the Spectrum of Diffuse Siderosis

Rishabh Agrawal MD, Benjamin Kaminski MD, Adam Wolberg DO, Maira Sarpi MD, Ibrahim Tuna MD
University of Florida, Gainesville, FL, USA

Clinical History

Diffuse superficial hemosiderosis results from chronic or repeated bleeding into the subarachnoid space, leading to gradual deposition of hemosiderin along the pial surfaces of the brain and spinal cord. The resulting iron accumulation promotes oxidative injury, demyelination, and neuronal loss. Involvement is classically infratentorial, particularly within the cerebellum and brainstem, but supratentorial and spinal extension are increasingly recognized. Patients often present with slowly progressive gait ataxia, sensorineural hearing loss, and myelopathic symptoms. We present a case series with varying degrees of diffuse siderosis involving the brain and spinal cord.

Imaging Findings

Awareness of this entity has grown with the broader use of iron-sensitive MRI sequences such as GRE, T2*, and SWI. On MRI, superficial hemosiderosis appears as a thin, hypointense rim outlining the affected surfaces on susceptibility-weighted or T2* sequences. Infratentorial disease most commonly involves the superior cerebellar vermis, brainstem, and cranial nerves. Supratentorial or cortical superficial siderosis presents as linear sulcal hypointensity along the cerebral convexities. Spinal involvement is characterized by circumferential low signal along the cord or nerve roots. GRE and SWI at 3T improve sensitivity compared with 1.5T imaging. Secondary findings may include focal atrophy or white-matter changes. Associated abnormalities such as ventral dural tears, CSF-venous fistulae, or epidural fluid collections are best demonstrated with CT or dynamic subtraction myelography.

Discussion

Conditions that can mimic superficial hemosiderosis include laminar cortical necrosis, subarachnoid calcification, vascular malformations, and magnetic susceptibility artifacts. Distinguishing features of true hemosiderosis are its continuity along pial surfaces and pronounced blooming on SWI. Evaluation should include MRI of the entire neuroaxis with high-resolution susceptibility sequences, followed by targeted myelography or CT angiography when a bleeding source is suspected. In cases of cortical siderosis, work-up for cerebral amyloid angiopathy or prior convexity subarachnoid hemorrhage is warranted.

Teaching Point

Diffuse superficial hemosiderosis represents a chronic hemorrhagic process rather than a single disease. Identifying and repairing the bleeding source – most often a spinal dural defect – is critical to prevent further neurologic deterioration. Radiologists play a key role by recognizing the characteristic imaging pattern and guiding subsequent leak-localization studies. Familiarity with this entity allows timely diagnosis and intervention, improving long-term outcomes for affected patients.

References

Kumar N. Neuroimaging in superficial siderosis: an in-depth look. *AJNR Am J Neuroradiol*. 2010;31(1):5-14. doi:10.3174/ajnr.A1628

Kumar N, Cohen-Gadol AA, Wright RA, et al. Superficial siderosis. *Neurology*. 2006;66(8):1144-1152. doi:10.1212/01.wnl.0000208510.76323.5b

Schievink WI, Maya MM, Harris J, et al. Infratentorial Superficial Siderosis and Spontaneous Intracranial Hypotension. *Ann Neurol*. 2023;93(1):64-75. doi:10.1002/ana.26521

Weidauer S, Neuhaus E, Hattingen E. Cerebral Superficial Siderosis : Etiology, Neuroradiological Features and Clinical Findings. *Clin Neuroradiol*. 2023;33(2):293-306. doi:10.1007/s00062-022-01231-5

Images/Tables

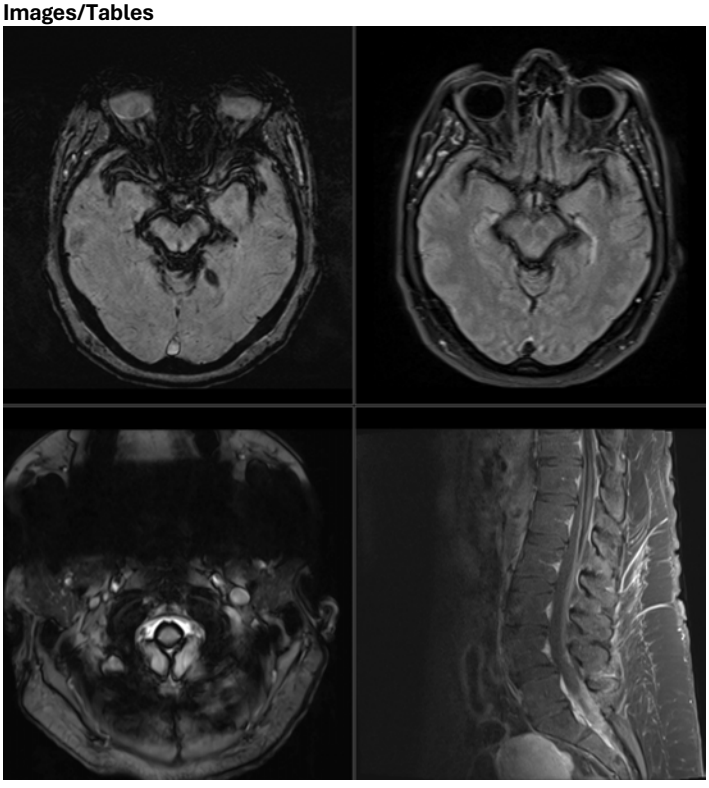

336 Reading Between the 'Pages': Neuroradiologic Insights into Pediatric Posterior Reversible Encephalopathy Syndrome (PRES) Induced by Traumatic Page Kidney

Sammar M Ghannam MD, MPH[1], Melissa Donate MD[2], Moawiz Saeed BS[1], Achint Singh MD[3]

[1]University of Texas at San Antonio, San Antonio, Texas, USA. [2]The University of Texas Southwestern Medical Center, Dallas, Texas, USA. [3]Charlotte Radiology, Charlotte, North Carolina, USA

Clinical History

14-year-old male presents with new onset headache, vision changes, emesis, and seizure following diagnosis of a left renal subcapsular hematoma and grade 4 renal laceration due to a sports injury a few days prior. Found to be hypertensive with systolic blood pressures in 160-180s.

Imaging Findings

CT of the abdomen and pelvis revealed a large 8.5 cm left renal subcapsular hematoma and a Grade IV renal laceration. Magnetic resonance (MR) imaging of the brain demonstrated symmetric cortical and subcortical FLAIR hyperintensity without enhancement bilaterally in the posterior parietal and occipital lobes. No diffusion weighted imaging (DWI) hyperintensities or hemorrhage.

Discussion

Posterior reversible encephalopathy syndrome (PRES) is an acute clinico-radiographic neurological syndrome characterized by vasogenic edema affecting the cortical and subcortical parietal and occipital lobes (most common) as a result of altered integrity of the blood-brain barrier. Symptoms include headache, visual disturbances, nausea, vomiting, and seizures. Most common etiologies include severe hypertension, renal failure, sepsis, preeclampsia, autoimmune disease, certain immunosuppressants, and chemotherapy. Of note, PRES is underdiagnosed and rarely reported in pediatric patients [3,4, 5]. Reports suggest PRES in pediatric patients is caused by renal disease and other causes similar to adults. In this case, acute severe hypertension was a clinical manifestation of the subcapsular hematoma resulting in external compression of the renal parenchyma, causing renal hypoperfusion, activation of the renin-angiotensin-aldosterone (RAAS) system, and leading to significant hypertension (Page kidney phenomenon) [4].

Magnetic Resonance (MR) imaging is the preferred imaging modality for diagnosis. Three hemispheric pattern variants of FLAIR hyperintensity showing edema may be encountered: holohemispheric, superior frontal sulcal, and primary parietal-occipital (most common). The parietal and occipital lobes are most commonly affected, followed by the frontal lobes, the inferior temporal-occipital junction, and the cerebellum. Focal/patchy areas of FLAIR hyperintense edema can also be seen in the basal ganglia, brain stem, and deep white matter which may cause hydrocephalus and brainstem compression. Diffusion restriction, mild leptomeningeal enhancement, and hemorrhage can be seen. While the imaging findings in children follow a classic presentation, they have a higher reported incidence of involvement of atypical regions such as the frontal lobes, brainstem, and cortex [3]. Treatment involves addressing the source of hypertension, blood pressure control and management of neurologic symptoms[4]. In our case of traumatic Page kidney, this required percutaneous drainage of the hematoma and initiation of antiepileptics. The timely care of PRES in this patient resulted in reversal of neurological symptoms. PRES should be considered in children presenting with encephalopathy/seizures, hypertension, or renal disease since delayed diagnosis and treatment may result in permanent neurological damage.

Teaching Point

1. Recognize the characteristic imaging findings of posterior reversible encephalopathy syndrome (PRES) using a case-based approach.
2. Identify Page kidney as a rare cause of pediatric hypertension and review the proposed pathophysiologic mechanisms.
3. Discuss the role of imaging in evaluating new-onset encephalopathy without acute head trauma for prompt diagnosis and management.
4. Discuss the role of the radiologist in diagnosing neuroradiologic diseases caused by systemic illnesses.

References

1. Whitworth PW, Dyer RB. The "page kidney." Abdom Radiol 2017;42(9):2387-88. DOI: https://doi.org/10.1007/s00261-017-1139-y
2. Rajiah P, Suman G, Vijay K, et al. Multisystem imaging manifestations of kidney failure. RadioGraphics 2024 Jul 17. [Epub ahead of print] DOI: https://doi.org/10.1148/rg.230124.q1
3. Sharma S, Tiwari S, Yadav T, et al. Magnetic resonance imaging patterns and perfusion changes of posterior reversible encephalopathy syndrome in children with clinical outcome correlation. Pediatr Radiol 2024;54(11):1884-95. DOI: https://doi.org/10.1007/s00247-024-06045-w
4. Bartynski WS. Posterior reversible encephalopathy syndrome, part 1: Fundamental Imaging and clinical features. AJNR Am J Neuroradiol 2024;45(12). DOI: https://doi.org/10.3174/ajnr.45-12.s100
5. Smyth A, Collins CS, Thorsteinsdottir B, et al. Page kidney: Etiology, renal function outcomes and risk for future hypertension. J Clin Hypertens (Greenwich) 2012;14(4):216-21. DOI: https://doi.org/10.1111/j.1751-7176.2012.00601.x

Images/Tables

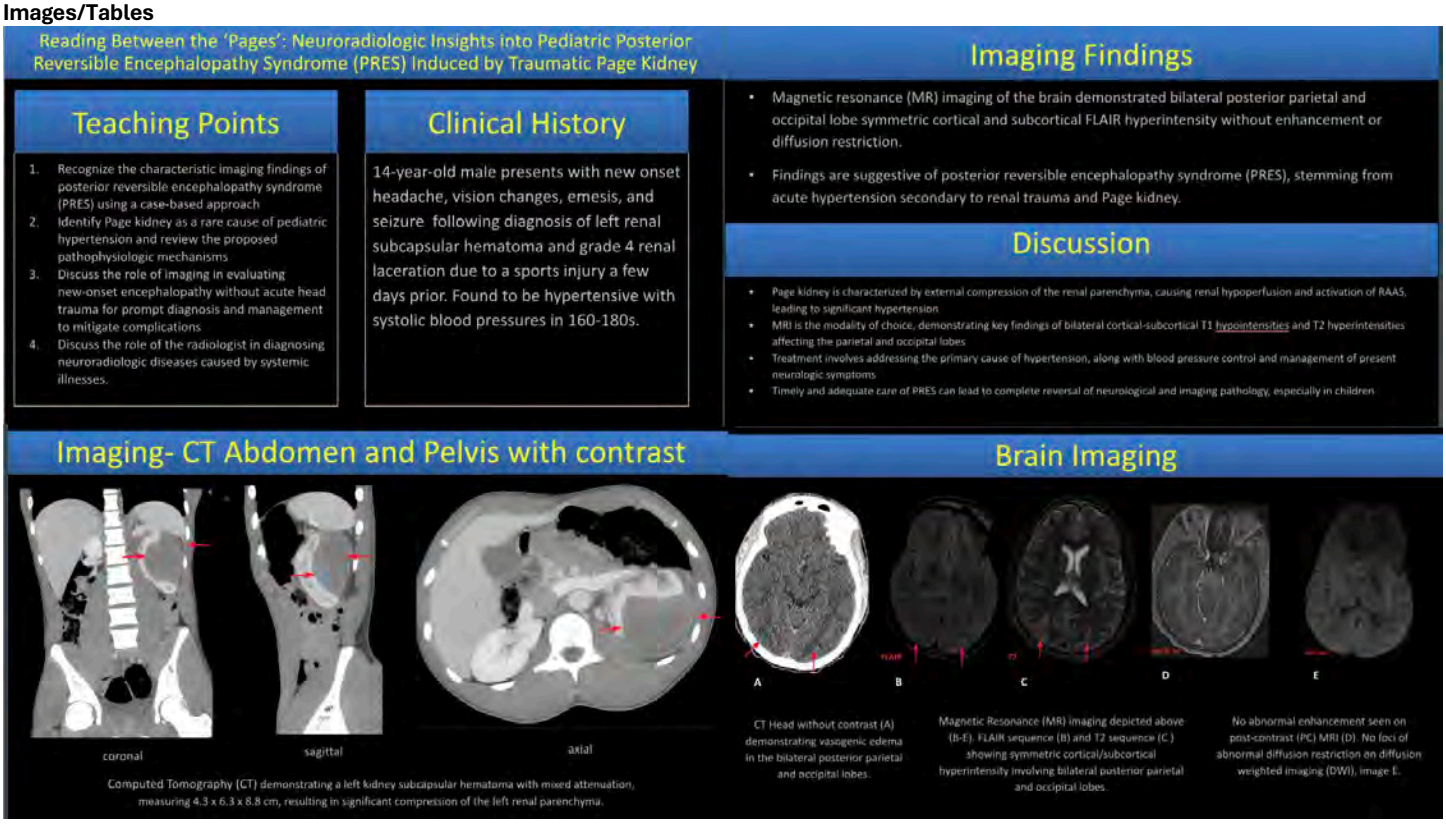

359 **Rhombencephalosynapsis with Hydrocephalus and Bipolar Disorder**

Mira A Zineddin BS, Barton F Branstetter MD
University of Pittsburgh School of Medicine, Pittsburgh, Pennsylvania, USA

Clinical History

A 43-year-old female with bipolar disorder presented to the emergency room with acute psychosis. MRI was performed to exclude organic causes of psychosis, upon which enlarged ventricles and a ventriculoperitoneal shunt were discovered. Further questioning revealed a diagnosis of hydrocephalus and strabismus at age 1, which resulted in ventriculoperitoneal shunt placement. After childhood, she was lost to neurosurgical care until she re-presented with psychiatric symptoms.

Imaging Findings

MRI and CT reveal complete midline fusion of the cerebellar hemispheres, the dentate nuclei, and the superior cerebellar peduncles, as well as cerebellar vermis agenesis and an abnormally shaped fourth ventricle, consistent with rhombencephalosynapsis (Figure). Asymmetrical lateral ventricular enlargement, aqueductal stenosis, and a ventriculoperitoneal shunt are also present.

Discussion

Rhombencephalosynapsis is a rare congenital anomaly involving midline fusion of the cerebellar hemispheres and internal cerebellar structures. Outcomes can range from mild to severe ataxia and cognitive difficulties. This patient also presented with hydrocephalus, which is the most common supratentorial feature associated with rhombencephalosynapsis.[1] It usually results from aqueductal stenosis caused by fusion of the superior colliculi, inferior colliculi, or superior cerebellar peduncles.[2] This patient's psychiatric presentation is noteworthy, as bipolar disorder has been linked to both hydrocephalus[3] and cerebellar pathology such as rhombencephalosynapsis,[4] suggesting that these conditions are possible organic causes of mania or secondary bipolar disorder.

Teaching Point

The neurological and psychiatric manifestations of rhombencephalosynapsis are highly variable. Given its association with bipolar disorder, rhombencephalosynapsis can be considered a potential organic contributor to mood disorders, particularly when comorbid hydrocephalus is observed. The radiologic findings of rhombencephalosynapsis may be subtle on CT and MRI, so a high level of suspicion for this otherwise rare disease is needed when excluding organic causes of psychiatric disorders.

References

1. Fouda MA, Kim TY, Cohen AR. Rhomboencephalosynapsis: Review of the literature. *World Neurosurgery* 2022;159:48–53. DOI: https://doi.org/10.1016/j.wneu.2021.12.062
2. Ishak GE, Dempsey JC, Shaw DW, et al. Rhombencephalosynapsis: A hindbrain malformation associated with incomplete separation of midbrain and forebrain, hydrocephalus and a broad spectrum of severity. *Brain* 2012;135:1370–86. DOI: https://doi.org/10.1093/brain/aws065
3. Tunel M, Cakmak S, Tamam L, et al. A case of simultaneous mania and idiopathic normal pressure hydrocephalus: Etiology or comorbidity? *Turkish Journal of Psychiatry* 2019;30:290–4. DOI: https://doi.org/10.5080/u23340
4. Ozturk BT, Guvendik T, Agac UN, et al. Gómez-López-Hernández syndrome: An adult case diagnosed after psychiatric symptoms. *Psychiatry Research Case Reports* 2023;2:100150. DOI: https://doi.org/10.1016/j.psycr.2023.100150

Images/Tables

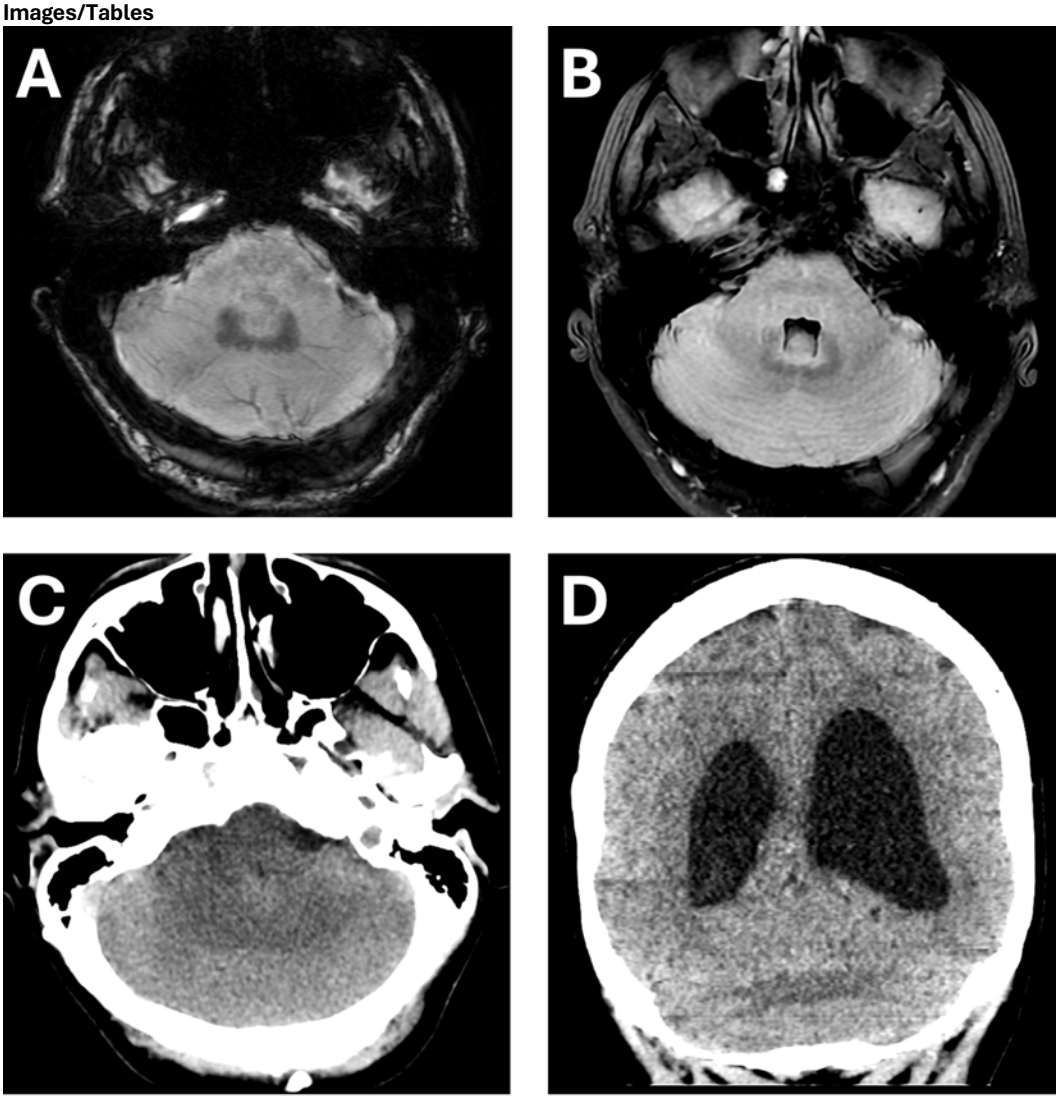

Figure. Axial susceptibility-weighted MRI reveals fusion of the dentate nuclei (A). On axial FLAIR images (B), the cerebellar vermis is absent and the cerebellar hemispheres are fused, with an abnormally shaped fourth ventricle. CT imaging in axial (C) and coronal (D) planes demonstrates midline fusion of the cerebellar hemispheres with continuous white matter across midline.

---

372 **Anti-NMDA Receptor Encephalitis: Subtle MRI Findings, Dramatic Outcomes — A Tale of Two Patients**

Prashant K Gupta MD, Robert Llanos MD
Newark Beth Israel Medical Center, Newark, NJ, USA

Clinical History

Two female patients presented with acute neuropsychiatric symptoms and were ultimately diagnosed with anti-NMDA receptor encephalitis.

Case 1: A 20-year-old woman developed abrupt agitation, bizarre behavior, and psychosis. CT head, CSF, and infectious studies were unremarkable. MRI brain showed subtle bilateral FLAIR hyperintensity in the medial temporal lobes, insulae, medial frontal lobes, and caudate nuclei as well as foci of FLAIR hyperintensity in bilateral frontal subcortical white matter without diffusion restriction or enhancement. CT abdomen revealed a right ovarian dermoid cyst. Serum anti-NMDAR antibody was positive (1:100). Despite high dose steroids, IVIG, and dermoid removal, she deteriorated with cardiac arrest and expired.

Case 2: A 15-year-old girl presented with seizures and encephalopathy. MRI brain showed similar bilateral FLAIR hyperintensities involving limbic and basal ganglia regions, with additional punctate foci of FLAIR hyperintensity in right frontal subcortical white matter. CT abdomen showed a left ovarian dermoid cyst. Serum and CSF were both positive for anti-NMDAR antibodies. After oophorectomy, steroids, IVIG, plasmapheresis, rituximab, and tocilizumab, she recovered significantly.

Imaging Findings

Both patients had normal initial CT heads but demonstrated subtle symmetric limbic (medial temporal lobes, insula, medial frontal lobes) and basal ganglia FLAIR hyperintensities as well as frontal subcortical white matter FLAIR hyperintense foci on MRI brain without diffusion restriction or enhancement.

CT abdomen/pelvis confirmed ovarian teratomas (dermoid cysts) in both, establishing a paraneoplastic trigger.

CT study also showed patchy lower lobe pneumonia in both, likely from aspiration or immunosuppression.

Discussion

Anti-NMDA receptor encephalitis is a potentially reversible autoimmune encephalitis, usually affecting predominantly young females, frequently associated with ovarian teratomas containing neural tissue. The disorder presents with psychiatric symptoms, seizures, dyskinesias, and autonomic instability.

MRI brain can be normal in up to > 50% of cases. When abnormal, nonspecific cortical and subcortical T2/FLAIR hyperintensities are seen without significant contrast enhancement or diffusion restriction with subsequent atrophy in follow up study, predominantly in the frontotemporal and cerebellar regions. Such findings, though subtle, are pivotal clues distinguishing autoimmune from infectious etiologies.

These two cases highlight how nearly identical imaging can lead to contrasting outcomes. Early recognition, prompt tumor removal, and aggressive immunotherapy can lead to complete recovery, whereas delayed diagnosis may be fatal. Radiologists play a key role in initiating the diagnostic cascade by recognizing this imaging pattern in young females with acute psychosis or encephalopathy.

Teaching Point

- Anti-NMDAR encephalitis should be considered in young females with acute psychosis or seizures and subtle limbic MRI abnormalities.
- MRI may reveal bilateral FLAIR hyperintensity in the medial temporal lobes, insulae, frontal cortices, and basal ganglia without enhancement or diffusion restriction.
- Normal CT does not exclude autoimmune encephalitis.
- Always search for an ovarian teratoma; its removal significantly improves prognosis.
- Early recognition and immunotherapy can lead to full recovery, while delays may be fatal.

References

1. Klontzas ME, Kearns C, Sheikhbahaei S, et al. Anti–NMDA-Receptor Encephalitis. *Radiographics* 2022;42(7):E199-E200. DOI: https://doi.org/10.1148/rg.220173
2. Hartung TJ, Bartels F, Kuchling J, et al. MRI findings in autoimmune encephalitis. *Rev Neurol (Paris)* 2024;180(9):895-907. DOI: https://doi.org/10.1016/j.neurol.2024.08.006

Images/Tables

CASE 1

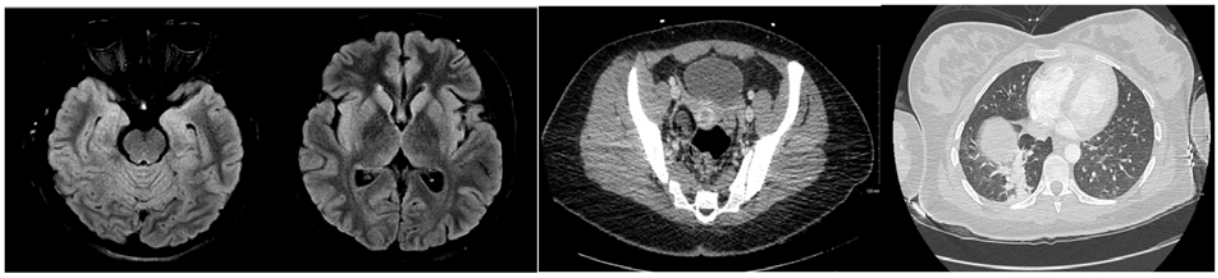

Image 1 shows symmetrically increased FLAIR signal intensity in bilateral medial temporal lobes. Image 2 demonstrates symmetrically increased FLAIR signal intensity in bilateral insula, medial frontal lobes and caudate heads along with bilateral frontal subcortical white matter FLAIR hyperintense foci. Image 3 demonstrates right adnexal dermoid. Image 4 shows right lower lobe consolidation.

CASE 2

Image 1 demonstrates symmetrically increased FLAIR signal intensity in bilateral medial temporal lobes. Image 2 shows symmetrically increased FLAIR signal intensity in bilateral insula, medial frontal lobes and caudate heads as well as right frontal subcortical white matter FLAIR hyperintense foci, not well seen in this image. Image 3 demonstrates left adnexal dermoid. Image 4 shows left>right lower lobe ground glass opacities.

375 Dual Energy Crisis: Dengue Encephalitis and Myelitis in a Teen with Underlying Mitochondrial Disease

Sawsan O Tabaza MD[1], Karen Moeller MD[2], Thierry Huisman MD[2], Nilesh Desai MD[2], Stephen Kralik MD[2], Lamson Tran[3], Huy B Tran MD[2]
[1]UTHealth Houston, Houston, Texas, USA. [2]Baylor College of Medicine, Houston, Texas, USA. [3]Texas A&M, Houston, Texas, USA

Clinical History

A 15-year-old boy with a confirmed NDUFV1 homozygous variant complex I deficiency (mitochondrial disease) and asthma became acutely ill during his holiday abroad. He manifested progressive respiratory distress, headache, fever, and diffuse joint pain. His situation deteriorated quickly; he became lethargic, unable to walk, and experienced seizure-like activity, which necessitated intubation. On examination, he became areflexic with weakness in his lower more than upper extremities.

Blood tests revealed leukopenia, thrombocytopenia, coagulopathy, and elevated creatine kinase (1480 U/L). Serology was positive for dengue IgM, confirming hemorrhagic dengue fever in its critical phase. A CT of the head revealed multifocal intraparenchymal and intraventricular hemorrhages. MRI of the brain and spine demonstrated findings consistent with encephalitis and cervicothoracic myelitis.

Because of his critical status and the risks of long-distance transfer, he was admitted to a tertiary pediatric center, where he was given high-dose intravenous methylprednisolone (1 g × 5 days), intravenous immunoglobulin, and plasma exchange. His neurological function gradually improved, and a follow-up MRI done three weeks later showed significant reduction in changes related to both encephalitis and myelitis. After three weeks of intensive neurorehabilitation, he was discharged home for outpatient therapy.

Imaging Findings

The initial MRI revealed T2/FLAIR hyperintensities with restricted diffusion and multifocal hemorrhages on SWI, findings consistent with hemorrhagic viral encephalitis. The cervical and upper thoracic spinal cord showed long-segment T2 hyperintensity and swelling, compatible with myelitis. Follow-up imaging demonstrated significant interval improvement with decreased edema and resolving hemorrhage.

Discussion

Dengue encephalitis is a rare but serious manifestation of dengue virus infection, reported in fewer than 1% of cases. Both dengue and mitochondrial disorders preferentially involve energy-dependent deep gray structures such as the thalami and brainstem, leading to overlapping imaging patterns. In this patient, the coexistence of mitochondrial energy failure and viral cytotoxic injury created a 'dual energy crisis,' resulting in extensive hemorrhagic and inflammatory changes.

Recognizing infectious overlap prevents misdiagnosis as metabolic flare, ensures confirmatory serology and CSF testing, guides safe management by avoiding anticoagulants or NSAIDs, and supports timely immunotherapy for optimal neurologic recovery.

Teaching Point

- Infectious encephalitis might be present along with metabolic disease, giving rise to the imaging findings that are different but similar.
- The signal from the bilateral thalamus together with the presence of petechial hemorrhage on SWI should make one think of dengue encephalitis rather than metabolic decompensation.
- Dengue serology or CSF PCR is necessary for the confirmation of CNS infection.
- Due to the risk of bleeding, refrain from using anticoagulants and NSAIDs; immunomodulatory therapy might support recovery.
- This case illustrates the neuroradiologist's function in detecting the twofold mechanisms of injury, viral and mitochondrial, in the same deep gray matter areas, thus directing timely and safe patient management.

References

1. Carod-Artal FJ. Neurological complications of dengue virus infection. *Lancet Neurol.* 2013;12(9):906-919. doi:10.1016/S1474-4422(13)70150-9
2. Soares CN, Cabral-Castro MJ, Peralta JM, Freitas MR, Puccioni-Sohler M. Neurologic manifestations of dengue infection: a case series and review of the literature. *Neurology.* 2011;77(6):624-630. doi:10.1212/WNL.0b013e318228c136
3. Chung CC, Lee WT, Chen C, et al. MRI findings in dengue encephalitis. *Neuroradiology.* 2017;59(9):921-928. doi:10.1007/s00234-017-1871-4
4. Uttal L, Nascene DR, Flanagan SR, et al. MR imaging of pediatric mitochondrial disorders: pattern recognition. *Radiographics.* 2020;40(4):1047-1065. doi:10.1148/rg.2020190169
5. Chakravarty A, Dubey S, Kumar S, et al. Dengue myelitis: MRI features and short-term outcome. *J Neurol Sci.*2014;346(1-2):176-180. doi:10.1016/j.jns.2014.08.005

Images/Tables

FIG. 1. Multifocal intracranial hemorrhage. **A.** Coronal noncontrast CT demonstrates parenchymal hematomas in the right frontal lobe. **B.** T1WI without contrast also demonstrates small IVH (arrow). **C.** T2WI without contrast demonstrates additional parenchymal hematoma in the left temporal lobe with surrounding edema (arrow).

FIG. 2. Parenchymal findings of mitochondrial complex 1 deficiency on axial FLAIR images. **A.** Increased T2/FLAIR signal in the bilateral dentate nucleus (arrow, right dentate nucleus). **B.** Increased T2/FLAIR signal in the periaqueductal grey matter (arrow). **C.** Increased T2/FLAIR signal in the medial thalami (arrow) and subcortical white matter of the frontal lobes (asterisk) and the corpus callosum.

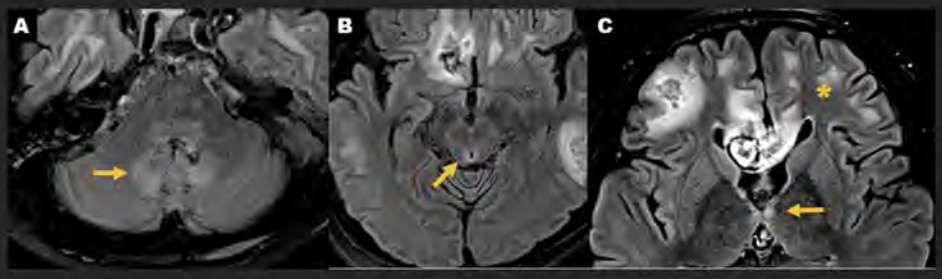

FIG. 3. Spine findings that are in keeping with the history of mitochondrial disorder. A. Sagittal T2WI shows hyperintense signal in the dorsal cord (arrow). B. Hyperintense signal in the central grey matter and posterior columns on axial T2WI. C. There is patchy enhancement in the cord on the postcontrast sagittal T1WI (arrows).

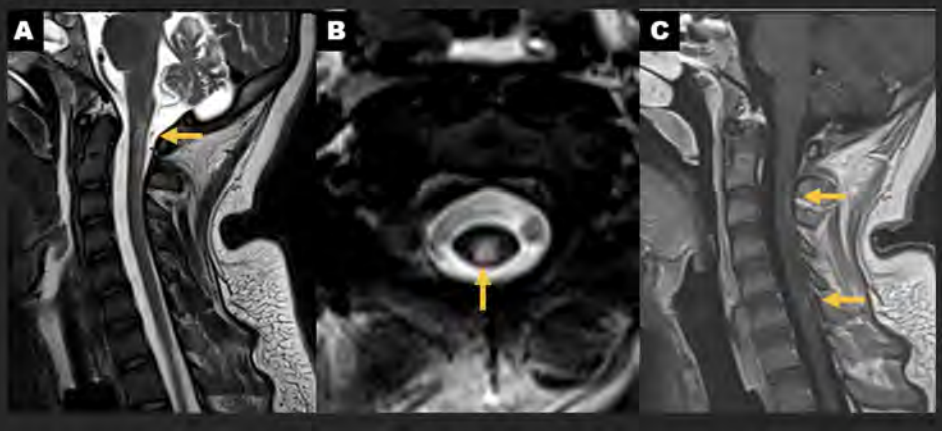

377 When Pumping Iron Gets You Weaker: Beta-Propeller Protein-Associated Neurodegeneration

Richard Liang DO, Paul K Lee MD
Northwell Health/Long Island Jewish Hospital, New Hyde Park, NY, USA

Clinical History

A 15-year-old female patient presented with seizures, spastic quadriparesis (lower extremities greater than upper extremities), and vision impairment. The patient also exhibited global developmental delay since infancy. Previous brain MRIs were essentially unremarkable, except for mild cerebral and cerebellar volume loss. An electroencephalogram (EEG) demonstrated bilateral cerebral slowing and bitemporal spikes, raising concerns for a generalized seizure disorder. Recently, genetic testing identified a mutation in the WDR45 gene. A follow-up brain MRI was subsequently ordered.

Imaging Findings

A non-contrast-enhanced MRI of the brain demonstrated pronounced hypointense susceptibility signal in the bilateral globus pallidus and substantia nigra. There was also hypointense T2 signal in the same regions. These findings suggest a disorder of neurodegeneration with brain iron accumulation (NBIA).

Discussion

Beta-propeller protein-associated neurodegeneration (BPAN) is a rare disorder of NBIA that presents with global developmental delay, seizures, autistic-like features, and movement disorders. It is estimated to affect 1 in 2-3 million individuals and is more prevalent in females. While imaging may appear normal in early childhood, some subtle early findings include a thinned corpus callosum, cerebellar and cerebral atrophy, and delayed myelination. When imaging is performed later in childhood, typical findings include T2 and susceptibility-weighted hypointense signal in the globus pallidus and substantia nigra, corresponding to iron deposition. Signal abnormalities in the substantia nigra may appear more prominent than that of the globus pallidus. Genetic testing reveals a pathogenic variant in the WDR45 gene, an X-linked gene involved in autophagy. Other NBIA disorders, such as pantothenate kinase-associated neurodegeneration (PKAN), can demonstrate similar MRI findings to BPAN, with differentiation based on the affected gene.

Teaching Point

Neuroimaging combined with genetic testing is essential for diagnosing disorders of NBIA, such as BPAN. Although imaging may be normal in early childhood, follow-up imaging later in childhood is important for diagnosis.

References

1. Larsh T. Characteristic Neuroimaging Findings in β-propeller Protein-associated Neurodegeneration. J Pediatr Neurosci. 2021;16(3):264-265. doi:10.4103/jpn.JPN_161_20
2. Chiapparini L, Zorzi G. Early Neuroimaging Markers in β Propeller Protein-Associated Neurodegeneration. AJNR Am J Neuroradiol. 2022;43(12):1815-1816. doi:10.3174/ajnr.A7723
3. Papandreou A, Soo AKS, Spaull R, Mankad K, Kurian MA, Sudhakar S. Expanding the Spectrum of Early Neuroradiologic Findings in β Propeller Protein-Associated Neurodegeneration. AJNR Am J Neuroradiol. 2022;43(12):1810-1814. doi:10.3174/ajnr.A7693

Images/Tables

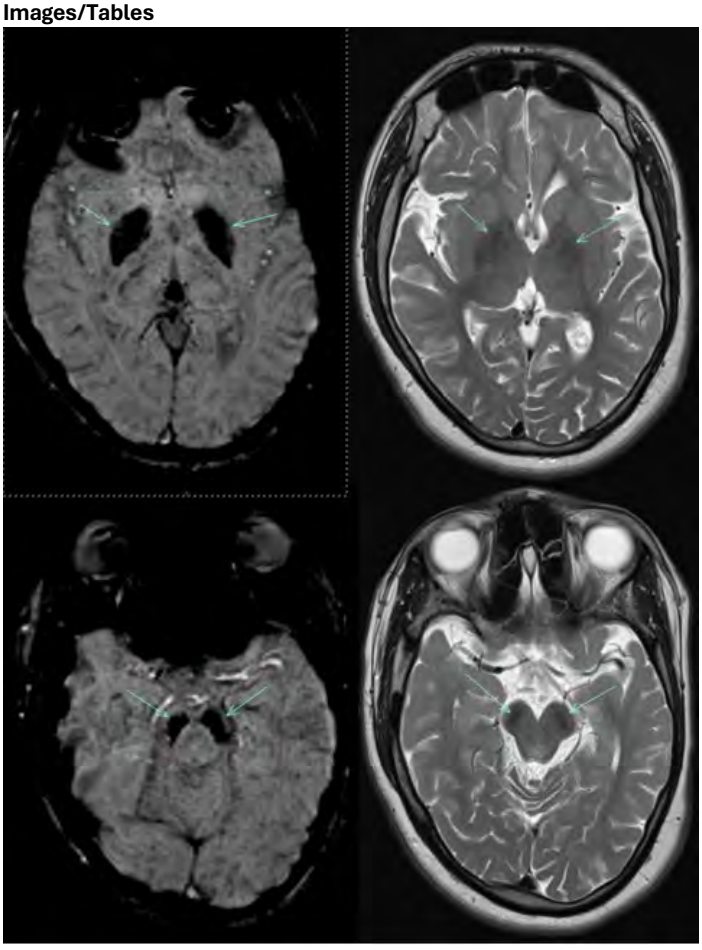

381 Cerebral Amyloidoma: A Rare Mimic of Infiltrative and Neoplastic Intracranial Lesions

Dhruv Shetty MBBS, Prasanna Vibhute M.D., Amit Desai M.D., Neetu Soni M.B.B.S., M.D.
Mayo Clinic, Jacksonville, Florida, USA

Clinical History

We reviewed 10 patients (9 female, aged 43–74) with histologically confirmed CA. Presenting symptoms—varying by lesion location—included aphasia, cognitive decline, confusion, seizures, motor and gait disturbances, visual deficits, headaches, and paresthesia. Initial differential diagnoses were broad, including CNS lymphoma, primary tumors, neurosarcoidosis, infection, demyelination, and vasculitis. All underwent brain biopsies confirming Congo red–positive amyloid with apple-green birefringence. Seven had no evidence of systemic amyloidosis on further workup.

Imaging Findings

MRI in a majority of the 10 patients showed solitary lesion in subcortical or periventricular white matter of the frontal, parietal, or occipital lobes; less often in basal ganglia, thalamus, cerebral peduncles, pons, or cerebellum. Lesions appeared iso- to hypointense on T1, typically hypointense on T2, exhibited homogenous or heterogeneous post-contrast enhancement with minimal perilesional edema and mass effect and absent diffusion restriction. CT often showed poorly defined lesions, sometimes with hyperattenuating calcifications.MR spectroscopy (one patient) showed broad peaks without clear NAA or creatinine. FDG PET (one patient) revealed focal photopenia, and Amyvid PET CT (one patient) showed little to no amyloid-β deposition. Of nine patients with follow-up imaging, three had mild progression, indicating cerebral amyloidoma's indolent nature.
Image caption: Histopathologically proven left frontal lobe cerebral amyloidoma T1, T2 and FLAIR hypointense with heterogeneous enhancement, minimal perilesional edema without mass effect. Corresponding lesion is hyperattenuating on CT. Amyloid deposits in the brain biopsy specimens demonstrate Congo red positivity (black arrow in F).-

Discussion

Cerebral amyloidomas are rare brain lesions, can mimic aggressive lesions on imaging, making diagnosis difficult without histopathological confirmation. Amyloidoma should be considered for atypical, enhancing white matter lesions with minimal edema. While FDG PET and amyloid PET can assist in characterization, but are not standard diagnostic tools. Most cases are stable or improve after surgical resection, with a low risk of recurrence or systemic amyloidosis; gross-total resection offers the best prognosis. No malignant transformation or systemic spread has been reported. Imaging surveillance is important, as recurrence is rare but possible. Longitudinal imaging supports their typically indolent course, with only mild progression observed in a minority of patients. These findings highlight the need to recognize CA's imaging features for accurate diagnosis and management.

Teaching Point

- Cerebral amyloidomas typically exhibit a characteristic MRI appearance and should not be mistaken for primary brain tumors, lymphoma, or tumefactive demyelination.
- Definitive diagnosis requires tissue sampling with Congo red staining demonstrating apple-green birefringence.
- CT: hyperattenuating white matter masses with calcifications; MRI: T1/T2 hypointense, enhancing lesion with little perilesional edema and mass effect.
- No specific serum biomarkers; systemic workup usually negative.
- Recognizing amyloidoma avoids unnecessary aggressive therapy.
- Most cases are stable; prognosis is excellent post-resection.

References

- Rincón-Arias N, Romo JA, Galvis KA, et al. Long-Term Progression of a Residual Cerebral Amyloidoma: An Illustrative Case and Systematic Review. *World Neurosurg*. 2024;190:e1100-e1115. doi:10.1016/j.wneu.2024.08.081
- Miller-Thomas MM, Sipe AL, Benzinger TL, et al. Multimodality Review of Amyloid-related Diseases of the Central Nervous System. *Radiographics*. 2016;36(4):1147-1163. doi:10.1148/rg.2016150172

Images/Tables

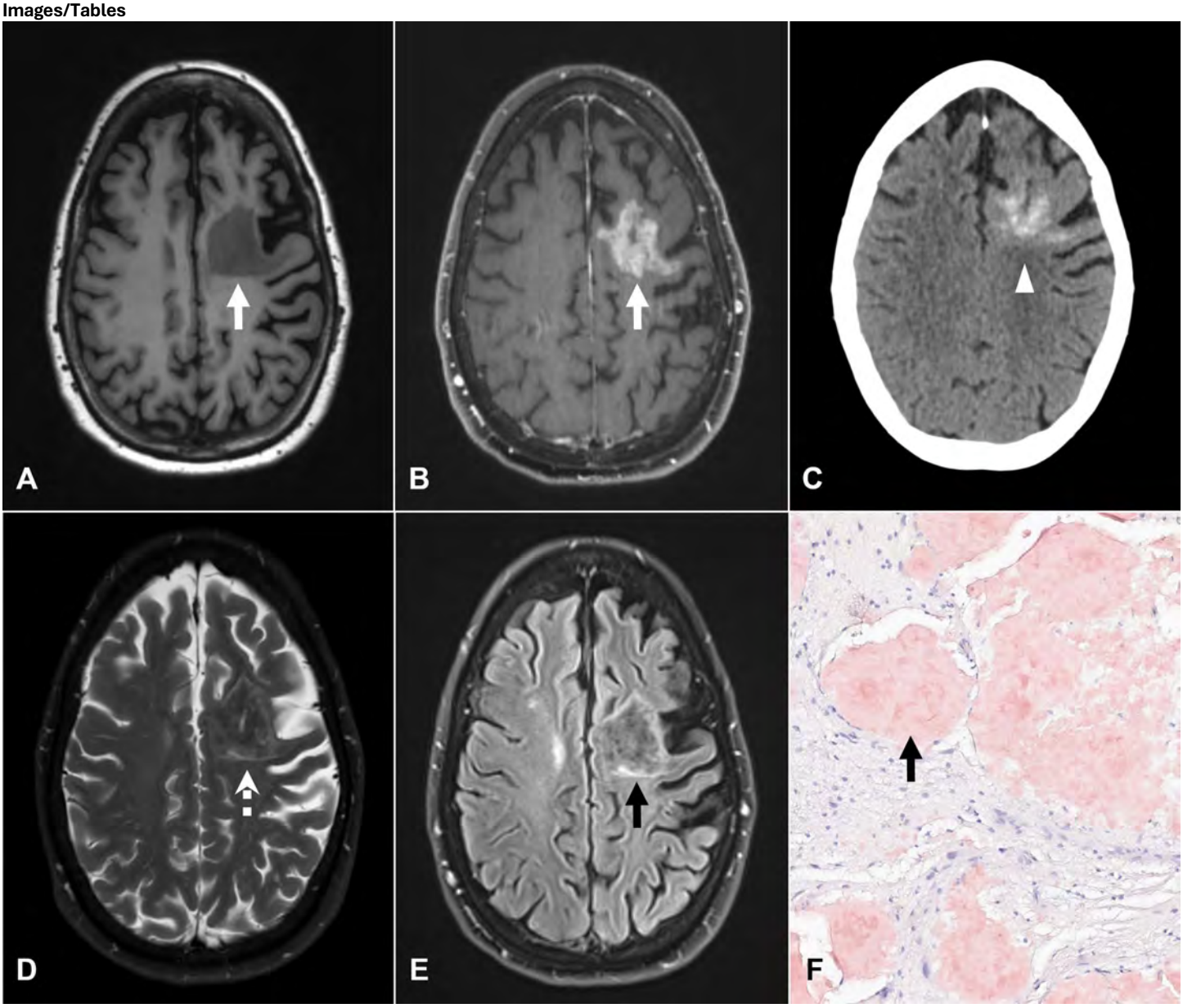

386 A Rare Case of Accessory Extraocular Muscle with Restrictive Strabismus

Shruti Kumari MD, Ameya Nayate MD
University Hospitals, Case Western Reserve University, Cleveland, OH, USA

Clinical History

A 4-year-old boy was referred for evaluation of vertical primary restrictive strabismus (supraduction deficit (movement is turning in) associated with head tilt (chin up)) in the left eye. MRI orbits with IV contrast were performed and demonstrated findings consistent with an anomalous extra-ocular muscle (AEM) (Figs. 1 and 2). The patient had a left inferior rectus disinsertion/reinsertion and orbital band biopsy which showed a left eye anomalous muscle band. In the follow-up surgery, left orbital accessory muscle myectomy was performed and sent for pathological analysis (Fig. 3). A month later, the final surgical procedure with accessory muscle band release was performed and patient showed improved visual acuity (20/20), good alignment (orthotropic in primary gaze) with moderate to severe (-2-3) limitation of supraduction of the superior oblique muscle remaining.

Imaging Findings

MRI orbits show a left intraconal lesion isointense to extraocular muscles on T1, with similar enhancement on post-contrast images extending to the orbital apex. Histology shows skeletal muscle fibers in fascicles.

Discussion

We present a rare finding of AEM in the left eye that caused restrictive strabismus and head tilting, with histopathological analysis and MRI being used to confirm the findings and surgical resection improving symptoms. To our knowledge, this is the first case which concurrently shows the MRI with contrast findings along with histopathology of the AEM in a single patient. As higher-resolution orbital imaging is increasingly used in the evaluation of strabismus, supernumerary AEMs inevitably will be encountered. preoperative recognition can better inform surgical management decisions especially since there are a few instances of AEMs detected during surgery, prompting an abrupt change in surgical plan.

Etiology of AEM remains unclear. In 1911, Whitnall proposed that AEMs may represent an atavistic retractor bulbi muscle, normally found in reptiles, amphibians, and some ruminants, originating at the orbital apex and inserting on the posterior surface of the ocular globe. Another hypothesis suggests that these structures might occur as a result of anomalous innervation of the primitive extraocular muscles during embryogenesis. AEM may

represent extraocular muscle tissue that was never properly innervated or lost innervation during development. The factors which favor the AEM being a vestigial remnant of retractor bulbi include the origin from the orbital apex with forward extension to insert on the sclera underneath, the conical shape and location between the optic nerve and inferior rectus muscle. However, the poor characterization of whether eyeball retraction is present and the absence of multiple tendon slips surrounding the optic nerve do not favor this theory.

Teaching Point

AEMs are a rare cause of strabismus. We present MRI and histopathology findings of AEM in a pediatric patient who presented with restrictive strabismus of the left eye. The presence of an AEM should be included in the differential diagnosis of patients with atypical restrictive strabismus, especially when globe retraction is observed with the patient looking straight ahead and confirmed with MRI orbits with IV contrast. Awareness of such anomalies can improve the search pattern of radiologists evaluating patients with atypical strabismus as these are amenable to surgical resection.

References

1. Lueder GT, Dunbar JA, Soltau JB, Lee BC, McDermott M. Vertical strabismus resulting from an anomalous extraocular muscle. *J AAPOS*. 1998;2(2):126-128. doi:10.1016/s1091-8531(98)90078-7
2. Khitri MR, Demer JL. Magnetic resonance imaging of tissues compatible with supernumerary extraocular muscles. Am J Ophthalmol. 2010;150(6):925-931. doi: 10.1016/j.ajo.2010.06.007
3. Lueder GT. Anomalous orbital structures resulting in unusual strabismus. *Surv Ophthalmol*. 2002;47(1):27-35. doi:10.1016/s0039-6257(01)00285-5
4. Chaves AC, Paiva C, Carvalho S. Accessory Extraocular Muscle: A Rare Cause of Strabismus. *J Belg Soc Radiol*. 2024;108(1):109. Published 2024 Nov 30. doi:10.5334/jbsr.3807
5. Dobbs MD, Mawn LA, Donahue SP. Anomalous extraocular muscles with strabismus. *AJNR Am J Neuroradiol*. 2011;32(9): E167-E168. doi:10.3174/ajnr. A2291

Images/Tables

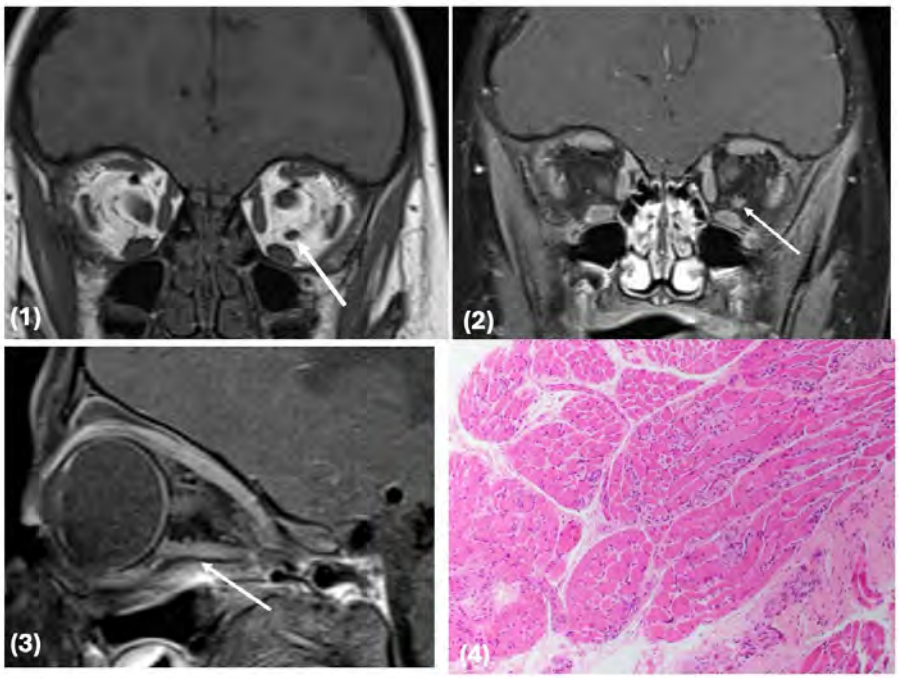

Fig. 1: MRI orbits. Coronal T1 without contrast. White arrow depicts a structure in the left intraconal fat with similar appearance and signal as the extra-ocular muscles. Figs. 2 and 3: MRI orbits, coronal and sagittal T1 post contrast. White arrows depict structures in the left intraconal fat with similar enhancement and appearance as the extra-ocular muscles. Figure 3 depicts the posterior extent of the structure to the orbital apex. Fig 4.: H&E showing skeletal muscle fibers arranged in fascicles with mild variation in fiber size (10x magnification).

---

389 Rare Case of Aortic Spinal Fistula

Aman Jaiswal MD

UTHealth Houston, Houston, Texas, USA

Clinical History

A 69-year-old male with history of remote cervical spine injury and subsequent quadriplegia, hypertension, atrial fibrillation, and recent fall with spinal fracture presented for elevated blood pressure with systolic measurements greater than 180 mmHg over the days prior to presentation. The patient became hemodynamically stable in the ED. Limited chart review from an outside institution revealed the patient had a Chance fracture at L2 3 months prior. Imaging at this current admission demonstrated an aortic spinal fistula at the L1-L2 level. Given the patient's co-morbidities and need for a high-risk open surgical approach, the patient and his family decided on hospice and comfort care measures.

Imaging Findings

CTA chest, abdomen and pelvis: There is a background of nearly completely fused and ankylosed rigid spine. There are abnormally distracted, angulated, and remodeled L1 and L2 vertebral bodies with adjacent new bone formation. Vascular outpouching from the posterior aspect of the abdominal aorta at L1-L2 (A) with extravasation of contrast filling the distracted space between the L1-L2 vertebral body osseous elements and extending posteriorly towards the spinal canal (B, C). These findings are consistent with ruptured aortic pseudoaneurysm.

MRI entire spine without IV contrast: Redemonstrated nearly completely ankylosed rigid spine and distracted remodeled L1-L2 vertebral bodies. T2 hypointense lobulated signal consistent with hemorrhage fills the distracted space between the L1-L2 vertebral body osseous elements and corresponds to the ruptured pseudoaneurysm/contrast extravasation on CT (D). The hemorrhage continues from the aorta, through the osseous elements, and into the spinal canal. Hemorrhage fills the thecal sac from L2 through the sacral spinal canal with dark T2 hemorrhage surrounding the cauda equina nerve roots (D, E) as well as the inferior conus medullaris (D, F). These findings are consistent with aortic spinal fistula. Of note, there is prior cervical spinal cord injury with myelomalacia from C5-C7 (G).

Discussion

Many cases of aortic fistula described in the literature include aortoenteric fistulas but very few between the aorta and spinal column, and often in the context of a prior aortic aneurysm repair. This case presents a rare example of an aortic spinal fistula with connection from the posterior aspect of the abdominal aorta to the spinal canal and thecal sac. The patient's ankylosed and rigid spine in the context of remote cervical spinal cord injury is consistent with Charcot spine. A background of Charcot spine and recent history of Chance fracture at L2 likely led to the L1-L2 osseous abnormality and contributed to creation of the aortic spinal fistula.

Teaching Point

Aortic spinal fistula is a rare variant of aortic fistula that may be seen in the background of Charcot spine and recent vertebral fracture. Imaging characteristics associated with the fistulous tract through the vertebral column can potentially mimic other pathologies of the spine such as discitis/osteomyelitis and malignancy.

References

Farnsworth P, Bailey K, Baardsen E, et al. An aortic wall to vertebral body fistula presenting as a lytic lesion. *J Radiol Case Rep* 2020;14:1-9. DOI: https://doi.org/10.3941/jrcr.v14i9.3270

Images/Tables

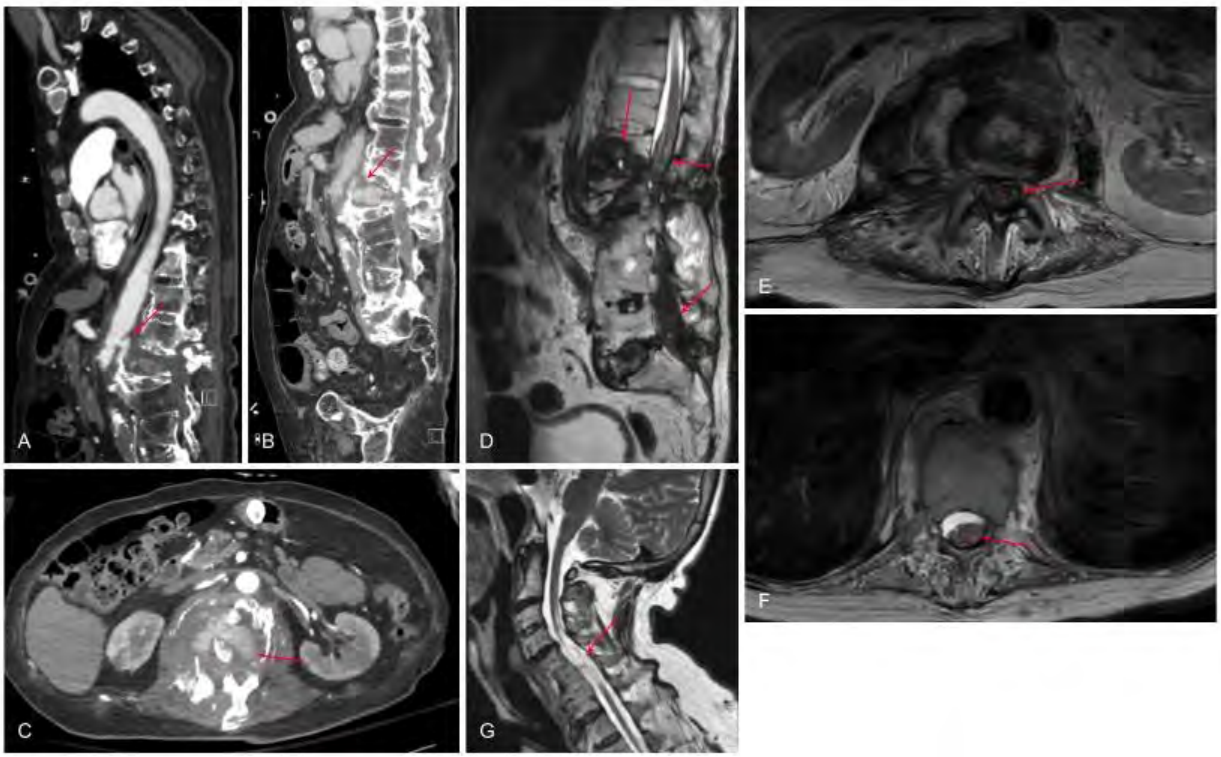

---

399 Eye Don't Believe It - A Curious Case of Orbital Lipolysis

Newton V Nagirimadugu MD, Kavin D Mistry MD, Israel L Saramago MD
St. Luke's University Health Network, Bethlehem, PA, USA

Clinical History

A 37 y/o male with diabetes, chronic pancreatitis, and a BMI of 19 presented due to hyperglycemia complicated by hyperglycemic hyperosmolar state (HHS). A CT head without contrast was ordered. Abnormal imaging findings prompted a follow up MRI brain and orbits with and without contrast.

Imaging Findings

Axial and coronal noncontrast CT images demonstrate diffuse inflammatory changes involving both the intraconal and extraconal orbital fat and visualized subcutaneous facial fat (A, B).

On MR, T2-weighted Dixon water-only images show increased signal within the orbital fat and visualized subcutaneous temporal fat (C), while T1-weighted Dixon fat-only post-contrast images demonstrate diffusely infiltrative enhancement in these regions on a background that appears to have regions of fat saturation (D). Axial FLAIR and T2-weighted fast spin echo sequences confirm persistently increased signal in the same regions (E, F). Coronal T2 orbits fat saturated sequence demonstrates symmetrically bright signal in both orbital fat and subcutaneous facial fat (G) and the coronal T1 orbits precontrast image demonstrates diffusely decreased signal in regions involved by fat which should be bright (I) – opposite to expected findings. These findings are characteristic of the "pseudo fat-saturated" appearance. On the T1-weighted Dixon fat only postcontrast images (H, J), there is symmetrically diffuse infiltrative enhancement in both orbital fat and visualized subcutaneous facial tissues. Finally, axial post-contrast 3D

T1-weighted images with obliqued reformats demonstrate symmetric optic nerve sheath enhancement involving optic nerves, orbital apices, canalicular segments, and optic chiasm (K). These findings reflect a diffuse edematous infiltrative enhancing process with loss of the normal fat signal on fat only and T1 imaging.

Discussion

Orbital lipolysis is most often described in the context of anorexia nervosa, though it may occur in any patient with malnutrition (1). These patients exist in a global catabolic state with increased metabolic demand that drives adipose breakdown. The process of fatty acid degradation produces oxidative stress and chronic inflammation, which contributes to the abnormal orbital fat signal seen on imaging. Increased endothelial permeability has been proposed as an additional mechanism, accounting for enhancement of the fat (2).

On CT, orbital lipolysis appears as decreased orbital fat volume with variable attenuation and occasional inflammatory stranding. MRI demonstrates altered fat signal and enhancement without a discrete soft tissue mass. In advanced disease, nearly complete fat destruction can produce a so-called "pseudo–fat sat" effect, where the orbit mimics fat suppression not because of pulse sequencing, but due to lipolysis itself (3, 4). The differential diagnosis includes thyroid ophthalmopathy, sclerosing orbital pseudotumor, silent sinus syndrome, chronic corticosteroid exposure, post-radiation or postsurgical change, lymphoma, metastasis, and scirrhous orbital tumor. Unlike most of these processes, orbital lipolysis is characterized by progressive enophthalmos rather than proptosis. Scirrhous breast cancer metastasis and silent sinus syndrome represent notable exceptions, as both can also cause enophthalmos (5).

Teaching Point

Orbital lipolysis should be considered in malnourished patients, as it presents with enophthalmos rather than the more typical proptosis of orbital disease. CT and MRI generally demonstrate nonspecific inflammatory enhancing changes in all fat tissues with a characteristic "pseudo–fat sat" appearance.

References

1. Demaerel P, Daele MC, De Vuysere S, et al. Orbital fat edema in anorexia nervosa: a reversible finding. AJNR Am J Neuroradiol 1996;17:1782–4.
2. Demaerel P, Dekimpe P, Muls E, et al. MRI demonstration of orbital lipolysis in anorexia nervosa. Eur Radiol 2002;12:S4–6.
3. Yu S, Kwong WK, Law YY, et al. Pseudo fat-saturation and orbital lipolysis in cancer cachexia: a diagnostic trap. Hong Kong Med J https://doi.org/10.12809/hkmj2310913.
4. Kalelioglu T, Patel SH. Orbital Lipolysis. Radiology 2023;307:e221947.
5. Novitskaya E, Rene C. Enophthalmos as a sign of metastatic breast carcinoma. CMAJ 2013;185:1159.

Images/Tables

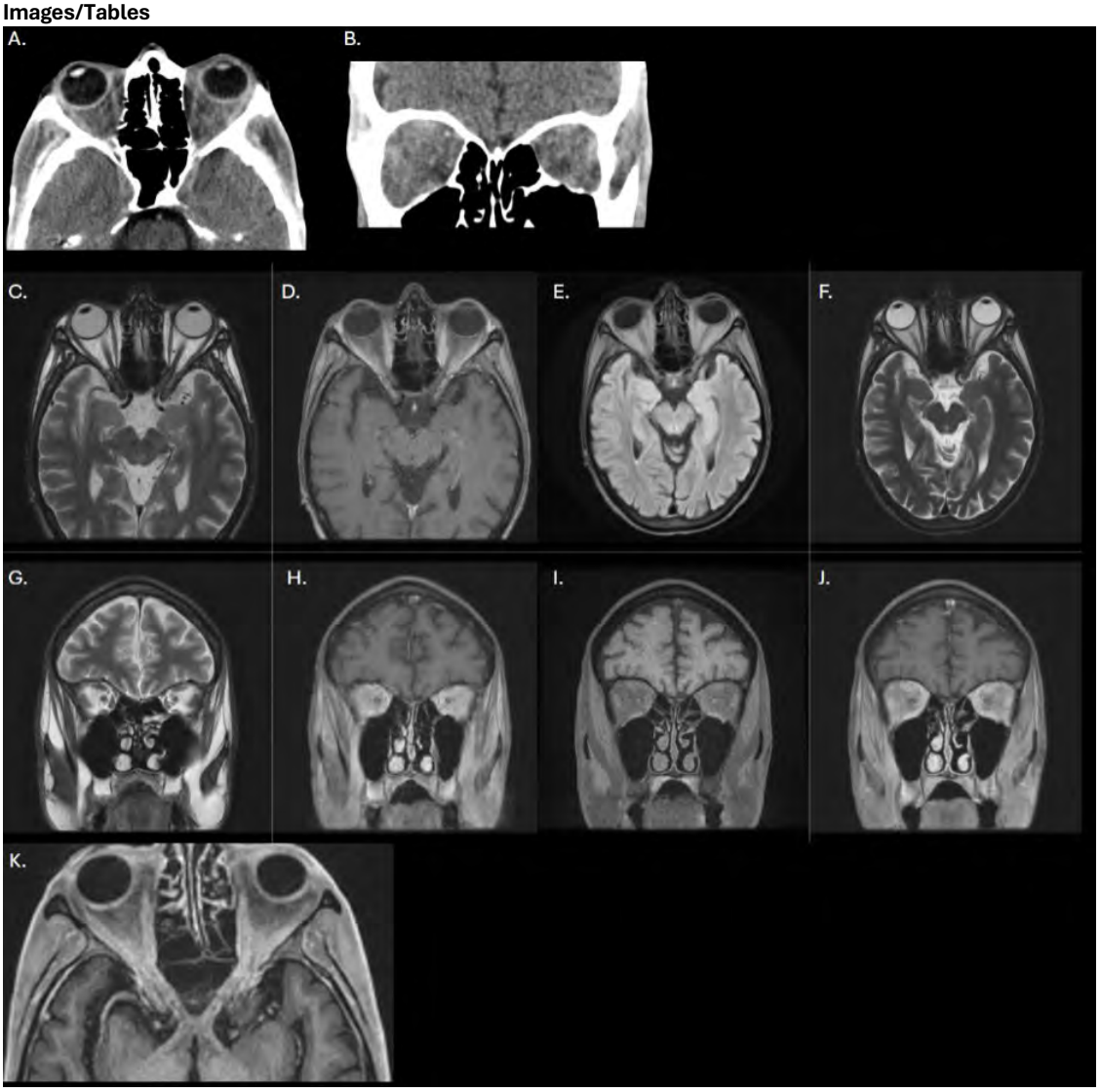

408 Recurrent Middle Cranial Fossa Epidermoid Cyst with MCA Involvement: Importance of Long-Term Follow-Up

D'Shaun Adams MD, Anthony Santisi MD
Cooper University Hospital, Camden, NJ, USA

Clinical History

A 33-year-old male presented to the emergency department with seizures. Imaging revealed a left middle cranial fossa mass consistent with epidermoid cyst. The patient underwent surgical resection including careful dissection of mass off of left proximal middle cerebral artery (MCA) branches. The mass had a 'pearly white' macroscopic appearance. Pathology was consistent with epidermoid cyst. Post-operative computed tomography (CT) scan (not shown) demonstrated expected post-surgical findings. Post-operative magnetic resonance imaging (MRI) was not performed. The patient presented to the emergency department following an assault, 13 months after surgery. Imaging revealed residual/recurrent epidermoid cyst, new chronic infarcts in the left corona radiata and severe left MCA stenosis. The patient underwent re-resection, with biopsy-proven residual/recurrent epidermoid cyst, and indirect extracranial–intracranial (EC–IC) bypass. On outpatient follow-up, the patient has been seizure-free and clinically doing well.

Imaging Findings

Figure 1) MRI of the brain with axial diffusion-weighted (DWI (a) and ADC (b)), FLAIR (c) and post-contrast T1 fat-saturated (d) sequences at initial presentation reveals a non-enhancing mass in the left middle cranial fossa which restricts diffusion and demonstrates heterogeneous/'dirty' signal on FLAIR. Imaging features are consistent with epidermoid cyst.

Figure 2) Follow up MRI with axial diffusion-weighted (DWI (e) and ADC (f)) and FLAIR sequences (g and h) demonstrates incomplete FLAIR suppression of the resection cavity with layering fluid-fluid level which restricts diffusion. Findings are suspicious for residual or recurrent epidermoid cyst. There are also new chronic infarcts in the left corona radiata, an internal border zone. Figure 3) CT angiography of the head (i) reveals severe left MCA stenosis, confirmed on digital subtraction angiography (j).

Discussion

Intracranial epidermoid cysts are rare, benign, and usually congenital lesions, accounting for ~1% of intracranial tumors [1]. Rarely, epidermoid cysts can be acquired following surgery/trauma. An epidermoid cyst arises from ectodermal inclusion of epithelial cells during neural tube closure between the 3rd-5th weeks of embryogenesis. The inclusion gradually desquamates keratin and cholesterol over time, leading to the formation of a slow-growing cyst lined by stratified squamous epithelium. Epidermoid cysts most commonly involve the cerebellopontine angle cistern (40–50%), parasellar/suprasellar region (10–15%), and posterior fossa (10–15%). Middle cranial fossa involvement is relatively rare, representing approximately 5–10% of reported cases [2].

When located in the middle cranial fossa, epidermoid cysts can mimic arachnoid cysts or cystic neoplasms on imaging. Clinical presentation may include seizures due to proximity to the temporal lobe. Proximity to the MCA and its branches raises concern, as large or recurrent lesions may cause vessel encasement, narrowing, and/or ischemic complications, as seen in this case. Complete surgical resection can be challenging because of adherence to neurovascular structures. Subtotal resection increases the risk of recurrence (~21%) which underscores the importance of long-term surveillance imaging [3].

Teaching Point

Although benign, epidermoid cysts can demonstrate clinically significant recurrence if not completely resected. Although rare, when occurring in the middle cranial fossa, patients may present with symptoms of seizures or vascular compromise. Long-term imaging surveillance is critical to detect recurrence and prevent neurologic complications.

References

Chen S, Ikawa F, Kurisu K, *et al.* Quantitative MR evaluation of intracranial epidermoid tumors by fast FLAIR and echo-planar DWI. AJNR Am J Neuroradiol 2001;22:1089-96.

Osborn AG, Preece MT. Cerebral epidermoid tumors. Radiology 2006;239:650-64. DOI: https://doi.org/10.1148/radiol.2393050823

Shear BM, Jin L, Zhang Y, *et al.* Extent of resection of epidermoid tumors and risk of recurrence: case report and meta-analysis. J Neurosurg 2020;133:291-301. DOI: https://doi.org/10.3171/2019.4.JNS19598

Images/Tables

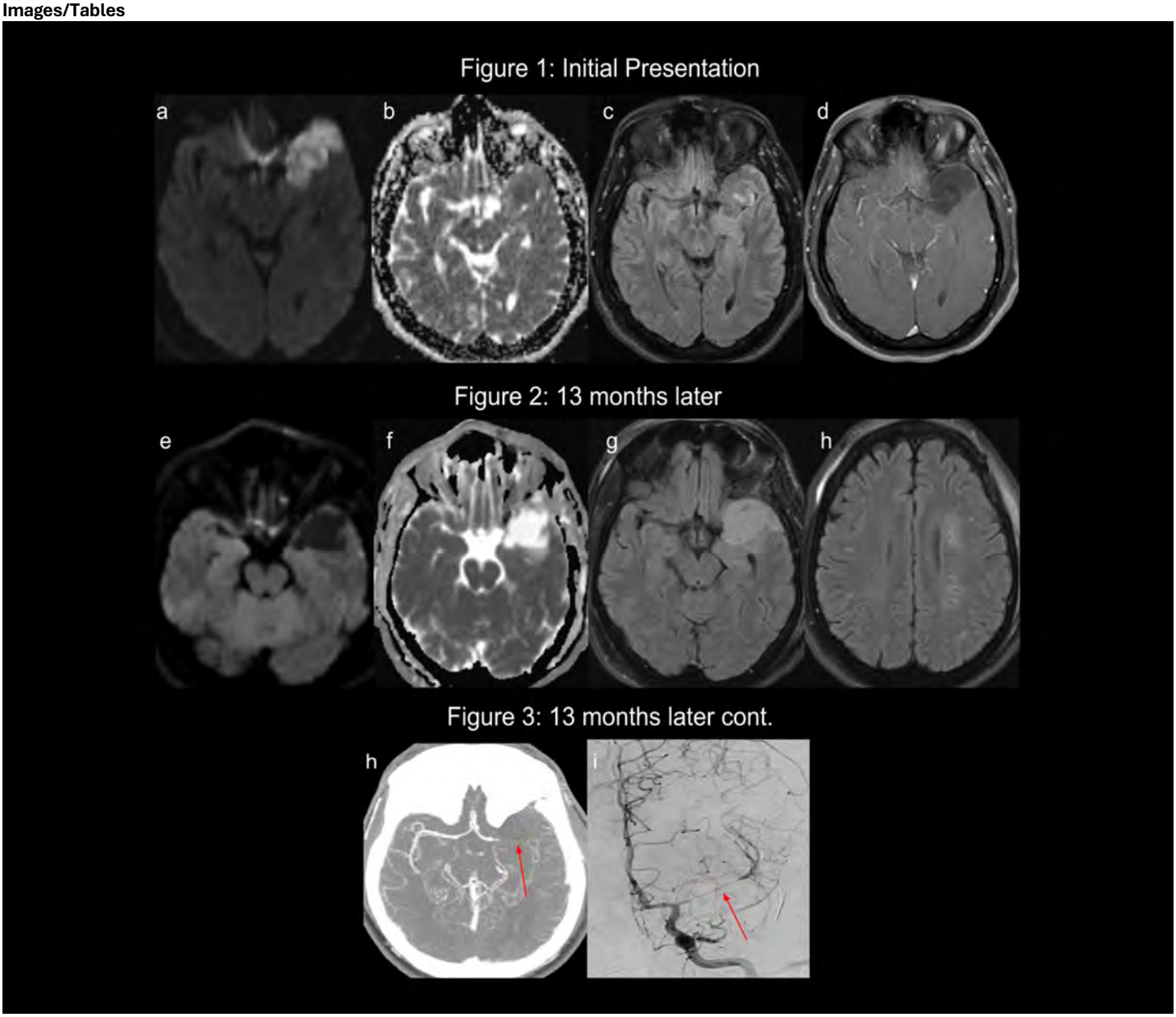

416 Imaging Evolution of SMARCB1-Deficient Sinonasal Carcinoma Treated with Radiosurgery

Roshan Gill Medical Doctor[1], Brandon Friedman D.O.[2], Alec Brown D.O.[1], Jessica Telleria-Cano Medical Doctor[1]
[1]Larkin Community Hospital, Miami, FL, USA. [2]Larkin Community Hospital, South Miami, Florida, USA

Clinical History

A 40-year-old woman presented in November 2024 with persistent headaches during pregnancy. MRI at that time demonstrated diffuse left frontal sinus opacification and a probable sphenoid retention cyst. She was referred to otolaryngology for further evaluation. A subsequent CT of the face revealed osseous destruction involving the frontoethmoidal region. The patient underwent endoscopic biopsy on May 27, 2025, which demonstrated SMARCB1-deficient sinonasal carcinoma (SDSC).

Preoperative PET/CT and MRI of the face obtained on June 2, 2025, confirmed the extent of disease. The patient underwent radiosurgery on June 13, 2025, followed by adjuvant chemotherapy. Follow-up imaging was performed on September 25, 2025.

Imaging Findings

Figures A and B represent preoperative studies from June 2, 2025. Figures C and D represent postoperative studies from September 25, 2025.

Preoperative:

Axial T1-weighted images demonstrate a mass centered in the left frontal sinus with extension through both the inner and outer tables of the frontal bone (A). Axial fat-saturated post-gadolinium T1-weighted images reveal an enhancing mass involving the left frontal scalp soft tissues and bilateral frontal sinuses (left greater than right), with associated bilateral enhancing dural thickening (B).

Postoperative:

Axial T1-weighted images demonstrate a decreased size of the mass centered in the left frontal sinus with reduced extension through the outer table (C). Axial MPRAGE sequences show a marked interval decrease in the size of the lesion and significant reduction in bilateral dural thickening and enhancement (D).

Discussion

SMARCB1-deficient sinonasal carcinoma (SDSC) is a rare and highly aggressive malignancy of the sinonasal tract characterized by inactivation of the SMARCB1 tumor suppressor gene, a core component of the SWI/SNF chromatin remodeling complex. Patients typically present with nonspecific symptoms such as facial pain or headache, and disease is often advanced at diagnosis.

SDSC frequently demonstrates extensive local invasion involving multiple paranasal sinuses, and is associated with high rates of recurrence, locoregional spread, distant metastasis, and poor prognosis.

The standard of care involves multimodal therapy, including radical surgical resection and adjuvant chemotherapy. While radiotherapy is not traditionally a first-line modality, emerging evidence suggests a role for stereotactic radiosurgery in unresectable or recurrent cases, or as part of a palliative approach.

This case demonstrates the imaging characteristics of SDSC before and after radiosurgery, illustrating notable tumor volume reduction and decreased dural enhancement, supporting the potential value of radiosurgery as an adjunctive treatment in select patients.

Teaching Point

Imaging plays a critical role in both the preoperative and postoperative evaluation of SMARCB1-deficient sinonasal carcinoma. Preoperative imaging is essential for defining the full extent of disease and guide surgical and therapeutic planning. Post-treatment imaging is equally important for assessing response to therapy, differentiating residual or recurrent tumor from post-surgical changes, and monitoring for disease progression. Careful comparison of serial studies enables radiologists to provide meaningful input on treatment efficacy and long-term management in this aggressive malignancy.

References

Wang, Ru, et al. “Clinical Diagnosis and Treatment Analyses on SMARCB1 (Integrase Interactor 1)-Deficient Sinonasal Carcinoma: Case Series with Systematic Review of the Literature.” *World Neurosurgery*, vol. 161, May 2022, pp. e229–e243, pubmed.ncbi.nlm.nih.gov/35123020/, https://doi.org/10.1016/j.wneu.2022.01.114.

Contrera, Kevin J, et al. “Impact of Clinical Factors and Treatments on SMARCB1 (INI-1)-Deficient Sinonasal Carcinoma.” *Otolaryngology--Head and Neck Surgery : Official Journal of American Academy of Otolaryngology-Head and Neck Surgery*, vol. 169, no. 2, Aug. 2023, pp. 435–440, pubmed.ncbi.nlm.nih.gov/36856048/, https://doi.org/10.1002/ohn.310.

Parsel, Sean M., et al. “SMARCB1-Deficient Sinonasal Carcinoma: Systematic Review and Case Report.” *World Neurosurgery*, vol. 136, 27 Jan. 2020, pp. 305–310, www.sciencedirect.com/science/article/abs/pii/S1878875020301480?via%3Dihub, https://doi.org/10.1016/j.wneu.2020.01.130.

Images/Tables

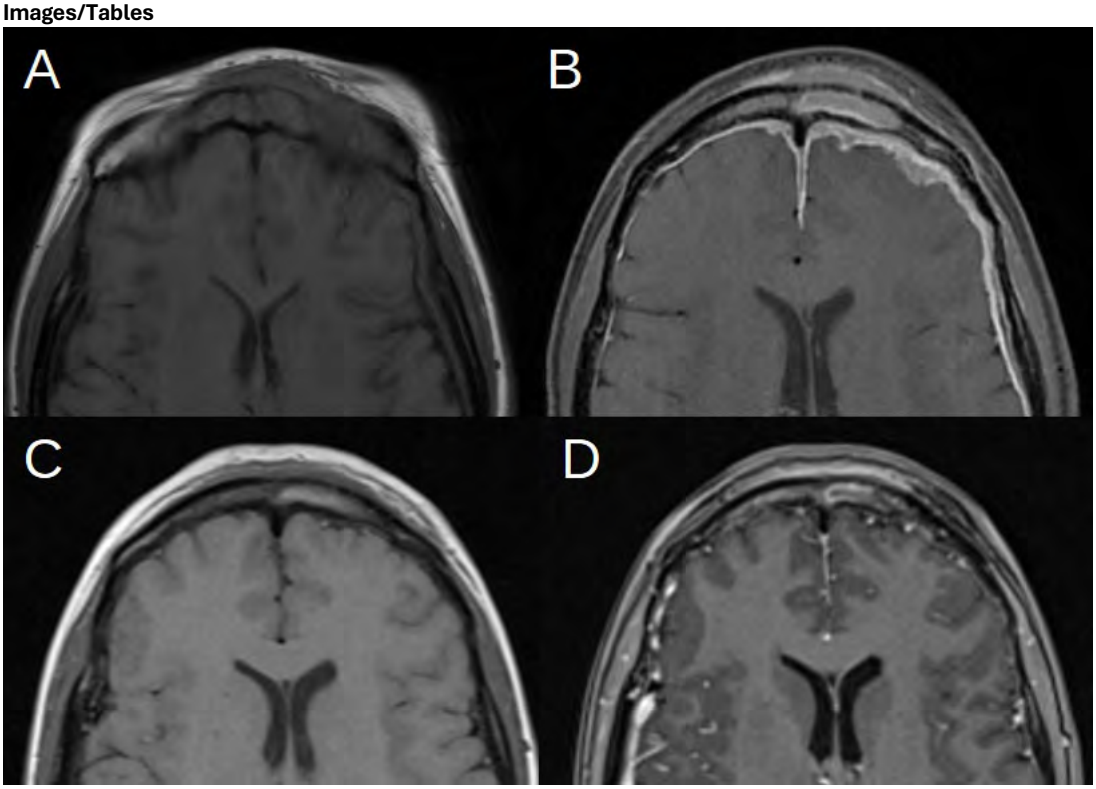

432 Aneurysm at the Crossroads: Where the Spine Meets the Brain

Jedediah Bondy[1], Muhammad Altaf D.O[2], Nirav Patel D.O[2], Yaqub Murad M.D[2], Fahim Bachu[1], Meha Patel MD[3], Victor David Ivancev[1], Mozhan Hagigatian[1], Sinja Kriete[1], Sammy Khalouf[1], Sara Khanipour Roshan M.D[2]

[1]Lake Erie College of Osteopathic Medicine (LECOM), Erie, PA, USA. [2]ChristianaCare Department of Radiology, Newark, Deleware, USA. [3]Mount Sinai West, New York, NY, USA

Clinical History

A 67-year-old woman with hypertension presented with a sudden thunderclap headache and vomiting while exercising. Initial examination revealed expressive aphasia, dysarthria, and mild weakness in all extremities. Non-contrast CT demonstrated diffuse subarachnoid hemorrhage (SAH) centered in the basal cisterns and prepontine region with intraventricular extension and hydrocephalus. She was intubated for airway protection and transferred to the neurocritical care unit, where an external ventricular drain was placed and medical management with nimodipine, levetiracetam,

and nicardipine was initiated. CTA of the head and neck revealed subtle irregularity of the distal left vertebral artery near the anterior spinal artery (ASA) origin, suspicious for a small aneurysm or fenestration.

Imaging Findings

CTA demonstrated irregularity of the distal left vertebral artery (V4 segment) adjacent to the ASA origin, with limited evaluation due to bone artifact and vascular overlap. Subsequent digital subtraction angiography (DSA) confirmed a 1.5–2 mm saccular aneurysm at the vertebral–ASA junction. Oblique projections revealed collateral ASA supply from the contralateral vertebral artery, confirming bilateral perfusion. Three-dimensional rotational angiography (3D-DSA) provided detailed visualization of the aneurysm neck and its relationship to the vertebral artery. Given the small size and critical spinal cord supply, endovascular treatment was deferred to prevent ischemic injury. The patient was managed conservatively with cerebrospinal fluid diversion and strict hemodynamic control, resulting in stable follow-up imaging and gradual neurological improvement.

Discussion

Aneurysms of the anterior spinal artery are exceedingly rare, representing fewer than 1% of intracranial aneurysms. They most commonly arise at the vertebral–ASA junction, where vessel angulation and hemodynamic stress predispose to wall weakness. While CTA is often the first-line modality for suspected aneurysmal SAH, its sensitivity is limited in the posterior fossa due to bone artifact and the small caliber of perforating vessels. DSA remains the diagnostic gold standard, providing superior spatial and dynamic resolution, while 3D-DSA enhances delineation of aneurysm morphology and its relation to branch vessels. In this case, recognition of bilateral ASA collateralization was critical in avoiding endovascular intervention that could have compromised spinal cord perfusion. Conservative management was successful, consistent with prior reports describing spontaneous stabilization of small ASA aneurysms. This case emphasizes the need for individualized management strategies in posterior circulation SAH, balancing hemorrhagic risk against spinal ischemic complications.

Teaching Point

ASA aneurysm rupture is a rare but important cause of posterior circulation SAH. When diffuse prepontine hemorrhage occurs without a clear CTA source, DSA with 3D reconstruction should be performed. Identifying ASA collateralization is essential before intervention to prevent catastrophic spinal cord infarction.

References

1. Raz E, Shapiro M, Nossek E, et al. Neuroanatomy of the vertebrobasilar perforators: implications for aneurysm treatment. *J Neurointerv Surg.* 2024;17(8):848–858.
2. Westerlaan HE, van Dijk MJ, Jansen-van der Weide MC, et al. Diagnostic accuracy of CTA in small posterior circulation aneurysms. *Stroke.* 2014;45(6):1618–1620.
3. Nisson PL, Goyal N, Taussky P, et al. Ruptured anterior spinal artery aneurysm: case report and literature review. *World Neurosurg.* 2021;148:e67–e72.
4. Ohkuma H, Suzuki S, Shimamura N, et al. Management of aneurysms in the vertebrobasilar system. *Neurosurgery.* 2019;84(3):652–660.
5. Ali F, Reddy V, Dublin AB. Anatomy, Back, Anterior Spinal Artery. *StatPearls [Internet].* Treasure Island (FL): StatPearls Publishing; 2025.

Images/Tables

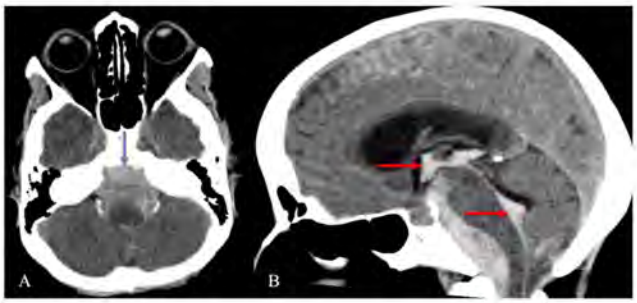

Figure 1. Non-Contrast CT Head Demonstrating Diffuse Subarachnoid Hemorrhage With Intraventricular Extension
(A) Axial non-contrast CT head demonstrates diffuse subarachnoid hemorrhage centered in the prepontine cistern (blue arrow), extending into the basal cisterns and perimesencephalic spaces. (B) Sagittal non-contrast CT head from the same exam shows intraventricular extension of hemorrhage into the third and fourth ventricles (red arrows), consistent with Modified Fisher Grade 4 SAH. Mild ventricular enlargement is present, suggesting early hydrocephalus.

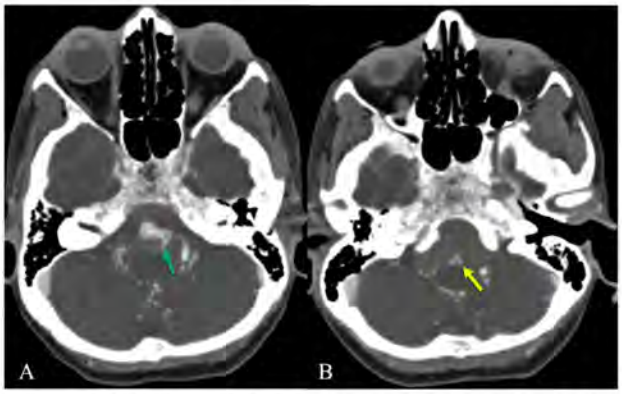

Figure 2. CT Angiography Demonstrating Left Vertebral–Anterior Spinal Artery Junction Aneurysm
(A) Axial CTA head demonstrates the origin of the anterior spinal artery arising from the distal left V4 segment of the vertebral artery (green arrow). (B) Axial CTA head at a slightly inferior level shows a small, irregular outpouching arising from the anterior spinal artery, consistent with a 2 mm saccular aneurysm (yellow arrow).

Figure 3. Digital Subtraction Angiography (DSA) Confirming Left Vertebral–Anterior Spinal Artery Aneurysm and Collateral Flow
(A) Magnified lateral projection demonstrates a 1.5 mm irregular aneurysm (orange arrow) arising from the anterior spinal artery at its junction with the left vertebral artery, consistent with a ruptured ASA aneurysm. (B) Oblique projection demonstrates a collateral vessel (purple arrow) from the contralateral vertebral artery supplying the ASA, confirming bilateral perfusion and explaining the decision to avoid endovascular occlusion.

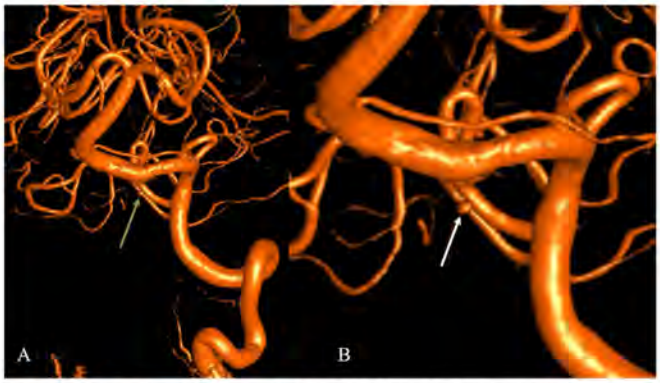

Figure 4. Three-Dimensional Rotational Digital Subtraction Angiography (3D-DSA) of the Left Vertebral–Anterior Spinal Artery Junction Aneurysm
(A) Three-dimensional reconstruction of the left vertebral artery demonstrates a 1.5–2 mm saccular aneurysm (tan arrow) arising from the anterior spinal artery at its vertebral junction. (B) Magnified view provides detailed delineation of the aneurysm neck and morphology (white arrow), confirming its midline projection and proximity to the ASA origin.

---

439 The Thalamic Tempest: Unraveling A Case of Acute Necrotizing Encephalitis in Childhood

Nicholas Mynarski MD, Alan Johnson MD
Northwell Health, New Hyde Park, NY, USA

Clinical History

A 2 year old previously healthy male with no significant past medical history presented to the ED with fever of 107.0 F in the setting of COVID-19 infection with associated cough, non-bloody diarrhea and new altered mental status. Initial sepsis workup was performed, including lumbar puncture, initiation of antibiotics, non-contrast CT Head, and subsequently recommended contrast-enhanced MR Brain examinations.

Imaging Findings

Initial CT Head demonstrated bilateral thalamic hypodensities of which encephalitis, cerebritis, ischemia, or other etiologies could not be excluded. Contrast enhanced MR Head demonstrated punctate thalamic microhemorrhage on SWI, marked edema and swelling of the bilateral thalami on T2/FLAIR weighted sequences with associated areas of diffusion restriction with a layered appearance on ADC mapping, and patchy peripheral enhancement of pontine cavitations. Subsequent contrast-enhanced MR Head status post treatment, including methylprednisolone, IVIG, tocilizumab, and PLEX, demonstrated decreased bilateral thalamic edema with associated decreased diffusion restriction and resolution of pontine enhancement.

Discussion

Although nonspecific, these findings were thought to represent acute necrotizing encephalopathy (ANE) of childhood in the setting of COVID-19 infection with differential diagnosis including acute disseminated encephalomyelitis, other viral encephalitides, acute hemorrhagic encephalitis, Leigh syndrome, embolic infarction, and septic emboli. The vast majority of these other entities were excluded based upon negative laboratory and CSF results.

ANE is a rare type of acute encephalopathy, usually preceded by a viral febrile illness, characterized by rapid neurological deterioration and widespread brain necrosis.[1] Radiologic assessment plays a critical role in the diagnosis of ANE. MRI is pivotal, often revealing bilateral symmetric edema within the thalami and brainstem. A hallmark imaging feature, particularly on DWI/ADC MR sequences, is the trilaminar sign. This distinct pattern comprises a combination of vasogenic edema (T2 shine-through in the outermost bright ring), cytotoxic edema (true restricted diffusion in the

middle dark ring), and hemorrhage (central high signal).[2] Recognizing this highly specific sign is critical for differentiating ANE from other acute encephalopathies.

Teaching Point

Neuroradiologists should recognize the unique imaging characteristics of acute necrotizing encephalitis (ANE), including the trilaminar sign, to facilitate prompt diagnosis and treatment of this often-fatal condition.

References

1. Wu X, Wu W, Pan W, Wu L, Liu K, Zhang HL. Acute necrotizing encephalopathy: an underrecognized clinicoradiologic disorder. Mediators Inflamm. 2015;2015:792578. doi: 10.1155/2015/792578. Epub 2015 Mar 22. PMID: 25873770; PMCID: PMC4385702.
2. Vanjare HA, Selvi BT, Karuppusami R, Manesh A, Gunasekaran K, Prabhakar AT, Mannam P, Jasper A. Clinical and Radiologic Findings of Acute Necrotizing Encephalopathy in Young Adults. AJNR Am J Neuroradiol. 2020 Dec;41(12):2250-2254. doi: 10.3174/ajnr.A6803. Epub 2020 Oct 29. PMID: 33122207; PMCID: PMC7963253.

Images/Tables

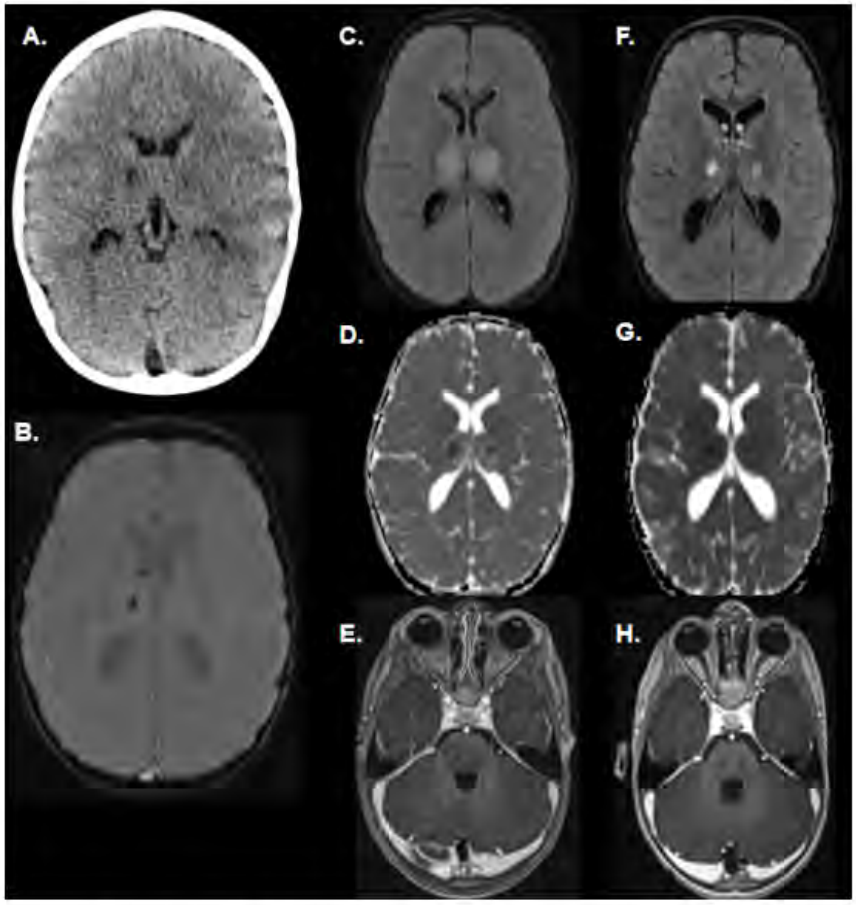

Figure 1: Multimodality Radiologic Assessment of Acute Necrotizing Encephalitis Pre- and Post-Treatment. Initial noncontrast CT head demonstrated nonspecific bilateral thalamic hypodensities (Figure 1A). Contrast enhanced MR Head demonstrated punctate thalamic microhemorrhage on SWI (Figure 1B), marked edema and swelling of the bilateral thalami on T2/FLAIR weighted imaging (Figure 1C) with associated areas of diffusion restriction with a layered appearance on ADC mapping (Figure 1D), and patchy peripheral enhancement of pontine cavitations (Figure 1E). Subsequent contrast-enhanced MR Head status post treatment, demonstrated decreased bilateral thalamic edema (Figure 1F) with associated decreased diffusion restriction (Figure 1G) and resolution of pontine enhancement (Figure 1H).

---

447 Bilateral Facial Nerve Palsy In A Patient With CAR-T therapy.

Diego J Cebrian Chaustre MD, Yoshimi Anzai MD, MPH, Blair A Winegar MD
Univerisity of Utah Health, Department of Radiology, Neuroradiology Section, Salt Lake City, Utah, USA

Clinical History

76-year-old male patient with known monoclonal gammopathy of undetermined significance (MGUS) who rapidly progresses to Plasma Cell Leukemia (PCL), with extensive osseous involvement. He initiated Dexamethasone, Cyclophosphamide, Etoposide and Cisplatin (DCEP) chemotherapy regimen, Monoclonal antibody therapy with talquetamab, and Chimeric Antigen Receptor T-cell (CAR-T) therapy. Later developed Grade I cytokine release syndrome (GR1 CRS - only fever >38C, without hypotension). 24 days following CAR-T therapy, the patient developed left facial nerve palsy, with subsequent right facial nerve palsy on day 40.

Imaging Findings

Initial brain MRI with contrast performed approximately 4 weeks after the initiation of CAR-T therapy showed asymmetric enhancement of the left facial nerve in the internal auditory canal (IAC) fundus as well as stable/known abnormal marrow signal through the calvarium, secondary to multiple

myeloma (MM). Follow-up MRI performed two weeks later showed progressive enhancement now involving the distal canalicular and labyrinthine segments of the bilateral facial nerves.

Discussion

Cranial neuropathy is recognized as an uncommon, but distinctive neurotoxicity related to CAR-T therapy, usually responsive to steroids.

The pathologic mechanism of neurotoxicity after BCMA CAR-T therapy is not well understood. It has been considered secondary to immune cell-effector activated neurotoxicity syndrome (ICANS), and although cytology shows elevated CAR-T T-cells and cytokines in CSF, autopsies and pathologic specimens have demonstrated very few T-cells and no CAR-T T-cells in the affected nerves of patients suffering with neurotoxicity. ICANS often coexists with cytokine release syndrome (CRS) — about 70–80% of ICANS cases follow or overlap with CRS.

This case presents a relatively acute onset of initially unilateral, then subsequently bilateral facial nerve palsy, as well as linear (non-mass-like) enhancement of the canalicular and labyrinthine segments of the bilateral facial nerves, shortly after BCMA CAR-T therapy. If the patient's medical history was not known or the therapeutic agents were not recognized, potential differential diagnosis may include bilateral idiopathic Bell palsy, infectious etiologies (e.g. Lyme disease, Herpes Zoster neuritis, HIV), or inflammatory conditions (sarcoidosis, Guillain-Barre/Miller Fisher syndrome). Less likely, given onset timing, malignancy (e.g. intracranial MM/PCL, leptomeningeal metastasis, lymphoma), or even neuropathic manifestations of other systemic diseases, such as diabetic cranial neuropathy.

The timing also follows a similar pattern as those demonstrated on the CARTITUDE -1/2 and CARTITUDE 5- programs, in which asymmetric onset of bilateral facial neuropathy presented in several patients, especially after presenting with mild CRS.

It is important to note that distinguishing immune mediated cranial neuropathy from ICANS can be challenging. Although ICANS has been reported on talquetamab therapy, cranial neuropathy has not been associated with ICANS, and lack of clinical manifestation of encephalopathy and diffuse white matter changes and BBB disruption, favor CAR-T immune-mediated facial neuritis.

Teaching Point

Bilateral facial nerve palsy following CAR-T therapy likely represents a distinct immune-mediated cranial neuropathy rather than an ICANS variant. Awareness of the therapeutic regimen, with its clinical presentation and imaging correlates, is important for neuroradiologists to distinguish this immune-related neuritis from other causes of bilateral facial palsy.

References

Patrick KL et al. Chimeric Antigen Receptor T-Cell–Mediated Bilateral Facial Nerve Palsy. J Neuroimmunol. 2023.
van de Donk NWCJ et al. Cranial Nerve Impairment in the CARTITUDE Clinical Program. Biol Blood Marrow Transplant. 2024.
Cohen AD et al. Neurotoxicity After BCMA-Directed CAR T-Cell Therapy for Multiple Myeloma. Blood Cancer J. 2024.

Images/Tables

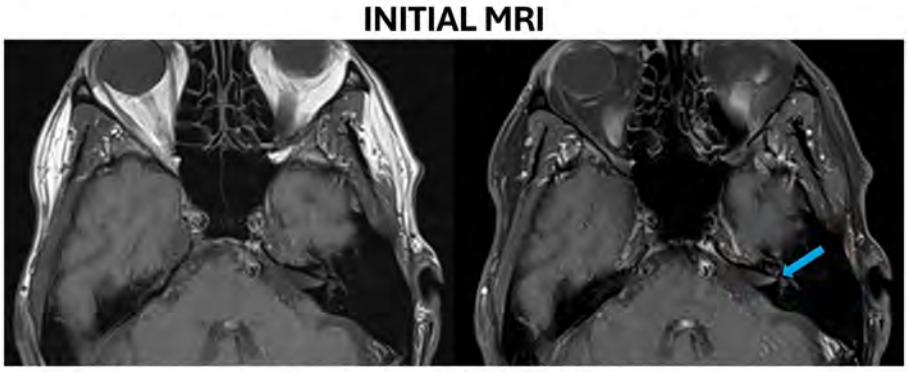

Fain enhancement in the left IAC fundus.

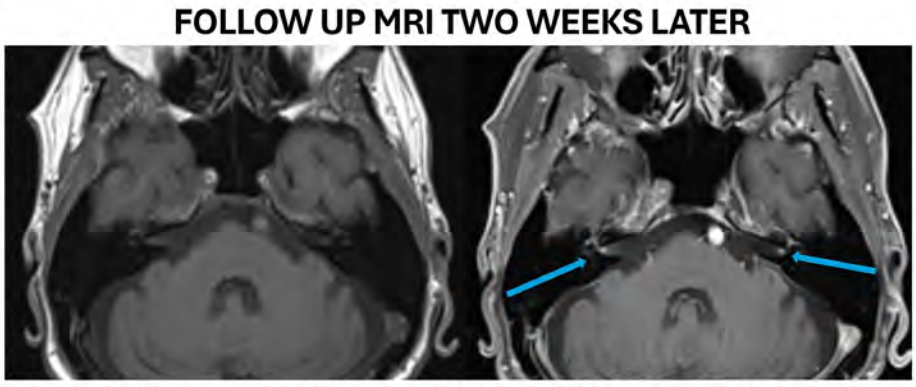

Increased degree of enhancement of the distal canalicular and labyrinthine segments of the facial nerves bilaterally.

---

448 A Patchwork of Pain and Pigment: A Case Report on Multiple Glomuvenous Malformations

Hadassah Stein MD, Paul K Lee MD
Northwell at North Shore/Long Island Jewish, Manhasset, New York, USA

Clinical History

A 21 year female with history of innumerable tender blue-purple plaques distributed across her neck, trunk and extremities presents for tonsillectomy. The patient had a prior diagnosis of multiple glomuvenous malformations. MRI head and neck were obtained to evaluate for pharyngeal involvement prior to surgery.

Imaging Findings

Image Description

Left image is an axial T1 postcontrast MRI, middle image is a coronal T2 MRI and right image is an axial T2 MRI. A malformation appearing as a cobblestone pattern of avidly enhancing (blue arrow) and markedly T2 hyperintense (red and yellow arrows) soft tissue lesions primarily cutaneous and subcutaneous in location most prominently involving the bilateral occipital and posterior cervical soft tissues. Involvement of the left posterior pharyngeal wall (yellow arrow) and posterior surface of the mucosal torus tubarius was noted for presurgical planning prior to tonsillectomy.

Discussion

Glomuvenous malformations or "glomangiomas" are hamartomatous lesions affecting the skin and subcutaneous tissue. They are characterized histologically by the presence of glomus cells in vascular smooth muscle. Glomus cells are believed to have a thermoregulatory role. Familial cases demonstrate an autosomal dominant, incomplete penetrance inheritance pattern and are due to mutations in the glomulin gene (GLMN; 1p22.1). Some patients can have associated malformations of different internal organs including the trachea, nerve, bone and gut. Malignant transformation of these glomus tumors to glomangiosarcomas is rare but will present as a locally infiltrative lesion.

On physical exam, lesions may appear as hard and tender blue or pink pebbly plaques that fail to completely empty with compression. Multiple grouped papules can combine to form plaques. These malformations are often more painful than the typical nonhereditary venous malformation warranting treatment for symptomatic relief. Treatment options include surgery, endovascular laser treatment, embolization and sclerotherapy. Embolic agents include coils, vascular plus and sclerosing agents. Surgery is best used in conjunction with sclerotherapy and embolization as part of staged management of large or treatment resistant lesions.

Alternative venous malformations that may initially be on the differential include cutaneomucosal venous malformations and blue rubber bleb nevus syndrome, which are both related to vascular smooth muscle recruitment and have relatively increased risk for consumptive coagulopathy and iron deficiency anemia. Their different gene responsible for these malformations alter a different molecular signalling pathway, which lends itself to a different targeted therapy.

Imaging is pivotal in characterizing these lesions. Glomuvenous malformations are often hypoattenuating on unenhanced CT with delayed peripheral enhancement. On MRI, these lesions appear as lobular cobblestone T2 hyperintense foci demonstrating low to intermediate T1 signal with avid homogeneous enhancement and intervening septa. Dynamic time-resolved contrast enhanced MR will demonstrate subtle arterial enhancement, early venous shunting and progressive filling of dilated venous spaces. Ultrasound will exhibit a well-defined hypoechoic lesion with increased posterior acoustic enhancement.

Teaching Point

Glomuvenous malformations should be considered in the differential when assessing patients with multiple venous malformations as there are implications for treatment and management. Imaging is pivotal in further characterizing venous malformations. Interventional radiology can perform procedures including embolization and sclerotherapy for symptomatic relief of painful lesions.

References

Behr GG, Johnson CM. Vascular anomalies: hemangiomas and beyond. Part 2. Slow-flow lesions. AJR Am J Roentgenol 2013;200:423–436.

Flors L, Norton PT, Hagspiel KD. Glomuvenous malformation: magnetic resonance imaging findings. Pediatr Radiol 2015;45:286–290. doi:10.1007/s00247-014-3086-x

Jha A, Khunger N, Malarvizhi K, Ramesh V, Singh A. Familial disseminated cutaneous glomuvenous malformation: treatment with polidocanol sclerotherapy. J Cutan Aesthet Surg 2016;9:266–269. doi:10.4103/0974-2077.197083

Khan MS, Sohail AH, Hilal K, Maan MHA. Glomuvenous malformation of the neck. Int J Angiol 2020;29:267–271. doi:10.1055/s-0039-1694059

McMahon MH, Tahir N, Balasubramanian M. GLMN causing vascular malformations: the clinical and genetic differentiation of cutaneous venous malformations. *BMJ Case Rep* 2022;15(6):e246114. doi:10.1136/bcr-2021-246114. PMID: 35732373; PMCID: PMC9226952.

Images/Tables

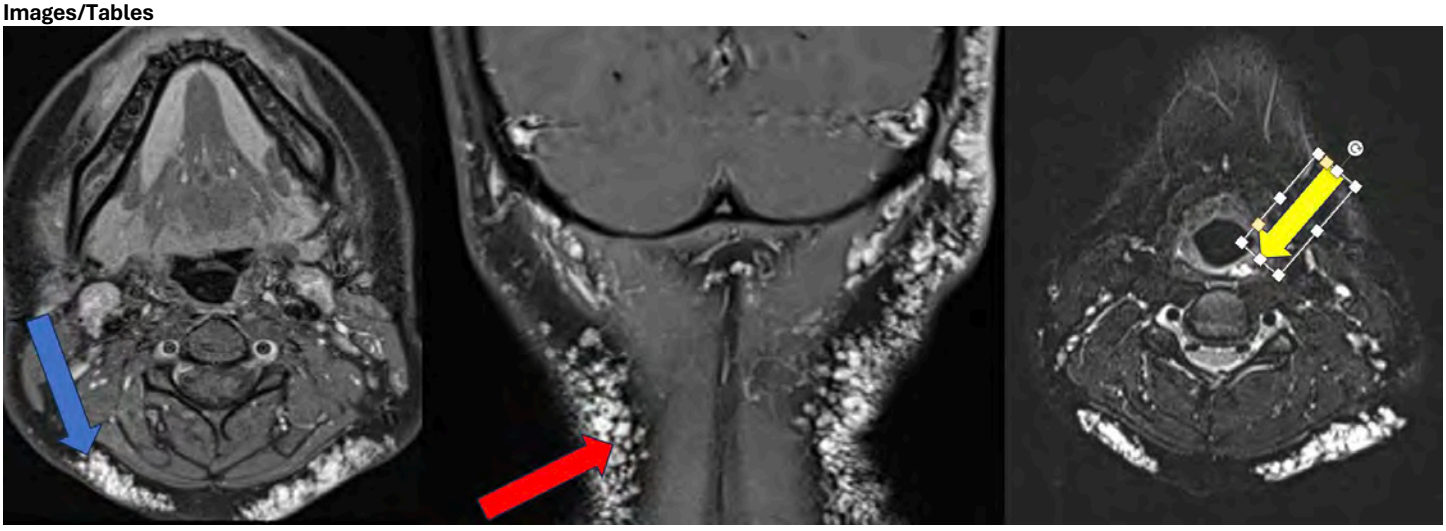

---

449 Radiologic Diagnosis of Cerebral Air Embolism: A Rare but Critical Entity

Adam L Stroh DO, Jennifer McCarty MD

UTHealth Houston, Houston, Texas, USA

Clinical History

A 70 year-old-male with a history of AML s/p remote bone marrow transplant, graft vs host disease and pulmonary fibrosis initially presented to an outside hospital after a mechanical ground level fall wherein he sustained a scalp laceration without loss of consciousness. Initial imaging workup showed pneumomediastinum and no acute intracranial findings.

Early the following morning, the patient reported bilateral visual loss and was found to have punctate acute ischemic infarcts in the bilateral occipital lobes. Shortly afterwards, mental status declined and he became encephalopathic with a GCS of 3, tachycardic with respiratory distress, hypoxia and fever. A repeat CT head in the early afternoon showed right frontal intravascular air.

The patient was transferred to our institution the next day in order to potentially undergo hyperbaric oxygen therapy. A repeat CT the following day showed resolution of air, and MRI brain with and without contrast showed findings consistent with extensive sequela of recent cerebral air embolism. By then, the patient was not deemed a candidate for hyperbaric treatment and was subsequently treated with FiO2 at 100%.

Imaging Findings

Non-contrast CT showed extra-axial intravascular air along sulci in superior right frontal lobe extending to the paracentral lobule.

Repeat CT head showed resolution of air with new right frontoparietal parenchymal hypoattenuation in the region of prior air, consistent with acute ischemic infarcts from cerebral air embolism.

MRI brain with and without contrast showed findings consistent with extensive sequela of recent cerebral air embolism with extensive bihemispheric (right more than left) mixed cytotoxic and vasogenic edema with a predominant distal vascular bed/watershed distribution, with associated avid perivascular and leptomeningeal enhancement throughout these regions.

Discussion

Cerebral air embolic ischemic infarcts are rare, yet potentially catastrophic events. The air may enter via the arterial or venous route, including iatrogenic (most often) causes such during invasive procedures (i.e. central venous catheter manipulation, intravascular injection, endovascular procedures, surgeries) or non-iatrogenic causes such as trauma or decompression sickness.

The pathophysiology of injury with cerebral air embolic infarcts is comprised of three main mechanisms which account for the MR imaging manifestations, including direct ischemia from end artery occlusion by the gas emboli (cytotoxic edema), inflammation and blood-brain-barrier breakdown resulting from a gas-bubble related foreign body reaction (enhancement), and elevated venous pressure promoting vasogenic edema and potentially venous infarctions.

While CT may directly show the extra axial air, it is not a reliable/sensitive finding given the rapidity at which it may be resorbed (as shown in this case with the resolution of air on CT the following day).

Clinically, patients often present with nonspecific encephalopathic symptoms. Treatment includes hyperbaric oxygen therapy (if appropriate) and 100% FiO2.

Teaching Point

The MR imaging patterns of cerebral air embolic infarcts is characterized by a distal border-zone predominant pattern of mixed cytotoxic and vasogenic edema along with leptomeningeal and perivascular enhancement. Of note, the finding of enhancement in the acute phase is a relatively underrecognized/underreported feature, only recently brought to attention in a case series published in AJNR in August 2024.

References

Vincent M. Timpone, Andrew L. Callen. Characteristic MR Imaging Findings of Cerebral Air Embolism Infarcts: A Case Series. American Journal of Neuroradiology Aug 2024, DOI: 10.3174/ajnr.A8349

Tabata, H., Kitaguchi, H., Terajima, Y., & Shindo, K. (2016). Cerebral air embolism with pneumomediastinum resulting from Emesis: A case report. Journal of Stroke and Cerebrovascular Diseases, 25(10). https://doi.org/10.1016/j.jstrokecerebrovasdis.2016.07.008

Images/Tables

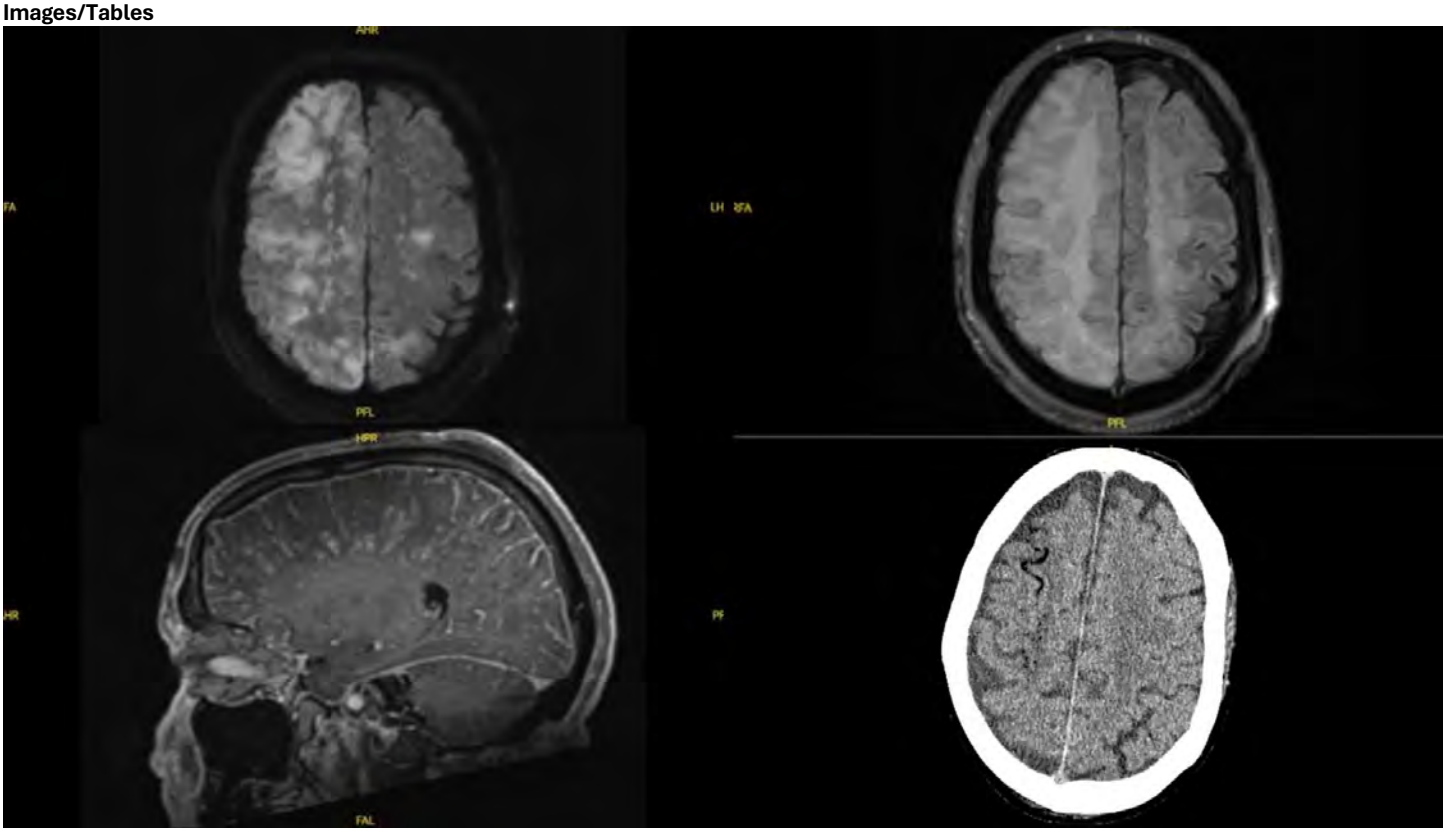

469 An Unusual Case of a High Grade Pleomorphic Xanthoastrocytoma

Sean Andresen MD, Alexandra Reis MD
Santa Barbara Cottage Hospital, Santa Barbara, California, USA

Clinical History

A 30 year old male with no significant past medical history presented for evaluation of acute severe headache and vomiting. Imaging revealed a 4 cm right superior temporal gyrus mass with associated hemorrhage and surrounding vasogenic edema. Craniotomy and tumor resection were subsequently performed and notably the tumor exhibited adhesion to without invasion of the overlying dura. Initial tissue histological exam yielded findings suspicious for infiltrating glioma. The mutational/chromosomal profile of this resected mass yielded findings shared between glioblastoma as well as pleomorphic xanthoastrocytoma (PXA). Given the methylation profile, a high grade PXA, possibly anaplastic, was felt to be the more likely diagnosis. Treatment following craniotomy was tailored to that of a high grade glioma and so the patient received radiation, temozolomide, and dabrafenib given presence of BRAF V600E mutation. Approximately one year following initial diagnosis and mass resection, follow up MRI demonstrated new nodular enhancement along the resection cavity representing tumor recurrence. A second craniotomy with resection was performed and subsequent histological tissue analysis confirmed the recurrence of tumor.

Imaging Findings

On noncontrast CT imaging, the initial mass within the superficial right temporal lobe was lobulated in appearance and demonstrated mixed hyperdensity. On contrast-enhanced MRI, the 4 cm mass demonstrated central T2 hypointensity and T1 hyperintensity with associated susceptibility-weighted blooming artifact felt to represent acute hemorrhage. There was irregular T2/FLAIR mildly hyperintense tissue surrounding this hemorrhage with associated heterogeneous enhancement. No diffusion restriction was identified. Adjacent dural thickening and enhancement with a long dural tail was noted. There was moderate surrounding vasogenic edema in addition to effacement of regional sulci.

Discussion

Pleomorphic xanthoastrocytoma (PXA) is a rare tumor accounting for less than 1% of astrocytomas. This mass typically arises in children and young adults with a mean age of onset of 26.The imaging findings associated with PXAs tend to be varied however there are a number of findings commonly seen. In our young adult patient, a superficial mass within the temporal lobe with reactive dural tail were suggestive of PXA. Previous reports indicate that PXAs tend to be cystic with an enhancing mural nodule, however a review of adult-onset PXAs found that typically PXAs arising specifically in adulthood are more often solid as was seen in our patient. A mass of larger size with slightly inconspicuous margins, associated hemorrhage, heterogeneous enhancement, and surrounding vasogenic edema seen in our patient were features shared with a more aggressive underlying tumor such as anaplastic PXA (WHO grade III) or glioblastoma. Ultimately, the lesion demonstrated both overlapping imaging and histopathological features which made distinction challenging. A precise diagnosis and WHO grade has remained elusive.

Teaching Point

Our case illustrates an atypical PXA with imaging characteristics overlapping those of more aggressive neoplasms, highlighting the diagnostic challenges posed by shared radiologic features.

References

1. Yan, J., Cheng, J., Liu, F, Liu, X. Pleomorphic xanthoastrocytomas of adults: MRI features, molecular markers, and clinical outcomes. Sci Rep 2018;8:14275.https://doi.org/10.1038/s41598-018-32273-w
2. Rippe D, Boyko O, Radi M, Worth R, Fuller G. MRI of Temporal Lobe Pleomorphic Xanthoastrocytoma. *J Comput Assist Tomogr.* 1992;16(6):856-9. doi: 10.1097/00004728-199211000-00004.
3. Crespo-Rodríguez AM, Smirniotopoulos JG, Rushing EJ. MR and CT imaging of 24 pleomorphic xanthoastrocytomas (PXA) and a review of the literature. *Neuroradiology* 2007;49(4):307-15. doi: 10.1007/s00234-006-0191-z.
4. Kahramancetin N, Tihan T. Aggressive behavior and anaplasia in pleomorphic xanthoastrocytoma: a plea for a revision of the current WHO classification. CNS Oncol 2013;2(6):523-30. doi: 10.2217/cns.13.56.

Images/Tables

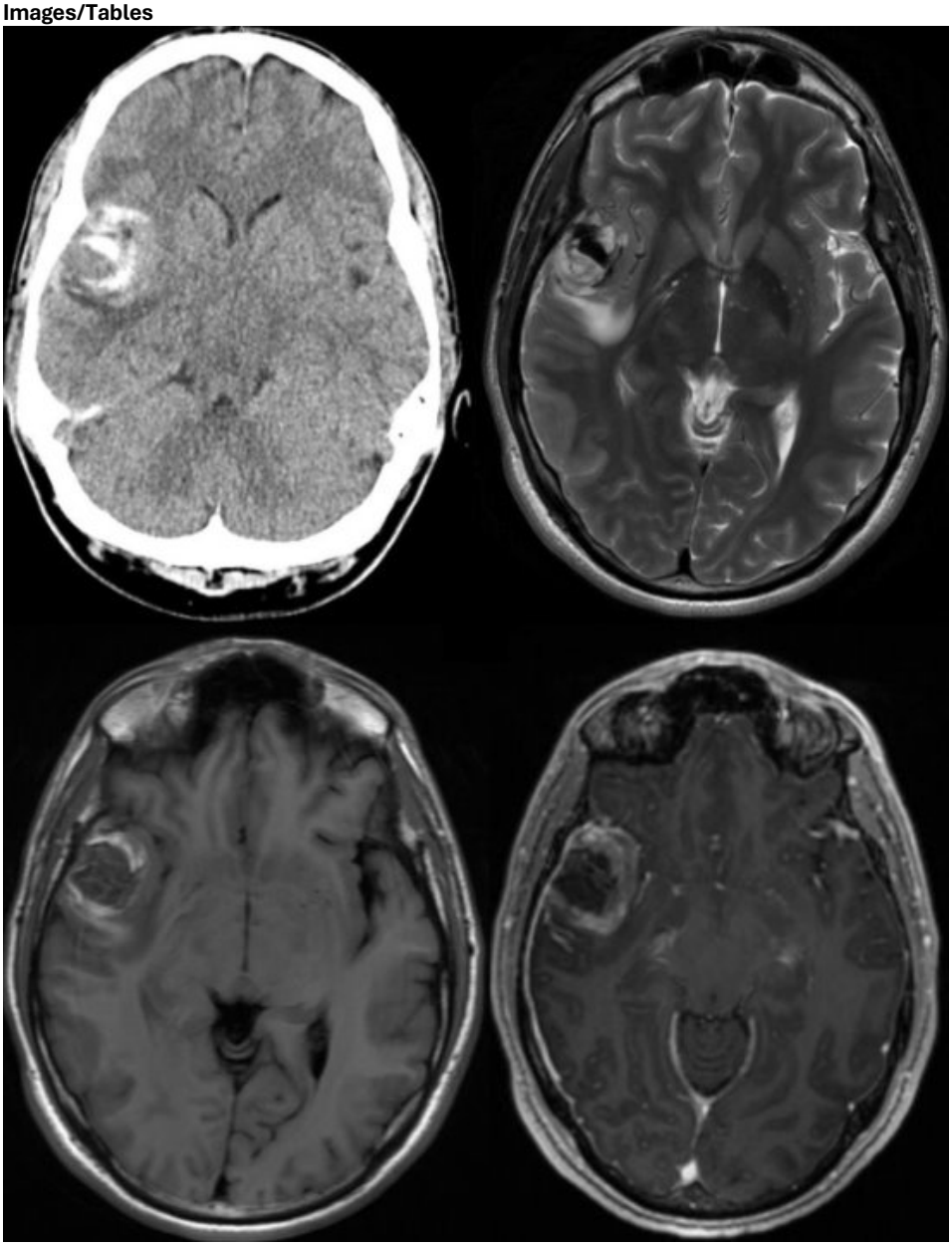

476 A Rare Case of Intramedullary Solitary Fibrous Tumor of the Spinal Cord

Steven Robinson, William Gibson, Hong Li MD, Panagiotis Sideras
Columbia University, New York, NY, USA

Clinical History

This is a case of a 74 year old female with no relevant past medical history. She initially presented in 1994 with left hand weakness. She was diagnosed with a spinal cord tumor and underwent resection and radiation, although information about that diagnosis and treatment is limited at this time. Symptoms recurred in 2018 and she underwent resection #2 that year after imaging showed tumor recurrence. Unfortunately, left hand symptoms kept reoccurring and she underwent resection #3 in 2021. In March 2025, she developed numbness and weakness in her right hand. This, along with imaging evidence of progression, prompted resection #4. After this, she has experienced worsening left upper and lower extremity spasticity and hemiparesis.

Imaging Findings

Serial imaging from 2008 shows slow interval growth of an expansile intramedullary spinal cord mass at C2-C4. The mass is T1 isointense to the cord with heterogenous T2 hyperintensity and moderate enhancement. There is a small amount of spinal cord edema associated with the lesion.
The lesion measured 2.2cm craniocaudal in 01/2025 and 2.7cm in 07/2025, despite interval resection in March of that year. In October 2025, the lesion demonstrated continued growth, measuring 3.0cm .
The adjacent vertebral bodies were normal.

Discussion

Solitary fibrous tumors (formerly hemangiopericytoma) are tumors of mesenchymal origin which can occur anywhere in the body, although they most commonly occur in the pleura. Other common sites include the meninges and less commonly the orbit, abdominal cavity, and extremities. Characteristically, they present as circumscribed, lobulated soft tissue masses with low to intermediate T1 and T2 signal due to the high fibrous component. Avid enhancement is typical. Myxoid components can be T2 hyperintense. They are rarely malignant but can become

symptomatic from compression of adjacent structures. Treatment, if any, is typically surgical excision with evidence that combined surgery and radiation may reduce recurrence rates, which are reported between 10-30%.

Teaching Point

Although there are characteristic locations and imaging appearances, because solitary fibrous tumors can occur anywhere in the body and may have variable imaging characteristics, this should be in the differential for most circumscribed soft tissue masses. Once diagnosed, long term imaging surveillance is recommended due to relatively high rates of recurrence.

In the case presented, there are no distinguishing features to suggest an intramedullary solitary fibrous tumor prospectively. However, this did not have the typical imaging characteristics of more common intramedullary tumors such as ependymoma or astrocytoma. Unfortunately, this case shows multiple recurrences despite multiple resections and prior radiation therapy.

References

Yang C, Xu Y, Liu X. Spinal Intramedullary Solitary Fibrous Tumor: A Rare and Challenging Diagnosis. *Cancer Manag Res*. 2019 Dec 10;11:10321-10326. doi: 10.2147/CMAR.S231019.

Images/Tables

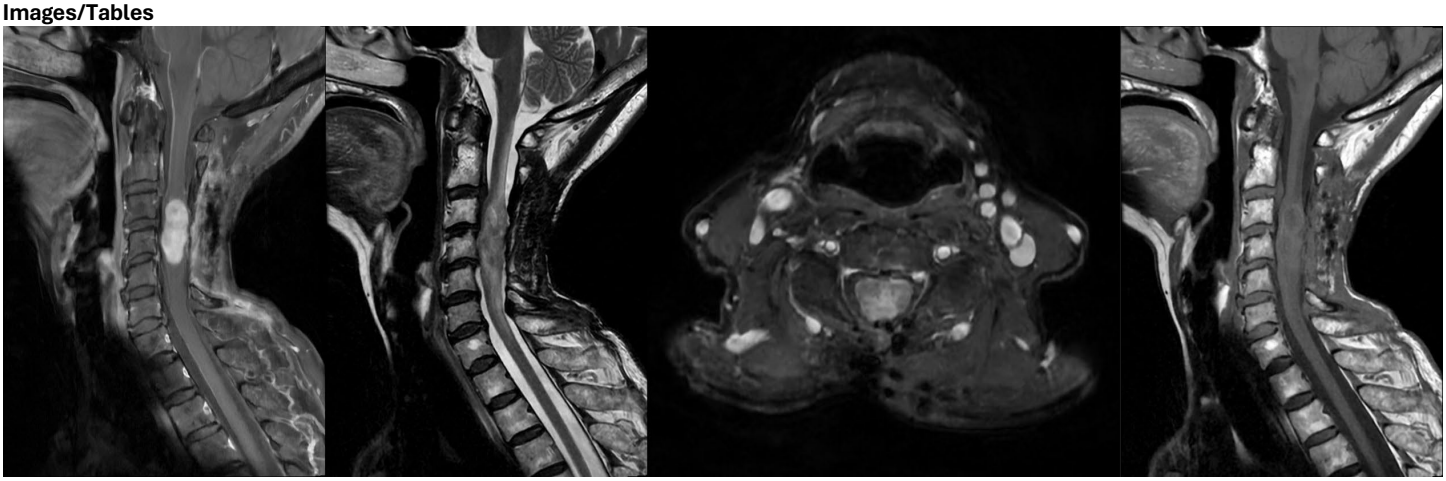

---

478 Fourth Recurrence of a Multifocal Myxopapillary Ependymoma with Superficial Siderosis

Santiago Quiceno-Ramirez MD[1], Alejandro Hernandez MS[2], Martin Eduardo Renjifo MD[3], Juan Camilo Márquez MD[4]

[1]Centro de Investigaciones Clínicas, Fundación Valle del Lili, Cali, Valle, Colombia. [2]Facultad de Ciencias de la Salud, Universidad Icesi, Cali, Valle, Colombia. [3]Fundación Valle del Lili, Cali, Valle, Colombia. [4]Departamento de Radiología, Fundación Valle del Lili, Cali, Valle, Colombia

Clinical History

We present a 50-year-old patient with a ten-year history of recurrent and multifocal MPE, whose initial presentation was a lumbosacral mass treated with surgical resection. The clinical course has been marked by multiple recurrences: a first recurrence at L1-L4 treated with resection and laminectomy, a second recurrence managed with radiotherapy, and a third recurrence manifesting as a multifocal T10-L1 extradural lesion and multiple lesions within the filum terminale.

This third recurrence was surgically resected, with a postoperative spine MRI confirming successful resection and no evidence of residual epidural mass. The patient now returns for follow-up, where surveillance imaging reveals a fourth recurrence, demonstrating a new epidural mass at the T9-T12 level with bilateral neural foraminal extension. All recurrent lesions have been pathologically confirmed as MPE.

Notably, surveillance neuroimaging of the brain demonstrated the presence of superficial siderosis along the folia of both cerebellar hemispheres and the cerebellar vermis.

Imaging Findings

Initial imaging (third recurrence):

MRI thoracic spine: There is a homogeneously enhancing nodular tissue occupying the anterolateral epidural space from T11 extending caudally, causing severe spinal canal stenosis. The enhancing lesion extends into the neural foramina, with expansion of the left T12-L1 foramen. MRI lumbar spine: There are multiple enhancing nodular lesions involving the paraspinal soft tissues, the epidural and intradural spaces, and infiltrating the L2 and L3 vertebral bodies, consistent with infiltrative disease. Additionally, multiple enhancing nodular foci are seen within the intradural space among the cauda equina nerve roots at the L1-L2 and L5 levels, as well as within the sacral canal, with the latter causing remodeling of the adjacent bony structures.

2-year post-op follow up (fourth recurrence):

MRI spine: Expected postoperative changes and posterior instrumented fusion from T10 to L2, which causes magnetic susceptibility artifact. A homogeneous enhancing epidural soft tissue mass is present, causing significant spinal canal stenosis. The lesion extends through the neural foramina bilaterally, compressing the exiting nerve roots. Sagittal sequences were limited by significant artifact from the posterior instrumented fusion and are not shown.

Axial brain SWI sequences show characteristic hypointense linear signal lining the folia of the cerebellar hemispheres and vermis, consistent with superficial siderosis.

Discussion

This case illustrates a rare multifocal recurrence of myxopapillary ependymoma and the different ways in which this ependymal tumor could reappear years later after the initial diagnosis.

Currently, there are a handful of case reports in which the multifocal presentation of this tumor is discussed and its treatment options are reviewed. Multifocality has been linked to worst clinical outcomes and a more aggressive tumoral behavior.

This tumor is often seen as a well-defined heterogeneous intradural tumor with hyperintensity on T2WI and isointensity on T1WI. Authors have also described contrast enhancement of this mass due to its high vascularity.

Teaching Point

Multifocal recurrent MPE is a rare entity. Despite its good prognosis, it has a high propensity for metastasis and recurrence due to easy cerebrospinal fluid dissemination. Patient history, previous histopathological confirmation, and radiological characterization of these lesions are key for identification of recurrences.

References

Tabor, J.K., Ryu, B., Schneider, D. et al. Multifocal lumbar myxopapillary ependymoma presenting with drop metastasis: a case report and review of the literature. Spinal Cord Ser Cases 8, 43 (2022). https://doi.org/10.1038/s41394-022-00513-x

Liu T, Yang C, Deng X, et al. Clinical characteristics and surgical outcomes of spinal myxopapillary ependymomas. Neurosurg Rev. 2020 Oct 1;43(5):1351–6.

Montero AS, Tran S, Amelot A, et al. Clinical characteristics and long-term surgical outcome of spinal myxopapillary ependymoma: a French cohort of 101 patients. J Neurooncol. 2021 May;152(3):491–9.

Images/Tables

---

487 Ependymoma (Ependy-maybe): MR and Microscopy Don't See Eye to Eye

Carlo Castro MD, Andrew Campbell MD, David Bartlett MD, Emery Price MD, Benjamin Cho MD, Benjamin Huang MD
University of North Carolina at Chapel Hill, Chapel Hill, NC, USA

Clinical History

A 54-year-old man with a history of hypertension and neurofibromatosis type 1 with café-au-lait spots and cutaneous neurofibromas presents with 1 week of headaches.

Imaging Findings

Unenhanced head CT demonstrated a 4th ventricular mass with internal calcifications. Brain MRI with contrast demonstrated a 4th ventricular mass extending through the left foramen of Luschka into the left cerebellopontine angle and the porus of the internal auditory canal, medially displacing and partially encasing the left vertebral artery and encasing the left posterior inferior cerebellar artery (PICA) at its origin. The mass was slightly hyperintense on T2WI, enhanced heterogeneously, and contained numerous small foci of blooming on SWI. There was no diffusion restriction in the mass.

Discussion

On neuropathologic review, the mass exhibited overlapping features of both ependymoma and subependymoma. Histologically, two distinct morphologic patterns were identified. Some regions showing clustered nuclei within a fibrillary, nodular background characteristic of subependymoma, while other areas demonstrated increased cellularity, nuclear atypia, and perivascular pseudorosettes more consistent with ependymoma. The specimen from this case has been submitted to the NIH for methylation profiling, which remains pending at this time.

Posterior fossa ependymal tumors can be categorized into three molecular subgroups based on DNA methylation profiling, cytogenetic features, and gene expression patterns: *posterior fossa subependymoma* (PFSE), *posterior fossa group A* (PFA), and *posterior fossa group B* (PFB). Subependymomas are typically indolent WHO grade I neoplasms, whereas posterior fossa ependymomas are more aggressive, corresponding to WHO grades II or III. Mixed ependymoma–subependymoma tumors have been described, showing variable proportions of differentiation but generally aligning epigenetically with the subependymoma profile. Clinically, subependymomas represent the least aggressive end of the spectrum. Mixed lesions are intermediate, and pure ependymomas are the most aggressive, with recurrence risk following this same gradient.

Emerging evidence supports the concept of a shared precursor cell for ependymomas and subependymomas, with subsequent divergence into separate subclones—or possible metaplastic or dedifferentiation processes—accounting for the mixed histologic features observed in some lesions.

Teaching Point

1. Mixed ependymoma–subependymoma tumors can show overlapping histologic features, but DNA methylation profiling is essential to define their true molecular subgroup (PFSE, PFA, or PFB). Morphology alone can be misleading—molecular data determine prognosis and potential aggressiveness.
2. Pure subependymomas are WHO grade I; pure ependymomas (PFA/PFB) are WHO grade II/III and more aggressive. Mixed lesions can range in ependymal differentiation, but recurrence risk and aggressiveness generally follow a spectrum: subependymoma < mixed < pure ependymoma. Current models propose a common precursor with early divergence into subclones; therefore, surveillance and treatment should be individualized based on the lesion's molecular subgroup, extent of resection, and histologic grade.
3. A fourth ventricular mass with calcifications, heterogeneous enhancement, T2 hyperintensity, and SWI blooming, extending through the foramen of Luschka strongly suggests an ependymal tumor and informs surgical planning.

References

1. Thomas C, Thierfelder F, Träger M, et al. TERT promoter mutation and chromosome 6 loss define a high-risk subtype of ependymoma evolving from posterior fossa subependymoma. *Acta Neuropathol* 2021;141:959–70.
2. Wagner MW, Jabehdar Maralani P, Bennett J, et al. Brain Tumor Imaging in Adolescents and Young Adults: 2021 WHO Updates for Molecular-based Tumor Types. *Radiology* 2024;310:e230777.
3. Leclerc T, Levy R, Tauziède-Espariat A, et al. Imaging features to distinguish posterior fossa ependymoma subgroups. *Eur Radiol* 2023;34:1534–44.
4. Sabin ND, Hwang SN, Klimo P, et al. Anatomic Neuroimaging Characteristics of Posterior Fossa Type A Ependymoma Subgroups. *AJNR Am J Neuroradiol* 2021;42:2245–50.

Images/Tables

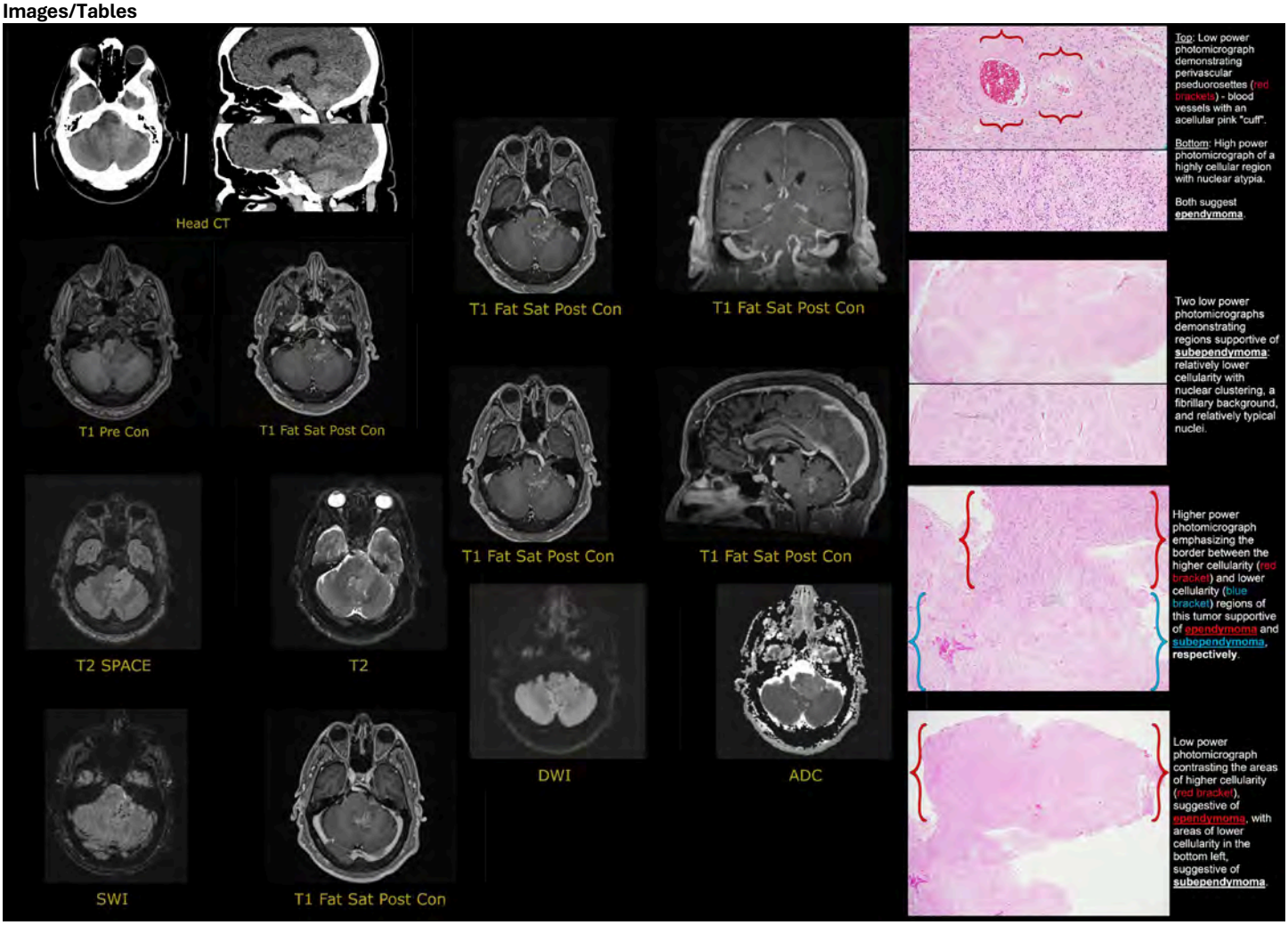

---

503 A Constant Thorn in the Throat: When the Body Betrays Itself

Nga T Nguyen MD[1], Lawrence E Ginsberg MD[2]

[1]The University of Texas Medical Branch, Galveston, Texas, USA. [2]The University of Texas Medical Branch, Galveston, TX, USA

Clinical History

A middle-aged man with a four-year history of Eagle syndrome presented with progressively increased right neck pain, exacerbated by tongue movement and mouth opening. His associated symptoms included increasing morning dysarthria, drooling, dysphagia, and odynophagia.

Physical examination revealed a firm, tender right submandibular region. On neurological examination, he was found to have a right-sided House-Brackmann Grade VI facial palsy. Flexible fiberoptic laryngoscopy was unremarkable for mass or lesion. Imaging studies, including plain film, computed tomography (CT), and magnetic resonance imaging (MRI) were subsequently obtained.

Imaging Findings

A CT neck from 3 years previously revealed significant enlargement of the right styloid process, ossification of the stylohyoid ligament, and pseudo-articulation with the right superior hyoid cornu. A repeat CT redemonstrated similar findings. Because of the new clinical symptoms of right facial neuropathy, MRI of the skull base was subsequently obtained and showed dramatic abnormal enhancement surrounding the styloid process. This enhancement extended posteriorly to the occipitomastoid suture and stylomastoid foramen, suggesting irritation and inflammation of the foraminal facial nerve aspect. These findings correlated with the patient's clinical symptoms and were regarded as a plausible explanation for right facial nerve paralysis.

Discussion

Eagle Syndrome is a condition characterized by facial pain resulting from an abnormally elongated styloid process and/or the ossification of the stylohyoid ligament, leading to local tissue and neurovascular impingement [1]. The syndrome traditionally involves cranial nerve and carotid vessel impingement[2]. Additionally, jugular vein compression has also been recently documented in the literature[3]. The glossopharyngeal and trigeminal nerves are most involved in cases of impingement[4]. Facial nerve involvement in patients with Eagle syndrome is exceptionally rare but has been reported in the literature; however, those cases were without clear radiologic or surgical evidence to suggest active inflammation in a particular segment[5]. Meanwhile, facial nerve inflammation at the stylomastoid foramen in this particular case was strongly supported by MRI findings and eventually confirmed intraoperatively.

The diagnostic process requires both thorough physical examination and appropriate imaging studies. Symptomatic patients typically present with signs of nerve compression, such as facial pain exacerbated by head movement, a foreign body sensation in the throat, dysphagia, and headaches[1]. Treatment modalities encompass both medical and surgical options. For the above patient, initial conservative management, including NSAIDs and oral steroids failed. He subsequently underwent trans-cervical styloidectomy with mastoidectomy. Intraoperatively, swelling and inflammation were confirmed at the inferior portion of the mastoid segment of the facial nerve. Simulation of the facial nerve at the second genu resulted in movement of the stapedius tendon, but no movement of the digastric muscle or facial muscles could be evoked by stimulation of the intratemporal segment. Therefore, nerve decompression was performed. Postoperatively, the patient reported marked improvement in pain and dysphagia.

Teaching Point

Eagle Syndrome is a diagnosis reserved specifically for patients with symptomatic elongation of the styloid process and/or calcification of the stylohyoid ligament. Clinical symptoms typically result from impingement or compression of adjacent neurovascular structures. The glossopharyngeal, trigeminal and less likely, facial nerves can be involved.

References

1. Murtagh R, Caracciolo J, Fernandez G. CT Findings Associated with Eagle Syndrome. AJNR Am J Neuroradiol. 2001;22(7):1401-2
2. Chuang W, Short J, McKinney A, et al. Reversible Left Hemispheric Ischemia Secondary to Carotid Compression in Eagle Syndrome: Surgical and CT Angiographic Correlation. AJNR Am J Neuroradiol. 2007;28(1):143-5
3. Zhao X, Cavallo C, Hlubek RJ, et al. Styloidogenic Jugular Venous Compression Syndrome: Clinical Features and Case Series. *Oper Neurosurg*. Dec 1 2019;17(6):554-561. doi:10.1093/ons/opz012
4. Shin JH, Herrera SR, Eboli P, et al. Entrapment of the glossopharyngeal nerve in patients with Eagle syndrome: surgical technique and outcomes in a series of 5 patients. *J Neurosurg*. Dec 2009;111(6):1226-30. doi:10.3171/2009.1.Jns08485
5. Al-Hashim M, Al-Jazan N, Abdulqader A, et al. Eagle's syndrome with facial palsy. *J Family Community Med*. May-Aug 2017;24(2):128-130. doi:10.4103/jfcm.JFCM_134_16

Images/Tables

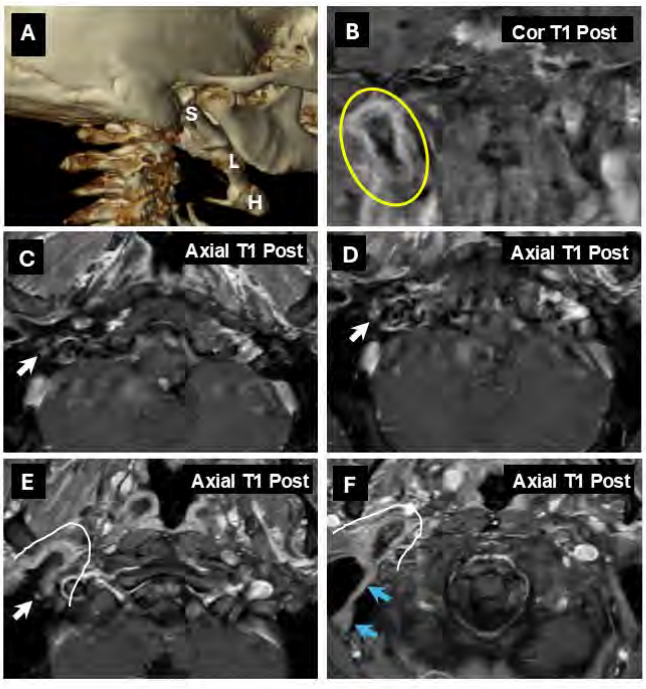

Figure 1. A. Three-dimensional (3D) reconstruction from the computed tomography (CT) of the neck shows an elongated right styloid process (S) and ossification of the stylohyoid ligament (L) which articulates with the hyoid bone (H). B. Contrast enhanced T1-weighted magnetic resonance imaging (MRI) of the skull base in coronal view illustrates dramatic abnormal enhancement surrounding the styloid process (yellow oval). C-F. Contrast enhanced T1-weighted MRI of the skull base in axial views demonstrates abnormal enhancement of the stylomastoid foramen and mastoid segment of the facial nerve (white arrows in C-E). Enhancement surrounding the styloid process (curved white lines in E and F) extends to the occipital mastoid suture region (blue arrows in F).

511 Brain MRI Findings in the Setting of Hypoglycemic Encephalopathy

Joel Thomas MD, Jack Rigsbee BS, Manu S Goyal MD
Mallinckrodt Institute of Radiology, Washington University School of Medicine, St. Louis, MO, USA

Clinical History

This retrospective case series included 11 patients for whom hypoglycemia was listed as one of the principal hospital problems and a brain MRI was obtained during their admission. Assessment of diffusion-weighted imaging (DWI) abnormalities in deep grey matter, cortex, cerebellum, and subcortical white matter structures was completed and compared among patients. Clinical characteristics and outcomes were also noted and assessed in the context of the distribution of the patient's DWI abnormalities.

Imaging Findings

11 patients underwent MRI within 0-5 days of being treated for hypoglycemic encephalopathy. Restricted diffusion involved the cortex (n=7) in the majority of patients in this series, with variable sparing of the peri-Rolandic and medial occipital regions. DWI abnormalities in deep grey matter structures, including the hippocampi, were also frequently seen (n=9), with simultaneous cortical and deep grey matter abnormalities in most patients (n=7). Diffusion restriction in subcortical white matter (n=3) and the cerebellum (n=3) was less common, as was overlap between involvement of both the cortex and subcortical white matter (n=2). One patient in this cohort (patient 8) was an outlier with a minimum blood glucose of 61 mg/dL, minimal findings on MRI (restricted diffusion in the left hippocampus), and minimal symptoms (clouding of consciousness at presentation that resolved by discharge).

Discussion

Hypoglycemic encephalopathy is a common emergent presentation of altered mental status. However, there is a paucity of literature regarding brain MRI findings in these patients given its rapidly identifiable cause and potential reversible nature with glucose administration. Existing literature outlines some patterns of injury on imaging, most notably bilateral, symmetric diffusion-restricted lesions involving the cerebral cortex and deep grey nuclei, and less commonly the white matter[1]. DWI lesions have been shown to variably resolve or persist depending on the duration and severity of hypoglycemia[1,2]. In this study, we redemonstrated the findings of cortical and deep grey matter restricted diffusion previously established in hypoglycemic encephalopathy. Cortical involvement was variable, with cases of medial occipital and peri-Rolandic sparing, although not consistently. This case series demonstrated occasional involvement of the white matter as seen in past studies[3], though with only 3 cases of subcortical white matter involvement. Additionally, imaging findings varied among patients with similar outcomes, indicating the distribution of restricted diffusion alone is likely not predictive of neurologic recovery.

Teaching Point

Hypoglycemic encephalopathy is associated with variable imaging findings on MRI that do not necessarily correlate with clinical outcome. In this cohort, patterns of injury included diffuse cortical involvement (with variable sparing of the peri-Rolandic and medial occipital cortex), in addition to variable involvement of deep grey nuclei and, to a lesser extent, subcortical white matter.

References

1. Kang, EG, Jeon, SJ, Choi, SS, et al. Diffusion MR imaging of hypoglycemic encephalopathy. *AJNR Am J Neuroradiol*, 2010;31(3):559-564. DOI: https://doi.org/10.3174/ajnr.A1856

2. Johkura, K, Nakae, Y, Kudo, Y, et al. Early diffusion MR imaging findings and short-term outcome in comatose patients with hypoglycemia. *AJNR Am J Neuroradiol*, 2012;33(5):904-909. DOI: 10.3174/ajnr.A2903

3. Ma, JH, Kim, YJ, Yoo, WJ, et al. MR imaging of hypoglycemic encephalopathy: lesion distribution and prognosis prediction by diffusion-weighted imaging. *Neuroradiology*, 2009;51(10):641-649. DOI: 10.1007/s00234-009-0544-5

Images/Tables

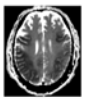

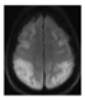

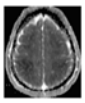

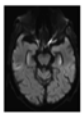

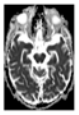

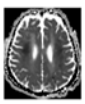

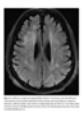

518 Subarachnoid Pneumocephalus Following Epidural Injection: A Stroke Mimic Managed Conservatively

Janelle Azar[1], Andres Samos[1], Roman Montes De Oca[1], Muhammad Aziz MD[2]
[1]FIU Herbert Wertheim College of Medicine, Miami, FL, USA. [2]FIU Herbert Wertheim College of Medicine, Miami, Florida, USA

Clinical History

A 56-year-old woman with type 2 diabetes, hypertension, and prior myocardial infarction presented with acute right-sided weakness immediately after fluoroscopy-guided cervical epidural and facet joint injections at C3–4, C4–5, and C5–6 for chronic neck pain. Shortly post-procedure, she developed chest discomfort, somnolence, and right arm and leg paresthesia with weakness. On arrival, her vital signs were stable, and she was alert and oriented, with intact cranial nerves and comprehension. Initial neurological examination revealed 4/5 strength in the left extremities and progressive right-sided weakness, from 3/5 at the deltoids to 1/5 at her fingers. Sensation to light touch and pinprick was reduced circumferentially on the right, and deep tendon reflexes were absent in the right arm with a negative Babinski sign. Her gait was wide-based and limited by pain. Laboratory studies, including electrolytes and coagulation panel, were unremarkable.

Imaging Findings

Initial non-contrast computerized tomography (CT) scan of the head demonstrated persistent scattered foci of subarachnoid pneumocephalus, mostly visualized at the bifrontal regions, and no acute intercranial hemorrhage, midline shift, or hydrocephalus (Figure 1). Brain magnetic resonance imaging (MRI) showed similar findings of pneumocephalus and mild chronic microvascular ischemic changes (Figure 2). Additionally, a cervical MRI demonstrated a T2-hyperintense cord signal spanning the C3-T5 levels with no evidence of cord infarct (Figure 3). Scattered foci of intrathecal and epidural air were also visualized throughout the spine, with mild nonspecific prevertebral soft tissue edema and moderate spinal canal stenosis at the C6 to C7 level.

Discussion

The patient was managed conservatively with high-flow oxygen via a non-rebreather mask, head elevation, and intravenous dexamethasone tapered over several days. By day four, her neck and back pain improved, and she was able to ambulate independently. Right-sided weakness remained most pronounced distally in the right arm with absent reflexes and decreased sensation, though near-baseline strength returned in all other extremities. A repeat CT on day five (Figure 4) demonstrated complete intracranial air resorption. She was discharged to an inpatient rehabilitation center for continued recovery.

Management of pneumocephalus involves high-concentration oxygen to accelerate air resorption, corticosteroids for edema, and supportive care. Evidence comparing hyperbaric oxygen therapy (HBOT) with high-flow normobaric oxygen remains limited and inconsistent. A 2014 review by Paiva et al. found faster radiologic resolution with HBOT but no improvement in neurological outcomes compared with 100% FiO_2 via a non-rebreather mask.[1] A recent systematic review identified only three heterogeneous studies and none directly comparing these oxygen-delivering modalities[2], highlighting a persistent gap in the data.

Teaching Point

In conclusion, we present a rare case of pneumocephalus with associated cervical cord injury following epidural and facet injections, manifesting as acute hemiparesis mimicking stroke. This case underscores the need for more comparative data to inform care across facilities with different resources. In situations where facilities lack access to HBOT, conservative management with high-flow oxygen, corticosteroids, and supportive care remains an effective and practical approach. As highlighted by this case, such management can lead to full radiologic and clinical recovery while avoiding delays associated with HBOT transfer or availability.

References

1- Paiva WS, de Andrade AF, Figueiredo EG, et al. Effects of hyperbaric oxygenation therapy on symptomatic pneumocephalus. *Ther Clin Risk Manag*. 2014;10:769-773. DOI:10.2147/TCRM.S45220
2- Kim BJH, Ji MY, Chen JCC, et al. Use of oxygen therapy for pneumocephalus: a systematic review. *Neurosurg Rev*. 2024;47(1):30. DOI:10.1007/s10143-023-02261-4

Images/Tables

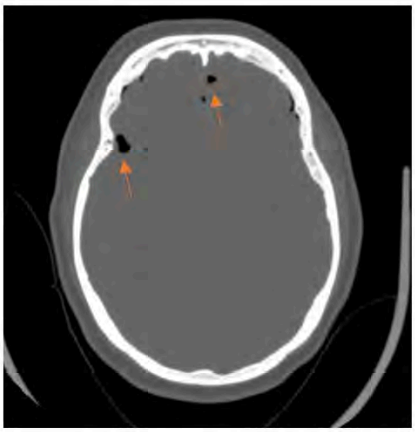

Figure 1: brain CT showing scattered foci of trapped air, consistent with pneumocephalus.

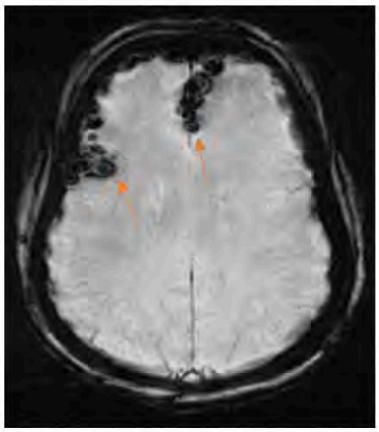

Figure 2: brain MRI showing similar findings of pneumocephalus within the bifrontal subarachnoid space. No evidence of infarct or midline shifts.

Figure 3: cervical MRI showing right-sided long segment T2 hyper-intense cord signal abnormality spanning the C3 through the partially visualized T5 level. Scattered foci of intrathecal and epidural air was also visualized throughout the spinal canal.

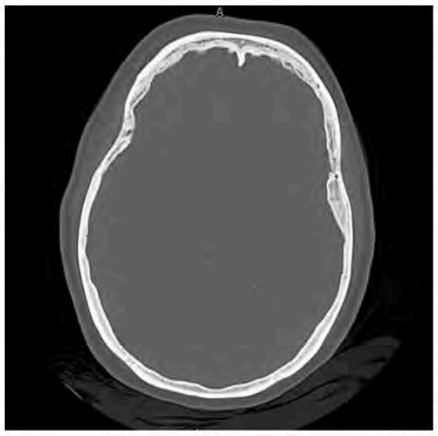

Figure 4: brain CT showing resolution of the pneumocephalus 5 days after initial CT in figure 1.

---

519 Calling It Right: Multiparametric MRI Predicts DCVax-L Response in a Long-Term GBM Survivor

Archith Rajan PhD[1], Daniel Gewolb MD[2], Ajay Kumar MD, PhD[1], Laiz Laura de Godoy MD, PhD[1], Arati Desai MD, MAS[3], Steven Brem MD[4], Zissimos Mourelatos MD[5], Suyash Mohan MD[6], Sanjeev Chawla PhD[1]

[1]Division of Neuroradiology, Department of Radiology, Perelman School of Medicine at the University of Pennsylvania, Philadelphia, Pennsylvania, USA. [2]Miller School of Medicine, University of Miami, Miami, Florida, USA. [3]University of Pennsylvania, Philadelphia, PA, USA. [4]Department of Neurosurgery, Perelman School of Medicine at the University of Pennsylvania, Philadelphia, Philadelphia, Pennsylvania, USA. [5]Clinical Pathology and Laboratory Medicine, Perelman School of Medicine at the University of Pennsylvania, Philadelphia, PA, USA. [6]Division of Neuroradiology, Department of Radiology, Perelman School of Medicine at the University of Pennsylvania, Philadelphia, PA, USA

Clinical History

A 63-year-old woman presented with seizures, aphasia and left facial weakness. MRI demonstrated a left frontal contrast-enhancing mass. Near-total resection confirmed the diagnosis of GBM (IDH-wildtype, MGMT-methylated, EGFRvIII-negative). She completed standard-of-care concurrent chemoradiation therapy (KPS 90) and enrolled on an autologous tumor lysate-loaded dendritic cell vaccine (DCVax-L)[1] trial (NCT00045968). Over 31 months post-resection, she received 10 doses (dose=0.15 ml per injection). Two subsequent craniotomies showed predominantly viable malignant glioma with superimposed treatment effects. Overall survival was 64 months from initial surgery and 60 months from DCVax-L initiation.

Imaging Findings

The purpose of this study was to investigate the potential utility of a previously developed multiparametric MRI-based prediction model[2] in evaluating treatment response in long-surviving glioblastoma patient treated with DCVax-L. The patient underwent serial MRI scans at 10 time points beginning two weeks prior to DCVax-L initiation (Figure **A–B**). Multiparametric MRI model consisted of predictive probabilities (PP) of tumor progression computed from diffusion and perfusion MRI-derived parameters from contrast enhancing regions (CERs). The model consisted of three parameters: median values of fractional anisotropy (FA), coefficient of linear anisotropy (CL) and maximum relative cerebral blood volume (rCBVmax). The absence of detectable CER within the tumor bed precluded the multiparametric MRI data analysis three times during treatment. At other 7 time points, the PP values were used to characterize the lesion as true progression (TP, if PP $\geq$ 50%) or pseudoprogression (PsP, if PP < 50%)[3]. We sought to ascertain the number of time points for which our model correctly classified the lesion as TP or PsP using histopathology/mRANO criteria as ground truths in the final diagnosis of TP or PsP. When tumor specimens were available from repeat surgery (n=2), histopathological analyses were used to classify between TP (>25% malignant viable neoplasm; and PsP (<25% malignant viable neoplasm). In the absence of histopathology (n=5), modified RANO criteria[4] were used to determine TP or PsP.

Our predictive model using PP values correctly identified all time points with TP (n =3) and PsP (n =4). These findings reflect a significant concordance between the model's diagnostic performance and final diagnosis as determined by histopathology/mRANO criteria[3] (Figure **D**).

Our predictive model using PP values correctly identified all time points with TP (n =3) and PsP (n =4). These findings reflect a significant concordance between the model's diagnostic performance and final diagnosis as determined by histopathology/mRANO criteria[4] (Figure **D**).

Discussion

Our multiparametric MRI-based prediction model correctly classified enhancing lesion as TP or PsP at each time point during treatment. We believe that this is a very promising finding given the fact that glioblastomas are extremely heterogeneous neoplasms in nature and immunotherapy trigger profound inflammatory response at the tumor bed.

Teaching Point

- Multiparametric MRI-based prediction model can assess treatment response in a long-surviving patient with glioblastoma receiving DCVax-L.
- Multiparametric MRI data analysis may allow for refined prognostication and improved “go/no-go” decision-making in real time with regard to changes in immunotherapy regimen in neuro-oncology.

References

1. Liau, LM., Ashkan K., Brem S et al. (2023). Association of autologous tumor lysate-loaded dendritic cell vaccination with extension of survival among patients with newly diagnosed and recurrent glioblastoma: a phase 3 prospective externally controlled cohort trial. *JAMA oncology*, *9*(1), 112-121.
2. Wang, S, Martinez-Lage M, et al. (2016). Differentiating tumor progression from pseudoprogression in patients with glioblastomas using diffusion tensor imaging and dynamic susceptibility contrast MRI. American Journal of Neuroradiology, 37(1), 28-36.
3. de Godoy, LL, Chawla S, et al. (2023). Assessment of treatment response to dendritic cell vaccine in patients with glioblastoma using a multiparametric MRI-based prediction model. *Journal of Neuro-Oncology*, *163*(1), 173-183.
4. Ellingson BM, Wen PY, Cloughesy TF. Modified criteria for radiographic response assessment in glioblastoma clinical trials. Neurotherapeutics. 2017 Apr 1;14(2):307-20.

Images/Tables

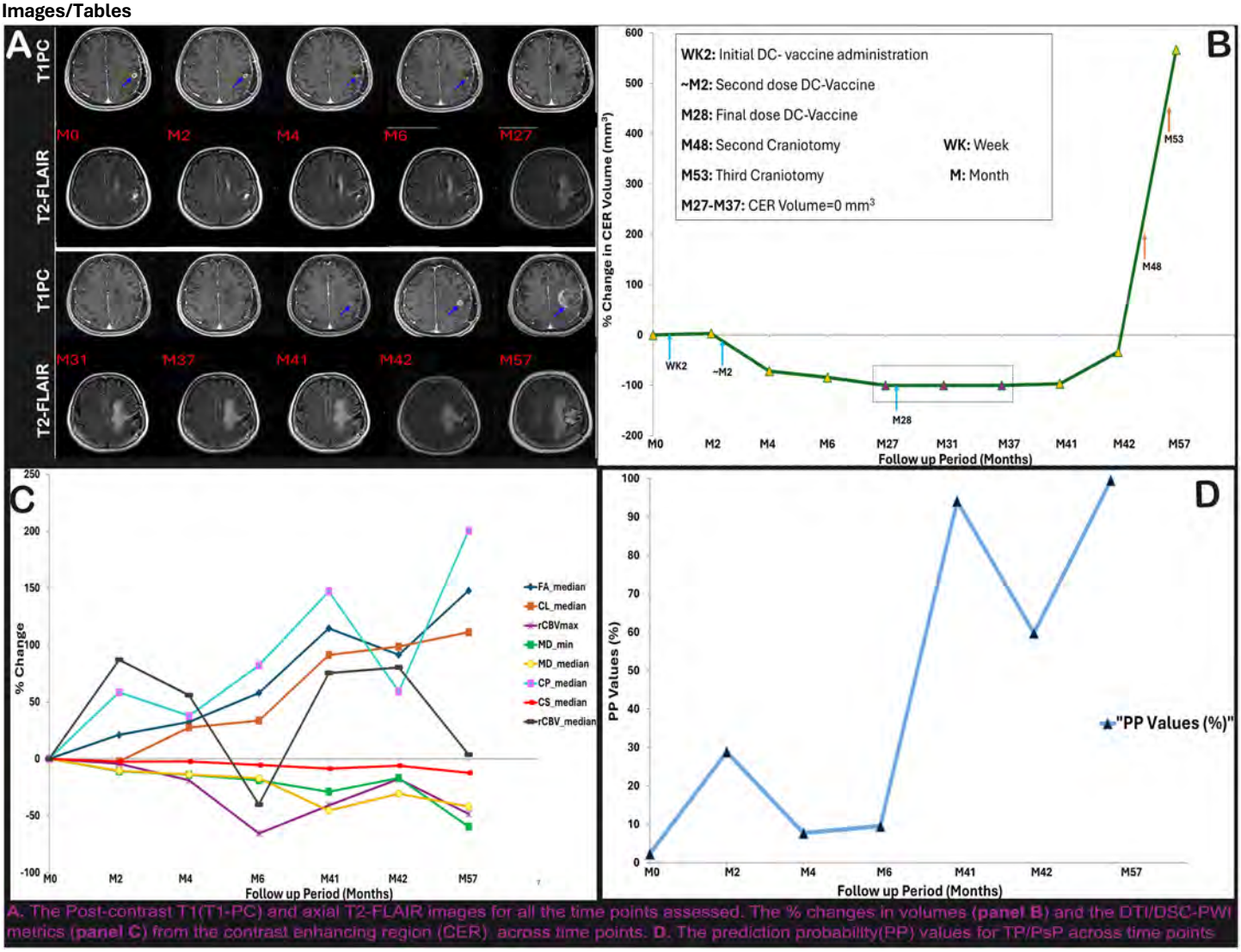

A. The Post-contrast T1(T1-PC) and axial T2-FLAIR images for all the time points assessed. The % changes in volumes (**panel B**) and the DTI/DSC-PWI metrics (**panel C**) from the contrast enhancing region (CER) across time points. **D**. The prediction probability(PP) values for TP/PsP across time points

---

523 An Unintended Intra-arterial Injection of Contrast During CT Angiography.

Sanidhya Shailendra Karve MD, Jay Starkey MD, Reza Moein Taghavi
Oregon Health and Science University, Portland, Oregon, USA

Clinical History

A 68-year-old female was found unresponsive. A CT angiogram was ordered to look for a large vessel occlusion. 50 ml Omnipaque 350 was administered via 20G IV access needle at the rate of 5ml/sec using power injector. On contrast injection, the patient experienced excruciating pain in the right arm.

Imaging Findings

Intense opacification of the right subclavian artery and its branches. The aortic arch and its branches were not opacified. Right vertebral artery and its branches, including the anterior spinal, posterior inferior cerebellar artery (PICA), and medullary branch, all the way up to distal posterior cerebral artery (PCA), were opacified. Intracranially, contrast crosses midline through the basilar artery via the left PCA and left superior cerebellar artery (SCA).

Right hemicord enhancement from the C4 level upward. Intense posterior circulation parenchymal enhancement with sharp territorial demarcation. Symmetrical enhancement of bilateral thalami, midbrain, paramedian parietal lobes, and occipital lobes. Ipsilateral enhancement involving the right cerebellum, right half of the medulla and pons, with sharp midline demarcation. Relative contralateral medial cerebellar non-enhancement, which was likely due to left PICA sparing and probable left AICA agenesis/hypoplasia. Left SCA territory superolateral cerebellar enhancement noted.

Later, a CT angiogram repeated using left arm intravenous access, showed a normal arterial phase angiogram with a right M1-M2 bifurcation aneurysm. No fetal PCAs were identified, which explain the lack of anterior circulation involvement in the previous angiogram. No injection site complications were noted.

Discussion

Unintended intra-arterial (IA) contrast injection is rare and may occur due to variations in the vascular anatomy of the upper limb. Aberrant superficial ulnar artery or a high bifurcating brachial artery are most commonly mistaken for a vein and accidentally cannulated [1]. Other risk factors include morbid obesity, lack of technical expertise, or vigilance etc.

Imaging findings can vary widely based on the type of injection (power or manual), scan timing, bolus triggering setting, and vascular anatomic variants. Common variants are fetal PCAs, dominant vertebral artery, and bovine aortic arch [2,3]. Being aware of the enhancement pattern, cannulation

history, and recognizing the subclavian arterial injection on the scan is crucial to avoid misinterpreting it as a pathology [2,3]. It could be confused with abnormal leptomeningeal enhancement, Lhermitte-Duclos disease, and vascular malformations, depending on the pattern of enhancement.
Signs of intra-arterial cannulation are intense pain on contrast injection, pulsatile retrograde flow, etc. Because the contrast injection is against the flow in the artery, there is risk of arterial clot or dissection. In addition, contrast extravasation may occur[4] . Finally, while the bolus dose and contrast concentration is similar to interventional angiography, rapid injection of a large bolus may lead to contrast encephalopathy[5]. Modifying the bolus tracking protocol by putting region of interest at the mid-aortic arch avoids starting scan in cases of left-sided intra-arterial injection or right-sided intra-arterial injection with a weak retrograde flow and prevents unnecessary radiation. Ultrasound guidance is not fool proof as our case demonstrates[3,4].

Teaching Point

Radiologists should be aware of the possibility of an intra-arterial contrast injection with its unique imaging patterns and potential complications.

References

1. Gupta P, Gulati GS, Guleria M. Contrast injected, scan triggered, but where has contrast gone?. *Indian J Radiol Imaging*. 2012;22(3):186-187. doi:10.4103/0971-3026.107180
2. Wong M, Brennan D, Gaillard F. Unusual enhancement patterns from inadvertent arterial contrast injection during CT angiography. *J Clin Neurosci*. 2020;78:406-408. doi:10.1016/j.jocn.2020.04.094
3. Zhang H, Kumar S. Unintended intra-arterial injection of contrast of an intracranial CT angiography. *Radiol Case Rep*. 2018;14(1):41-43. Published 2018 Oct 6. doi:10.1016/j.radcr.2018.09.005
4. Sen S, Chini EN, Brown MJ. Complications after unintentional intra-arterial injection of drugs: risks, outcomes, and management strategies. *Mayo Clin Proc*. 2005;80(6):783-795. doi:10.1016/S0025-6196(11)61533-4
5. Meijer FJA, Steens SCA, Tuladhar AM, et al. Contrast-induced encephalopathy-neuroimaging findings and clinical relevance. Neuroradiology. 2022;64(6):1265-1268. doi:10.1007/s00234-022-02930-z

Images/Tables

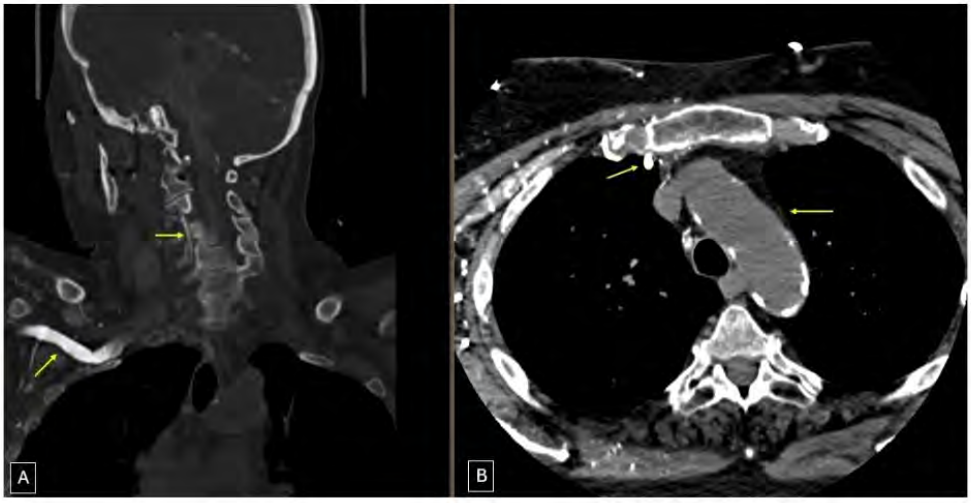

Figure 1: Coronal view (A) and axial view (B) of CT Angiogram demonstrating contrast opacification of right subclavian and its vertebral artery/anterior thoracic artery branches. Contrast doesn't reach arch of aorta and its other branches due to weak retrograde flow. This is indicative of a right sided intra-arterial contrast injection.

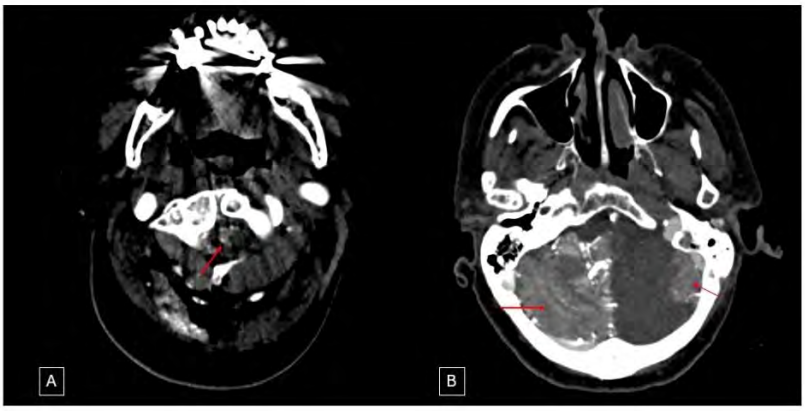

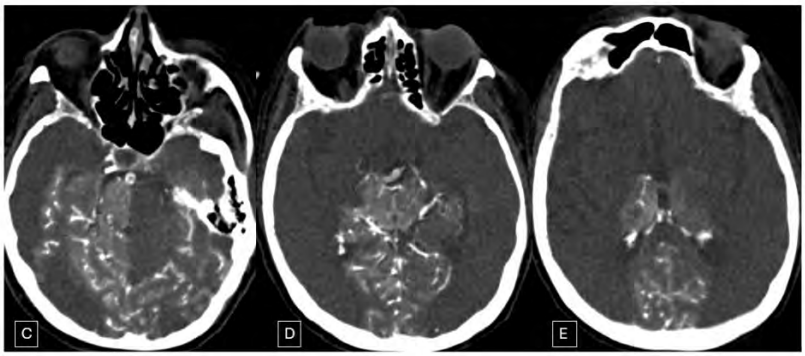

Figure 2: Axial CT Angiogram following intra-arterial contrast injection demonstrating enhancement in following areas: right cervical hemicord (A), entire right cerebellum/medulla and contralateral superolateral cerebellum, sparing left medial cerebellum/left half of medulla (B), right pons and bilateral occipital lobes (C), entire midbrain, bilateral thalami and paramedian parietal lobes (D,E).

Figure 3: CT Angiogram with a normal intravenous contrast administration was performed using left sided venous access later. Abnormal enhancement has vanished with an early arterial phase study showing contrast predominantly in the intracranial arteries (A, B). Incidentally detected inferiorly directed tiny saccular aneurysm seen at the right M1-M2 MCA bifurcation (B).

548 Trigeminal Neuralgia Associated with Congenital Anomalies of Meckel's Cave: Two Case Reports and Review of the Literature

Asayel Alzahrani, Omamah Qawalh, Reem Adas, Aisha Halawani, MD
Ministry of National Guard Health Affairs, Jeddah, Mecca, Saudi Arabia

Clinical History

Two female patients presented with unilateral trigeminal neuralgia (TN) in the absence of neurovascular compression.

Patient 1: A 46-year-old woman experienced paroxysmal electric-shock pain in the right maxillary and mandibular territories, refractory to carbamazepine (1.6 g/day). There was no prior trauma, infection, or demyelinating disease.

Patient 2: A 28-year-old woman reported episodic burning pain in the left ophthalmic and maxillary distributions with mild facial hypoesthesia. Symptoms partially improved with gabapentin.

Both underwent dedicated 3 T MRI of the skull base with thin-section constructive-interference-in-steady-state (CISS) and 3D SPACE sequences for detailed evaluation of the trigeminal pathway.

Imaging Findings

Patient 1: Axial and coronal CISS images showed complete absence of the right Meckel's cave with loss of the normal CSF pouch and marked atrophy of the cisternal trigeminal nerve (1.2 mm versus 2.5 mm contralateral) (arrowhead).

Patient 2: Axial and coronal CISS images show a hypoplastic left trigeminal nerve entering an enlarged, laterally displaced Meckel's cave centered within the petrous apex (arrowhead).

Discussion

Meckel's cave is a CSF-containing dural recess that houses the trigeminal ganglion. Congenital absence or malformation of this space is uncommon but has been increasingly recognized as a structural correlate of TN on high-resolution MRI. The cave develops from a dural evagination of the posterior fossa; incomplete formation or aberrant extension can lead to aplasia, hypoplasia, or displacement (1). Loss or alteration of the surrounding CSF space may expose the ganglion to chronic mechanical or microvascular stress, resulting in nerve thinning and neuropathic pain (2, 3).

Jain et al. (4) described seven patients with unilateral absence of Meckel's cave and ipsilateral trigeminal-nerve atrophy, none showing neurovascular contact. Cleary et al. (5) reported three similar cases that improved after stereotactic radiosurgery. Lin et al. demonstrated that reduced Meckel's-cave volume and "flatness" on radiomic analysis were associated with primary TN even in the absence of vascular conflict.

Our cases represent two ends of a congenital spectrum, complete aplasia with nerve atrophy and hypoplasia with ectopic expansion, both had ipsilateral TN. Recognition of these congenital variants is clinically relevant to avoid unnecessary vascular decompression. In such cases, medical therapy or ganglion-directed procedures may be more appropriate. When no vascular contact is seen, careful bilateral assessment of Meckel's-cave morphology on high-resolution CISS or FIESTA sequences can help identify these subtle anomalies.

Teaching Point

Congenital anomalies of Meckel's cave (including aplasia, hypoplasia, and ectopic expansion) are rare structural causes of trigeminal neuralgia. In patients without neurovascular compression, high-resolution evaluation of Meckel's-cave morphology can help uncover potential structural correlates of trigeminal neuralgia and assist in management planning.

References

1. Malhotra A, et al. Neuroimaging of Meckel's cave in normal and disease conditions. Insights Imaging. 2018;9(4):499–510.
2. Cruccu G, Di Stefano G, Truini A. Trigeminal neuralgia. Continuum (Minneap Minn). 2017;23(2):396–420.
3. Jain A, et al. Absence of Meckel cave: a rare cause of trigeminal neuralgia. AJNR Am J Neuroradiol. 2021;42(9):1610–1614.
4. Cleary DR, et al. Three cases of trigeminal neuralgia with radiographic absence of Meckel's cave. Stereotact FunctNeurosurg. 2019;97(4):249–254.
5. Lin J, et al. Flatness of the Meckel cave may cause primary trigeminal neuralgia: a radiomics-based study. J Headache Pain. 2021;22(1):99.

Images/Tables

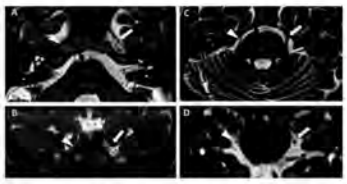

Figure 1: (A) Axial and (B) coronal CISS images show an absence of CSF space on the right Meckel's cave (arrowhead) as compared with the normal left Meckel's cave (arrow). (C) Axial and (D) coronal CISS images in the same patient show atrophy of the right trigeminal nerve (arrowhead) as compared with the normal trigeminal nerve of left side (arrow).

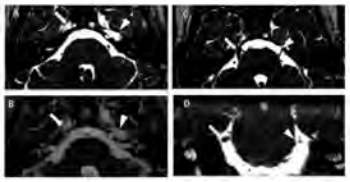

Figure2: A) Axial and (B) 3D CISS images demonstrate an enlarged, abnormally positioned left Meckel's cave (arrowhead) centered within the left petrous apex. The abnormally positioned Meckel's cave is causing deformity & expansion of the petrous apex, as compared with the normal apex of the right Meckel's cave (arrow). (C) Axial and (D) coronal CISS images show the left trigeminal nerve (arrowhead), which appears congenitally hypoplastic and deviates laterally by approximately 35° from its expected course, (compared with the normal right trigeminal nerve (arrow).

Table 1. Summary of Published Literature on Absent or Hypoplastic Meckel's Cave Associated with Trigeminal Neuralgia

Journal Name	Year	First Author	Paper Title	Number of Cases	Imaging Findings
The Journal of Radiology Case Reports	2024	Jacob Schroeder	Trigeminal neuralgia in the context of an undetectable Meckels cave.	1	Non-visualization/undetectable Meckel's cave ipsilateral to TN; cisternal trigeminal nerve atrophy documented on 3D sequences.
Radiology Case Reports	2023	Ali Al-Smair	Absent Meckel's cave as a possible cause of trigeminal neuralgia	1	Ipsilateral absent Meckel's cave on MRI; ipsilateral trigeminal symptoms; imaging excluding other causes.
Indian Journal of Radiology and Imaging	2022	Asma Alhlumi	Absence of Meckel's Cave with Trigeminal Neuralgia.	1	Ipsilateral absence of Meckel's cave with atrophy of cisternal trigeminal nerve on 3T MR; no neurovascular contact found.
American Journal of Neuroradiology	2021	A. Jusi	Absence of Meckel Cave: A Rare Cause of Trigeminal Neuralgia	7	Unilateral absence of Meckel's cave on high-res MRI in all; ipsilateral trigeminal nerve atrophy (reduced CSA); No neurovascular conflict in these patients.
The Journal of Headache and Pain	2021	Jinzhi Lv	Flatness of the Meckel cave may cause primary trigeminal neuralgia: a radiomics-based study	112	Quantitative morphologic changes (eg, "flatness"; shape features) of the Meckel's cave were significantly associated with PTN, especially in patients without neurovascular contact.
Pakistan Journal of Radiology	2020	Khanchan Shuldani	Absent Meckel's cave on MRI in a clinically-diagnosed TN.	1	Unilateral absent Meckel's cave identified on MRI in a patient with TN; no significant vascular conflict.
Stereotactic and Functional Neurosurgery	2019	Daniel R. Cleary	Three Cases of Trigeminal Neuralgia with Radiographic Absence of Meckel's Cave	3	Absent or hypoplastic ipsilateral Meckel's cave; no other compressive lesions identified on thin-cut MR.

---

578 CT Appearance of Morgagnian Cataract

Valeria Ortega Apraez M.D., Pedro Diaz-Marchan M.D., Kuang-chun Jim Hsieh M.D.
Baylor College of Medicine, Houston, Texas, USA

Clinical History

64-year-old female with hypertension, heart failure, and smoking history presented to the ER after head trauma. Head and Maxillofacial CT performed for trauma evaluation revealed an incidental Morgagnian cataract in the left eye, previously diagnosed by Ophthalmology.

The patient reported a long history of gradually progressive, painless vision loss in the left eye and mild visual decline in the right eye. Ophthalmologic examination showed left Morgagnian lens with significant zonular loss from 3 to 12 o'clock. Intraocular pressure was 18 mmHg. The right eye had a dense white cataract with some visual fields preserved.

Imaging Findings

Left ocular lens with dense nucleus posteriorly (red arrow) and hypodense, liquified anterior cortex (blue arrow) correlates with a photo of a Morgagnian cataract. Zonular attachments maintain lens position, and the significant zonular loss likely accounts for the subtle posterior lens subluxation. For comparison, another partially dislocated lens from the literature is provided. Following complete zonular disruption, the lens may dislocate posteriorly layering in the vitreous as shown or, less commonly, anteriorly. Trauma accounts for over half of lens dislocations, though nontraumatic lens dislocations can occur with systemic connective tissue disorders, such as Marfan and Ehler-Danlos syndrome. Acute traumatic cataracts have been described as hypoattenuating, with a mean attenuation difference of 30 HU when compared to the contralateral lens due to increased fluid within the lens. Surgical treatment of cataracts involves lens extraction and replacement with an intraocular lens implant. The presence of a lens implant, known as pseudophakia, appears on imaging as a thin linear hyperdensity.

Discussion

A Morgagnian cataract represents a hypermature cataract characterized by complete liquefaction of the lens cortex and a dense, sunken nucleus within the capsule. On CT, its appearance is likely attributed to the liquefaction of the lens cortex, with increased fluid contributing to decreased attenuation. The advanced stage of this kind of cataract may lead to secondary complications such as lens dislocation, inflammation, or glaucoma. Diagnosis is clinical, and treatment involves surgical lens extraction.

Teaching Point

CT correlate of Morgagnian cataract is an ocular lens with a liquified (hypodense) cortex and a dense dependent layering nucleus.

References

1. Sukhija J, Kaur S. Morgagnian cataract. N Engl J Med. 2014;370(24):2326. DOI:10.1056/NEJMicm1312140

2. Hua X, Dong Y, Wang L, et al. Intraocular lens implantation performed first to protect the posterior capsule in Morgagnian cataracts during phacoemulsification. Int J Ophthalmol. 2019;12(7):1215-8. DOI: 10.18240/ijo.2019.07.25
3. Kubal WS. Imaging of orbital trauma. Radiographics. 2008 Oct;28(6):1729-39. DOI: 10.1148/rg.286085523
4. Boorstein JM, Titelbaum DS, Patel Y, Wong KT, Grossman RI. CT diagnosis of unsuspected traumatic cataracts in patients with complicated eye injuries: significance of attenuation value of the lens. AJR Am J Roentgenol. 1995 Jan;164(1):181-4. DOI: 10.2214/ajr.164.1.7998535

Images/Tables

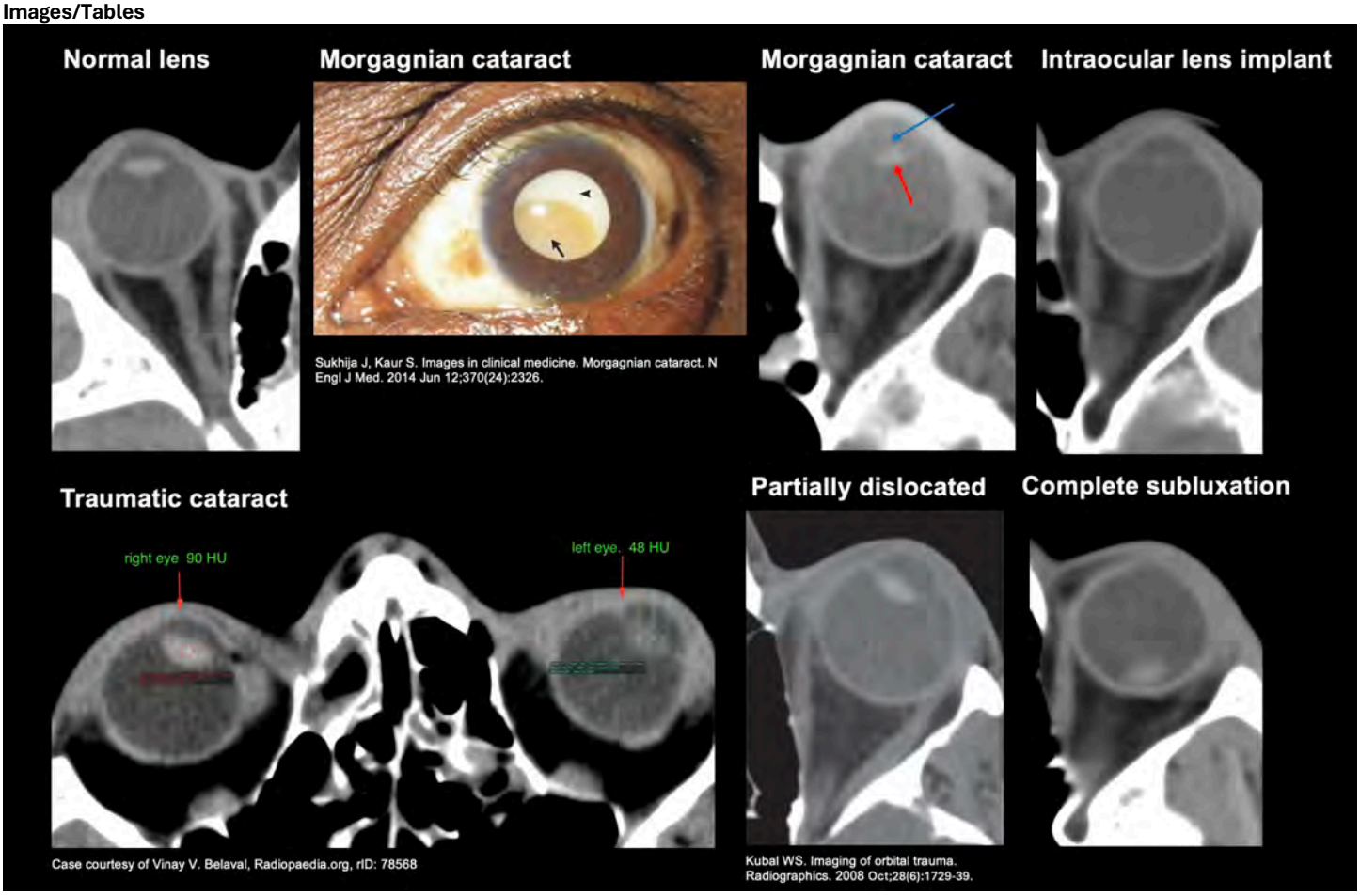

---

587 A Case report of the MRI features of Isolated Cytomegalovirus (CMV) Retinitis in an HIV patient.

Nafisa Paruk MBChB, FCRad Diag SA[1], Richard Wiggins MD, FACR[2]
[1]Drs Oosthuizen & Ebrahim Incorp.., Pretoria, Gauteng, South Africa. [2]University of Utah, Salt Lake City, Utah, USA

Clinical History

A 52 year old, HIV positive male patient presented with decreased visual acuity in the left eye, seizures and pyrexia. MRI and ophthalmic findings of CMV retinitis were noted.

CSF analysis detected viral meningitis not seen on the MRI

Imaging Findings

Left ocular CMV retinitis:

T1: Isointense to minimally hyperintense.

T2 FLAIR and T2: Hyperintense.

Diffusion restriction with low ADC, peripheral T2 shine through.

Postcontrast T1: Enhancement.

SWI : Punctate haemorrhages

Discussion

CMV retinitis occurs concurrently with viral meningitis in severely immunocompromised patients, as in HIV, patients receiving immunotherapy, chemotherapy and organ transplants.

It is the most common opportunistic ocular disease in HIV patients and carries a poor prognosis resulting in irreversible blindness.

The disease is slowly progressive and undetectable in its early stages. Hence the importance of early screening, especially in low socioeconomic groups.

The incidence has decreased to 0.3% since the initiation of HAART.

Risk factors include severe systemic or local ocular immunosupression, CD4 counts less than 50cells/mm3, low socioenomic areas , especially in areas with lack of resources for screening and some immunocompetent patients.

Clinically, presentation may be asymptomatic, present with decreased visual acuity, scotomas, vitreal floaters and photopsias. Pain and photophobia are uncommon. CMV oculopathy may present with retinitis, uveitis, corneal endotheliitis and iridocyclitis. Vitreal inflamamtion may be the earliest sign.

1/3 of patients present with retinal detachment if infiltrative disease exceeds 25%. Optic nerve atrophy and papillitis (4%) are rare.

Causes of blindness include retinal destruction, retinal detachment and IRU (Immune Reconsitution Uveitis) due to HAART.
Pathophysiology: CMV retinitis is a double stranded DNA herpes virus which occurs from primary infection or reactivation of the latent virus in myeloid progenitor cells and other tissues. Histopathology reveals pathognomonic CMV intracellular eosinophilic inclusions or "owl's eyes".
The definitive diagnosis is made on PCR, OCT, vitreous biopsy, aqueous tap and consequent histopathology as in this case. Bedside ultrasound detects retinal detachment.
MRI and lumbar puncture are essential to evaluate for CMV meningitis and encephalitis.
It is important to differentiate it from Acute Retinal Necrosis (ARN), which has less severe necrosis, since the treatments differ. Other differential diagnoses include HIV retinopathy and syphilitic haemorrhagic necrotising retinitis, the latter being a mimic of CMV retintis.
Management includes prompt treatment to avoid blindness, routine screening to detect viral loads, CD4 counts, RBC and fundoscopy.
The administration of HAART decreases CMV retinitis by 90%,despite the paradoxical increase in T cell reactivation on dead CMV.
Treatment includes intravitreal antiviral therapy and immunotherapy as given in this patient.
Longterm followup is required to avoid retinal detachment and blindness.

Teaching Point

Suspect CMV retinitis in an immunocompromised patient who presents with an acute onset of visual disturbance.
It is a slowly progressive disease which may go undetected in its early stages.
Hence, the importance of screening in high risk and low socioeconomic areas in order to enhance early detection and avoid irreversible blindness.
MRI may detect CMV early, before the systemic features of meningitis or encephalitis.
Early antiviral treatment and long term followup to avoid irreversible blindness, like retinal detachment.

References

Hassan-Moosa R, Chinappa T, Jeena L, Visser L, Naidoo K. Cytomegalovirus retinitis and HIV: Case reviews from KwaZulu-Natal Province, South Africa. S Afr Med J. 2017 Sep 22;107(10):843-846. doi: 10.7196/SAMJ.2017.v107i10.12740.
Kobayashi R, Hashida N. Overview of Cytomegalovirus Ocular Diseases: Retinitis, Corneal Endotheliitis, and Iridocyclitis. Viruses. 2024 Jul 11;16(7):1110. doi: 10.3390/v16071110. PMID: 39066272; PMCID: PMC11281654.
Patel SS, Rutzen AR, Marx JL, Thach AB, Chong LP, Rao NA. Cytomegalovirus papillitis in patients with acquired immune deficiency syndrome. Visual prognosis of patients treated with ganciclovir and/or foscarnet. Ophthalmology. 1996 Sep;103(9):1476-82. doi: 10.1016/s0161-6420(96)30480-6.
Zhang J, Kamoi K, Zong Y, Yang M, Zou Y, Miyagaki M, Ohno-Matsui K. Cytomegalovirus Retinitis: Clinical Manifestations, Diagnosis and Treatment. Viruses. 2024 Sep 7;16(9):1427. doi: 10.3390/v16091427.

Images/Tables

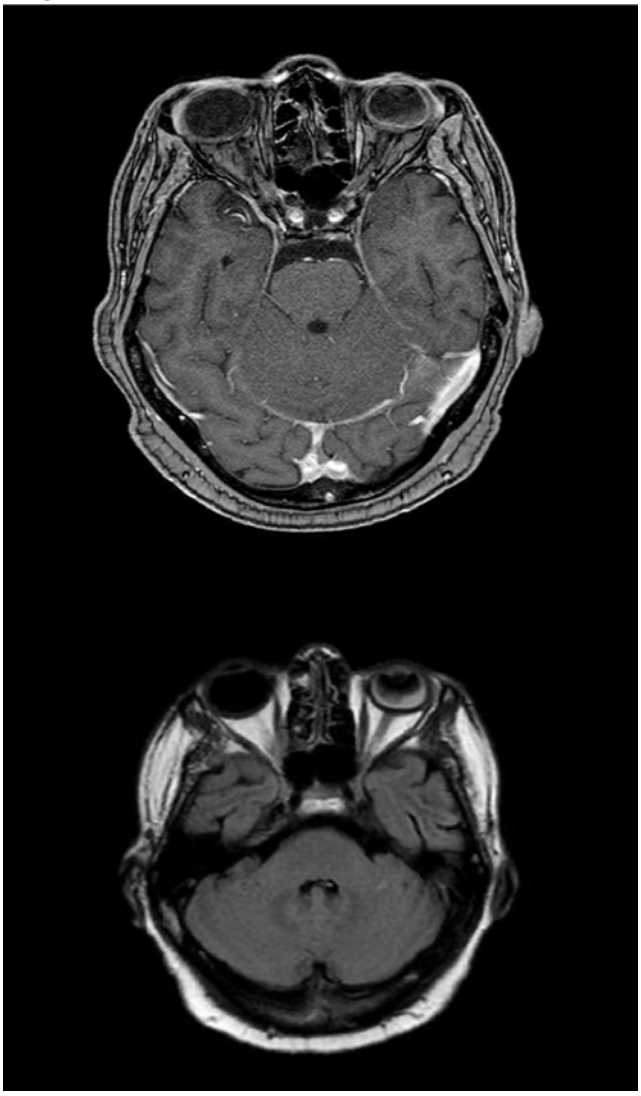

603 When the Eagle Strikes the Vein: A Case of Styloid-Induced Venous Sinus Thrombosis

Neud Kiros MD[1], Ahmad Chehab MD[2], Abeer Abukamil BS[3], Ahmad Chehab MD[1], Ali Luqman MD[1], Kamil Abu-Shaban MD[1], Mehdy Haidar MD[1], Ay-Ming Wang MD[1]

[1]Corewell Health William Beaumont University Hospital, Royal Oak, Michigan, USA. [2]Corewell Health East William Beaumont University Hospital, Royal Oak, MI, USA. [3]Wayne State University School of Medicine, Detroit, Michigan, USA

Clinical History

41-year-old male with no prior relevant medical history presented to the emergency department with severe neck pain and occipital headaches radiating bilaterally to the temporal regions. He also reported diplopia and "tunnel vision." He had presented two weeks earlier with similar symptoms and was advised outpatient follow-up. Initial CT head and cervical spine were unremarkable.

Imaging Findings

Brain MRI/MRV demonstrated heterogeneous signal and enhancement in the left transverse and sigmoid sinuses and jugular bulb, initially thought to reflect possible motion artifact. However, CT venography was recommended for further assessment. The MRI also showed subtle left posterior occipital subdural hemorrhage. CT venogram revealed bilateral elongated styloid processes (3.2 cm), with significant compression of the proximal left internal jugular vein at the level of the cranio-cervical junction. Small filling defects were identified in the left transverse and sigmoid sinuses and jugular bulb. A repeat MRV without motion artifact confirmed findings consistent with nonocclusive dural venous sinus thrombosis.

Discussion

Eagle syndrome refers to symptomatic elongation of the styloid process or calcification of the stylohyoid ligament. It is critical to distinguish this from asymptomatic elongation, which is commonly seen incidentally on imaging.

A subset, known as styloidogenic jugular venous compression syndrome, can result in venous outflow obstruction, with clinical manifestations ranging from chronic headaches to pseudotumor cerebri. In this case, CT venography revealed left internal jugular vein compression at the cranio-cervical junction level by a 3.2 cm left styloid process, with associated nonocclusive dural venous sinus thrombosis . These imaging findings correlated with the patient's occipital headaches and visual symptoms, meeting the threshold for Eagle syndrome.

Initial MRV demonstrated heterogeneous signal in the left dural sinuses, initially attributed to motion artifact. CT venography clarified this by confirming thrombus and identifying the underlying structural cause. This case underscores the diagnostic value of cross-sectional venography in cases of equivocal MRV, and reinforces that Eagle syndrome should only be diagnosed when there is both anatomic compression and attributable symptoms.

Teaching Point

In patients with dural venous sinus thrombosis and no clear hypercoagulable risk factors, consider extrinsic venous compression from elongated styloid processes, known as styloidogenic jugular venous compression syndrome as an underrecognized but surgically treatable cause. Importantly, Eagle syndrome should only be diagnosed when there is both anatomic compression and corresponding symptoms or complications such as headaches or thrombosis as in our case.

References

Zhao X, Cavallo C, Hlubek RJ, et al. Styloidogenic jugular venous compression syndrome: clinical features and case series. *Oper Neurosurg (Hagerstown)* 2019;17:554–561. DOI: https://doi.org/10.1093/ons/opz012

Images/Tables

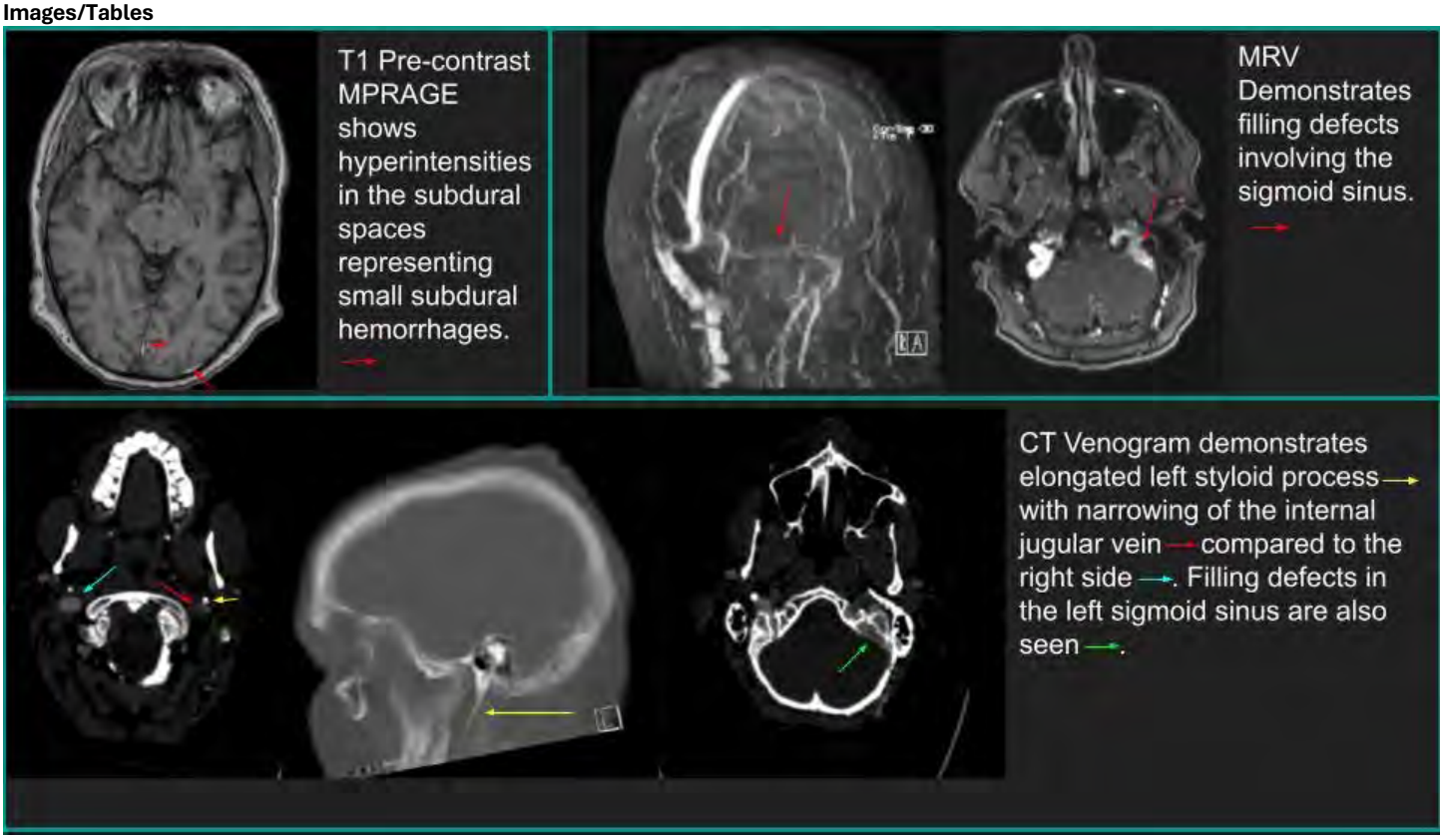

612 Craniospinal Neurosarcoidosis with Nodular Leptomeningeal and Parenchymal Enhancement and Hydrocephalus

Younus Syed DO, Amna Ajam MD
The Ohio State University Wexner Medical Center, Columbus, Ohio, USA

Clinical History

A 47-year-old woman presented with progressively worsening headaches over several months, without focal neurological deficits or constitutional symptoms. Her medical history was unremarkable, and she denied prior infections, autoimmune disease, or malignancy.

Cerebrospinal fluid (CSF) analysis demonstrated a lymphocytic pleocytosis and elevated protein concentration, with normal glucose. Extensive infectious work-up, including testing for tuberculosis, Lyme disease, HIV, and fungal pathogens, was negative. Posterior fossa biopsy demonstrated non-caseating granulomas, raising concern for neurosarcoidosis.

Imaging Findings

Brain MRI showed extensive nodular leptomeningeal enhancement involving the basal cisterns, subarachnoid spaces, and left cavernous sinus. Additional nodular foci were present along both sylvian fissures. A left posteromedial temporal-lobe intraparenchymal lesion demonstrated interval enlargement and vasogenic edema. Enhancement extended along the right optic tract, optic chiasm, and pituitary stalk, indicating hypothalamic–optic pathway involvement. Chronic ventricular enlargement had mildly progressed, compatible with communicating hydrocephalus secondary to leptomeningeal obstruction.

MRI of the spine revealed multifocal nodular intradural and intramedullary enhancement spanning the spinal canal, with overall improvement compared to prior imaging except for mild interval enlargement at the dorsal craniocervical junction. Persistent but improved cord edema extended from the craniocervical junction to the upper cervical levels. Moderate-to-severe spinal canal stenosis was noted at the craniocervical junction and C2–C3.

Given the imaging, histopathology and CSF profile, a presumptive diagnosis of neurosarcoidosis was made. The patient was started on high-dose corticosteroids (prednisone 60 mg daily, tapered to 20 mg maintenance) and referred for neuro-immunology follow-up. Symptomatic improvement was noted upon discharge.

Discussion

Sarcoidosis is a multisystem granulomatous disease characterized by non-caseating granulomas. Neurological involvement occurs in 5-26% of cases [2] and may be the only manifestation of the disease. Neurosarcoidosis remains a diagnosis of exclusion, requiring integration of clinical, radiologic, CSF, and histopathologic data. MRI often demonstrates leptomeningeal or dural enhancement, parenchymal granulomas, or cranial nerve involvement. Communicating hydrocephalus, as in this case, results from impaired CSF resorption due to meningeal inflammation.

First-line therapy involves corticosteroids (prednisone 0.5–1 mg/kg daily), which result in clinical stability or improvement in up to 80% of patients. Refractory or relapsing cases may benefit from steroid-sparing immunosuppressants such as methotrexate, azathioprine, or mycophenolate. In severe or resistant disease, anti-TNF agents may be considered. [1] [2] [3]. Risk factors for relapse include parenchymal lesions, elevated CSF protein, low CSF glucose, and oligoclonal bands, underscoring the need for close follow-up and tailored immunosuppression.

Teaching Point

- Leptomeningeal and basal cisternal enhancement in conjunction with communicating hydrocephalus should prompt consideration of neurosarcoidosis in the differential, particularly when infectious work-up is negative.
- Non-caseating granulomas on biopsy remain the diagnostic cornerstone.
- Parenchymal nodular lesions may coexist with leptomeningeal disease and can mimic neoplastic or infectious etiologies.
- Serial imaging is valuable in distinguishing neurosarcoidosis from progressive malignant or infectious processes, given its potential for partial regression or fluctuation.
- Early corticosteroid therapy can result in significant clinical improvement and prevent irreversible neurologic sequelae.

References

1. Ibitoye RT, Wilkins A, Scolding NJ. Neurosarcoidosis: a clinical approach to diagnosis and management. J Neurol. 2017 May;264(5):1023-1028. doi: 10.1007/s00415-016-8336-4. Epub 2016 Nov 22. PMID: 27878437; PMCID: PMC5413520.
2. Barreras P, Stern BJ. Clinical features and diagnosis of neurosarcoidosis - review article. J Neuroimmunol. 2022 Jul 15;368:577871. doi: 10.1016/j.jneuroim.2022.577871. Epub 2022 Apr 18. PMID: 35523055.
3. Stern BJ, Royal W 3rd, Gelfand JM, Clifford DB, Tavee J, Pawate S, Berger JR, Aksamit AJ, Krumholz A, Pardo CA, Moller DR, Judson MA, Drent M, Baughman RP. Definition and Consensus Diagnostic Criteria for Neurosarcoidosis: From the Neurosarcoidosis Consortium Consensus Group. JAMA Neurol. 2018 Dec 1;75(12):1546-1553. doi: 10.1001/jamaneurol.2018.2295. PMID: 30167654.
4. Nitsch L, Skowasch D, Courtin E, Duffau P, Otto C, Ruprecht K, Dambietz C, Heming M, Meyer Zu Hörste G, Byg KE, Kindler C, Gutzwiller J, Pretzsch R, Proebstel AK, Weller JM, Zimmermann J. Factors Associated With Relapse in Patients With Neurosarcoidosis. Neurology. 2025 Jun 10;104(11):e213705. doi: 10.1212/WNL.0000000000213705. Epub 2025 May 15. PMID: 40373242.
5. Bathla G, Singh AK, Policeni B, Agarwal A, Case B. Imaging of neurosarcoidosis: common, uncommon, and rare. Clin Radiol. 2016 Jan;71(1):96-106. doi: 10.1016/j.crad.2015.09.007. Epub 2015 Oct 23. PMID: 26506463.

Images/Tables

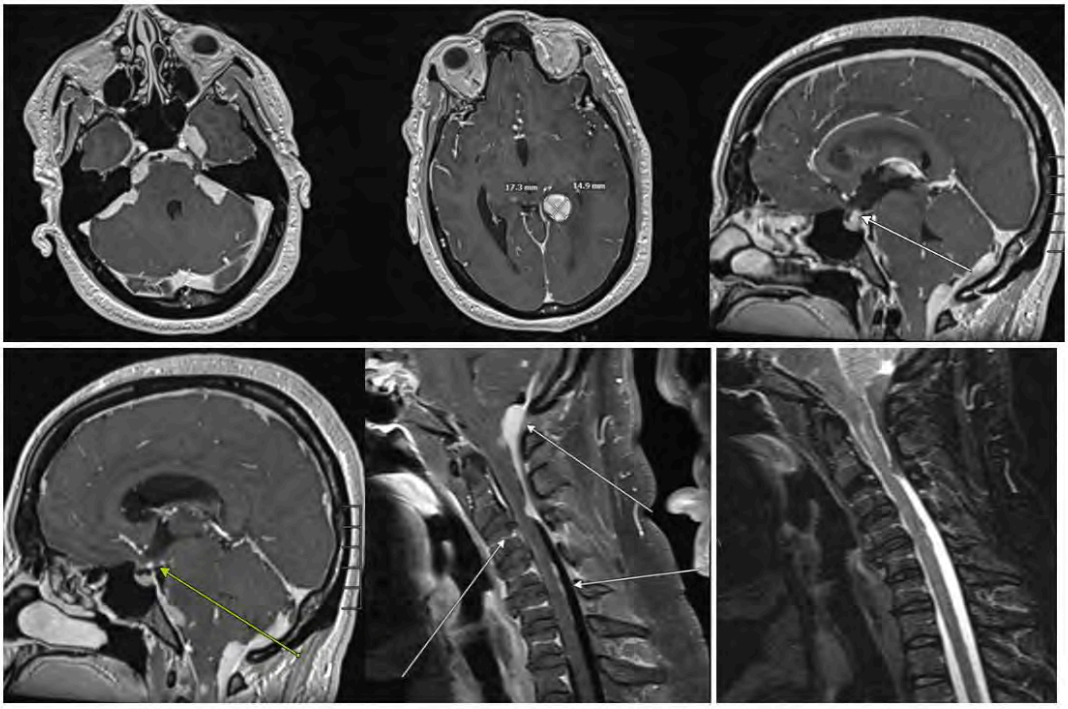

Figure 1-2, 5-6: Contrast-enhanced brain and cervical spine MRI showing nodular leptomeningeal enhancement at the skull base and basal cisterns, extending to C3, with severe C2–C3 cord compression, upper cervical cord edema, and an enhancing left parietal nodule.

Figure 3-4: Nodular enhancement of the pituitary stalk and optic chiasm.

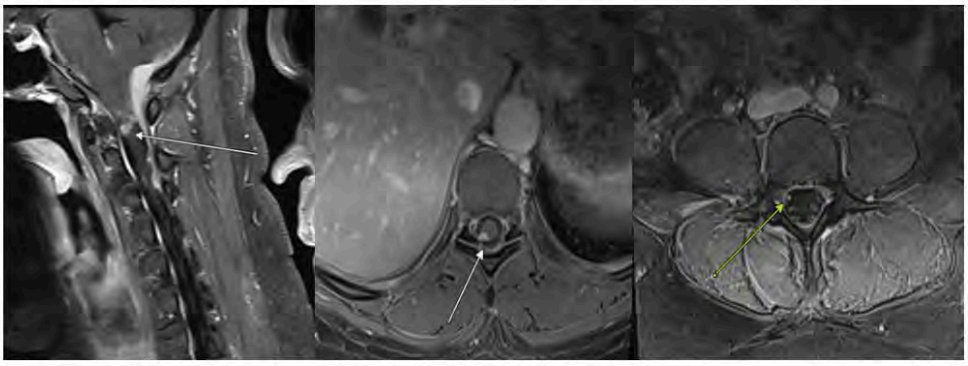

Figure 7-9: MRI of the spine demonstrating nodular intramedullary and dorsal cord lesions with leptomeningeal involvement of cauda equina nerve roots.

621 "Aceruloplasminemia: Distinctive MRI features of a Rare, One in Two-Million Culprit of Neurovisceral Iron Deposition"

Ahmed R. Farhat D.O., Dhairya Lakhani M.D., Joe Joseph M.D., Jarunee Intrapiromkul M.D.
West Virginia University School of Medicine, Department of Neuroradiology, Morgantown, West Virginia, USA

Clinical History

A 28-year-old woman presented with fatigue, anxiety, unintentional weight gain, and paresthesia of the extremities. Laboratory evaluation revealed markedly elevated serum ferritin levels, approximately eight times the upper limit of normal, raising concern for hemochromatosis. MRI of the liver demonstrated mild hepatic iron overload, but HFE gene testing revealed a normal phenotype. Core liver biopsy confirmed iron deposition, and cardiac MRI showed a borderline low T2* value, suggesting early myocardial involvement. Despite serial phlebotomy, ferritin levels remained persistently elevated. Given the patient's young age, high ferritin, undetectable serum ceruloplasmin, and confirmed systemic iron overload, aceruloplasminemia was suspected. Genetic testing confirmed a homozygous pathogenic variant in the *ceruloplasmin* gene. Brain MRI further demonstrated extensive cerebral iron accumulation.

Imaging Findings

T2-weighted and T2*-weighted gradient-echo images of the brain revealed diffuse hypointensity and susceptibility involving the dentate nuclei, cerebellar folia, cerebral cortex, basal ganglia, thalami, red nuclei, substantia nigra, superior colliculi, and choroid plexus. The symmetric, simultaneous, and uniform distribution of iron deposition throughout both supratentorial and infratentorial structures is highly characteristic of aceruloplasminemia and distinguishes it from other forms of neurodegeneration with brain iron accumulation.

Discussion

Aceruloplasminemia (ACP) is a rare autosomal recessive disorder caused by mutations in the *ceruloplasmin* gene, leading to the absence of ceruloplasmin ferroxidase activity and resulting in systemic and cerebral iron accumulation. It is the only known iron overload disorder associated with both visceral and brain deposition. Clinically, ACP may present with diabetes mellitus, retinal degeneration, and progressive neurodegeneration. It is classified within the neurodegeneration with brain iron accumulation (NBIA) spectrum, which encompasses disorders characterized by excessive brain iron deposition, particularly in the basal ganglia. MRI plays a pivotal role in early recognition, showing diffuse and synchronous T2 and T2* hypointensities in deep gray matter and cortical regions. In the setting of elevated ferritin, low transferrin saturation, and undetectable ceruloplasmin levels, these radiologic findings strongly support the diagnosis of ACP.

Teaching Point

There are more than ten subtypes of NBIA, each with distinct imaging characteristics. Pantothenate kinase–associated neurodegeneration (PKAN), the most common form, demonstrates the classic "eye-of-the-tiger" sign—central T2 hyperintensity within the globus pallidus surrounded by hypointense iron deposition. Wilson disease may show T2 hypointensity in the lentiform nuclei and thalami, often accompanied by caudate atrophy and white matter hyperintensity. Neuroferritinopathy (NFT) exhibits multifocal, asymmetric iron accumulation in the basal ganglia, cortex, and dentate nuclei, sometimes progressing to cystic degeneration of the caudate and putamen. In contrast, aceruloplasminemia shows diffuse, symmetric, and homogeneous iron deposition across cortical and deep gray matter structures, while hereditary or secondary hemochromatosis typically spares the basal ganglia. Recognition of these distinctive MRI patterns enables radiologists to accurately differentiate ACP from other NBIA disorders and facilitates timely diagnosis and treatment.

References

1) Grisoli M, Barbeau D, Morel J, et al. MR Imaging of Cerebral Cortical Involvement in Inherited Aceruloplasminemia. *Am J Neuroradiol.* 2005;26(3):657-661.
2) Lehéricy S, Roze E, Goizet C, Mochel F, et al. MRI of neurodegeneration with brain iron accumulation. *Curr Opin Neurol*. 2020;33(4):462-473.
3) Li CK, Lau CY, Chin KH, Chu CY. Aceruloplasminemia with Neurodegenerative Condition: A Case Report. *Hong Kong J Radiol.* 2025;28(2):e107-10. doi:10.12809/hkjr2417845.
4) Xiao Y, Zhu C, Jiang F, et al. Novel ceruloplasmin gene mutation causing aceruloplasminemia with diabetes in a Chinese woman: a case report. *Ann Palliat Med.* 2022;11(7):2516-2522. doi:10.21037/apm-21-1086.
5) Marchi G, Busti F, Lira Zidanes A, et al. Aceruloplasminemia: A severe neurodegenerative disorder deserving an early diagnosis. *Front Neurosci.* 2019;13:325. doi:10.3389/fnins.2019.00325.

Images/Tables

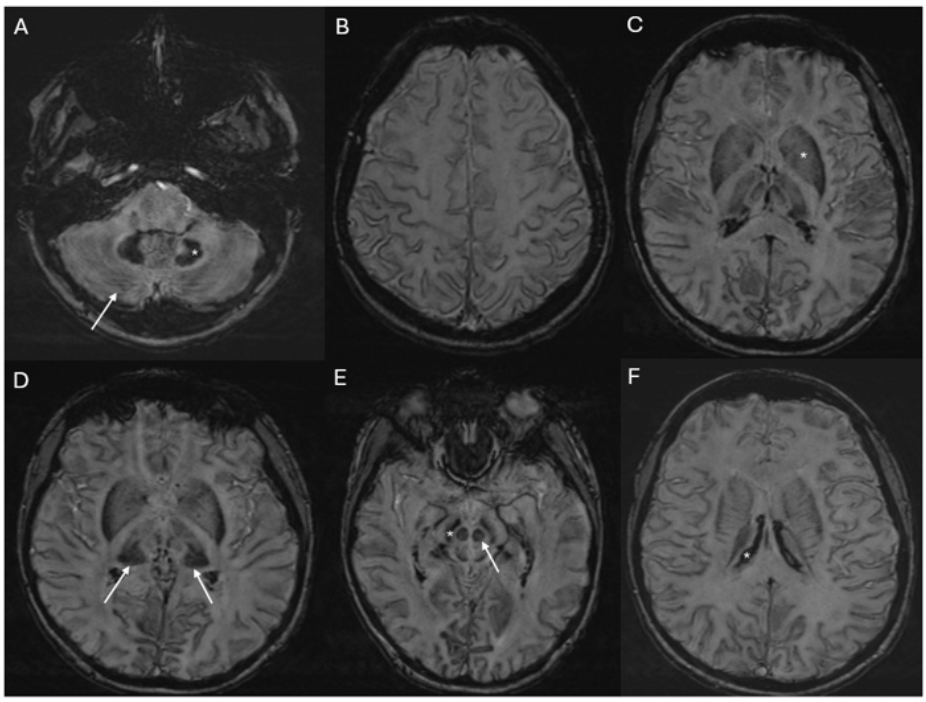

Magnetic resonance imaging (MRI) of the brain demonstrated diffuse susceptibility on susceptibility weight imaging (SWI) in the dentate nuclei (asterisk) and cerebellar folia (Fig. 1A; arrow), the supratentorial gyri (Fig. 1B), the bilateral basal ganglia (Fig. 1C; asterisk), bilateral thalami (Fig. 1D; arrows), red nuclei (arrow) and substantia nigra (asterisk) of the midbrain (Fig. 1E), and choroid plexus (Fig. 1F; asterisk).

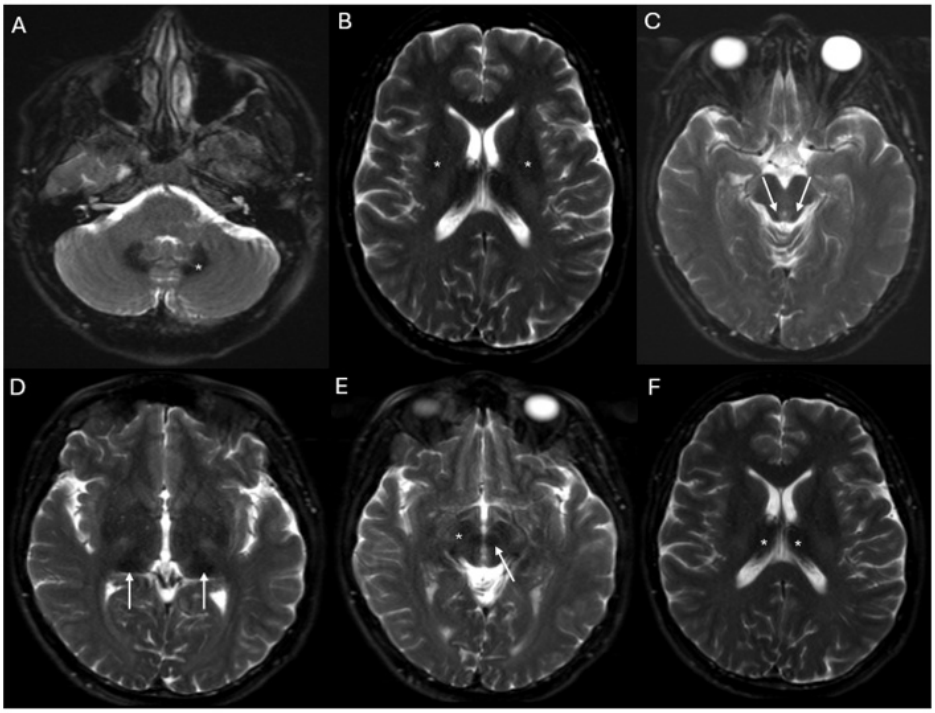

Magnetic resonance imaging (MRI) of the brain demonstrated marked hypointensity on T2-weighted images in the dentate nuclei (Fig. 1A; asterisk), the bilateral basal ganglia (Fig. 1B; asterisk), the bilateral superior colliculi (Fig. 1C; arrows), bilateral thalami (Fig. 1D; arrows), red nuclei (arrow) and substantia nigra (asterisk) of the midbrain (Fig. 1E), and choroid plexus (Fig. 1F; asterisk).

672 **When Nerves Swell in Silence: The Infraorbital Clue to IgG4-Related Disease.**

Kamaljeet Singh MBBS, MD, DNB[1], Shivaprakash Hiremath MD[2], Santanu Chakraborty MBBS, FRCPC[1]
[1]The University of Ottawa, Ottawa, Ontario, Canada. [2]The University of Toronto, Toronto, Ontario, Canada

Clinical History

A 49 year old patient presented with dryness of the mouth. Physical examination was normal. Blood work also came as normal , so was symptomatically treated. Patient was doing well on conservative therapy but soon developed complaints of recurrent sinusitis, for which CT PNS was done.

Imaging Findings

CT sinuses revealed significant enlargement of the bilateral inferior orbital foramen with concerns for bilateral infraorbital nerve thickening. Brain and orbit MRI with contrast was recommended for further assessment. MR revealed isointense T1, mildly hypointense T2 infiltrative enlargement and enhancement of the bilateral infraorbital nerves with associated expansion of the infraorbital canals extending posteriorly to the pterygopalatine fossa and anteriorly into the premaxillary soft tissues. Mild prominence of right lacrimal gland was seen. No extraconal soft-tissue thickening were noted. Both globes, intraorbital fat and extraocular muscles were unremarkable. Both optic nerves were of normal size, symmetric signal intensity and does not show enhancement following gadolinium

Discussion

IgG4-related disease (IgG4-RD) is a systemic fibroinflammatory condition characterized histopathologically by lymphoplasmacytic infiltrates rich in IgG4-positive plasma cells, storiform fibrosis, and obliterative phlebitis.Previously named myriad of diseases such as Mikulicz's disease, autoimmune pancreatitis, hypophysitis, Riedel's thyroiditis, Kuttner tumor etc were found to be having similar clinical and laboratory features which were found to be similar to IgG4-related disease (IgG4-RD) initially first recognized in 2001.

IgG4-related disease can affect orbits as well. Orbital involvement (IgG4-ROD) often affects the lacrimal glands, extraocular muscles, orbital fat, and branches of the trigeminal nerve. Bilateral infraorbital nerve enlargement is a distinctive radiological sign, present in up to 53% of IgG4-ROD cases, but is rarely reported in other orbital diseases. This case highlights the importance of recognizing this pattern for accurate diagnosis.

Teaching Point

Bilateral infraorbital nerve thickening and enhancement is a highly specific radiologic indicator of IgG4-related orbital disease.

References

1. Deshpande V, Zen Y, Chan JK, Yi EE, Sato Y, Yoshino T, Klöppel G, Heathcote JG, Khosroshahi A et al. Consensus statement on the pathology of IgG4-related disease. Mod Pathol. 2012 Sep;25(9):1181-92. doi: 10.1038/modpathol.2012.72. Epub 2012 May 18. PMID: 22596100.
2. Tiegs-Heiden CA, Eckel LJ, Hunt CH, Diehn FE, Schwartz KM, Kallmes DF, Salomão DR, Witzig TE, Garrity JA. Immunoglobulin G4-related disease of the orbit: imaging features in 27 patients. AJNR Am J Neuroradiol. 2014 Jul;35(7):1393-7. doi: 10.3174/ajnr.A3865. Epub 2014 Mar 13. PMID: 24627453; PMCID: PMC7966591.

Images/Tables

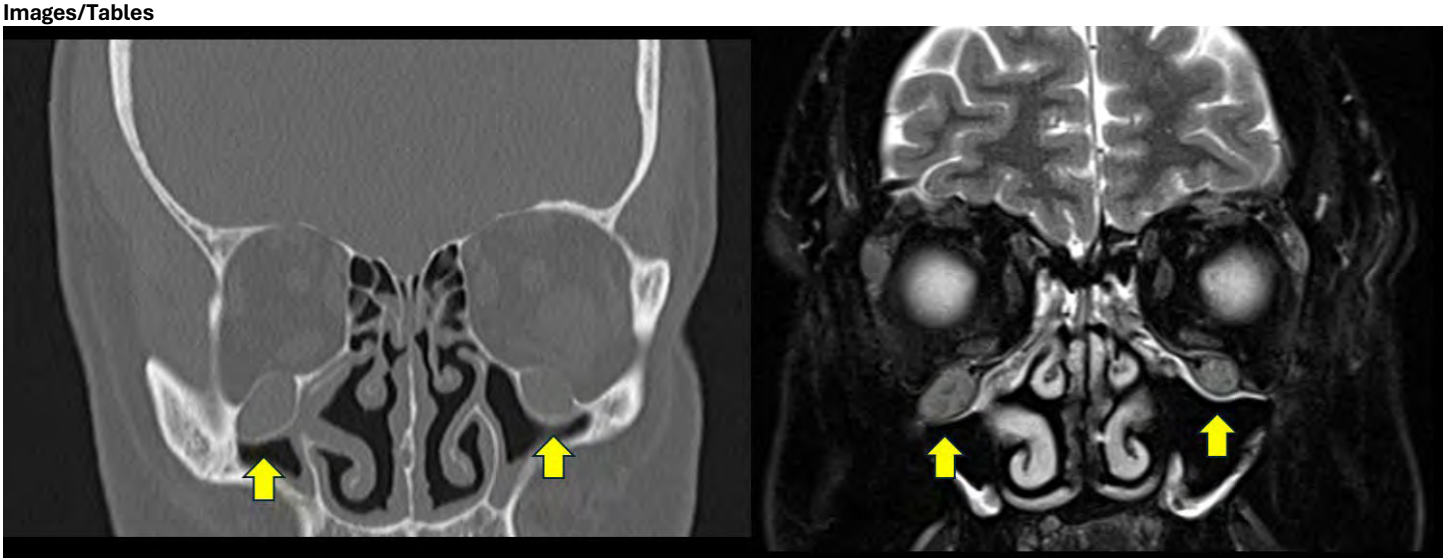

CT Orbits Coronal Bone window showing expanded infra-orbital foramen. MRI T2FS Cor shows thickened infra-orbital nerves.

682 **Spontaneous Pneumorrhachis Secondary To Acute Asthma Exacerbation**

Gautam Menon, Arathi Menon
Royal Free London NHS Foundation Trust, London, London, United Kingdom

Clinical History

Whilst traumatic and iatrogenic aetiologies of pneumorrhachis are more widely recognised, spontaneous pneumorrhachis is very rare. In particular, only few cases of pneumorrhachis associated with acute asthma exacerbation have been reported in the literature. Here, we present such a case in a 19 year old male with known asthma and a four day history of productive cough.

Imaging Findings

After a chest radiograph showed the presence of pneumomediastinum (Figure 1A), the patient proceeded to CT which ruled out oesophageal and tracheal injuries, and demonstrated the additional findings of pneumothoraces and pneumorrhachis (Figures 1B and 1C). Despite normal neurological exam, he proceeded to MRI which did not demonstrate any new concerning findings - as expected, the epidural free air was better appreciated on CT (Figure 1D).

Discussion

We discuss the pathophysiology of spontaneous pneumorrhachis and review the literature reporting the association between pneumorrhachis and acute asthma exacerbations. The aim of this case report is to add to the limited existing literature and to better understand this rare pathology.

Teaching Point

- Pneumorrhachis is characterised by the presence of free air in the spinal canal.
- Spontaneous pneumorrhachis is a rare sequela of acute asthma exacerbation, often seen with spontaneous pneumomediastinum i.e. Hamman syndrome.
- CT is the investigation of choice for detecting pneumorrhachis; in the absence of neurological symptoms, MRI is rarely indicated.
- Although often an asymptomatic epiphenomenon, awareness of spontaneous pneumorrhachis is important to allow for early recognition and optimal care of possible neurological compromise.

References

Zhao CZ, Poci N, Niewodowski D, at al. Pneumorrhachis secondary to exacerbation of asthma: A case report and literature review. Respirol Case Rep. 2023 Oct 9;11(11):e01228. DOI: https://doi.org/10.1002/rcr2.1228

Images/Tables

Figure 1A

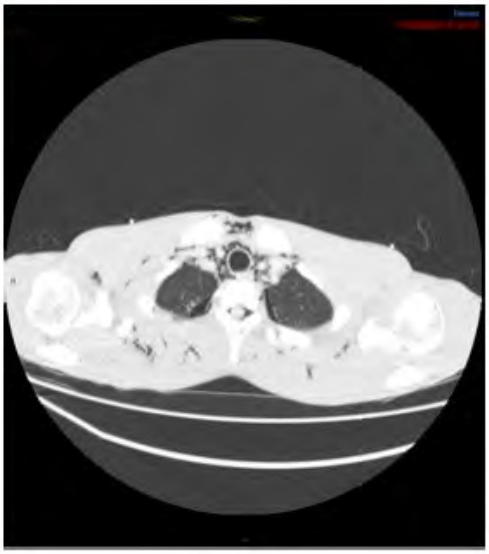

Figure 1B

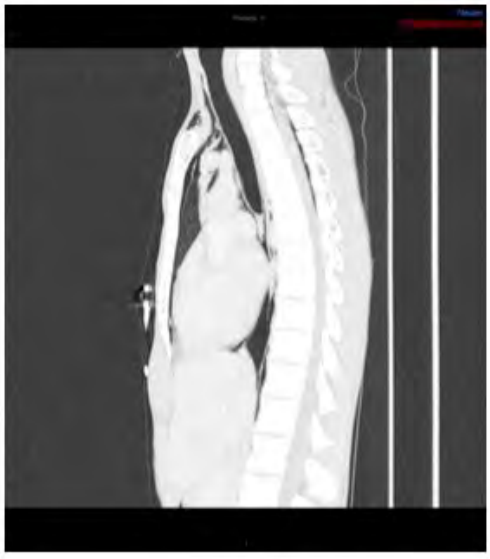

Figure 1C

Figure 1D

685 Beyond the Nose: Fluid Distention of Eustachian Tube in Mastoid CSF Leak Presenting with Rhinorrhea

Brandon Hanai DO[1], John Manov MD[2], Jerrin Varghese MD[1], Avraham Zlochower MD[2], Puneet Pawha MD[2]
[1]Northwell, Manhasset, NY, USA. [2]Northwell, New York, NY, USA

Clinical History

A 49-year-old female with no significant past medical history presented to an outside hospital after trauma. Patient had been struck by a bicyclist, fell backwards, and suffered injury to back of her head. Initial imaging at the outside hospital demonstrated a small subdural hemorrhage which was conservatively managed, and she was discharged.

Subsequently, the patient developed clear rhinorrhea from the left nostril and presented at our hospital for evaluation. Upon questioning, the patient reported feeling a sensation of fullness and pressure in the left ear with decreased hearing immediately after her trauma.

Imaging Findings

CT of the head and paranasal sinuses did not show a skull base defect along the sinonasal regions but did reveal left mastoid fluid with thinning of the tegmen mastoideum. A dedicated high-resolution temporal bone CT was obtained, demonstrating left middle ear and mastoid opacification and evidence of tegmen dehiscence (Figure 1).

MRI demonstrated a tract of fluid signal extending inferiorly from the tegmen mastoideum defect, suggesting a site of cerebrospinal fluid (CSF) leak (Figure 2). Additionally, a separate thin tract of fluid-like signal was also seen along the expected course of the left Eustachian tube, suggesting drainage of fluid from the tympanomastoid cavity into the nasopharynx, accounting for the patient's ipsilateral rhinorrhea (Figures 3, 4).

Discussion

Craniofacial trauma is the most common cause of CSF leak, responsible for approximately 80% of cases[1]. The most common locations of the culprit osseous defects are the cribriform plate, fovea ethmoidalis, and the floor of the sphenoid sinuses due to the thin bone in these regions and close approximation of subarachnoid spaces with the paranasal sinuses.

Iatrogenic CSF leak is not uncommon post-operatively after surgery involving the anterior skull base or tympanomastoid regions. Other causes of CSF leak include idiopathic intracranial hypertension (IIH). In this condition, chronic pressure upon the skull base may lead to development of dural and osseous defects which, depending upon their location, may lead to CSF rhinorrhea or otorrhea.

In cases of suspected traumatic CSF leak, presentation with rhinorrhea or otorrhea leads radiologists to search for skull base defects bordering the nose or ear, respectively. This presentation highlights a case of rhinorrhea apparently secondary to traumatic dehiscence of the mastoid tegmen. While previously documented, the possibility of this phenomenon is not well-recognized[2].

In this case, CSF was postulated to leak into the mastoid cells, course through the aditus ad antrum into the tympanic cavity, and then drain into the nasopharynx via the Eustachian tube. Although fluid signal was visualized along the entire Eustachian tube tract in this case, such findings may not always be captured on imaging, and radiologists should nevertheless remain aware of this potential route of CSF drainage from the ear.

Teaching Point

In cases of suspected CSF rhinorrhea, imagers should bear in mind the communication between the ear and nose provided by the Eustachian tube and scrutinize the bony margins of both regions as well as the Eustachian tube itself.

References

1. Le C, Strong EB, Luu Q. Management of Anterior Skull Base Cerebrospinal Fluid Leaks. *J Neurol Surg B Skull Base* 2016; 77(05): 404-411. DOI: 10.1055/s-0036-1584229
2. Waheed A, Amir F. Cerebrospinal fluid leak-associated ventriculitis - a case report. *Clin Med* (Lond). 2025 Jan;25(1):100279. DOI: 10.1016/j.clinme.2024.100279. Epub 2024 Dec 18. PMID: 39706573; PMCID: PMC11761854.

Images/Tables

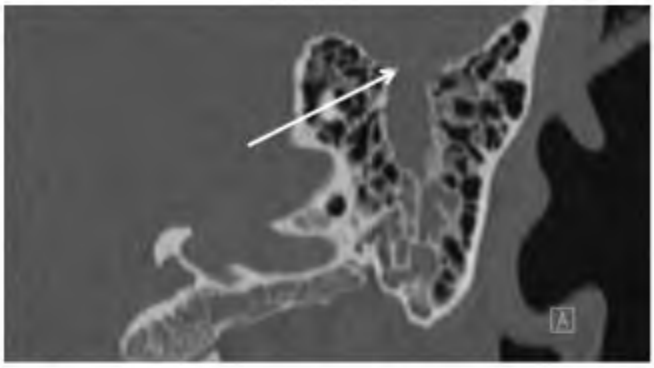

Figure 1

Figure 2

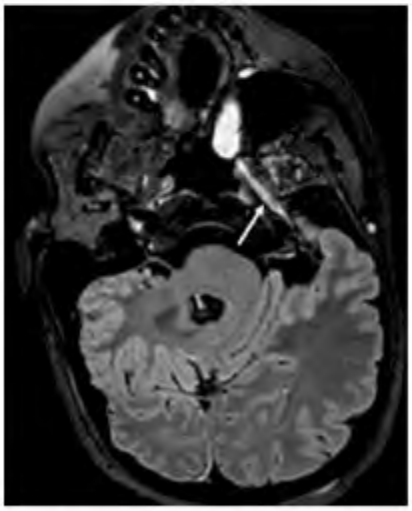

Figure 3

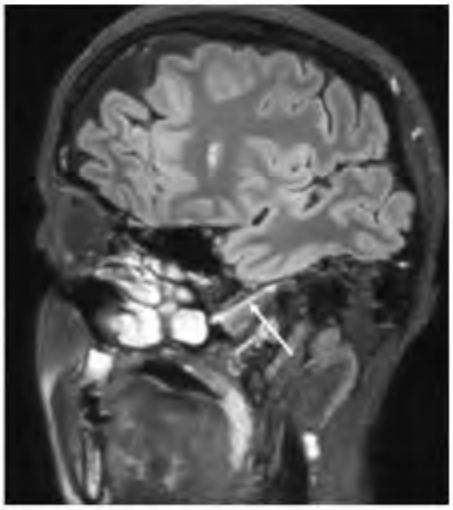

Figure 4

---

712 Aggressive Transcranial Mass of the Anterior Skull Base

Mira A Zineddin BS, Barton F Branstetter MD
University of Pittsburgh School of Medicine, Pittsburgh, Pennsylvania, USA

Clinical History

A 41-year-old female presented with a two-week history of blurry vision, sinus pressure, and frontal headaches. The patient reported anosmia and mild nasal obstruction for the past several months, but physical examination revealed no rhinorrhea, epistaxis, or external deformities. MRI revealed an elongated transcranial anterior skull base mass producing bone destruction and brain edema. Endonasal biopsy was performed, indicating a spindle cell neoplasm. The tumor was resected via a trans-cribriform endonasal approach with gross tumor resection and good clinical outcome.

Imaging Findings

MRI reveals a large, lobulated right sinonasal mass (5.2 x 3.0 x 2.8 cm) extending transcranially across the cribriform plate, with vasogenic edema in the medial frontal lobe indicating parenchymal invasion (Figure). Secondary obstruction of the right frontonasal and ostiomeatal drainage pathways causes entrapped secretions in the frontal and maxillary sinuses. The mass is heterogeneously hyperintense to brain on T2 images and intrinsically isointense to hypointense on T1 images. CT demonstrates loss of bone in the anterior skull base. However, careful review shows that the bone is being remodeled around the lesion rather than aggressively destroyed.

Discussion

Sinonasal schwannomas with intracranial invasion are extremely rare, accounting for less than 4% of all head and neck schwannomas with only around 17 previously published cases. Sinonasal schwannomas likely arise from nasal autonomic nerves or the ophthalmic and maxillary trigeminal nerve branches. Sinonasal schwannomas are typically hypointense to isointense to brain on T1 images and heterogeneously hyperintense on T2 images. A lobulated, heterogeneously enhancing presentation is typical, particularly in schwannomas greater than 1 cm.[1] However, the rare location and aggressive growth pattern of the schwannoma in this case could easily lead to misdiagnosis, as this sinonasal tumor presentation is more commonly expected for malignancies such as squamous cell carcinoma, sinonasal intestinal-type adenocarcinoma, melanoma, minor salivary tumor, sinonasal undifferentiated carcinoma, SMARC-B1 deficient sinonasal carcinoma, or esthesioneuroblastoma.[2]

Teaching Point

Despite their benign histology, sinonasal schwannomas can present with transcranial invasion, including aggressive growth that can lead to misdiagnosis. The nonspecific clinical symptoms and imaging presentation of schwannomas on MRI and CT increase the risk of misdiagnosis. Careful review of the CT images for remodeling of bone may provide a critical diagnostic clue.

References

1. Brahmbhatt P, Kumar T, Bhatt AA, et al. Sinonasal Schwannomas: Imaging findings and review of literature. *Ear, Nose & Throat Journal* 2023;104:645–50. DOI: https://doi.org/10.1177/01455613221150573
2. Lo Casto A, Lorusso F, Palizzolo E, et al. Uncommon nasal mass presentation: A radiological case series. *Journal of Personalized Medicine* 2024;14:1145. DOI: https://doi.org/10.3390/jpm14121145

Images/Tables

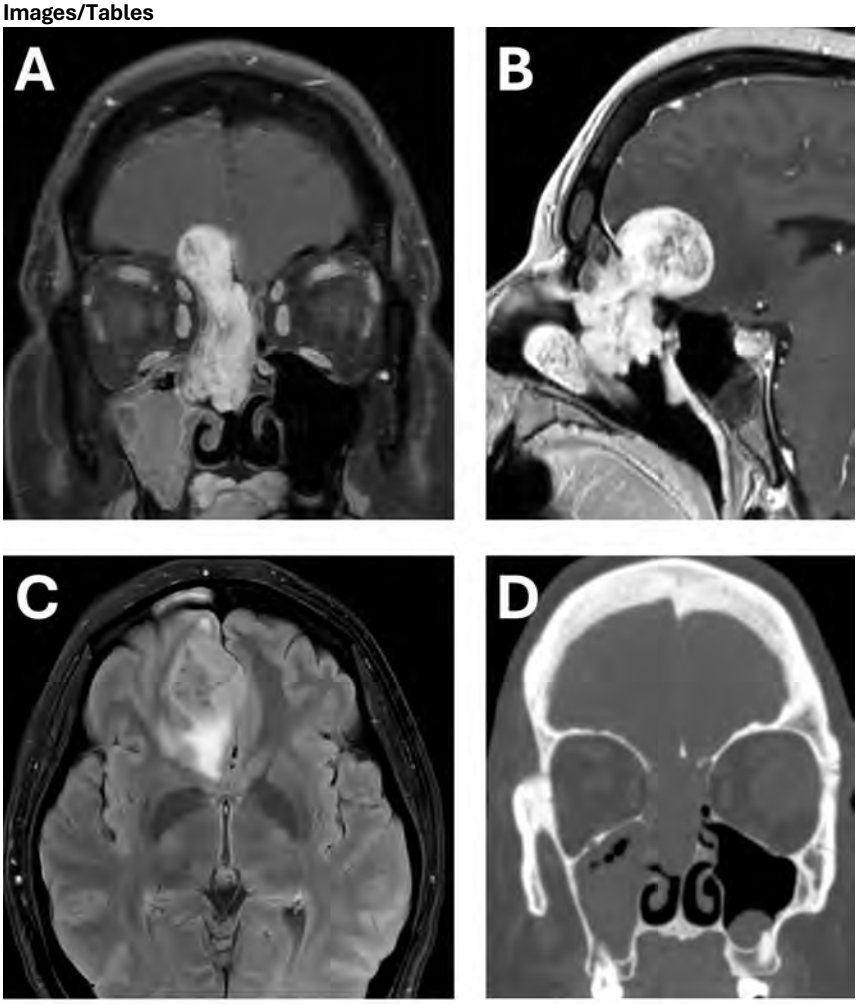

Figure. Post-contrast T1-weighted coronal MRI through the anterior skull (A) and reformatted sagittal 3D spoiled gradient recall imaging (B) reveal a large, lobulated sinonasal mass with intracranial invasion. T2-FLAIR MRI (C) highlights the mass's heterogeneous T2 signal and the vasogenic edema indicating brain invasion. Coronal CT (D) highlights bone loss with bone remodeling around the lesion rather than aggressive erosion.

736 Classic imaging manifestations of orbital metastatic gastrointestinal carcinoid

Alexandra Castro MD, Wigger Andrew MD, Aulino Joseph MD, Simone Montoya MD
vanderbilt university, Nashville, TN, USA

Clinical History

We present a series of patients with metastatic NET. The case we highlight in our abstract is a 66-year-old woman with history of small bowel neuroendocrine (NET) tumor resected in 2009 with metastatic recurrence in liver, lymph nodes, and bone who presented to the emergency department (ED) with acute right eye swelling, progressive proptosis, and vision loss. Physical examination revealed a right afferent pupillary defect with fixed dilated pupil, nonlight perceptible vision, upper and lower eyelid swelling, conjunctival injection, and chemosis. Orbital imaging revealed a disease process involving the myofascial cones bilaterally, as described below. Given history of metastatic NET elsewhere, and classic radiologic features, the decision was made to forego biopsy and proceed with radiation therapy.

Imaging Findings

CT demonstrates proptosis with enlargement of bilateral extraocular muscle (EOM) bellies with well-defined areas of low density in right lateral rectus muscle. MRI demonstrates proptosis with bilateral irregular nodular fusiform thickening of the EOMs. Ga-68 DOTATATE PET/CT and MIP images from a different patient demonstrated diffuse radiotracer uptake within the liver, lungs, spine and right lateral rectus muscle.

Discussion

Although orbital metastases are rare overall, NET has a propensity to metastasize to orbital structures; the majority are of gastrointestinal (GI) origin and extraocular muscle (EOM) involvement is typical. We present a series of cases showing the various classic imaging findings on different imaging modalities of metastatic NET. Pathophysiology is unknown but speculated to be due to increased somatostatin receptor numbers and increased vascularity of the EOMs. MRI is the gold standard for imaging, however, somatostatin receptor-based imaging such as Ga-68 DOTATATE PET has an increasing role in staging and monitoring response to treatment. Surgical biopsy may not be necessary in the setting of known metastatic NET with classic radiologic findings, such as presented in our cases, but intralesional hemorrhage and bony destruction are uncommon and should warrant biopsy. Mainstays of treatment include surgery for tumor debulking along with systemic chemotherapy, radiation, or biologics.

Teaching Point

- GI NET has a propensity to metastasize to the extraocular eye muscles.
- Classic radiologic features with a history of metastatic neuroendocrine tumor can obviate the need for surgical biopsy.
- MRI is gold standard with well defined, round or fusiform necrotic masses that are hyperintense on T2 imaging. Ga-68 DOTATATE PET has an increasing role.

References

1. Tayon KG, Kaila V, Sobti D, Vrcek I. Metastatic neuroendocrine carcinoma presenting with left lateral rectus enlargement and orbital cellulitis. Proc (Bayl Univ Med Cent). 2021 Jun 15;34(5):620-622. doi: 10.1080/08998280.2021.1930633. PMID: 34456492; PMCID: PMC8366931.
2. Das S, Pineda G, Goff L, Sobel R, Berlin J, Fisher G. The eye of the beholder: orbital metastases from midgut neuroendocrine tumors, a two institution experience. Cancer Imaging. 2018 Dec 6;18(1):47. doi: 10.1186/s40644-018-0181-5. PMID: 30522522; PMCID: PMC6282338.
3. Bonavolontà, G. , Strianese, D. , Grassi, P. , Comune, C. , Tranfa, F. , Uccello, G. & Iuliano, A. (2013). An Analysis of 2,480 Space-Occupying Lesions of the Orbit From 1976 to 2011. *Ophthalmic Plastic and Reconstructive Surgery, 29* (2), 79-86. doi: 10.1097/IOP.0b013e31827a7622.
4. Ryan, T. G., Juniat, V., Stewart, C., Malhotra, R., Hardy, T. G., McNab, A. A., … Selva, D. (2021). Clinico-radiological findings of neuroendocrine tumour metastases to the orbit. *Orbit*, *41*(1), 44–52. https://doi.org/10.1080/01676830.2021.1895845

Images/Tables

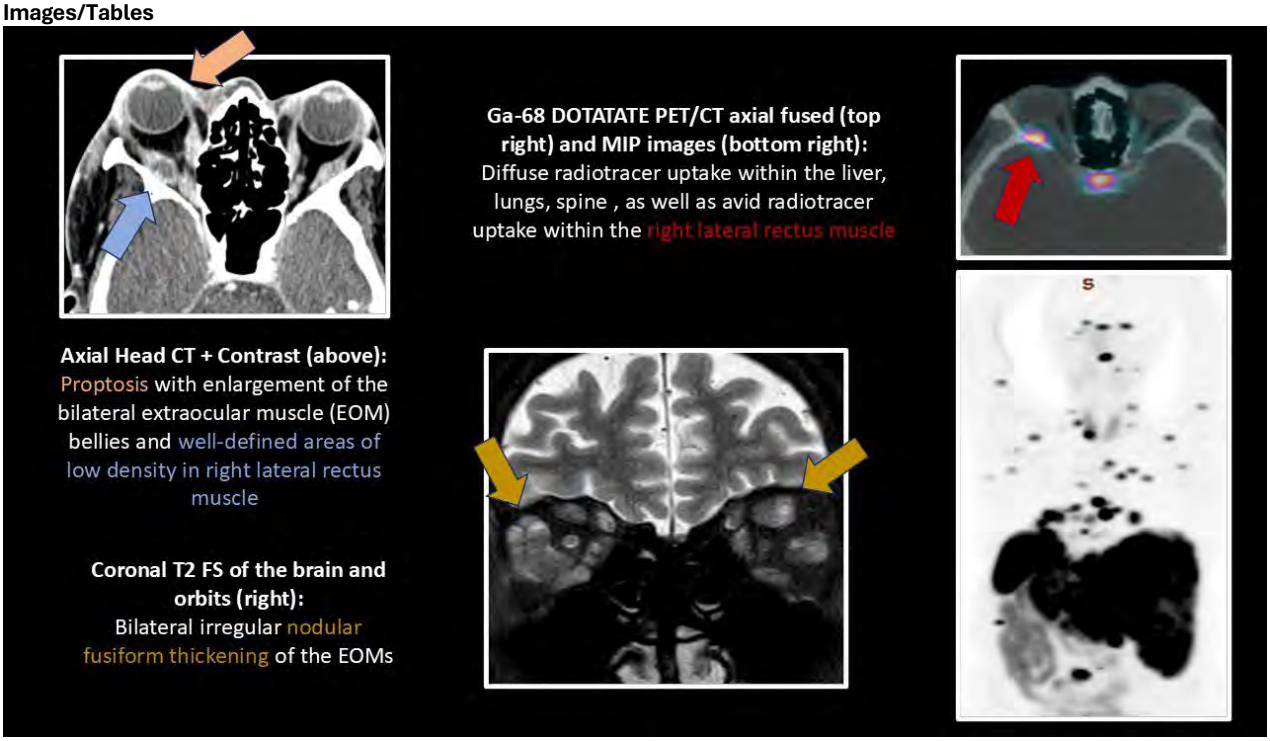

742 Cochlear Nerve Aplasia: An Uncommon Cause of Unilateral Sensorineural Hearing Loss in A Male Patient: A Case Report and Literature Review

Jana Hareesi Medical Intern[1], Samaher Thigah Senior diagnsotic radiology resident[2], Asayel Alzahrani Junior diagnsotic radiology resident[2], Aisha Halawani Neuroradiology Consultant[2]

[1]College of Medicine, King Saud Bin Abdulaziz University for Health Sciences, Jeddah, Mecca, Saudi Arabia. [2]Ministry of National Guard Health Affairs, Jeddah, Mecca, Saudi Arabia

Clinical History

we describe the case of a 68-year-old male presenting with right-sided hearing loss since childhood without a significant medical history. Otoscopic examination revealed intact tympanic membranes bilaterally, with no evidence of abnormalities. Pure-tone audiometry demonstrated profound sensorineural hearing loss in the right ear and mild sensorineural hearing loss in the left ear.

Imaging Findings

Magnetic resonance imaging (MRI) of the brain revealed the absence of the right cochlear nerve, confirming the diagnosis of cochlear nerve aplasia CNA.

Discussion

Sensorineural hearing loss (SNHL) is characterized by impaired auditory function resulting from structural or functional abnormalities of the inner ear or the vestibulocochlear nerve. Congenital SNHL may have a genetic origin, either as an isolated condition or as part of a syndromic presentation, or it may result from sporadic insults during fetal development. Cochlear nerve deficiency (CND) represents a subset of these cases and accounts for approximately 2% of congenital profound SNHL. CND is defined as a developmental abnormality involving either a cochlear nerve that is smaller in diameter than the ipsilateral facial nerve, termed cochlear nerve hypoplasia (CNH), or a complete absence of the cochlear nerve, referred to as cochlear nerve aplasia (CNA). The condition most commonly occurs unilaterally.

Teaching Point

Cochlear nerve deficiency should be considered among the differential diagnoses in patients presenting with congenital or long-standing unilateral sensorineural hearing loss. Moreover, MRI plays a crucial role in confirming the diagnosis and guiding further management.

References

1. Glastonbury CM, Davidson HC, Harnsberger HR, Butler J, Kertesz TR, Shelton C. Imaging findings of cochlear nerve deficiency. AJNR Am J Neuroradiol. 2002;23(4):635–643. PMID: 11950658; PMCID: PMC7975095.

2. O'Brien WT Sr, D'Arco F, Onofrj V, Koch BL. Nonsyndromic congenital causes of sensorineural hearing loss in children: an illustrative review. AJR Am J Roentgenol. 2021;216(4):1048–1055. doi:10.2214/AJR.20.23160.

Images/Tables

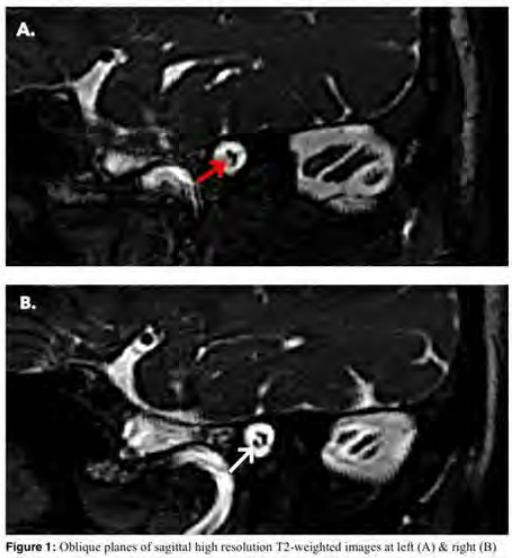

Figure 1: Oblique planes of sagittal high resolution T2-weighted images at left (A) & right (B) internal auditory canals that show a presence of cochlear nerve in the left side (white arrow), and absent cochlear nerve in the right side (red arrow).

Table 1: Literature Summary on Sensorineural Hearing Loss Associated with Cochlear Nerve Aplasia/Hypoplasia (CNA/H)

Journal Name	First Author	Year	Paper Title	Number of Cases	Imaging Findings
Wiley	Susmita Chennareddy HA	2024	Cochlear Implantation in Pediatric Cochlear Nerve Deficiency: A Systematic Review and Meta-Analysis	248	CNA/H
Otolaryngology–Head and Neck Surgery	Leyn B Shakhtour	2024	Evaluation of Cochlear Implantation in Children With Cochlear Nerve Absence or Deficiency	7	CNA/H
Acta Oto-Laryngologica	Niki Karpeta	2023	Vestibular function in children with vestibulocochlear nerve aplasia/hypoplasia	11	CNA/H
Wiley	Elina Kari	2019	A de novo SIX1 variant in a patient with a rare nonsyndromic cochleovestibular nerve abnormality, cochlear hypoplasia, and bilateral sensorineural hearing loss	2	Bilateral CNA
Cureus	Farid Alzhrani	2019	Value of Routine Magnetic Resonance Imaging for the Preoperative Assessment of Cochlear Implant Candidates	2	CNA/H
The Journal of International Advanced Otology	Özgür Sürmelioğlu	2016	Cochlear Implantation in Patient with Cochlear Nerve Deficiency: A Case Report	1	Bilateral CNA
Otology & Neurotology	Catherine S. Birman	2016	Cochlear Implant Outcomes in Cochlea Nerve Aplasia and Hypoplasia	32, 12	CNA, CNH (respectively)
The Journal of International Advanced Otology	Muhammed Dağkıran	2016	Radiological Imaging Findings of Patients with Congenital Totally Hearing Loss	10	CNA/H
Acta Oto-Laryngologica	Marco Carner	2009	Imaging in 28 children with cochlear nerve aplasia	9	CNA
SageJournals	Ken Ito	2005	Nonsyndromic isolated unilateral cochlear nerve aplasia without narrow internal auditorymeatus: a previously overlooked cause of unilateral profound deafness in childhood	2	Unilateral CNA
American Journal of Neuroradiology	S Furuta	2000	Reduced size of the cochlear branch of the vestibulocochlear nerve in a child with sensorineural hearing loss	1	CNH
Radiological Society of North America	J W Casselman	1997	Aplasia and hypoplasia of the vestibulocochlear nerve: diagnosis with MR imaging	3	CNA/H

747 Bilateral Cerebellar Infarcts due to Occlusion of Anatomic Variant Bihemispheric Posterior Inferior Cerebellar Artery

Isaiah Tan MD
University of Wisconsin School of Medicine and Public Health, Department of Radiology, Madison, WI, USA

Clinical History

A 61-year-old male with hypertension presented to the emergency department due to acute onset of dizziness 5 hours prior. He endorsed one episode of vomiting but denied trauma, headache, neck pain, weakness, or paresthesia. Blood pressure was elevated to 201/101. Neurologic physical examination - including mental status, cranial nerves, motor function, sensation, and coordination - was normal.

Imaging Findings

CTA of the head and neck demonstrated occlusion of a vessel presumed to represent the right posterior inferior cerebellar artery (blue arrow), as well as non-visualization of a left posterior inferior cerebellar artery (PICA). Follow-up MRI in the emergency department demonstrated diffusion restriction within the bilateral PICA territories consistent with acute infarcts. Retrospective review of a contrast-enhanced MRI performed a few years prior for a different indication demonstrated variant posterior fossa vascular anatomy, with a single vessel arising from the right vertebral artery (purple arrow) giving off branches (yellow arrows) supplying the right and left PICA territories.

Discussion

The patient was diagnosed with acute bilateral cerebellar infarcts due to occlusion of a bihemispheric PICA. He was treated with dual antiplatelet therapy, with thrombolytic therapy deferred due to the timing of his presentation.

Understanding vascular variants of the central nervous system is crucial for accurate diagnosis and management. Unilateral absence of a PICA is relatively common, occurring in 15–25% of individuals, and in these cases the PICA territory is typically supplied by the ipsilateral anterior inferior cerebellar artery (AICA). In contrast, a bihemispheric PICA, in which a single PICA supplies both PICA territories, is rare, with a reported incidence of 0.1–3.6%. Recognition of this variant is important because occlusion of a bihemispheric PICA can result in bilateral cerebellar infarcts and potentially impact clinical outcomes. Awareness of this entity also has treatment implications, as aneurysms have been reported at the origins of a bihemispheric PICAs, and parent vessel occlusion is typically not a feasible treatment option.

Teaching Point

The bihemispheric PICA represents an anatomic variant that should be recognized by neuroradiologists, neurologists, and neuroendovascular surgeons, as pathology involving this vessel – including ischemia – may have distinct clinical features, imaging findings, and therapeutic implications.

References

Carlson AP, Alaraj A, Dashti R, et al. The bihemispheric posterior inferior cerebellar artery: anatomic variations and clinical relevance in 11 cases. *J Neurointerv Surg* 2013;5:601-4. DOI: https://doi.org/10.1136/neurintsurg-2012-010527

Cullen SP, Ozanne A, Alvarez H, et al. The bihemispheric posterior inferior cerebellar artery. *Neuroradiology* 2005;47:809-812. DOI: https://doi.org/10.1007/s00234-005-1427-z

Hirayama T, Oishi H, Kazekawa K, et al. Bihemispheric posterior inferior cerebellar artery revisited: angiographic and embryologic considerations. *AJNR Am J Neuroradiol* 2014;35:320-324. DOI: https://doi.org/10.3174/ajnr.A3788

Images/Tables

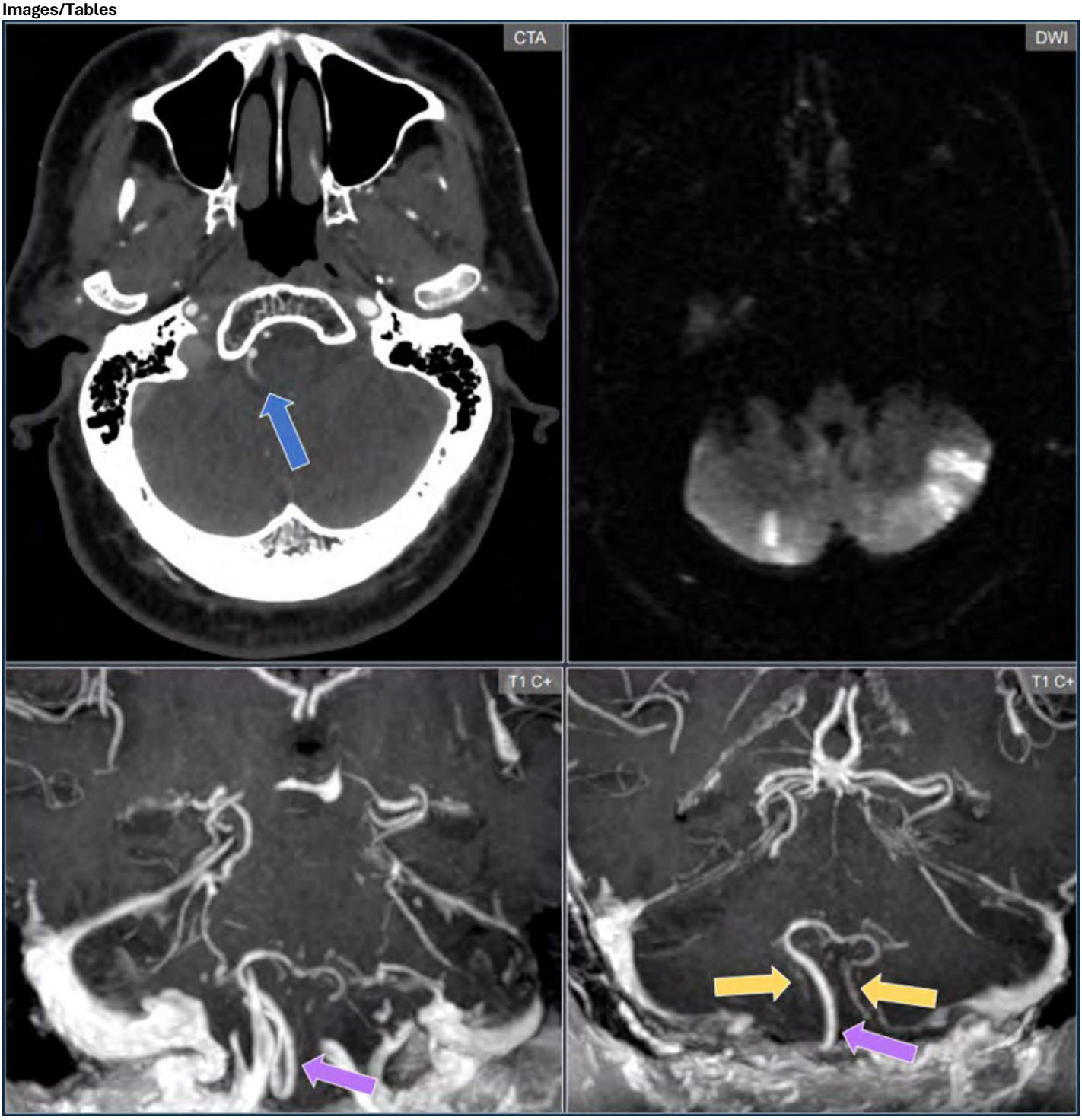

749 **Diffuse Marrow and Orbital Fat Signal Abnormality Mimicking Infiltrative Disease: A Case of "Flip-Flop" on MRI**

Mehdy Haidar MD[1], Alexander Pietroski MD[1], Kamil Abu-Shaban MD[2], Anant Krishnan[2]

[1]Corewell Health William Beaumont University Hospital, Royal Oak, 48073, USA. [2]Corewell Health William Beaumont University Hospital, Royal Oak, MI, USA

Clinical History

A 68-year-old male with a history of left tonsillar squamous cell carcinoma treated 5 months ago and reportedly negative recent PET and CT scans of the neck and body with eye pain with possible but uncertain remote history of trauma was sent in for imaging of the orbits. The patient has a feeding tube and was recently hospitalized and discharged for tube obstruction.

Imaging Findings

Orbital imaging revealed diffuse signal alterations involving the orbital and scalp fat, and marrow, characterized by low signal intensity on T1WI and high signal intensity on T2WI. In particular on the STIR sequence, there was lack of fat suppression in the orbits and adjoining soft tissues. Post-contrast images of the orbits showed diffuse enhancement of the retrobulbar intra-orbital fat without evidence of a discrete mass initially mimicking diffuse infiltration. Both globes appeared normal in morphology, the optic nerves were intact without compression and the extra-ocular muscles were normal in size. In addition, a left cavernous sinus mass was detected that was new from 6 months earlier head CT. Though the cavernous sinus mass

was concerning for neoplastic involvement, the more extensive findings in the fat of the orbits and particularly the bone marrow were favored to represent orbital lipolysis and a sequela of serous atrophy of the bone marrow with a “flip-flop” characteristic appearance. Subsequent discussion confirmed severe malnutrition from the cancer and recent feeding tube issues, with significantly low BMI.

Discussion

Serous atrophy of the bone marrow (SABM), or gelatinous transformation, is a metabolic response to catabolic stress or chronic illness. It involves depletion of marrow fat, hypoplasia of hematopoietic cells, and deposition of mucopolysaccharide-rich gelatinous material, leading to increased water content and a characteristic MRI pattern of diffuse low T1 and high T2 signal within marrow and adjacent fat-containing tissues. This case demonstrates the characteristic “flip-flop” pattern involving the marrow, scalp, and orbital fat, with diffuse retrobulbar enhancement but no discrete mass.

Recognition of SABM is essential, as its diffuse signal abnormalities may mimic infiltrative marrow disorders. Unlike malignant infiltration, which presents with focal enhancement and discrete nodules, SABM shows a homogeneous pattern without focal lesions. Understanding this distinction helps avoid unnecessary biopsies or imaging.

Pathophysiologically, SABM reflects advanced fat depletion replaced by water-rich gelatinous material in severe malnutrition or systemic wasting. Orbital findings represent lipid peroxidation of retrobulbar fat, called orbital lipolysis, resulting in diffuse loss of T1 signal and a “pseudo fat-saturated” appearance. Diffuse orbital enhancement likely reflects contrast leakage through compromised capillaries from the same catabolic process. Although uncommon, simultaneous marrow and orbital involvement underscores their shared etiology.

Teaching Point

Diffuse T1 hypointensity and T2 hyperintensity involving marrow, scalp, and orbital fat with preservation of normal anatomy and absence of focal mass should raise suspicion for serous atrophy of the bone marrow. Recognition of the characteristic “flip-flop” appearance, extending beyond bone marrow to orbital and subcutaneous fat, can prevent misdiagnosis of infiltrative disease and prompt evaluation for underlying systemic or nutritional disorders.

References

1. Toma T, Viegas S, Amiras D, Lord C. Recognising serous atrophy of bone marrow: a review of imaging findings. *Skelet Radiol.* 2025;54:2597-2606. doi:10.1007/s00256-025-04963-w.
2. Demaerel P, Dekimpe P, Muls E, Wilms G. MRI demonstration of orbital lipolysis in anorexia nervosa. Eur Radiol. 2002;12 Suppl 3:S4-S6. doi:10.1007/s00330-002-1365-7.

Images/Tables

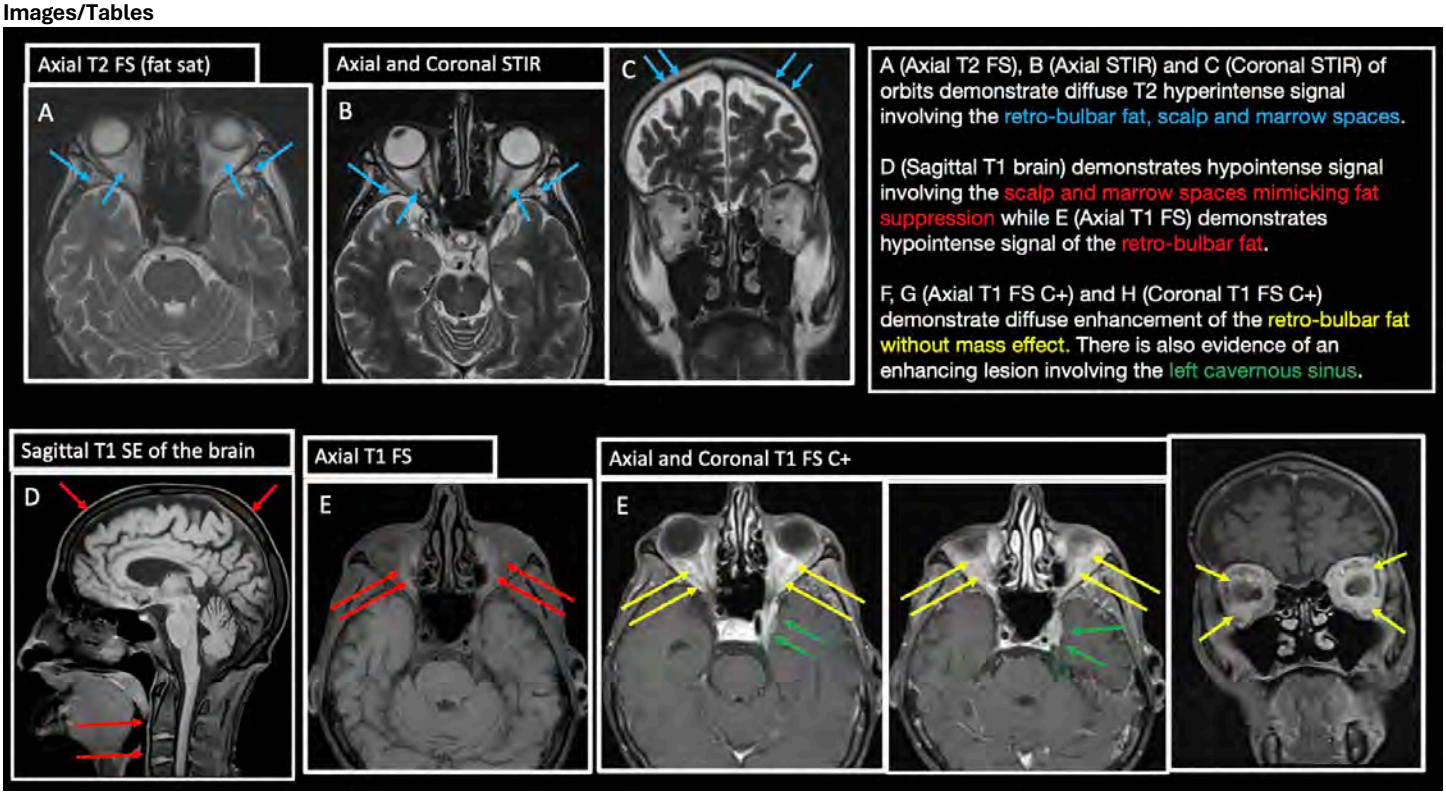

---

753 Challenging Neurovascular Cases from the Andes

Jose A. Bacalla MD, Vanessa I. Pineda Borja MD, Jheferson Contreras Grande MD
Instituto Nacional de Ciencias Neurologicas, Lima, Lima, Peru

Clinical History

CASE 1: 50-year-old male without relevant clinical history presents with temporal lobe epilepsy, quadriparesis and limb discoordination for 2 years.
CASE 2: 42-year-old male with mild congestion in the left eye, facial palsy, dysphagia, vertigo and sensory deficit in the left hemiface.
CASE 3. 35-year-old pregnant patient with mild quadriparesis and tingling sensation on her extremities

Imaging Findings

CASE 1:

Fig. 1 and Fig.4: Coronal T2 shows extensive signal change with mild mass effect on the left insular, left temporal white matter also involving the brainstem.

Fig.2 and Fig.3: Heterogeneous contrast enhancement with gyriform pattern in the regions with signal change.
Fig.5: Hemosiderin deposit in the subcortical temporal whitter matter.
Fig.6: CTA of the Head shows early and intense opacification of the left superior petrosal sinus.
Fig.7: DSA in fontal view demonstrates early opacification of the left superior petrosal sinus by a branch of the occipital artery.
Fig.8: DSA in lateral view confirms the aforementioned findings.

CASE 2:

Fig. 9 and Fig.10: Edema-like pattern in the brainstem with scattered foci of nodular-to-linear contrast enhancement.
Fig. 11 and Fig. 12: Axial and coronal FLAIR sequences demonstrate brainstem signal alteration with extension into the medulla oblongata.
Fig.13: Axial SWI depicts hemosiderin deposits in the left caudal pons.
Fig.14: DSA (lateral view) demonstrates opacification of a triangle-shaped structure corresponding to the left cavernous sinus.
Fig.15 DSA frontal view confirms a external carotid artery-to-cavernous sinus fistula.

CASE 3.

Fig.16: Sagittal T2 shows hypointense ovoid lesion in the spinal cord at the C4-C5 level with extensive myelopathic changes.
Fig.17: Axial gradient echo sequence shows a hypointense ovoid lesion, most likely hemosiderin deposit.
Fig.18: Axial T1 post-contrast depicts ovoid foci of enhancement in the left side (discontinuous arrow), raising suspicion for a vascular anomaly.
Fig.19: DSA demonstrates ovoid vascular lesion consistent with glomic arterio-venous malformation

Discussion

CASE 1: Initial diagnostic hypothesis included a tumoral process vs granulomatous atypical infection. Meticulous evaluation of the CTA findings, multidisciplinary clinical discussion and subsequent DSA were crucial for correct diagnosis.
Final Diagnosis: Dural occipital arterio-venous fistula with congestive changes and hemosiderin deposit in the left temporal, left insula and brainstem[1].
CASE 2: The initial appearance of MRI was non-specific, and inflammatory or infectious process were considered. The clinical picture revealed mild ocular congestion. Careful image review demonstrated early opacification of the left cavernous sinus, suggesting the possibility of an indirect fistula[2].
Final Diagnosis: External carotid artery-to-cavernous sinus fistula with brainstem venous congestion[3].
CASE 3: The presence of an ovoid hemosiderin deposit in the spinal cord associated with focal contrast enhancement was suspicious for a vascular anomaly, later confirmed by DSA.
Final Diagnosis: Spinal glomic AVM with conges<ve myelopathic changes.

Teaching Point

The common finding in our case series was the presence of hemosiderin deposits and atypical contrast enhancement in the affected regions, sugges<ng an underlying vascular anomaly. When a vascular lesion is suspected, meticulous review of clinical and imaging findings—along with the addition of DSA—is essencial for accurate diagnosis and appropriate management.

References

1.Miller TR, Gandhi D. Intracranial dural arteriovenous fistulae: clinical presentation and management strategies. *Stroke*. 2015;46(7):2017-2025. doi:10.1161/STROKEAHA.115.008228
2.Ringer AJ, Salud L, Tomsick TA. Carotid cavernous fistulas: anatomy, classification, and treatment. *Neurosurg Clin N Am* 2005; 16:279–95
3.Takahashi S, Tomura N, Watarai J, Mizoi K, Manabe H. Dural arteriovenous fistula of the cavernous sinus with venous congestion of the brain stem: report of two cases. *AJNR Am J Neuroradiol* 1999; 20:886–8
4. Alkhaibary A, Alharbi A, Alnefaie N, Alammar H, Arishy A, Alghanim N, *et al*. Spinal dural arteriovenous fistula: a comprehensive review of the history, classification systems, management, and prognosis. *Chin Neurosurg J* 2024; 10:1186/s41016-023-00355-y

Images/Tables

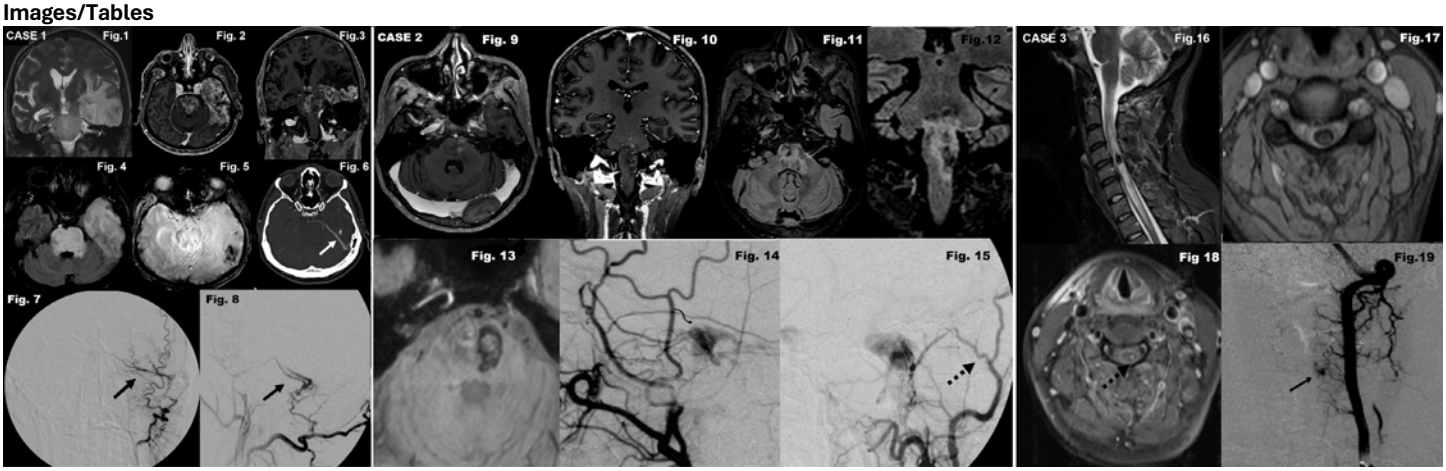

---

765 Dermatofibrosarcoma Protuberans in the Head and Neck: A Case Series.

Anisha Shetty MD[1], Kunal Shetty MD[2]
[1]Mayo Clinic, Scottsdale, AZ, USA. [2]Baylor Scott and White, Round Rock, TX, USA

Clinical History

Patient 1: 37yo male who presented with asymptomatic left supraclavicular exophytic mass present for 1 year. CT was performed for characterization. Biopsy was performed showing fibrosarcomatous DFSP. Dermatology performed Mohs surgery followed by adjuvant radiation therapy.

Patient 2: 6yo female who presented with a congenital slow growing, firm lesion at the vertex of her head. US was interpreted as a potential dermoid or epidermoid cyst with clinical exam thought to be more consistent with Port Wine stain. Biopsy demonstrated DFSP. CT and MR were performed for treatment planning. Mohs with reconstruction was done by plastic surgery and neurosurgery due to periosteal involvement.
Patient 3: 40yo female who presented after noticing a pimple on her right cheek approximately 5 years prior which appeared to be enlarging. Exam was notable for an erythematous nodule overlying the right anterior mandible. Biopsy demonstrated DFSP. MR and CT were performed for preoperative planning. Plastic surgery performed Mohs with reconstruction.

Imaging Findings

Patient 1: CT demonstrates a heterogeneously enhancing 4.5cm left supraclavicular mass involving the skin and subcutaneous tissue.
Patient 2: US demonstrates an isoechoic 5.4cm mass within the soft tissues at the skull vertex with mild internal vascularity. On CT, this lesion is seen as an ill-defined area of soft tissue thickening. On MR, the lesion is T2 hyperintense and T1 iso to hyperintense with enhancement. There is thinning of the underlying calvarium.
Patient 3: CT head shows a 3cm enhancing soft tissue mass overlying the right mandible and involving the right platysma without osseous involvement of the mandible. On MR, this lesion is T1 hypointense and T2 hyperintense with enhancement.

Discussion

Dermatofibrosarcoma protuberans (DFSP) is a rare adult and pediatric cutaneous soft tissue sarcoma that represents <0.1% of all malignancies and 1% of soft tissue sarcomas. The extremities and trunk are the most common locations of occurrence, accounting for 70-90% of cases, with the head and neck less common. On imaging, DFSP typically appears as a lobulated soft tissue mass involving the skin and subcutaneous fat. US demonstrates a hypoechoic or heterogeneous lesion with mild vascularity. CT features include hypo or isoattenuation with predominantly homogenous enhancement. On MR, DFPS is typically T1 hypointense and T2 hyperintense with enhancement. These carry a favorable prognosis, although they tend to locally recur in approximately 20-55% of cases making attention on follow up imaging vital. Rarely, metastatic disease is present and most often occurs within the lungs. Fibrosarcomatous transformation which occurs in approximately 10-20% of cases can lead to more aggressive disease. Treatment options include surgical resection, radiation therapy and Imatinib.

Teaching Point

1. DFSP is a rare cutaneous soft tissue sarcoma that can rarely appear in the head and neck in the pediatric and adult population.
2. As these can be locally aggressive, prompt identification is essential to reduce the need for an aggressive resection and extensive reconstruction.
3. After DFSP is confirmed with biopsy, preoperative imaging is done to help guide surgical planning.
4. Although carrying a favorable prognosis, DFSP tend to locally recur making attention on follow up imaging vital.

References

Choong P, Lindsay D, Khoo M, Saifuddin A. Dermatofibrosarcoma protuberans: the diagnosis of high-grade fibrosarcomatous transformation. *Skeletal Radiol*. 2021;50(4):789-799. doi:10.1007/s00256-020-03617-3

Torreggiani WC, Al-Ismail K, Munk PL, Nicolaou S, O'Connell JX, Knowling MA. Dermatofibrosarcoma protuberans: MR imaging features. *AJR Am J Roentgenol*. 2002;178(4):989-993. doi:10.2214/ajr.178.4.1780989

Millare GG, Guha-Thakurta N, Sturgis EM, El-Naggar AK, Debnam JM. Imaging findings of head and neck dermatofibrosarcoma protuberans. AJNR Am J Neuroradiol. 2014 Feb;35(2):373-8. doi: 10.3174/ajnr.A3650. Epub 2013 Aug 1. PMID: 23907249; PMCID: PMC7965745.

Thornton SL, Reid J, Papay FA, Vidimos AT. Childhood dermatofibrosarcoma protuberans: role of preoperative imaging. *J Am Acad Dermatol*. 2005;53(1):76-83. doi:10.1016/j.jaad.2004.11.071

Images/Tables

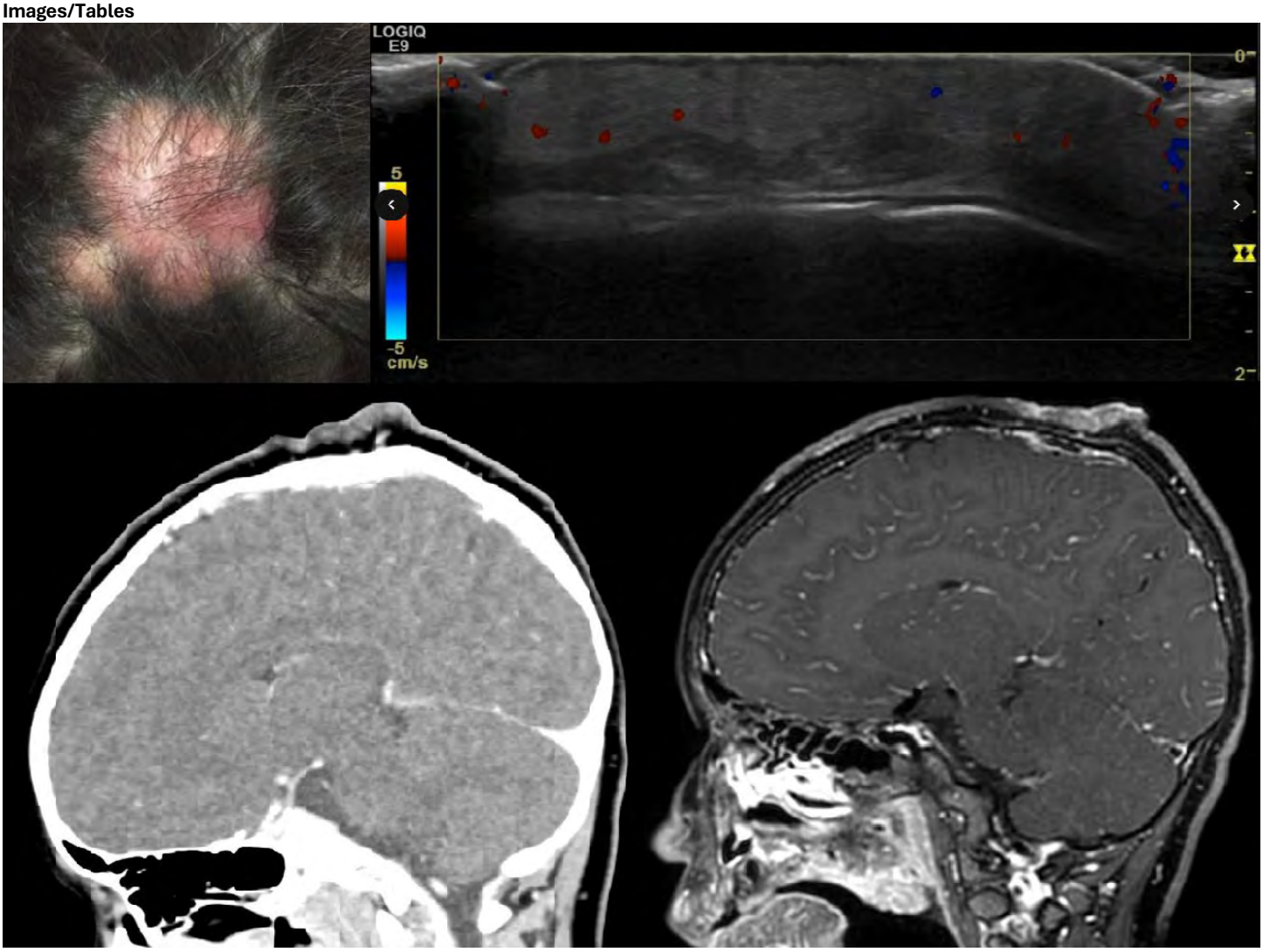

789 Single and Unusual: A Report of Two Cases of Solitary Fibrous Tumors in Atypical Intracranial Locations

Samaher Adnan Thigah Senior Diagnostic Radiology Resident[1], Afnan Samman Associate Consultant Neurosurgery[2], Alaa Samkari Pathologist[3], Reem Adas Neuroradiology Consultant[2]

[1]Ministry of National Guard Health Affairs, Jeddah, Makkah, Saudi Arabia. [2]King Abdulaziz Medical City National Guards Health Affairs - WR, Jeddah, Makkah, Saudi Arabia. [3]Department of Medicine, Faculty of Medicine, King Saud Bin Abdulaziz University for Health Sciences, Jeddah, Makkah, Saudi Arabia

Clinical History

The first patient was a 71-year-old woman, who presented with chronic headache, lethargy, and memory disturbance. The second patient was a 35-year-old man, who presented with chronic headaches, left facial numbness, and left facial palsy grade II. Both patients underwent advanced neuroimaging, including diffusion-weighted and perfusion sequences, for evaluation.

Imaging Findings

The first case revealed a mixed cystic-solid mass attached to the clinoid and extending into the ventricle. The solid component was markedly hypointense on both T1- and T2-weighted images, exhibited homogeneous enhancement, restricted diffusion, and no increase in perfusion.

The second case demonstrated a left CP angle mass that was isointense on T1 and markedly hypointense on T2, with homogeneous enhancement, no diffusion restriction, and no increased perfusion.

Discussion

Intracranial solitary fibrous tumors (SFTs) are rare mesenchymal neoplasms, accounting for less than 1% of all primary central nervous system tumors and may mimic more common CNS tumors on neuroimaging [1]. In our cases, SFTs arose in atypical locations at the central and posterior skull base. The differential considerations for the first case included atypical meningioma, glial tumor, and atypical central neurocytoma, while for the second case included meningioma and atypical schwannoma.

SFTs typically demonstrate marked T2 hypointensity, isointense or hypointense signal on T1, and homogeneous enhancement—imaging features attributed to their dense collagenous stroma and low water content [2,3]. These findings may overlap with meningiomas, which also enhance and can appear dural-based; however, meningiomas typically show isointense or mildly hyperintense T2 signal and increased perfusion due to rich vascularity [2]. Similarly, schwannomas may appear at the cerebellopontine angle with heterogeneous enhancement, T2 hyperintensity, and cystic degeneration, which are less typical features of SFTs. Glial tumors or central neurocytomas, though intraventricular, usually demonstrate T2 hyperintensity and variable perfusion, contrasting the low T2 signal and low perfusion seen in SFTs.

The imaging findings were correlated with histopathologic results after surgical resection. Histopathology confirmed solitary fibrous tumor, WHO grade II for the first case and WHO grade I for the second case.

Teaching Point

Intracranial SFTs can arise in unusual locations and mimic more common entities such as meningiomas, glial tumors or schwannomas. Magnetic resonance imaging features including marked T2 hypointensity, homogeneous enhancement, and absence of elevated perfusion—should raise suspicion for SFT and guide preoperative diagnosis.

References

1. Liu J et al. Front Oncol. 2022;12:915273. doi:10.3389/fonc.2022.915273.
2. Ginat DT et al. AJR Am J Roentgenol. 2011;196(3):487–495. doi:10.2214/AJR.10.4948.
3. Kim HJ et al. Korean J Radiol. 2005;6(3):136–142. doi:10.3348/kjr.2005.6.3.136.

Images/Tables

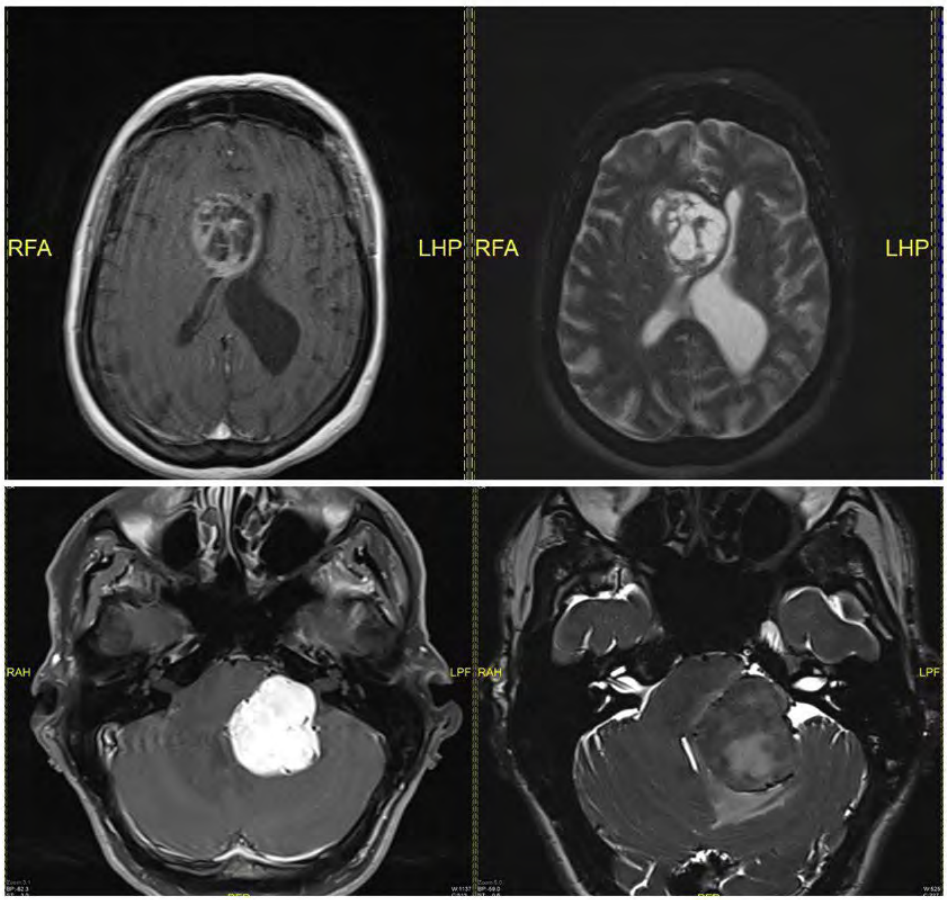

---

791 Lowe Syndrome: Neuroimaging Spectrum Including Rare Craniocervical Junction Dysplasia in an Adult Patient.

Huda Salah Zoori MD[1], David Timaran Montenegro MD[1], Luis Garcia MD[2], Nagore Siles MD[3], Cesar Palacios MD[4]

[1]UTHealth, Houston, Texas, USA. [2]Hospital General Regional No.1 IMSS Tijuana, Baja California, Mexico, Mexico. [3]San Pedro university Hospital, Logrono, La rioja, Spain. [4]Tecnológico de Monterrey, Monterrey, Nuevo Leon, Mexico

Clinical History

A 42-year-old male with genetically confirmed Lowe syndrome (oculocerebrorenal syndrome) is being followed secondary to to chronic epilepsy and developmental delay.His past medical history includes Fanconi syndrome diagnosed at 6 months of age, chronic kidney disease stage 3, congenital cataracts (removed in infancy), glaucoma (surgery in 2012), and moderate intellectual disability. The patient also has stereotypic behaviors, partial hearing loss, multiple sebaceous cysts, and mild scoliosis. Family history revealed a carrier mother and an affected half-brother, consistent with X-linked inheritance.

Imaging Findings

Brain MRI (non-contrast) demonstrates extensive bilateral periventricular T2/FLAIR hyperintensities with innumerable small cystic spaces, suggestive of chronic leukoencephalopathy and/or dilated Virchow–Robin spaces. The craniocervical junction shows dysplastic dens and flattened clivus with upper cervical canal narrowing and associated CSF effacement.

Discussion

Lowe syndrome is a rare X-linked recessive multisystem disorder caused by pathogenic variants in the OCRL1 gene, encoding the inositol-5-phosphatase OCRL-1. Loss of this enzyme disrupts phosphatidylinositol (4,5)-bisphosphate metabolism, leading to abnormal endosomal trafficking and actin regulation. The prevalence is estimated at 1 in 500,000 in the general population. The classic
triad includes dense congenital bilateral cataracts, intellectual impairment, and renal tubular dysfunction with slowly progressive renal failure. Other features include development delay, seizures, glaucoma, keloids, areflexia/hypotonia, dental anomalies,subcutaneous nodules, behavioral abnormalities and arthropathy, which can be observed in about 50 % of adult patients.

Neuroimaging findings typically include ventriculomegaly and periventricular/deep white matter T2 hyperintensities with associated cystic changes, often stable in size and distribution. Other findings more variable and non-specific are tigroid pattern with hypointense radially oriented stripes within the hyperintense cerebral white matter on T2-weighted images, brain atrophy, cerebellar hypoplasia, pachygyria, polymicrogyria, aberrant neuronal migration and subependymal cysts. Musculoskeletal implications are less described and include osteopenia, swollen/enlarged joints, scoliosis rickets, joint laxity, arthropathy and cervical abnormalities.

Teaching Point

Recognition of the oculocerebrorenal triad and distinctive MRI findings—including periventricular cystic leukoencephalopathy, and craniocervical junction dysplasia—broadens the imaging spectrum of Lowe syndrome.Identification of these features, particularly clival and odontoid dysplasia with canal stenosis, highlights the importance of multisystem evaluation and multidisciplinary management to mitigate neurological and renal complications in long-term survivors.

References

1. Lewis, R. A., Nussbaum, R. L., & Brewer, E. D. (2019). Lowe Syndrome. In: GeneReviews® [Internet]. Seattle (WA): University of Washington, Seattle (WA): University of Washington, Seattle; 1993–2025. PMID: 20301653.
2. Bökenkamp, A., & Ludwig, M. (2016). The oculocerebrorenal syndrome of Lowes An update. Pediatric Nephrology, 31(12), 2201–2212. https://doi.org/10.1007/s00467-016-3376-y
3. Sferopoulos, N. K. (2018). Oculocerebrorenal (Lowe) syndrome in the pediatric orthopedic practice: A review. Clinical Research in Pediatrics, 1(1), 1–5.
4. Won, J. H., Lee, M. J., Park, J. S., Chung, H., Kim, J. K., & Shim, J. S. (2010). Multiple epidermal cysts in Lowe syndrome. Annals of Dermatology, 22(4), 444–446. https://doi.org/10.5021/ad.2010.22.4.444
5. Sena, C., et al. (2022). Endocrine and behavioral features of Lowe syndrome and their potential molecular mechanisms. Journal of Medical Genetics, 59(12), 1171–1178. https://doi.org/10.1136/jmg-2022-108463

---

796 Intraventricular Cavernous Malformation: A Rare Entity in an Unusual Location

NAGORE SILES MD[1], Adam Stroh MD[2], Luis Gerardo García MD[3], Cesar Andrés Palacios MD[4], Jose Gavito-Higuera MD[2]
[1]San Pedro University Hospital, Logroño, La Rioja, Spain. [2]UTHealth Houston Medical Center, Houston, Texas, USA. [3]General Regional Hospital No1, Tijuana, Baja California, Mexico. [4]Tecnológico de Monterrey, Monterrey, Nuevo León, Mexico

Clinical History

A 51-year-old male presented to the Emergency Department with persistent occipital headaches for one month, accompanied by neck stiffness, low-grade fever, and night sweats. He denied focal neurological deficits, visual symptoms, or recent travel. Past medical history included hypertension, alcohol abuse with withdrawal seizures, and esophageal ulcer. He was initially treated for presumed migraine (sumatriptan), and a 10-day course of amoxicillin yielded no improvement.

Non-contrast CT and MRI revealed an intraventricular mass suspicious for neoplasm. Stereotactic biopsy demonstrated organizing hematoma with reactive changes; special stains excluded neoplasm and infection, consistent with cavernous malformation. The patient underwent surgical resection. Postoperative recovery was uneventful, with no recurrence or new neurological deficits.

Imaging Findings

CT demonstrated a lobulated, heterogeneous hyperdense lesion within the frontal horn of the left lateral ventricle, attached to the septum pellucidum, without calcifications or enhancement on angiographic CT.

MRI (Stealth protocol) revealed a well-defined, irregular intraventricular mass in the frontal horn of left lateral ventricle, with associated minimal T2/FLAIR hyperintensity in the genu of the corpus callosum, septum pellucidum and left frontal periventricular white matter suggestive of minimal perilesional edema related to recent intralesional hemorrhage. The lesion appeared isointense on T1W with peripheral hyperintense areas, heterogeneously hyperintense on T2W with a thin hypointense rim, and showed prominent blooming artifacts on SWI sequence, related with internal hemosiderin deposition. Contrast-enhanced images showed minimal heterogeneous enhancement, and there was restricted diffusion within the lesion corresponded to evolving recent hemorrhage. No hydrocephalus or midline shift was identified.

Discussion

Cerebral cavernous malformations (CCMs) are low-flow vascular malformations composed of dilated sinusoidal channels without intervening neural tissue. They represent 10–15% of central nervous system (CNS) vascular malformations, with intraventricular cavernomas accounting for only 2.5–10.8% of cases. The lateral ventricles are most frequently affected, followed by the third and fourth ventricles.

The absence of adjacent brain parenchyma allows these lesions to grow larger than parenchymal CCMs, and recurrent microhemorrhage contributes to enlargement. Symptoms typically arise from mass effect, hemorrhage, or hydrocephalus.

MRI is the diagnostic modality of choice, showing a characteristic “popcorn-like” appearance with mixed signal intensities and a hypointense rim on T2W and GRE/SW sequences, with prominent blooming artifact due to hemosiderin deposition. Minimal enhancement and lack of significant edema help differentiate CCMs from neoplastic lesions. The differential diagnosis includes central neurocytoma, ependymoma, or hemorrhagic metastasis. Histologically, cavernous malformations consist of thin-walled vascular channels lined by endothelium with insignificant intervening parenchyma. Complete surgical excision is recommended for symptomatic or enlarging intraventricular CCMs, while conservative management may be considered in asymptomatic lesions.

Teaching Point

Intraventricular CCMs are rare vascular lesions that can mimic intraventricular tumors on imaging. Recognizing their characteristic MRI features can prevent misdiagnosis and unnecessary biopsy. Although rare, cavernous malformation should be included in the diagnosis of intraventricular masses due to their high risk of intraventricular hemorrhage.

References

1. Kuroedov D, Cunha B, Pamplona J, Castillo M, Ramalho J. Cerebral cavernous malformations: Typical and atypical imaging characteristics. Journal of Neuroimaging. 2022 Dec;33(2):202–17. DOI:10.1111/jon.13072
2. Kivelev J, Niemelä M, Kivisaari R, Hernesniemi J. Intraventricular cerebral Cavernomas: A series of 12 patients and review of the literature. Journal of Neurosurgery. 2010 Jan;112(1):140–9. DOI:10.3171/2009.3.jns081693

3. Savith K. Intraventricular Cavernoma. Journal of Surgery and Surgical Research. 2018 Apr 30;001–2. DOI:10.17352/2455-2968.000049

Images/Tables

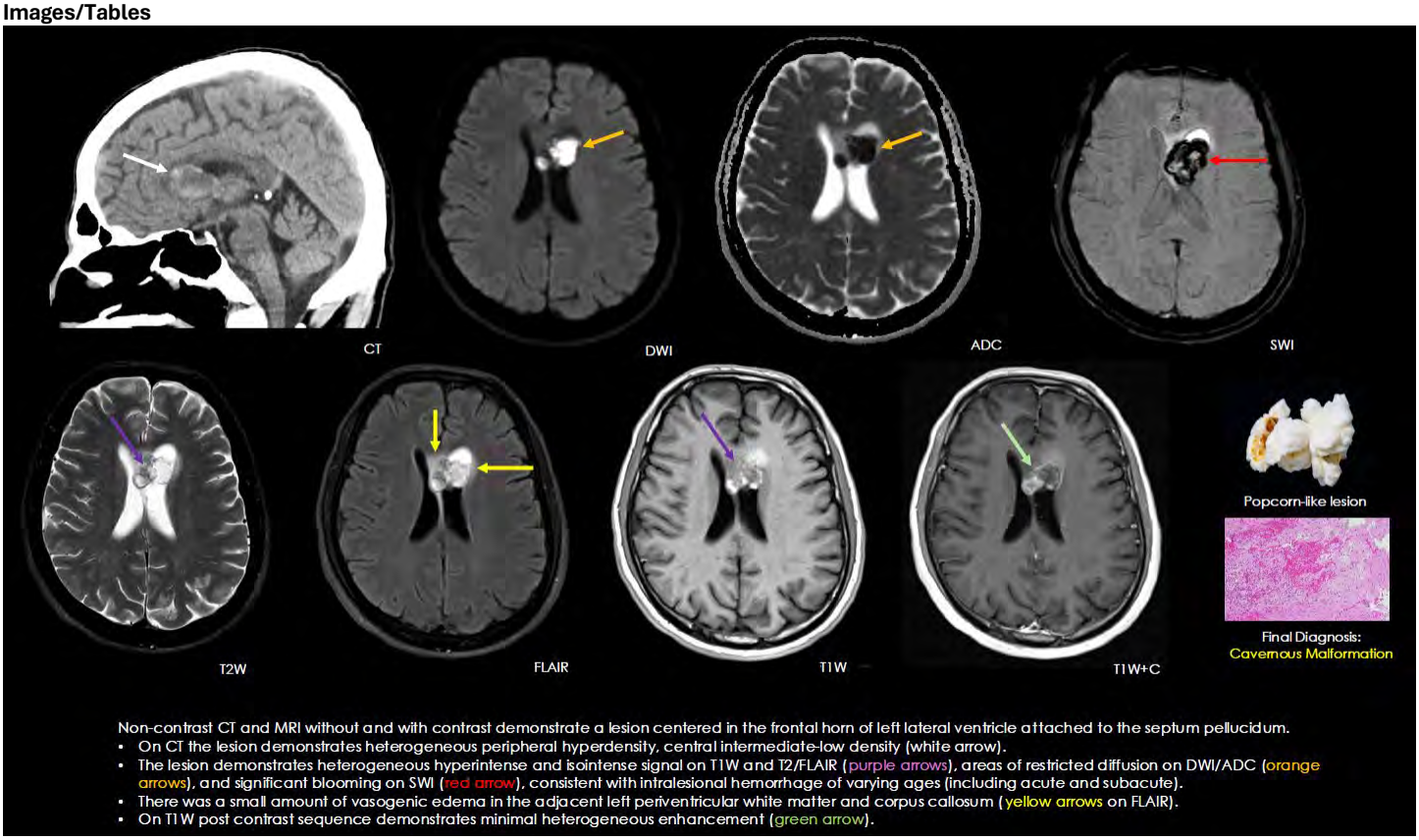

---

809 Intracranial Metastases from Uterine Leiomyosarcoma: A Systematic Review and Case Illustration

Ahmad Pour Rashidi M.D.[1], Laetitia Perronne M.D.[1], Chase Krumpelman MD[2], Yuri S Velichko PhD[1]

[1]Northwestern University, Feinberg School of Medicine, Chicago, IL, USA. [2]Northwestern University, Feinberg School of Medicine, Chicago, Illinois, USA

Clinical History

From 1989 to 2025, 39 individual cases of brain metastases from uterine leiomyosarcoma (ULMS) were identified in 34 previously published studies. We also included one new case from our institution that met all inclusion criteria, bringing the total number of cases analyzed to 40. As expected, all patients were female, with a median age of 51.5 years (range: 26–70). For patients who were still alive at the time of data collection, survival was calculated to the last known follow-up date. This right-censoring of data is a key limitation, as it inherently underestimates the true survival time for this subgroup and contributes to a poorer overall prognostic outcome. Four patients were excluded from the survival analysis because their survival time was not reported or could not be estimated. Therefore, for the remaining 36 patients, the average and median survival times after diagnosis of brain metastasis were 10.37 months and 5 months, respectively.

Imaging Findings

Nearly all patients underwent brain MRI (T1- and T2-weighted sequences), with or without accompanying CT imaging. Non-contrast CT scans, when performed, commonly revealed hyperattenuating lesions or evidence of osteolytic changes. Radiological findings were reported in 23 studies. Among MRI signal characteristics, T1 and T2 isointensity was observed in 4 (17.4%) cases, T2 hyperintensity in 5 (21.7%) cases, and a combination of T1 isointensity with T2 hyperintensity in 3 (13%) cases. Homogeneous contrast enhancement was the most frequently reported pattern, seen in 19 (82.6%) cases, while ring enhancement was described in 4 (17.4%) cases. Additional MRI features included necrosis in 14 (60.9%) cases and a dural-based lesion in 10 (43.5%) cases.

Discussion

Brain metastasis from ULMS is a lethal event with an extremely poor prognosis. Nonspecific imaging features create diagnostic challenges, necessitating histopathological confirmation. Current therapies, including surgery and radiotherapy, offer palliative benefit but do not significantly alter survival. The aggressive biological behavior demonstrated here underscores the urgent need for increased clinical awareness and collaborative research to develop more effective management strategies and improve outcomes for this devastating diagnosis.

Teaching Point

Brain metastasis from ULMS is a rare but lethal event characterized by nonspecific imaging features and an extremely poor prognosis. While current treatments, including surgery and radiotherapy, may offer symptomatic benefits, they do not appear to significantly alter the grim overall survival. Increased awareness and collaborative, prospective research are urgently needed to develop more effective management strategies and improve outcomes for this patient population.

References

Carrillo-Uzeta, A.A.; Varela-Avalos, E.; Agustin-Godinez, E.; Uehara-Gonzalez, J.A.; Medina-Romero, J.R.; Velazquez-Zamarripa, A.I.; et al. A neurosurgical approach to skull metastasis from uterine leiomyosarcoma: Illustrative case. *J. Neurosurg. Case Lessons* **2025**, *9*, CASE24769.

Images/Tables

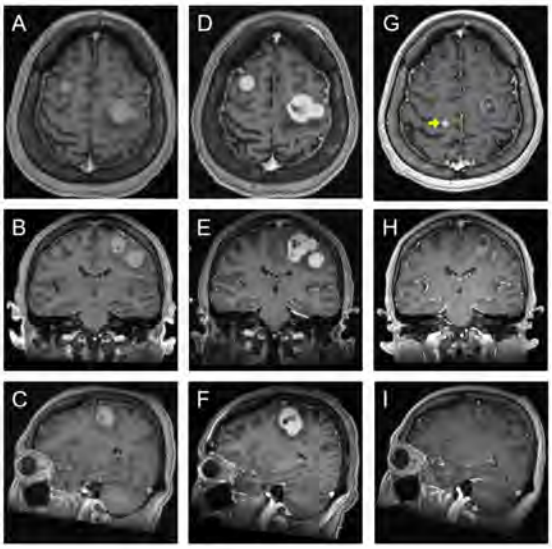

Axial, coronal and sagittal views of post-contrast T1-weighted brain MRIs in three different timepoints are seen. Left column (A&B&C) is related to the first scan upon the patient's admission. The second scan which was taken one week later, is seen in the middle column (D&E&F), and the third column (G&H&I) displays tumor changes two months after gamma-knife radiosurgery (GKRS). It is visible that the lesions has grown rapidly only after one week. Moreover, although an acceptable response to the GKRS is achieved, the new lesion (yellow arrow) has emerged concurrently.

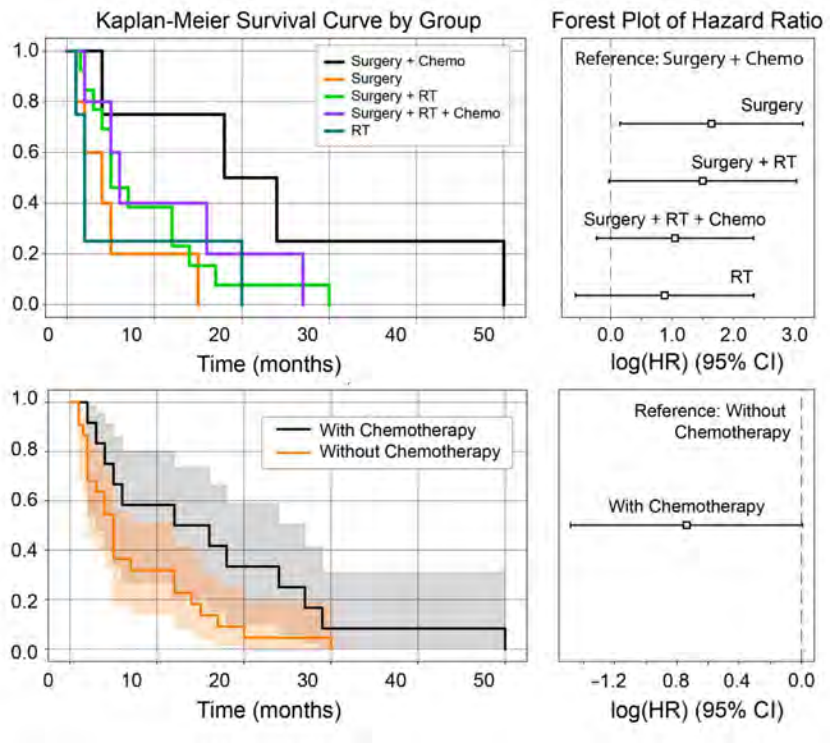

---

813 Fetal MRI Diagnosis of an Epignathus

Albert Gonzalez MD, Raul Barbieri MD, Daniella K Zanoni MD, Maria G Matheus MD, Maria V Spampinato MD
Medical University of South Carolina, Charleston, SC, USA

Clinical History

Patient was a 37-year-old female following with her obstetrician for routine prenatal care. On routine prenatal screening ultrasound, a cystic and solid facial mass was discovered and subsequently a fetal MRI was obtained at approximately 27 weeks gestation to further characterize the mass. Following a complex multidisciplinary discussion, the decision was made to deliver at 37 weeks gestation at the regional tertiary care center where an ex-utero intrapartum treatment (EXIT) to airway procedure would be performed to maintain the neonate's airway.

Imaging Findings

Axial, coronal, and sagittal T2 images from the fetal MRI demonstrated a complex partially cystic and solid mass arising from the palate and extending throughout the oral cavity of the fetus and anteriorly with a prominent component residing in the amniotic sac. The lesion resulted in mass effect on the oral cavity and airway. The solid components of the mass demonstrated variable signal with some solid components resembling well differentiated tissues (for example, the appearance of calvarium on the bottom left image).

Discussion

Imaging findings from the fetal MRI demonstrated a complex mass containing various differentiated tissues originating from the palate of the fetus. These findings are consistent with a teratoid tumor which when arising from the palate or pharyngeal tissues is referred to as epignathus.
As planned by the multidisciplinary team, the delivery occurred at approximately 37 weeks gestation during which the planned EXIT to airway procedure was performed. The tumor was surgically resected to secure the airway. The neonate was then transferred to the neonatal intensive care unit for monitoring.

Teaching Point

Teratoid tumors that arise from the oral cavity, specifically from the palate or pharyngeal tissues are termed epignathus. These tumors vary in presentation including variations of their origin, number, and levels of tissue differentiation, from poorly differentiated to well differentiated tissues. These tumors are often associated with a high risk of mortality due to their inherent proximity to the airway and risk of airway compromise. As a result, these tumors often require complex multidisciplinary discussions and planning to coordinate care at the time of delivery.

References

Freitas R, Alonso N, Azzolini T et al. Epignathus: Two Cases. Br J Oral Maxillofac Surg. 2008;46(4):317-9. doi:10.1016/j.bjoms.2007.06.012
Kumar B, Sharma SB. Neonatal oral tumors: congenital epulis and epignathus. J Pediatr Surg. 2008 Sep;43(9):e9-11. doi: 10.1016/j.jpedsurg.2008.03.055.
Oliveira-Filho AG, Carvalho MH, Bustorff-Silva JM et al. Epignathus: report of a case with successful outcome. J Pediatr Surg. 1998 Mar;33(3):520-1. doi: 10.1016/s0022-3468(98)90103-8.

Images/Tables

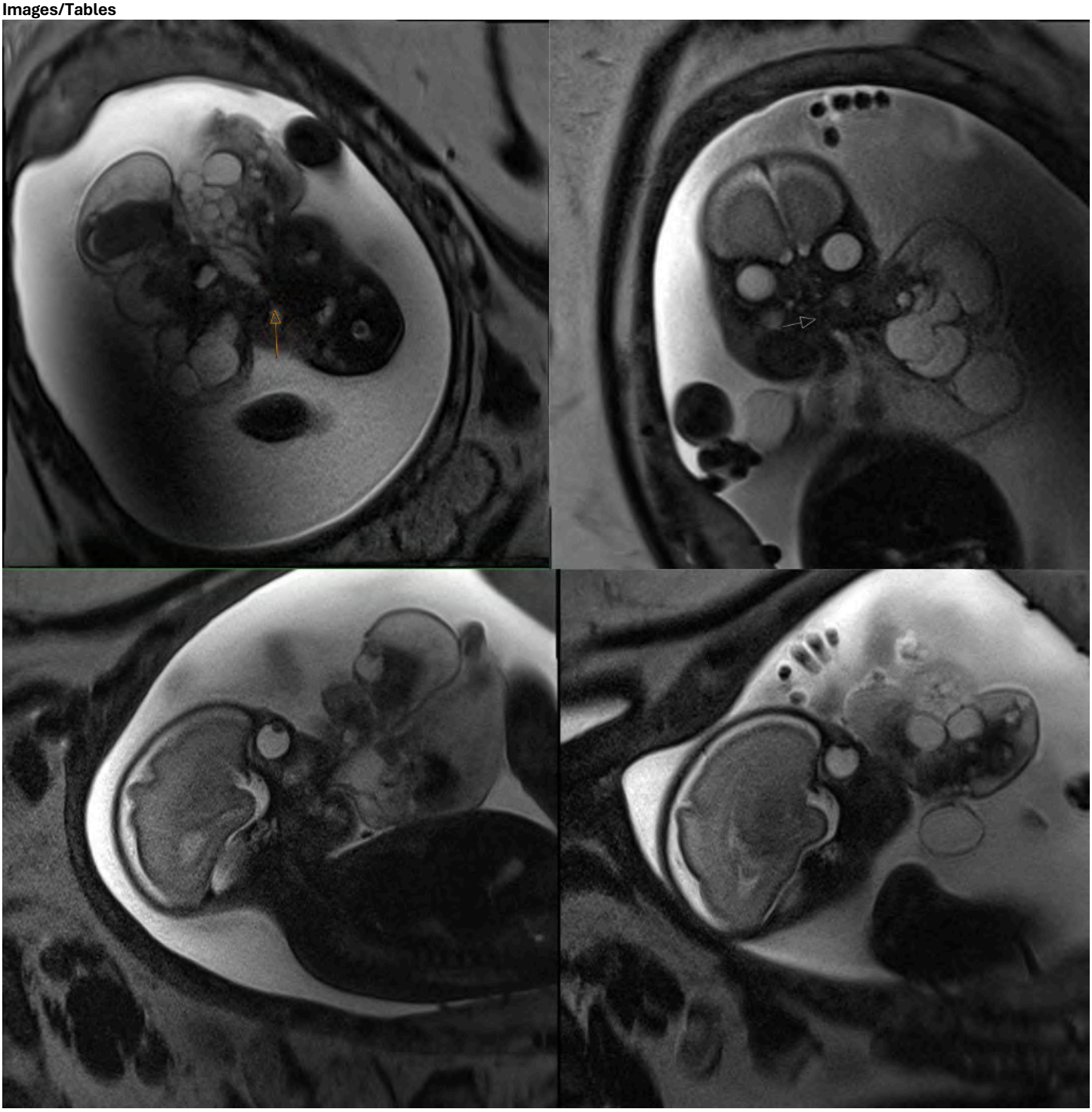

824 Cerebellar Endometriosis: When Gynecology Meets Neurosurgery.

Huda Salah Zoori MD[1], Luis Garcia MD[2], Nagore Siles MD[3], Cesar Palacios MD[4], Jose Gavito MD[1]

[1]UTHealth, Houston, Texas, USA. [2]Hospital General Regional No.1 IMSS Tijuana, Baja California, Mexico, Mexico. [3]San pedro university hospital, Lagrono, La rioja, Spain. [4]Tecnológico de Monterrey, Monterrey, Nuevo Leon, Mexico

Clinical History

A 14-year-old female with no prior medical history presented with recurrent, intermittent, and cyclic headaches that worsened over the preceding week. The headaches were throbbing in nature, predominantly frontal and occipital, and associated with photophobia, phonophobia, nausea, and dizziness. No history of trauma or focal neurological deficits. Outpatient non-contrast CT revealed a large posterior fossa cystic lesion exerting mass effect, prompting urgent neurosurgical referral. Suboccipital craniectomy achieved complete excision of a dark-blue cystic lesion. Postoperative recovery was uneventful. Histopathology demonstrated organized hemorrhage with hemosiderin-laden macrophages and focal benign epithelium, consistent with cerebellar endometriosis. Gynecologic evaluation revealed normal menstrual cycles and pelvic ultrasound.

Imaging Findings

Non-contrast CT of the brain demonstrated a well-circumscribed hyperdense lesion within the posterior aspect of the right cerebellar hemisphere, with an excentric hypodense nodular component lateral to the vermis. This lesion was partially compressing the fourth ventricle and resulting in mild supratentorial ventriculomegaly.

MRI revealed a large, well-defined, multiloculated cystic lesion projected in the posterior aspect of the right cerebellum. The dominant component was T1W hyperintense, with hypointense signal on T2W, FLAIR, SWI and DWI sequences, demonstrating the classic “T2 shading” sign, which strongly mirrors ovarian endometrioma. There was also an additional excentric heterogeneous and mildly enhancing nodule, projected posteromedial to the cyst, lateral to the vermis. This lesion caused mass effect to adjacent structures, resulting in mild tonsillar herniation and mild supratentorial ventriculomegaly.

Discussion

Endometriosis is a gynecologic disorder characterized by ectopic endometrial glands and stroma outside the uterus, causing cyclic hemorrhage, inflammation, and fibrosis.

While common in pelvic sites, CNS involvement is exceedingly rare; cerebellar localization is exceptional, with few reported cases (Sarma et al., 2004; Meggyesy et al., 2020). Proposed mechanisms include hematogenous or lymphatic spread, meningeal metaplasia, and perineural migration (Siquiara de Sousa et al., 2015).

MRI features often resemble ovarian endometriomas: T1W hyperintensity, T2W hypointensity (“T2-shading”), and chronic hemorrhage. Our case demonstrated these hallmark features.

Absence of pelvic disease does not exclude diagnosis; up to one-third of neuro-endometriosis cases lack peritoneal involvement (Siquiara de Sousa et al., 2015). Histopathologic confirmation may be challenging, as chronic hemorrhage and fibrosis obscure endometrial stroma (Van Buren et al., Radiology 2024).

Teaching Point

Cerebellar endometriosis, though exceedingly rare, should be considered in the differential diagnosis of hemorrhagic posterior fossa cysts in young females. Characteristic MRI findings can mimic neoplastic or vascular lesions. Awareness of this entity and its imaging parallels with ovarian endometriomas is essential for accurate preoperative assessment and multidisciplinary planning.

References

1. Thibodeau LL, Prioleau GR, Manuelidis EE, Merino MJ, Heafner MD. Cerebral endometriosis. J Neurosurg. 1987;66(4):609–610.
First reported intracranial case; right parietal hemorrhagic lesion with histologic confirmation of endometrial glands and stroma.
2. Ichida M, Gomi A, Hiranouchi N, et al. A case of cerebral endometriosis causing catamenial epilepsy. Neurology. 1993;43(12):2708–2709.
Second confirmed cerebral case; seizures recurring at onset of menses, resolved after danazol therapy.
3. Sarma D, Iyengar P, Marotta T, et al. Cerebellar endometriosis. AJR Am J Roentgenol. 2004;182(6):1543–1546.
First documented case of cerebellar involvement; cystic hemorrhagic lesion mimicking neoplasm.
4. Vilos GA, Hollett-Caines J, Abu-Rafea B, Ahmad R, Mazurek MF. Resolution of catamenial epilepsy after goserelin therapy and oophorectomy: case report of presumed cerebral endometriosis. J Minim Invasive Gynecol. 2011;18(1):128–130.
Catamenial neurological symptoms resolving with hormonal suppression and surgical menopause.
5. Siquiara de Sousa AC, D'Hooghe TM, et al. Neural involvement in endometriosis: review of anatomic distribution and mechanisms. Clin Anat. 2015;28(8):1029–1038.
Comprehensive review describing neuroendometriosisand alternate dissemination routes (hematogenous, lymphatic, perineural).
6. Antonio M, et al. A presumed case of cerebral endometriosis presenting with catamenial epilepsy. J Endometriosis Pelvic Pain Disord. 2020;12(1):1–3. Recent presumed cerebral endometriosis with seizures, no pelvic disease.
7. Meggyesy M, Friese M, et al. Cerebellar endometriosis: case report and literature review. J Neurol Surg A. 2020;81(3):260–266.
Second histologically proven cerebellar case; emphasizes diagnostic difficulty and recurrence.
8. Kido A, Togashi K, et al. MRI in the diagnosis of endometriosis and related diseases. Korean J Radiol. 2022;23(4):426–445.
Defines MRI hallmarks of endometriomas (T1 hyperintensity, T2 shading, hemosiderin foci) relevant to extrapleural sites.
9. Van Buren W, Feldman M, Shenoy-Bhangle AS, et al. Endometriosis imaging interpretation and reporting: RSNA expert consensus statement. Radiology. 2024;312(3):e233482.
RSNA consensus emphasizing imaging-pathologic correlation and recognition of extrapelvic endometriosis.

Images/Tables

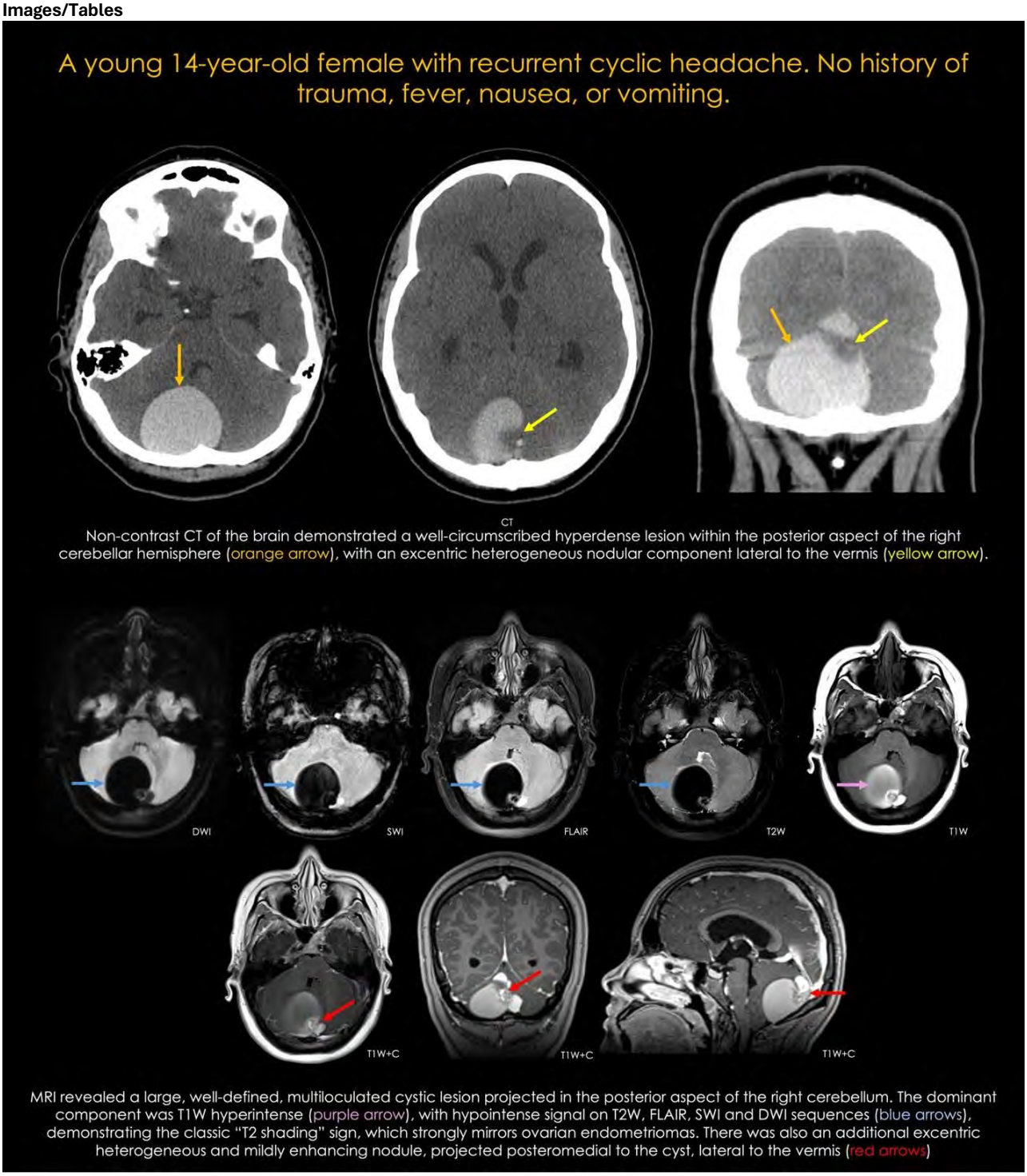

---

848 Medulloblastoma Masquerading as Cerebellitis

Derek W Grady MD, Diego J Cebrian Chaustre MD, Bradley D Weaver MD, PhD, Blair A Winegar MD, Karen L Salzman MD
University of Utah School of Medicine, Salt Lake City, UT, USA

Clinical History

A 44-year old female presented as an outpatient for recurring, transient episodes of confusion and headache. She had a history of lupus and rheumatoid arthritis. There was no known malignancy. Further review of the medical record revealed a recent and significant increase in fatigue and imbalance. She had a normal MRI of the brain in 2021 and a normal non-contrast head CT 9 months prior to presentation.

Imaging Findings

Non-contrast CT of the head demonstrated mass-like hyperdensity in the right cerebellar hemisphere causing localized mass effect and partial effacement of the fourth ventricle. There was increased ventricular caliber compared to prior imaging concerning for obstructive hydrocephalus. Concurrent MRI of the brain showed indistinct T2/FLAIR hyperintensity in the right cerebellar hemisphere associated with areas of nodular enhancement and diffusion restriction. There was no abnormal susceptibility to indicate hemorrhage. A subsequent MRI of the brain with vessel wall protocol showed normal vasculature.

Discussion

Based on patient demographics, a history of autoimmune disease, and vague neurologic symptoms, the primary differential included autoimmune versus infectious cerebellitis. Vasculitis was considered unlikely in the absence of hemorrhage; this diagnosis was further discounted by the negative vessel wall MRI. The combination of hyperdensity on CT and abnormal diffusion signal also raised suspicion for a hypercellular tumor (e.g., lymphoma or medulloblastoma).

The patient was admitted due to concern for obstructive hydrocephalus. CSF samples were collected after placement of a ventricular drain. Laboratory analysis was negative for autoimmune and infectious markers, which prompted a biopsy of the cerebellar lesion. Pathology revealed WHO Grade 4 medulloblastoma with sonic hedgehog (SHH)-activation and *TP53* wildtype.

Teaching Point

The most recent WHO 2021 CNS5 classification of medulloblastoma emphasizes molecular subgroups over traditional histologic categorization, which better informs risk-stratification, tailored treatment profiles, and prognosis. The four molecular subgroups include WNT-activated, SHH-activated and *TP53*-wildtype, SHH-activated and *TP53*-mutant, and non-WNT/non-SHH.

The most common molecular subgroup in adults is the SHH-activated and *TP53*-wildtype medulloblastoma, which commonly occurs in the lateral cerebellar hemisphere as in our case. Other common locations for medulloblastoma include the midline fourth ventricle, cerebellar peduncle/cerebellopontine angle cistern, and a nonfocal, diffusely infiltrating morphology.

When encountering a cerebellar lesion in the adult patient, a combination of hyperdensity and abnormal diffusion signal can suggest hypercellularity. In these cases, round blue cell tumors such as lymphoma and medulloblastoma may be appropriate differential considerations.

References

Louis DN, Perry A, Wesseling P, et al. The 2021 WHO Classification of Tumors of the Central Nervous System: a summary. *Neuro Oncol*. 2021;23(8):1231-1251. doi:10.1093/neuonc/noab106

Lazow MA, Palmer JD, Fouladi M, et al. Medulloblastoma in the Modern Era: Review of Contemporary Trials, Molecular Advances, and Updates in Management. *Neurotherapeutics*. 2022;19(6):1733-1751. doi:10.1007/s13311-022-01273-0

Choi JY. Medulloblastoma: Current Perspectives and Recent Advances. *Brain Tumor Res Treat*. 2023;11(1):28-38. doi:10.14791/btrt.2022.0046

Franceschi E, Giannini C, Furtner J, et al. Adult Medulloblastoma: Updates on Current Management and Future Perspectives. *Cancers (Basel)*. 2022;14(15):3708. Published 2022 Jul 29. doi:10.3390/cancers14153708

Images/Tables

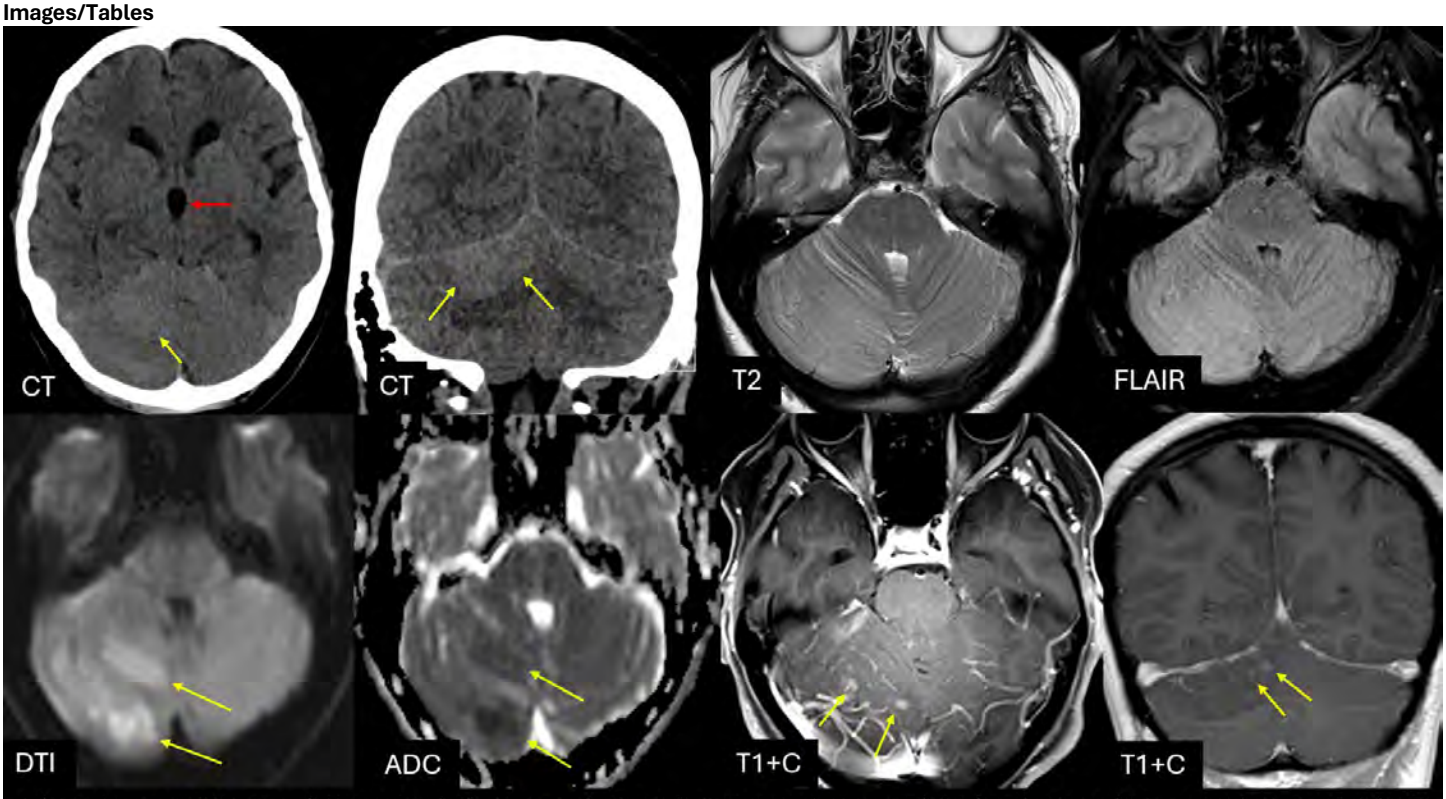

Axial and coronal CT shows mild hyperdensity in the posterior fossa (yellow arrows). Note partially visualized ventriculomegaly (red arrow). Axial T2 and FLAIR images show enlargement and hyperintensity in the right cerebellar hemisphere. Axial DTI trace and ADC images show restricted diffusion in the right cerebellar hemisphere (yellow arrows). Axial T1 C+ images show subtle nodular enhancement (yellow arrows).

---

851 Diffuse Leptomeningeal Glioneuronal Tumor: An Exceptionally Rare Entity with Diverse Imaging Features Illustrated Through Two Cases

Raihan Noman MD, Ada Baisre de Leon MD, Esther A Nimchinsky MD, PhD

Rutgers New Jersey Medical School, Newark, NJ, USA

Clinical History

Case 1: A 17-year-old non-binary person with no significant past medical history presented with papilledema.

Case 2: A 33-year-old man with a history of cervical spinal astrocytoma status post resection and radiation therapy 8 years prior, as well as intramedullary tumor resection 3 years prior, presented with abdominal pain, bowel/bladder incontinence, and scrotal pain/numbness.

Imaging Findings

Case 1: MRI of the brain with and without contrast demonstrated diffuse smooth leptomeningeal enhancement above and below the tentorium with some associated FLAIR signal abnormality. Histopathology showed neoplastic cells that are strongly and diffusely positive for synaptophysin and focally positive for S100 protein.
Case 2: MRI of the brain with and without contrast demonstrated scattered nodular leptomeningeal enhancement with associated FLAIR signal abnormality. A left insular parenchymal lesion was noted with nodular ependymal enhancement at the frontal horn of the left lateral ventricle. MRI of the thoracic and lumbar spine with and without contrast demonstrated extensive dural/leptomeningeal enhancement with multilevel severe cord compression, including the conus medullaris and cauda equina.

Discussion

Diffuse leptomeningeal glioneuronal tumor (DLGNT) is a rare entity that was first defined as a neuronal and mixed neuronal-glial tumor in the 2016 World Health Organization (WHO) classification of brain tumors.[1] DLGNT is primarily seen in the pediatric population with a male predilection and is only rarely encountered in adults. The imaging features are largely nonspecific, most frequently demonstrating diffuse or nodular leptomeningeal enhancement.[1] The imaging differential diagnosis remains broad, including infection (such as bacterial or tuberculous meningitis); primary diffuse leptomeningeal gliomatosis, a more aggressive entity; leukemia or leptomeningeal lymphomatosis, neurosarcoidosis; and disseminated high-grade and low-grade neoplasms.[1] Histopathology reveals several markers found in oligodendroglioma-like tumor cells as well as a recurrent molecular pattern of KIAA1549-BRAF fusion with 1p deletion and occasionally 1p/19q codeletion.[2,3] Several studies have suggested that parenchymal involvement is more common in adults, often appearing as solid-cystic lesions that extend to the superficial surface of the cerebral hemisphere, similar to our second case.[3]

Teaching Point

Although typically recognized as a pediatric tumor, DLGNT can also rarely occur in adults, sometimes demonstrating greater parenchymal involvement and variable imaging appearances.

References

1. Lakhani DA, Mankad K, Chhabda S, et al. Diffuse leptomeningeal glioneuronal tumor of childhood. AJNR Am J Neuroradiol 2020;41(11):2155–2159. DOI:10.3174/ajnr.A6737
2. De los Reyes-Nabhan NK, Scheil-Bertram S, Boppudi S, Carl B, Jussen D. Diffuse leptomeningeal glioneuronal tumor in adults: case report and literature review. Case Rep Oncol 2024;17(1):337–343. DOI:10.1159/000536400
3. Demir MK, Yapıcıer O, Kılıc T, et al. Diffuse leptomeningeal glioneuronal tumors: a case series of five patients with parenchymal forms and an analysis of the diagnostic challenges, treatment options and outcomes. Curr Med Imaging 2023;19(12). DOI:10.2174/1573405619666230213152949

Images/Tables

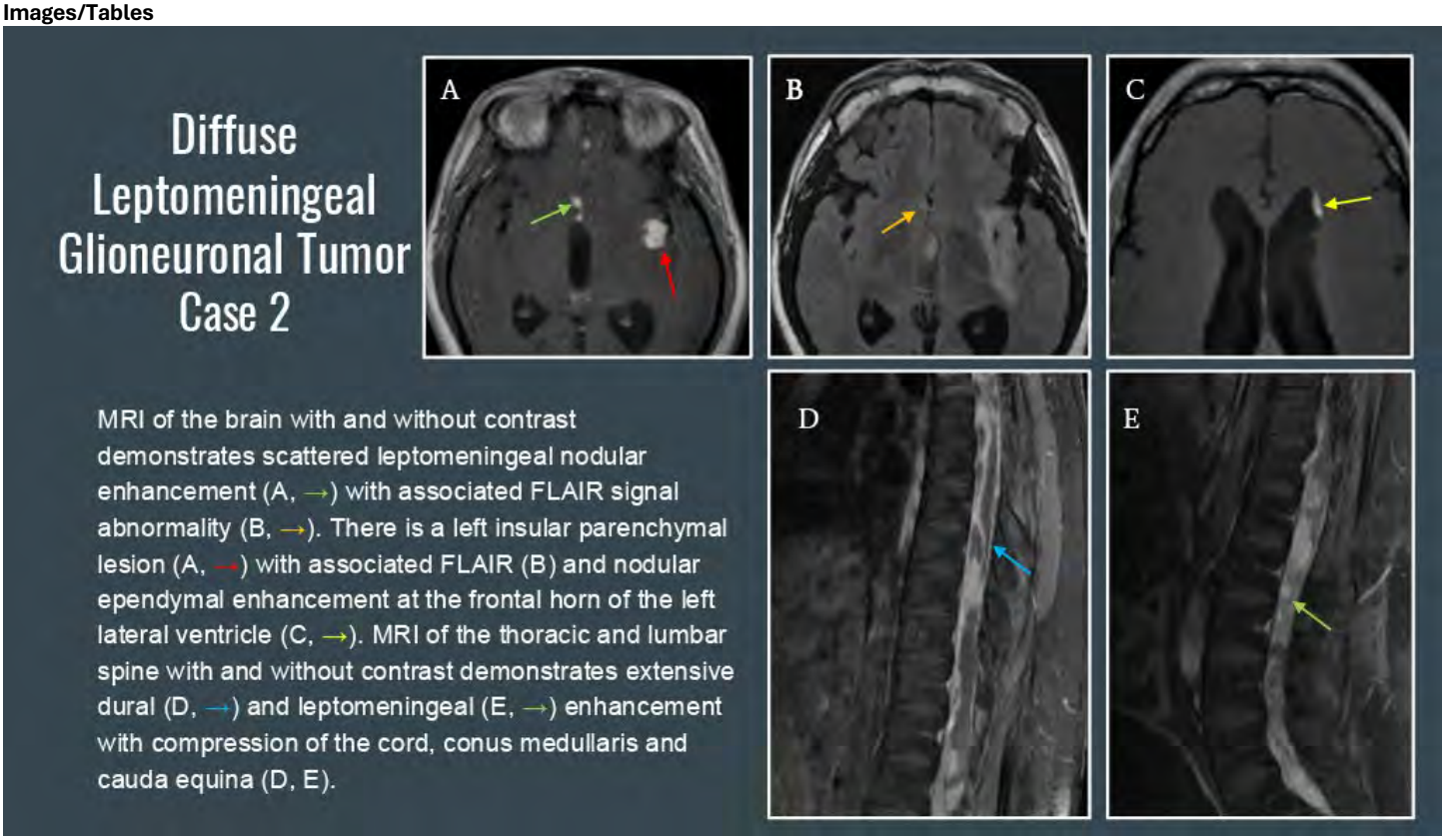

---

858 When Rosai–Dorfman Disease Masquerades as Meningioma: A Case of Intracranial Involvement

Grace Yoon MD, Gaurav Rana MD
Cook County Hospital, Chicago, IL, USA

Clinical History

A 36-year-old man presented with progressive headache and blurred vision for two weeks. Ophthalmologic evaluation showed bilateral papilledema; neurologic examination was otherwise unremarkable. Laboratory studies were unremarkable. CT and MRI of the brain demonstrated a dural-based enhancing mass, initially suspected to represent meningioma.

The patient underwent right frontal craniotomy with gross total resection. Histopathology revealed large histiocytes with abundant cytoplasm and emperipolesis, accompanied by perivascular plasmacytosis and fine fibrosis. Immunohistochemistry showed positivity for S100, CD68, CD163, CD4, BCL6, and Cyclin D1, with additional OCT2and ZBTB45 positivity and BRAF V600E negativity. Background T cells were CD3+, CD5+, and BCL2+; plasma cells were CD138+ and IgG+ with a small IgG4+ subset. Findings confirmed extranodal Rosai–Dorfman disease (RDD).
Postoperatively, the course was complicated by a cerebrospinal-fluid leak forming a right scalp collection, managed with aspirations, acetazolamide, and temporary lumbar drainage. The leak resolved, and the patient was discharged in stable condition on a steroid taper and continued acetazolamide.

Imaging Findings

Contrast-enhanced CT showed a 4.5 × 2.9 × 3.7 cm enhancing right temporal extra-axial mass with vasogenic edema, sulcal effacement, and 10 mm leftward midline shift. Two smaller enhancing dural-based lesions were noted in the right frontal lobe. MRI demonstrated lesions isointense to gray matter on T1 and hypointense on T2 with avid homogeneous enhancement, a dural tail, and surrounding edema, radiographically resembling multiple meningiomas. Persistent midline shift and right uncal herniation were present.

Discussion

Rosai–Dorfman disease (RDD), also known as sinus histiocytosis with massive lymphadenopathy, is a rare non-Langerhans cell histiocytic disorder characterized by proliferation of distinctive histiocytes demonstrating emperipolesis. Although RDD commonly involves lymph nodes, extranodal disease occurs in up to 40% of cases. Isolated intracranial involvement is rare, accounting for fewer than 5% of all RDD cases. Intracranial RDD typically presents as dural-based extra-axial lesions that radiologically resemble meningiomas, leading to frequent preoperative misdiagnosis. Lesions are usually isointense on T1- and hypointense on T2-weighted MRI, with homogeneous enhancement and variable perilesional edema. Histopathologic examination remains the gold standard for diagnosis. RDD histiocytes display abundant eosinophilic cytoplasm and emperipolesis within a mixed inflammatory background. Immunohistochemistry shows positivity for S100, CD68, and CD163, and negativity for CD1a. Surgical resection is the primary treatment, offering both diagnosis and symptom relief. Adjuvant corticosteroids, radiotherapy, or systemic therapies may be considered in cases of incomplete resection or recurrence. Prognosis is favorable after complete excision, though long-term follow-up is recommended due to potential recurrence or multifocal disease.

Teaching Point

Rosai–Dorfman disease should be considered in the differential diagnosis of dural-based enhancing lesions that mimic meningioma. Recognition of its imaging overlap and diagnostic histopathologic features is critical for accurate identification and management.

References

1. Abla O, Jacobsen E, Picarsic J, et al. Consensus recommendations for the diagnosis and clinical management of Rosai–Dorfman–Destombes disease. *Blood*. 2018;131(26):2877-2890. doi:10.1182/blood-2018-03-839639
2. Goyal G, Young JR, Koster MJ, Tobin WO, Vassallo R, Ryu JH, Davidge-Pitts CJ, Hurtado MD, Ravindran A, Sartori Valinotti JC, Bennani NN, Shah MV, Rech KL, Go RS; Mayo Clinic Histiocytosis Working Group. The Mayo Clinic Histiocytosis Working Group consensus statement for the diagnosis and evaluation of adult patients with histiocytic neoplasms: Erdheim-Chester disease, Langerhans cell histiocytosis, and Rosai–Dorfman disease. *Mayo Clin Proc*. 2019;94(10):2054-2071. doi:10.1016/j.mayocp.2019.02.023
3. Smith AB, Horkanyne-Szakaly I, Schroeder JW, Rushing EJ. From the Radiologic Pathology Archives: mass lesions of the dura—beyond meningioma: radiologic-pathologic correlation. *Radiographics*. 2014;34(2):295-312. doi:10.1148/rg.342130075
4. Sandoval-Sus JD, Sandoval-Leon AC, Chapman JR, et al. Rosai–Dorfman disease of the central nervous system: report of 6 cases and review of the literature. *Medicine (Baltimore)*. 2014;93(3):165-175. doi:10.1097/MD.0000000000000029
5. Rosai J, Dorfman RF. Sinus histiocytosis with massive lymphadenopathy: a newly recognized benign clinicopathologic entity. *Arch Pathol*. 1969;87(1):63-70.

Images/Tables

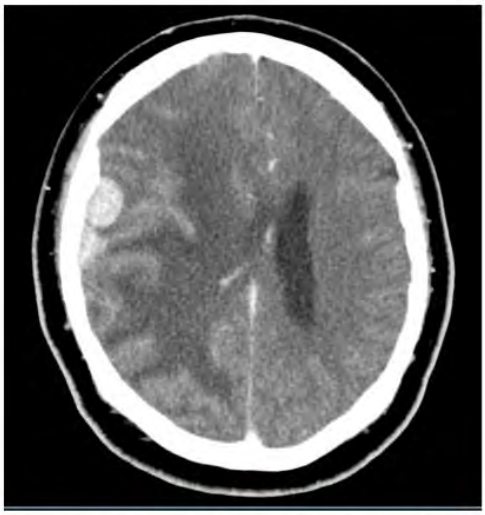

Post-contrast CT demonstrates avid enhancement of the temporal lesion and two smaller enhancing dural-based right frontal masses

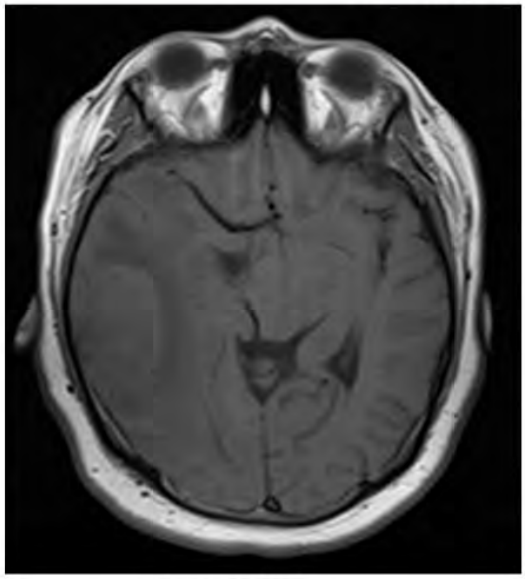

T1-pre contrast

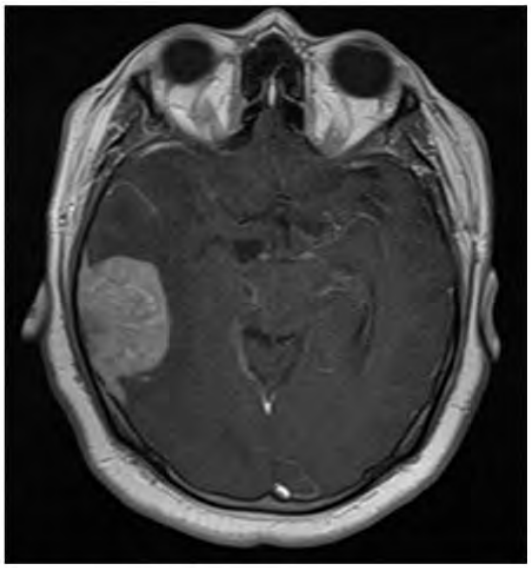

T1 post-contrast

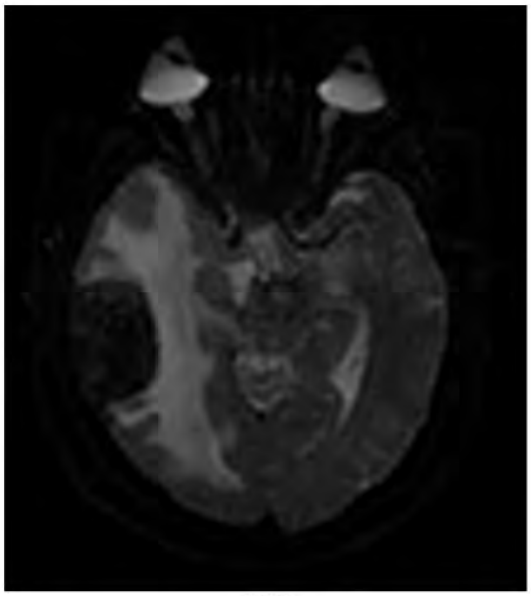

DWI

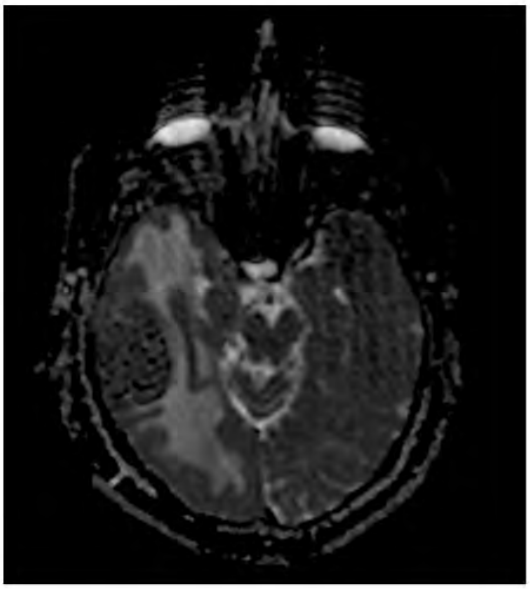

ADC

878 Endovascular Treatment for Intraorbital Arterio-venous Fistula: A case report

Wen-Hsien Chen PhD
Taichung Veterans General Hospital, Taichung, Taiwan, Taiwan

Clinical History

A 49-year-old male suffered from left eye proptosis and redness for 9 months. On ophthalmologic examination, extraocular movements are full and free, except for upward limitation in the left eye.

Imaging Findings

He received orbital CT scan, brain MRI and MR angiography (MRA) showing engorged left superior ophthalmic vein but symmetric bilateral cavernous sinuses. Time-resolved MRA revealed engorged, early enhanced left superior ophthalmic vein with reversed flow and draining to left facial vein, without early enhancement of left cavernous sinus. Intraorbital arterio-venous fistula (AVF) is considered. Digital subtraction angiography (DSA) showed early enhanced, reversed flow and engorgement of left superior ophthalmic vein, with feeding arteries from small branches of left ophthalmic artery and terminal branches of left internal maxillary artery. Endovascular embolization of the fistula was performed by trans-arterial Onyx infusion via catheterization of distal branches of left internal maxillary artery, combined with trans-venous coils embolization near the fistular region via catheterization of left facial vein to left superior ophthalmic vein. Final angiograms showed complete obliteration of the fistula with patent ophthalmic artery and central retinal artery. The left eye proptosis and redness improved after the procedure without vision loss.

Discussion

Intraorbital AVF is a rare subtype of AVF with venous drainage to engorged, reversed flow of superior ophthalmic vein causing proptosis and red eye. The clinical picture resembles that of more common conditions, such as carotid-cavernous fistulas or AVM in the orbital region. The common supplying arteries are branches of ophthalmic artery and distal branches of internal maxillary artery. Treatment goal of the AVF is to block the connection between arteries and veins. Due to hazard of retinal artery occlusion and blindness, trans-ophthalmic artery embolization is avoided. Trans-venous catheterization of superior ophthalmic vein with coil embolization near the fistula region combined with trans-arterial Onyx infusion at distal branches of internal maxillary artery is effective and safe treatment for the intraorbital AVF.

Teaching Point

1. Intraorbital AVF is a rare subtype of AVF mimicking carotid-cavernous fistula.
2. Treatment goal of the AVF is to block the connection between arteries and veins.
3. Trans-ophthalmic artery embolization is hazard and may lead to blindness.
4. Trans-venous coils embolization is effective and safe.

References

Su X, Song Z, Chen Y, et al. Intraorbital Arteriovenous Fistulas: Case Series and Systematic Review. Oper Neurosurg. 2024 Jul 1;27(1):23-30. doi: 10.1227/ons.0000000000001055. Epub 2024 Feb 2. PMID: 38305350.

Krylova, M., & Hauck, E. F. (2025). Intraorbital arteriovenous fistulas: illustrative case. Journal of Neurosurgery: Case Lessons, 9(23), CASE24857. https://doi.org/10.3171/CASE24857

Images/Tables

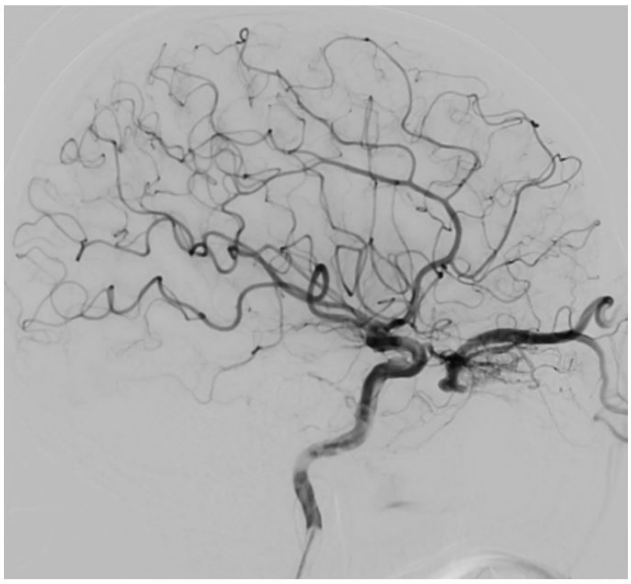

Lateral view of left ICA angiogram showed AVF of superior ophthalmic vein supplied by small branches of ophthalmic artery.

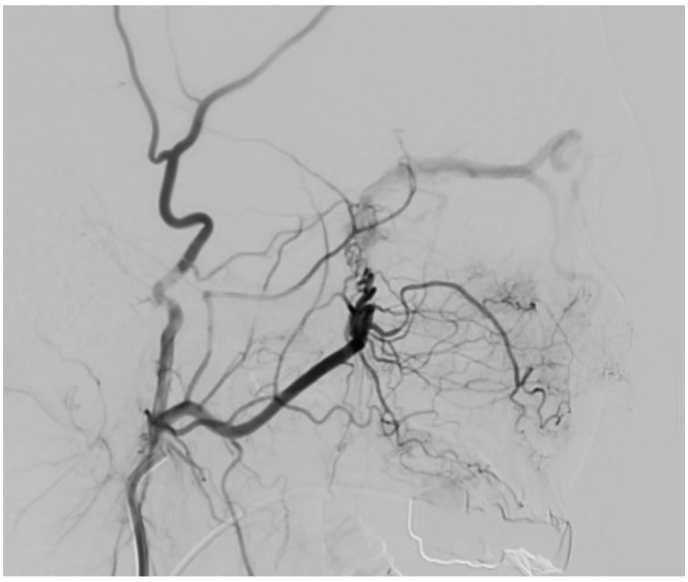

Lateral view of left ECA angiogram showed AVF of superior ophthalmic vein supplied by small branches of internal maxillary artery.

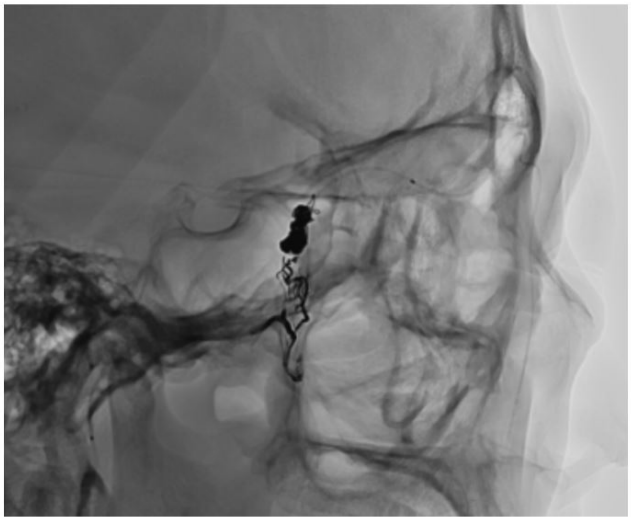

Onyx cast in feeding arteries and coils in superior ophthalmic vein.

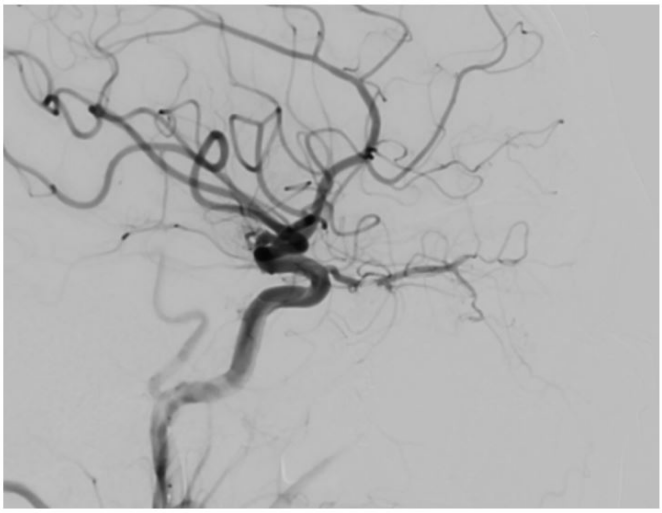

After embolization, lateral view of left CCA angiogram showed complete obliteration of the AVF.

---

879 Recognizing SMART Syndrome: Imaging Evolution, Pitfalls, and Differentiation from Recurrence

Junaid Kalair, Steve Fung
Houston, Texas, USA

Clinical History

A 62-year-old man with remote history of left temporooccipital glioblastoma treated by resection, temozolomide, and high-dose radiation therapy (60 Gy) 19 years earlier presented with new dysarthria, confusion, and falls. CT showed chronic posttreatment changes with extensive encephalomalacia in the left temporoparietooccipital region without acute abnormality. MRI showed new unilateral linear and micronodular leptomeningeal and cortical enhancement, diffuse mild cortical DWI hyperintensity with equivocal diffusion change confined to the prior radiation field without mass effect. CSF cytology and spinal MRI were negative for malignancy or infection. During admission, the patient had recurrent focal seizures, and interim MRI demonstrated small acute left occipital infarcts distinct from the enhancing regions. Over subsequent weeks, the leptomeningeal and cortical enhancement intensified with associated swelling. MR perfusion and spectroscopy were inconclusive. Multidisciplinary review favored SMART syndrome (stroke-like migraine after radiation therapy) over tumor recurrence or infectious meningitis. Corticosteroids and verapamil led to radiographic resolution and clinical improvement.

Imaging Findings

- Initial MRI: Extensive encephalomalacia with predominantly white-matter volume loss involving left temporal, parietal, and occipital lobes from prior resection and chemoradiation therapy. Superimposed new leptomeningeal and cortical enhancement, diffuse mild cortical DWI hyperintensity with equivocal diffusion change involving left temporal, parietal, occipital, and insular regions coinciding with prior radiation field without mass effect.

- Follow-up MRI: Increasing extent of leptomeningeal and cortical enhancement involving left temporal, parietal, occipital, insular, and to lesser degree frontal lobes, accompanied by increasing diffuse cortical thickening with T2 hyperintensity. Persistent diffuse mild cortical DWI hyperintensity in the same distribution with superimposed more pronounced DWI hyperintensity with restricted diffusion from small acute left occipital ischemic infarctions that developed in the interim.
- Post-treatment MRI: Near-complete resolution of leptomeningeal and cortical enhancement, confirming reversibility. Subcortical restricted diffusion and gyriform enhancement in left occipital region corresponding to evolving subacute-ischemic infarction and vascular dysregulation related to SMART syndrome.

Discussion

SMART syndrome is a delayed neurovascular complication of cranial irradiation resulting from radiation-induced endothelial injury, autoregulatory failure, and transient breakdown of the blood-brain-barrier (1). The consequence is episodic cortical hyperexcitability and reversible vasogenic edema that can occur years to decades after treatment (2).

Proposed pathways include endothelial dysfunction, impaired vasoreactivity, cortical spreading depression, and regional perfusion instability. These processes overlap with migraine and seizure physiology (3,4). The vascular and metabolic shifts explain the transient nature of the clinical symptoms and imaging abnormalities.

When new unilateral cortical or leptomeningeal enhancement develops within a prior radiation field, diagnosis should focus on:

1. Diffusion and perfusion: lack of restricted diffusion or hyperperfusion argues against disease recurrence.
2. Confinement: enhancement confined to the irradiated territory supports SMART.
3. Reversibility: resolution on follow-up imaging confirms the diagnosis and prevents unnecessary biopsy.

Treatment remains supportive with corticosteroids and calcium-channel blockers to reduce cortical edema, stabilize the endothelium, and restore autoregulatory balance (1,2).

Teaching Point

- SMART syndrome may occur months to decades after cranial irradiation.
- Imaging hallmark: reversible unilateral or asymmetric cortical and leptomeningeal enhancement within the radiation field.
- Assessment of diffusion, perfusion, and reversibility differentiates SMART from recurrence or infection.
- Recognition prevents unnecessary biopsy and guides appropriate management.

References

[1] Black DF, Bartleson JD, Bell ML, Lachance DH. SMART syndrome: stroke-like migraine attacks after radiation therapy. *Cephalalgia*. 2006;26(9):1137-1142. doi:10.1111/j.1468-2982.2006.01184.x

[2] Black DF, Morris JM, Lindell EP, Krecke KN, Worrell GA, Bartleson JD, et al. Stroke-like migraine attacks after radiation therapy (SMART) syndrome is not always completely reversible: a case series. *AJNR Am J Neuroradiol*. 2013;34(12):2298-2303. doi:10.3174/ajnr.A3602

[3] Zheng Q, Yang L, Tan L-M, Qin L-X, Wang C-Y, Zhang H-N, et al. Stroke-like migraine attacks after radiation therapy syndrome. *Chin Med J (Engl)*. 2015;128(15):2097-2101. doi:10.4103/0366-6999.161393

[4] Ota Y, Nemoto M, Gyoten T, Liao E, Shah G, Capizzano AA. Comprehensive update and review of clinical and imaging features of SMART syndrome. *AJNR Am J Neuroradiol*. 2023;44(6):626-639. doi:10.3174/ajnr.A7859

Images/Tables

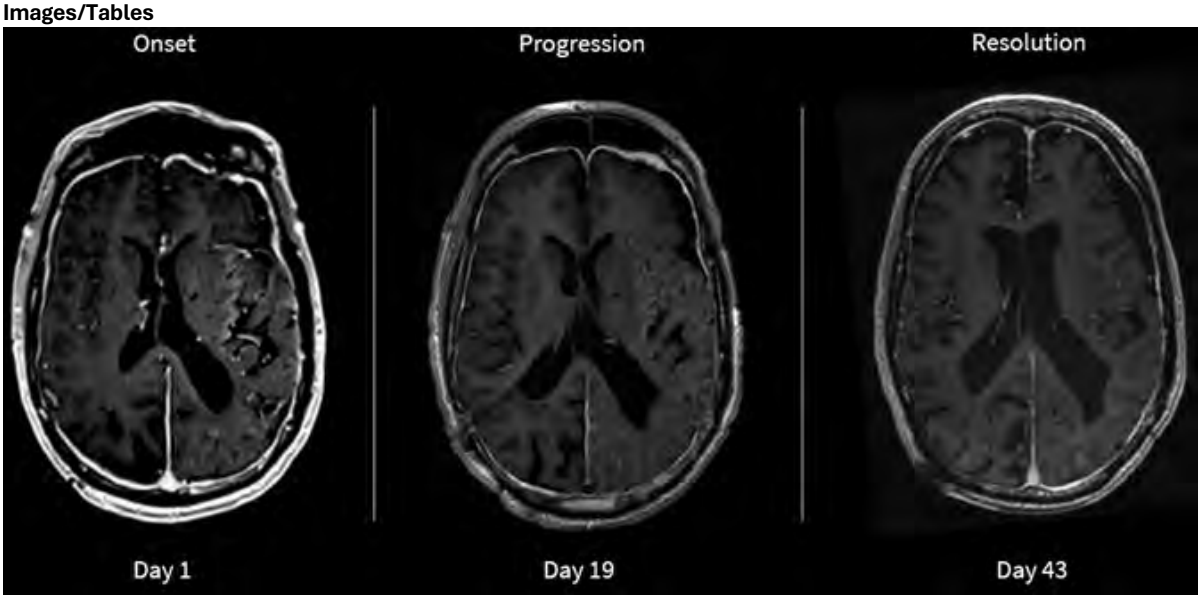

---

913 The Styloid-Pterygoid Line: An Alternative Landmark for CT-guided Biopsy Confirmation of Perineural Spread of V3 in the Masticator Space

Ivy T Vo B.S.[1], Brian Dahlin MD[2], Victor Sai MD[3], Nancy Pham MD[1]

[1]Stanford Health Care, Palo Alto, CA, USA. [2]Kaiser Permanente, Sacramento, CA, USA. [3]University of California - Los Angeles, Los Angeles, CA, USA

Clinical History

Six patients (three men, three women; mean age 63.8 years, range 40–79) with prior head and neck malignancies—including squamous cell carcinoma, basal cell carcinoma, and nasopharyngeal carcinoma—presented with symptoms or MRI findings suggestive of perineural spread (PNS) involving the mandibular division (V3) of the trigeminal nerve. All had abnormal enhancement and/or thickening of V3 within the infratemporal fossa, with several demonstrating denervation atrophy of the muscles of mastication and retrograde extension to Meckel's cave or the cavernous sinus.

Imaging Findings

MRI demonstrated characteristic signs of PNS, including enlargement and enhancement of the mandibular nerve, foraminal widening, and loss of perineural fat planes. Enhancement extended from the masticator space to Meckel's cave and the cavernous sinus in five of six cases. Denervation atrophy of the muscles of mastication was observed in five patients.

All patients underwent CT-guided fine-needle aspiration (FNA) using a transcondylar approach based on the styloid-pterygoid line, an anatomic landmark extending from the styloid process of the temporal bone to the pterygoid plates of the sphenoid bone. The mandibular nerve typically lies along the mid-portion of this line within the infratemporal fossa. Patients were positioned supine with the head rotated 30–45 degrees away from the biopsy side. A coaxial 19- and 22-gauge needle system was advanced through the condylar notch to approximately 10 mm proximal to the styloid-pterygoid line. Capillary technique was used to obtain samples without aspiration to minimize blood contamination.

Discussion

The CT-guided FNA was technically successful in all six cases. Histologic confirmation of PNS was achieved in five patients; the remaining patient showed inflammatory changes with no malignant cells, and follow-up MRI demonstrated resolution of abnormal enhancement. No patients experienced procedure-related complications such as hemorrhage, infection, or trigeminocardiac reflex.

This transcondylar approach using the styloid-pterygoid line offers a shorter and safer path to the mandibular nerve compared with traditional percutaneous access through the foramen ovale. It avoids critical neurovascular structures and reduces morbidity associated with skull base interventions. Prior literature on CT-guided trigeminal nerve biopsy is limited to small series, typically adapted from trigeminal neuralgia procedures. Our six-patient cohort represents one of the largest case series to date demonstrating the feasibility of this method for histologic confirmation of PNS. This approach is particularly valuable when open biopsy is contraindicated or technically challenging. It allows accurate diagnosis, helps distinguish tumor recurrence from post-treatment changes, and can prevent unnecessary surgery in patients with benign inflammatory enhancement.

Teaching Point

The styloid-pterygoid line serves as a practical, reproducible landmark for CT-guided transcondylar access to the mandibular nerve. This technique enables minimally invasive, reliable sampling of suspected perineural tumor spread while avoiding the risks associated with foramen ovale or open surgical biopsies.

References

Bartiromo, F., Cirillo, L., Caranci, F., Elefante, A., D'Amico, A., Tortora, F., Brunetti, A., & Cirillo, S. (2007). Trigeminal perineural spread of head and neck tumors. *The Neuroradiology Journal*, 20(1), 116–123. https://doi.org/10.1177/197140090702000119

Caldemeyer, K. S., Mathews, V. P., Righi, P. D., & Smith, R. R. (1998). Imaging features and clinical significance of perineural spread or extension of head and neck tumors. RadioGraphics, 18(1), 97–110. https://doi.org/10.1148/radiographics.18.1.9460111

Chang, P. C., Fischbein, N. J., McCalmont, T. H., Kashani-Sabet, M., Zettersten, E. M., Liu, A. Y., & Weissman, J. L. (2004). Perineural spread of malignant melanoma of the head and neck: Clinical and imaging features. American Journal of Ophthalmology, *137*(6), 1173–1174. https://doi.org/10.1016/j.ajo.2004.04.040

Doran, S., Whiriskey, R., Sheehy, N., Johnston, C., & Byrne, D. (2024). Perineural tumour spread in head and neck cancer: A pictorial review. Clinical Radiology, 79(10), 749–756. https://doi.org/10.1016/j.crad.2024.07.010

Yong, X. Z., Dillon, J., Smith, P., Salinas-La Rosa, C., & Jhamb, A. (2016). Novel ct-guided biopsy of isolated perineural spread of adenoid cystic carcinoma along the trigeminal nerve masquerading as chronic trigeminal neuropathy. *Journal of Medical Imaging and Radiation Oncology*, 61(1), 77–81. https://doi.org/10.1111/1754-9485.12557

Images/Tables

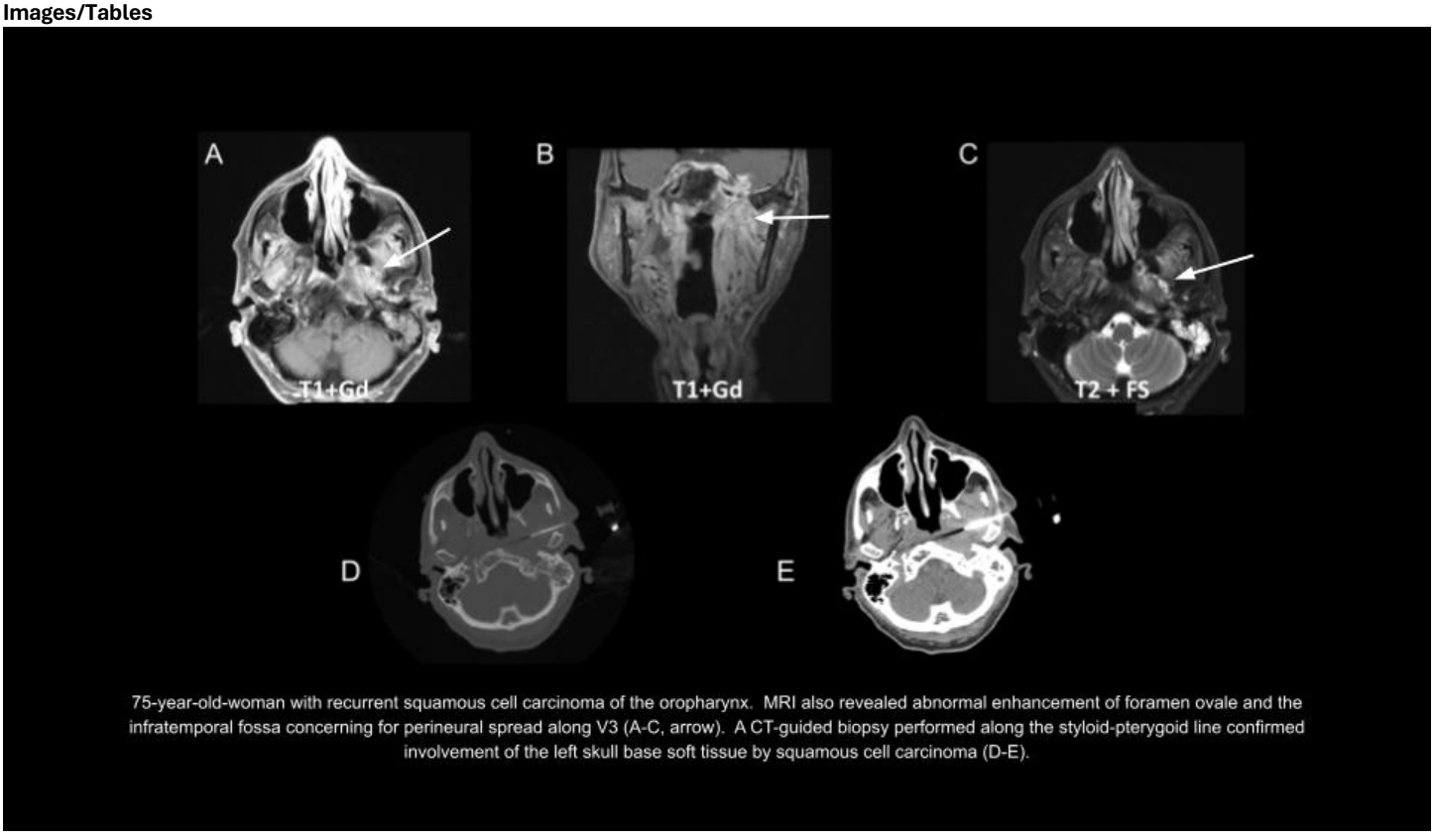

75-year-old-woman with recurrent squamous cell carcinoma of the oropharynx. MRI also revealed abnormal enhancement of foramen ovale and the infratemporal fossa concerning for perineural spread along V3 (A-C, arrow). A CT-guided biopsy performed along the styloid-pterygoid line confirmed involvement of the left skull base soft tissue by squamous cell carcinoma (D-E).

919 Sinonasal Lymphoma Mimicking Infectious and Inflammatory Processes in a Young Patient

Stephanie Vuong MD, Edward Kuoy MD
University of California Irvine, Orange, CA, USA

Clinical History

35-year-old male with history of diabetes presented for swelling and discoloration under the right eye as well as right nasal obstruction. Patient denied fevers, chills, coughs, epistaxis, and vision loss. On presentation, the basic metabolic lab panel was notable for glucose of 160 mg/dL (reference range 70-115 mg/dL) and blood chemistry panel demonstrated pancytopenia.

Imaging Findings

Initial sinus CT demonstrated severe right sinonasal opacification as well as right periorbital, extraconal orbital, nasolacrimal drainage apparatus region, peri-antral, and pterygopalatine fossa stranding. Additionally, there were erosive changes of the hard palate. Subsequent maxillofacial MR demonstrated predominantly right nasal cavity necrotic changes.

The patient underwent sinonasal surgery, but debridement of the necrotic regions was limited due to the extent of intraoperative hemorrhage.

The patient had worsening periorbital soft tissue swelling and underwent a follow-up maxillofacial MR exam 3 days after surgery that demonstrated short interval progressive soft tissue enhancement without significant worsening tissue necrosis.

Discussion

Surgical pathology results returned 4 days following surgery consistent with extranodal natural killer/T-cell lymphoma (NKTL). NKTL variant is a locally destructive tumor that may arise in the nasal cavity. On pathology, the angiocentric lymphoid infiltration may result in considerable necrosis and vascular destruction.

Infectious processes, particularly acute invasive fungal rhinosinusitis (AIFR) was a high differential consideration given the concerning areas of involvement including peri-antral, pterygopalatine process, and orbital with nasolacrimal drainage apparatus involvement. In this patient with a history of diabetes, while the glucose level notably was not markedly elevated, pancytopenia would make the immunocompromised patient susceptible to AIFR.

Idiopathic orbital inflammation (IOI) can involve various different sites, but typically clinically presents with pain. IgG4-related disease can present with soft tissue processes and osseous erosion but orbital disease commonly involve the extra-ocular muscle or lacrimal gland.

Other granulomatous processes such as the various vasculitides is a differential diagnosis, but sinus involvement oftentimes demonstrate osteitis, which this patient lacked.

Teaching Point

While imaging findings are non-specific, it is important to keep neoplasm, particularly an aggressive type such as NKTL, on the differential that can rapidly progress and present with overlapping concerning imaging features as infectious and inflammatory processes such as AIFS.

References

Ooi GC, Chim CS, Liang R, et al. Nasal T-cell/natural killer cell lymphoma: CT and MR imaging features of a new clinicopathologic entity. *AJR Am J Roentgenol* 2000 Apr;174(4):1141-5. doi: 10.2214/ajr.174.4.1741141.

Images/Tables

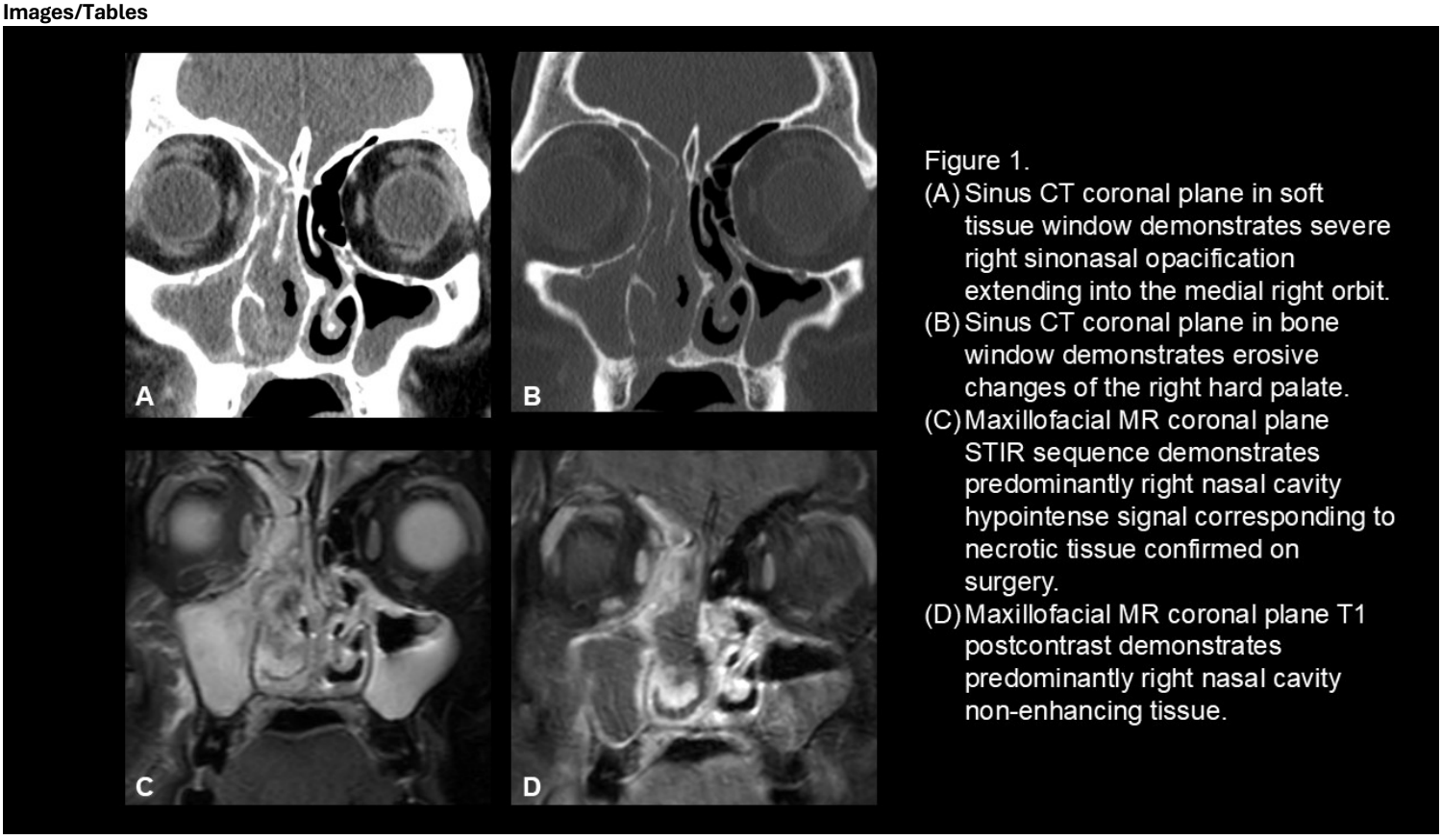

Figure 1.
(A) Sinus CT coronal plane in soft tissue window demonstrates severe right sinonasal opacification extending into the medial right orbit.
(B) Sinus CT coronal plane in bone window demonstrates erosive changes of the right hard palate.
(C) Maxillofacial MR coronal plane STIR sequence demonstrates predominantly right nasal cavity hypointense signal corresponding to necrotic tissue confirmed on surgery.
(D) Maxillofacial MR coronal plane T1 postcontrast demonstrates predominantly right nasal cavity non-enhancing tissue.

928 Immune Checkpoint Inhibitor-associated Perioptic Neuritis

Neud Kiros MD, Alina Sinha MD, Anant Krishnan MD
William Beaumont University Hospital, Royal Oak, MI, USA

Clinical History

A 47-year-old male with history of stage IV gastric cancer on nivolumab presented with blurry vision worse at close distances. Binocular horizontal diplopia was found on exam. Fundus exam demonstrated 4+ disc edema and hemorrhage bilaterally. Recent head MRI was negative for leptomeningeal enhancement. MR venogram and MRI orbits with contrast were ordered as well as lumbar puncture. The patient's next dose of immunotherapy was held. Opening pressure was normal, and MRV showed no evidence of dural sinus thrombosis. MRI of the orbits was positive for perioptic neuritis bilaterally, and the patient was started on a steroid taper with improvement in symptoms. Lumbar puncture cytology was positive for metastatic adenocarcinoma, and the patient has been receiving intrathecal chemotherapy.

Imaging Findings

MRI of the orbits showed thickening and enhancement along the bilateral optic nerve sheaths suggesting perioptic neuritis. This was not present on a head MRI which included fat-saturated sequences through the orbits two months prior. Differential diagnosis included infection, metabolic changes, demyelination, and sarcoidosis. Correlation with CSF analysis, recent medication changes, and concurrent systemic processes was recommended. Review of recent prior PET/CT and chest CT demonstrated perilymphatic micronodules and FDG-avid mediastinal and bilateral hilar lymphadenopathy, suggestive of sarcoidosis or sarcoid-like reaction. The patient had also undergone endobronchial biopsy of one of these lymph nodes six months prior, yielding non-necrotizing granulomatous inflammation.

Discussion

Perioptic neuritis is defined as inflammation of the optic nerve sheath. It is a distinct entity which can be associated with concurrent optic neuritis. There are a multitude of potential etiologies including vasculitis, autoimmune disorders, sarcoidosis, and medication. There have been a few reported cases of immune checkpoint inhibitor-associated optic and perioptic neuritis.

A well-described phenomenon in patients receiving immunotherapy is the sarcoid-like reaction. It is typically described in the chest with findings mimicking thoracic sarcoidosis such as mediastinal and bilateral hilar lymphadenopathy. We suspect there may be overlap between the immune checkpoint inhibitor-associated perioptic neuritis and the so-called sarcoid-like reaction also associated with immune checkpoint inhibitors. Treatment remains high-dose corticosteroids and the majority of patients show improvement in visual symptoms. Our patient was receiving nivolumab, an anti PD-1 immune checkpoint inhibitor, which was the suspected cause of the perioptic neuritis. The differential diagnosis includes sarcoidosis, although the lack of perioptic enhancement on the prior MRI would belie longstanding sarcoidosis. Metastatic disease is considered unlikely given the lack of imaging evidence for widespread intracranial leptomeningeal disease despite positive CSF cytology.

Teaching Point

The differential diagnosis for perioptic neuritis is broad. While sarcoidosis is a known secondary cause, the sarcoid-like reaction caused by immunotherapy is not often considered in the central nervous system. In the absence of imaging revealing leptomeningeal enhancement in the brain, bilateral perioptic neuritis is unlikely to be an isolated presentation of malignant CSF spread. In patients on immune checkpoint inhibitors, particularly with findings mimicking thoracic sarcoidosis, therapy-related side effects should be considered. Given the growing role of immunotherapy in many different cancers, the incidence of these lesser-known effects will likely increase. Knowledge of this entity can prevent unnecessary work-up.

References

Takada K, Fujiwara K, Ando E, et al. Optic perineuritis associated with nivolumab treatment for non-small cell lung cancer. *Case Reports in Oncology*. 2021;14(2):792-796. doi:10.1159/000516275

Mori S, Kurimoto T, Ueda K, et al. Optic neuritis possibly induced by Anti-PD-L1 antibody treatment in a patient with non-small cell lung carcinoma. *Case Reports in Ophthalmology*. 2018;9(2):348-356. doi:10.1159/000491075

Gyan C, Bonello M, Pinto AA. Immune checkpoint inhibitor-associated bilateral optic neuritis. *Practical Neurology*. Published online July 30, 2025. doi:10.1136/pn-2025-004640

Images/Tables

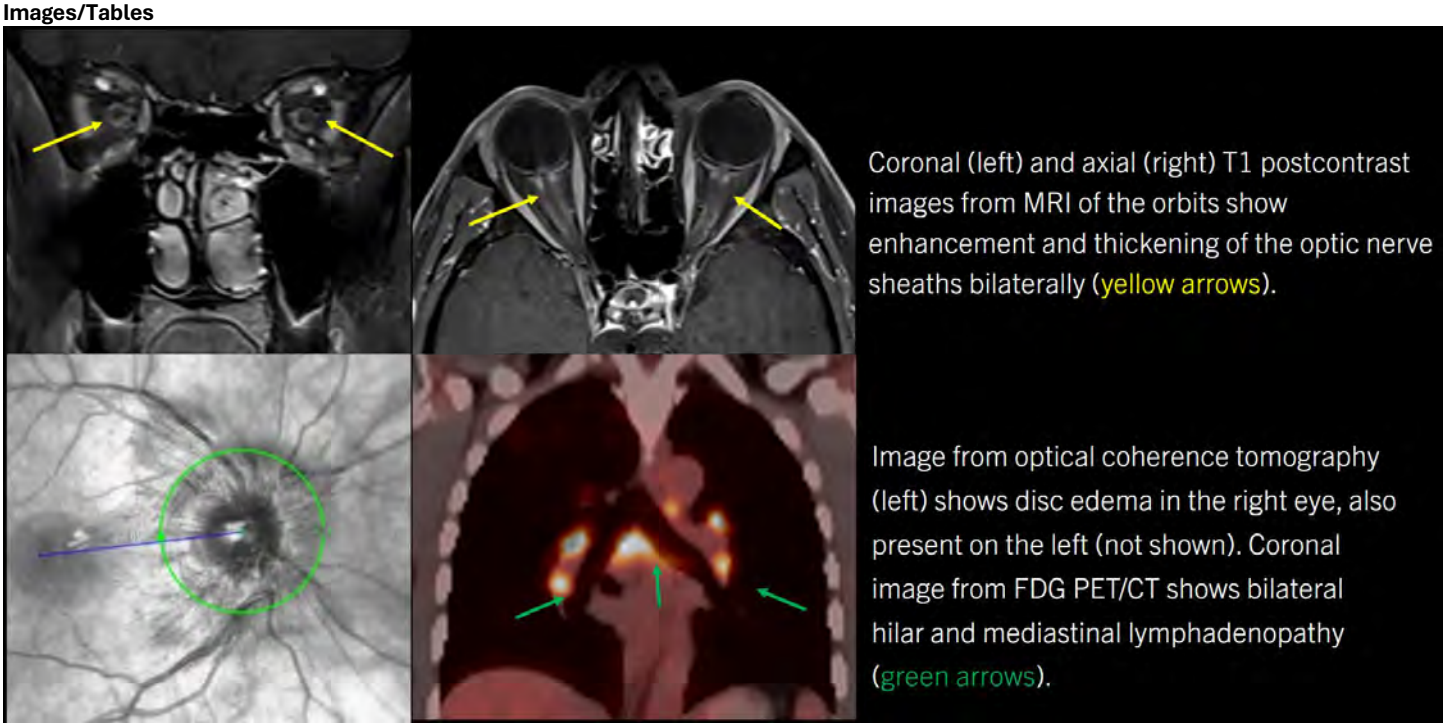

956 Ortner's Syndrome Secondary to Thoracic Aortic Ductus Diverticulum Aneurysm: A Rare Cause of Unilateral Vocal Cord Paralysis

Younus Syed DO, Rukya Masum MD
The Ohio State University Wexner Medical Center, Columbus, Ohio, USA

Clinical History

A 73-year-old male presented with persistent hoarseness five weeks prior to evaluation, with a consistently weak, raspy voice. The patient denied fatigue, neck pain, dysphagia, odynophagia, aspiration, respiratory difficulty, or stridor. He reported no constitutional symptoms, including weight loss, fever, or malaise, and denied symptoms of gastroesophageal reflux or recent upper respiratory infection.

Flexible nasolaryngoscopy with stroboscopy demonstrated left unilateral vocal cord paralysis. Subsequent evaluation with CT of the neck and chest was performed to determine the underlying etiology. The patient's primary complaint remained isolated dysphonia, which significantly affected his social and occupational functioning.

Imaging Findings

Contrast-enhanced CT imaging of the neck and chest demonstrated:

A 4.9 cm anteroinferiorly projecting ductus diverticulum aneurysm with peripheral calcified mural thrombus arising from the ductus diverticulum of the thoracic aorta. The lesion was identified along the expected course of the left recurrent laryngeal nerve (RLN).

Secondary indicators of left vocal cord paralysis were observed, including medialization and atrophy of the left true vocal fold, thickening of the left aryepiglottic fold, and asymmetric enlargement of the left piriform sinus and laryngeal ventricle.

No suspicious enhancing mass or pathologic lymphadenopathy was detected within the neck or upper mediastinum.

These findings are consistent with left recurrent laryngeal nerve palsy caused by mechanical compression from a ductus diverticulum aneurysm.

The patient was contacted for emergent evaluation due to the risk of rupture. No cardiothoracic symptoms were reported, and urgent referral to vascular and cardiothoracic surgery was arranged for further management.

Discussion

The left recurrent laryngeal nerve (RLN) branches from the vagus nerve, loops under the aortic arch, and ascends beside the trachea to the larynx [1]. Its long path makes it vulnerable to injury, especially from cardiovascular causes—such as aortic aneurysm, pseudoaneurysm, or enlarged pulmonary artery—leading to cardiovocal (Ortner's) syndrome, which causes left vocal cord paralysis [2-3].

In this case, an aneurysm arising from the ductus diverticulum—a developmental remnant of the fetal ductus arteriosus—was responsible for compressing the left RLN within the aortopulmonary window. Although hoarseness was the sole presenting symptom, the finding carried potentially fatal implications given the risk of aneurysm rupture.

Prompt recognition of vascular causes of isolated vocal cord paralysis is critical, as early diagnosis may be lifesaving. Radiologists are crucial in identifying subtle imaging signs of RLN palsy and tracing the nerve's anatomic pathway to uncover extralaryngeal pathology [2-3].

Teaching Point

- Isolated left vocal fold paralysis requires imaging from the skull base to the mediastinum to evaluate the recurrent laryngeal nerve.
- Thoracic aortic aneurysms or pseudoaneurysms, though rare, can cause cardiovocal syndrome and are life-threatening.
- Identifying CT signs such as medialized cord, laryngeal ventricle dilation, and piriform sinus asymmetry helps localize paralysis.
- In elderly or those with cardiovascular risk factors, consider vascular causes of hoarseness even without cardiopulmonary symptoms.
- Early identification and referral for repair are vital to prevent rupture.

References

1. Paquette CM, Manos DC, Psooy BJ. Unilateral vocal cord paralysis: a review of CT findings, mediastinal causes, and the course of the recurrent laryngeal nerves. Radiographics. 2012 May-Jun;32(3):721-40. doi: 10.1148/rg.323115129. Erratum in: Radiographics. 2012 Nov-Dec;32(7):2166. PMID: 22582356.

2. Semionov A, Kosiuk J. Ortner syndrome secondary to aortic aneurysm. Radiol Case Rep. 2016 Dec 27;12(1):29-30. doi: 10.1016/j.radcr.2016.11.024. PMID: 28228872; PMCID: PMC5310539.
3. Park JH, Chung JW, Joh JH, et al. Pseudoaneurysm of the ductus diverticulum: imaging findings and clinical significance. *J Vasc Interv Radiol.* 2003;14(4):467–471.

Images/Tables

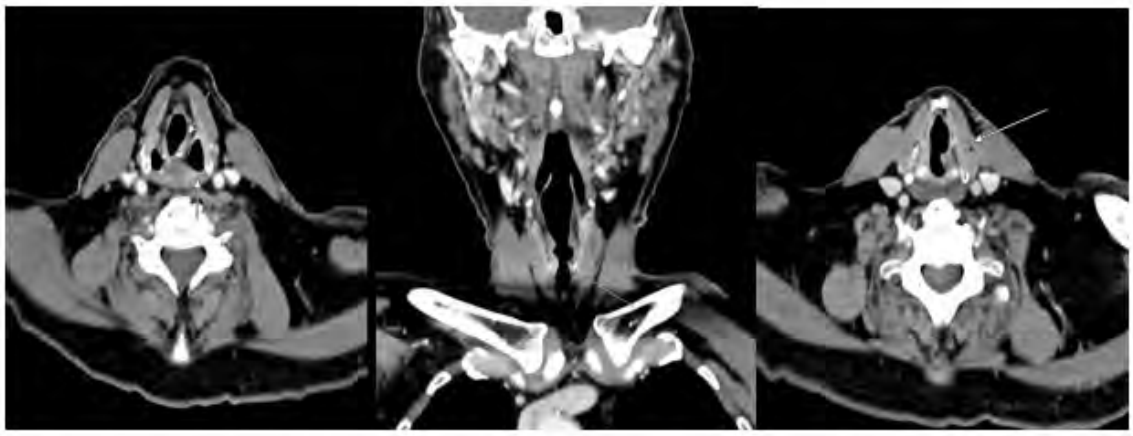

Figure 1-3: Contrast enhanced CT of the neck demonstrates thickening of the left aryepiglottic fold, asymmetric enlargement of the left piriform sinus and laryngeal ventricle, and thinning with medialization of the left vocal cord.

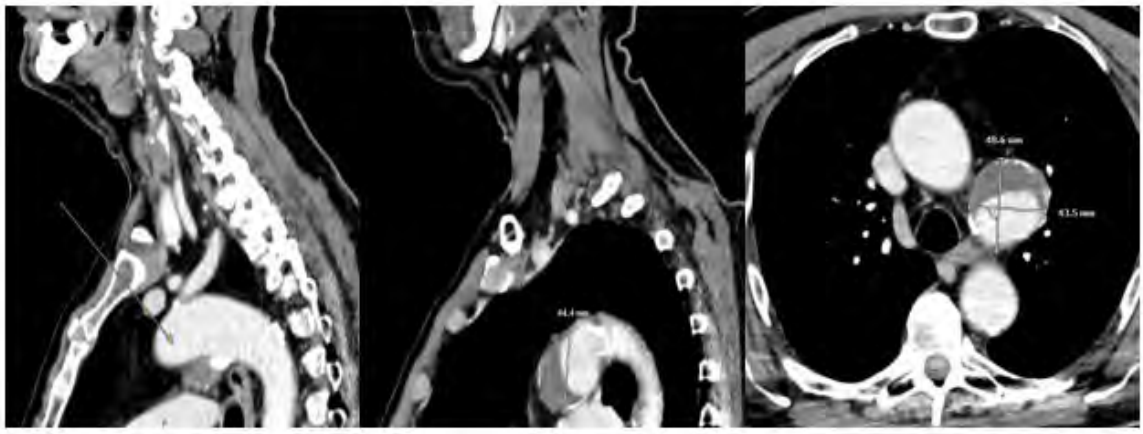

Figure 4-6: Contrast enhanced CT of neck and chest reveal anteroinferiorly projecting aneurysm with peripheral mural thrombus, arising from the ductus diverticulum of the thoracic aorta immediately distal to the origin of the left subclavian artery.

961 Invasive Fungal Sinusitis Presenting as Orbital Apex Syndrome in an Immunocompromised Patient

Michael Bowe MD
Hartford Hospital, Hartford, CT, USA

Clinical History

We report a case of orbital apex syndrome secondary to acute invasive fungal sinusitis. Our patient is a 77-year-old male with a history of bladder cancer undergoing neoadjuvant chemotherapy, complicated by type 2 diabetes mellitus, who initially presented with progressive, painless vision loss of the right eye over two weeks.

Imaging Findings

MR imaging of the orbits demonstrated enhancing soft tissue effacing the fat of the right orbital apex and encasing the right optic nerve. Enhancing tissue extended posteriorly along the ipsilateral right ethmoid sinus, sphenoid sinus, and right cavernous sinus. There was an area of nonenhancing necrotic right sphenoid sinus mucosa opposing the right orbital apex, a finding highly suspicious for invasive fungal infection. Subsequent CT maxillofacial imaging further reinforced suspicion of invasive fungal infection, revealing multiple areas of bony erosion throughout the sphenoid sinus and portions of the anterior cranial fossa floor. Biopsy later confirmed the presence of *Aspergillus*, and treatment was promptly initiated with antifungals alongside sinusectomy and debridement.

Discussion

Acute invasive fungal sinusitis (AIFS) is an aggressive infection usually affecting immunocompromised individuals with a tendency to progress rapidly due to reduced immunologic defense. Orbital apex syndrome (OAS) is a neuro-ophthalmic emergency characterized by dysfunction of cranial nerves II, III, IV, V1, and VI due to pathology at the orbital apex. Progressive AIFS can cause regional mass effect on, or directly infiltrate, the orbital apex tissues presenting clinically with OAS. Radiologic imaging plays a critical role in identification and characterization of AIFS. Key imaging features like pattern of spread, mucosal necrosis and bony erosions can be essential in distinguishing AIFS from malignancy.

Teaching Point

This case highlights the importance of early and accurate diagnosis of invasive fungal sinusitis in immunosuppressed patients to minimize morbidity and mortality. Delays in management can have catastrophic outcomes like irreversible vision loss, cavernous sinus thrombosis, and intracranial extension often with fatal outcomes. This case also emphasizes the need for ongoing research to improve outcomes and develop evidence-based guidelines for managing acute invasive fungal sinusitis in immunocompromised populations.

References

Dagher R, Calle S, and Learned K. Imaging approach for fungal sinusitis. *Current Opinion in Otolaryngology & Head and Neck Surgery* 2025; 33(1):56-63. DOI: 10.1097/MOO.0000000000001018

Images/Tables

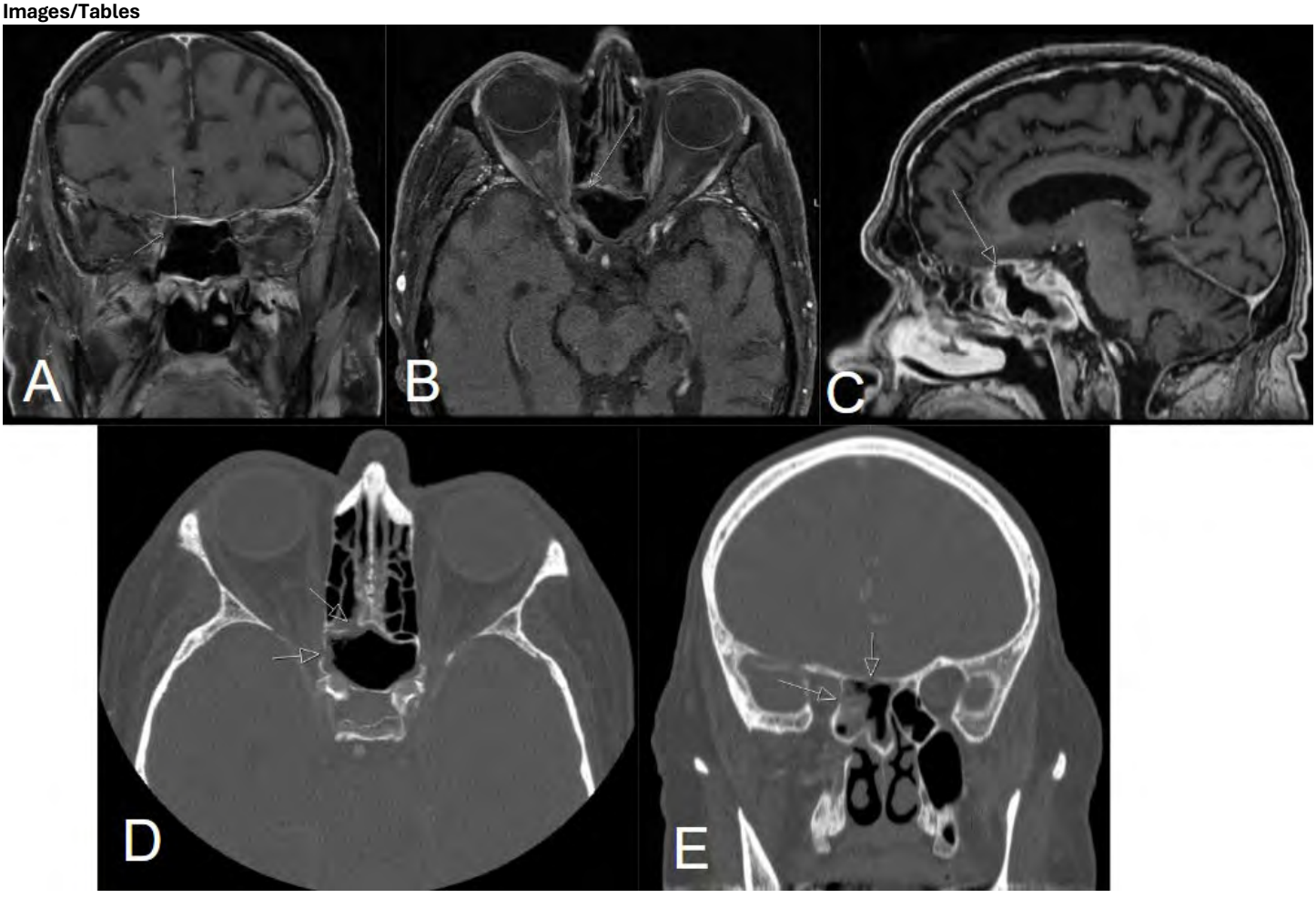

973 Beware of the Bolt Tract: Iatrogenic Scalp Pseudoaneurysm Following ICP Monitor Removal

Vatsal P Lal MD, Howard Gill MD, Anthony Higinbotham MD, Thomas J Eluvathingal Muttikkal MD
University of Virginia, Charlottesville, VA, USA

Clinical History

A 24-year-old male with no past medical history presented to the emergency department following a motor vehicle collision with a tree. The patient had an initial Glasgow Coma Scale (GCS) score of 7. Soon after, the patient was intubated for airway protection. The initial non-contrast head CT demonstrated multicompartment intracranial hemorrhage. Neurosurgery placed a right frontal intracranial pressure (ICP) bolt for monitoring, which was removed after 5 days as his clinical status improved. Approximately 12 days after removal, physical exam revealed new erythema and swelling over the bolt site, raising concern for infection along the tract and prompting further imaging.

Imaging Findings

CTA of the head and neck was obtained for evaluation of mental status changes and the bolt-site swelling. In addition to increased intraparenchymal hemorrhage, the CTA demonstrated a hypodense superficial fluid collection over the bolt tract with an internal arterially enhancing focus that increased on delayed images, consistent with a scalp arterial pseudoaneurysm. Ultrasound of the right frontal scalp demonstrated a rounded, heterogeneous collection with central "to-and-fro" flow on Doppler imaging, compatible with a partially thrombosed pseudoaneurysm.

Discussion

A pseudoaneurysm results from arterial wall disruption leading to a contained, extraluminal sac which remains in communication with the parent artery. While true aneurysms are bound by all three layers of the arterial wall, a pseudoaneurysm is bounded by clot and surrounding soft tissue. Scalp pseudoaneurysms are rare and the vast majority are secondary to blunt trauma, with only a small percentage due to penetrating injury or iatrogenic causes. Prompt recognition is imperative to avoid misdiagnosis as a hematoma or abscess.

Teaching Point

- Carefully survey all cranial hardware tracts and the adjacent soft tissues.
- A new or enlarging tract-site lesion should prompt bedside assessment for pulsatility and additional imaging.
- Ultrasound is the preferred first-line imaging study for assessment of a suspected scalp pseudoaneurysm.

References

1. Sueyoshi E, Ichiro S, Kazuaki N, et al. Visceral and peripheral arterial pseudoaneurysms. *AJR Am J Roentgenol* 2005;185(3):741–49. DOI:10.2214/ajr.185.3.01850741
2. Corvino A, Catalano O, Corvino F, et al. Superficial temporal artery pseudoaneurysm: what is the role of ultrasound? *J Ultrasound* 2016;19(3):197-201. DOI: 10.1007/s40477-016-0211-8

Images/Tables

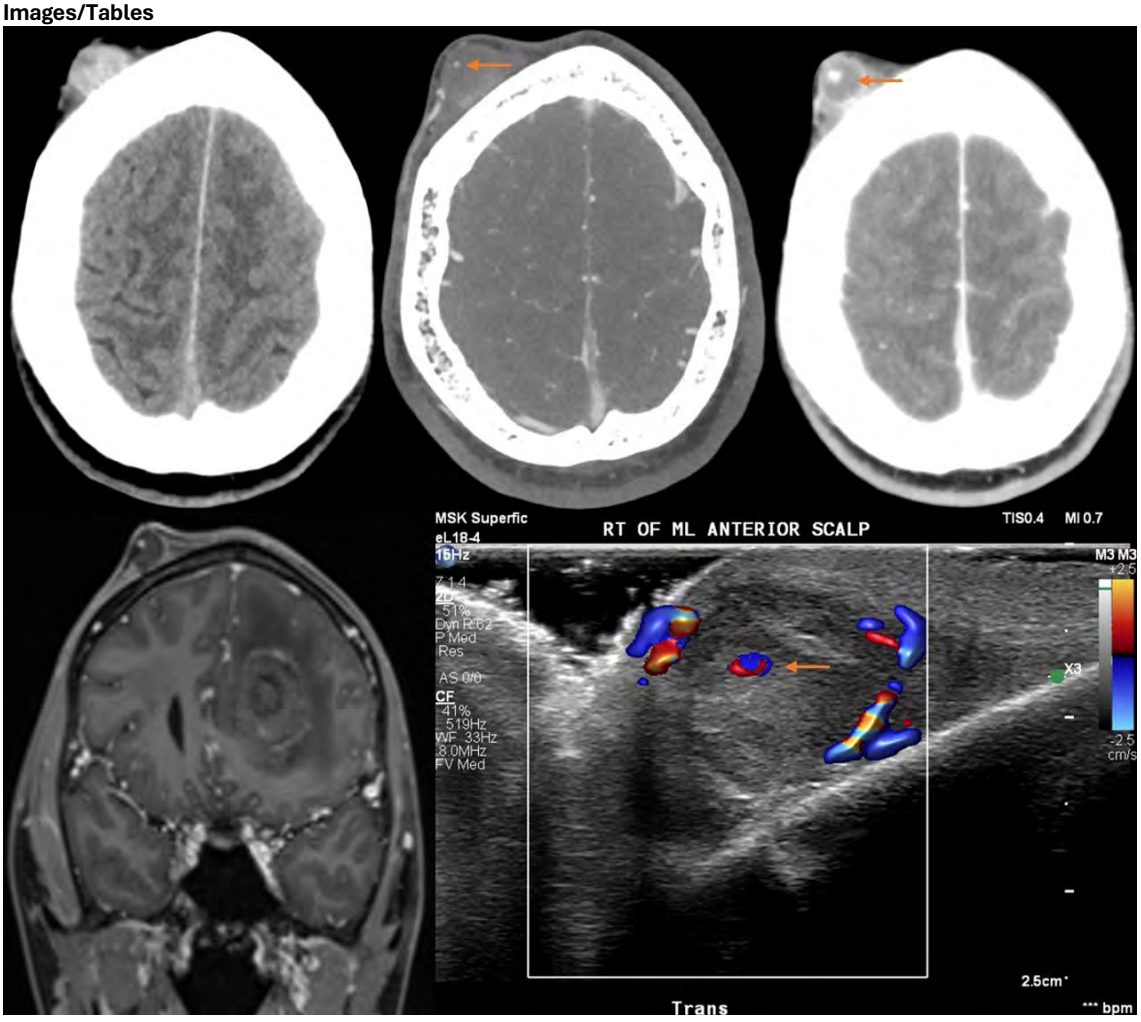

1040 Gut Feeling Gone South: Gastric Cancer Metastasizing to the Cauda Equina

Swastika Lamture, William Colantoni
University of Colorado and Anschutz Hospital, Aurora, Colorado, USA

Clinical History

A 46-year-old patient with a history of poorly differentiated gastric adenocarcinoma presented with back pain, perineal paresthesia.
Recent follow-up imaging demonstrated stable disease with no new intra-abdominal disease. Given the new onset of saddle anesthesia and altered bowel sensation, an MRI spine was ordered to evaluate for possible spinal cord or cauda equina compression secondary to metastatic disease.

Imaging Findings

Multiple well-defined T2 hypointense masses with homogenous postcontrast enhancement along the cauda equina nerve roots, suggestive of intradural cauda equina metastases. Few of these masses obliterated the spinal canal
Leptomeningeal enhancement in the caudal aspect of spinal cord suspicious for multiple meningeal carcinomatosis
Asymmetric heterogeneously enhancing thickening in the distal gastric wall

Discussion

Intradural cauda equina metastasis (ICEM) is an exceedingly rare manifestation of systemic malignancy, accounting for only ~1.5% of all spinal metastases. Most cases present as meningeal carcinomatosis, while focally restricted, space-occupying lesions within the caudal sac or dural sleeve of individual nerve roots are even less common and represent a distinct pathological entity.
A literature review identifies approximately 54 reported cases of cauda equina syndrome (CES) caused by non-CNS tumor metastases. Among these, 71.1% of patients had a prior diagnosis of malignancy—most commonly lung (44.4%), renal (16.7%), and breast (7.4%) primaries.
Five potential metastatic pathways have been proposed for ICEMs:

1. Hematogenous spread via the arterial system
2. Retrograde venous dissemination through the Batson venous plexus
3. Perineural lymphatic spread
4. Cerebrospinal fluid seeding
5. Direct invasion from adjacent structures

Due to their rarity and nonspecific presentation, ICEMs often mimic more common causes of cauda equina syndrome. Early recognition through MRI with contrast is essential to guide management and prevent irreversible neurological deficits. Prognosis remains poor, reflecting the advanced stage of systemic disease at presentation.

Teaching Point

- Intradural cauda equina metastasis is an exceptionally rare cause of cauda equina syndrome, representing about 1.5% of spinal metastases.
- Early neurological symptoms such as saddle anesthesia, back pain, and bowel/bladder dysfunction in a known cancer patient should prompt urgent spinal MRI.
- Intradural cauda equina metastasis can arise from hematogenous, venous, lymphatic, CSF, or direct invasion pathways.
- MRI with contrast remains the gold standard for diagnosis and helps distinguish intradural from extradural lesions.

References

Pagano, A., Iaquinandi, A., Fraioli, M. F., et al. (2021). Cauda equina syndrome from intradural metastasis of a non-neural tumor: case report and review of literature. *British Journal of Neurosurgery*, *37*(6), 1487–1494. https://doi.org/10.1080/02688697.2021.1958155
Paolo Palmisciano, Saif E. Zaidi, Nathan A. Shlobin et al.Intradural Cauda Equina Metastases: A Systematic Review of Clinico-radiological Features, Management, and Treatment Outcomes
Anticancer Research Apr 2022, 42 (4) 1661-1669; DOI: 10.21873/anticanres.15643

Images/Tables

T2 sagittal(A), T2 axial (B) and post contrast T1 fat suppressed sagittal(C) sections of the lumbar spine and contrast enhanced axial section through the abdomen (D)
Multiple T2 hypointense masses along the cauda equina, which are homogeneously enhancing (C). Few of these lesions are obliterating the spinal canal (A). There is leptomeningeal enhancement in the caudal aspect of the spinal cord (arrow in C)concerning for leptomeningeal carcinomatosis. Heterogeneously enhancing thickening of the distal gastric wall (arrow in D)

1059 Diffuse Brown Tumor Involvement Secondary to Primary Hyperparathyroidism: A Case-Based Imaging Review

RENATA TARRAF FERNANDES MD[1], Larissa Grazielle Souza Ribeiro MD[2], Anderson Aparecido Santim MD[2], Miraldo Santos Souza MD[3]
[1]Jales Cancer Hospital, Jales, sao paulo, Brazil. [2]Barretos Cancer Hospital, Barretos, sao paulo, Brazil. [3]Hospital das clínicas UFMG, Belo horizonte, Mina's gerais, Brazil

Clinical History

Case 1: A 45-year-old woman presented with a 4-year history of lower back pain and a previously treated tumor of the maxilla.
Case 2: An 18-year-old woman presented two months after sustaining trauma to the left shoulder. Radiographs revealed a lytic lesion in the humeral head.
Both patients, upon further evaluation, demonstrated diffuse lytic bone lesions and laboratory findings consistent with hyperparathyroidism, with imaging identifying a parathyroid nodule in each case.

Imaging Findings

In both cases, CT revealed multiple well-defined osteolytic lesions with sclerotic margins and cortical thinning. MRI demonstrated heterogeneous signal intensity due to cystic changes and hemosiderin deposits, along with heterogeneous post-contrast enhancement. Bone scintigraphy showed increased technetium-99m uptake.

Discussion

Brown tumor is a reactive osteolytic lesion secondary to hyperparathyroidism, resulting from excessive osteoclastic activity caused by persistent elevation of parathyroid hormone (PTH). On radiographs and CT, these lesions appear as well-defined, expansile, lytic bone defects with cortical thinning, possible endosteal scalloping, and sclerotic margins. They typically lack periosteal reaction and matrix mineralization.
MRI usually demonstrates heterogeneous signal intensity due to hemorrhage, cystic degeneration, and fibrous tissue components. Post contrast images show heterogeneous enhancement, typically moderate in the solid portions of the lesion. Bone scintigraphy shows increased uptake of technetium-99m methylene diphosphonate (^{99m}Tc-MDP), reflecting the high bone turnover and osteoclastic activity.
Brown tumors can be solitary or multiple. Although the mandible and ribs are the most common sites, diffuse skeletal involvement is uncommon and may mimic metastatic bone disease. Recognition of biochemical abnormalities, particularly elevated calcium and PTH levels, is essential for accurate diagnosis.
The main differential diagnoses include giant cell tumor, aneurysmal bone cyst, fibrous dysplasia, Langerhans cell histiocytosis, and osteoblastoma. More aggressive differentials include metastatic bone disease, multiple myeloma, and primary malignant bone tumors such as osteosarcoma or Ewing sarcoma.
Imaging plays a key role in defining lesion distribution and evaluating complications such as fractures or compressive effects. After parathyroidectomy, bone lesions typically regress or become sclerotic as a result of remineralization. Biopsy may be considered when imaging and clinical findings remain inconclusive.

Teaching Point

- Brown tumors are reactive osteolytic lesions secondary to prolonged hyperparathyroidism and may mimic malignant bone disease.
- Correlation of imaging findings with biochemical data (hypercalcemia and elevated PTH) is crucial for diagnosis and prevents unnecessary biopsy or oncologic work-up.

References

Carsote M, Ciobica ML, Sima OC, Valea A, Bondor CI, Geleriu A, Ticolea M, Nistor C, Rusu CC. Brown tumors: the hidden face of primary and renal hyperparathyroidism amid real-life settings. *J Clin Med* 2024;13(13):3847. doi:10.3390/jcm13133847
Liu Z, Yang H, Tan H, Song R, Zhang Y, Zhao L. Brown tumor of the cervical spine with primary hyperparathyroidism: a case report and literature review. Medicine (Baltimore) 2023;102(6):e32768. doi:10.1097/MD.0000000000032768
Jacquet-Francillon N, Prevot N. Brown tumors in nuclear medicine: a systematic review. *Ann Nucl Med* 2023;37(5):255–270. doi:10.1007/s12149-023-01832-1
Hong WS, Sung MS, Chun KA, Kim JY, Park SW, Lee KH, Lim HW, Lim YS, Yoo WJ, Chung MH. Emphasis on the MR imaging findings of brown tumor: a report of five cases. *Skeletal Radiol* 2011;40(2):205–213. doi:10.1007/s00256-010-0979-0

1076 Foley Catheter Induced Recanalization of M1 Occlusion

Matthew S Moler DO, Anthony Larder DO, Kevin Hammmond MD
University of Cincinnati, Cincinnati, OH, USA

Clinical History

A 34-year-old male with notable past medical history of hypertension presented to the emergency department with acute onset of profound left sided weakness, left facial droop, and left sided numbness. Symptoms began 15 minutes prior to arrival at the emergency department and NIH stroke scale was 23. He denied prior history of stroke, diabetes, or hypercoagulability. Patient was noted to be hypertensive at time of presentation, with blood pressure 160/110 mmHg.
There was initial concern for Moya-Moya disease, thus TNK was deemed high risk and not administered. Treatment with endovascular thrombectomy was pursued and a foley catheter was placed in preparation for the procedure. Foley catheter placement was noted to be extremely uncomfortable for the patient, and he was noted to be loudly screaming with a spike in blood pressure to 185/117 mmHg. He was subsequently able to move his left upper extremity.

Imaging Findings

Noncontrast CT of the head was performed and unremarkable with an ASPECT score of 10. CTA of the head was performed and demonstrated occlusion of the right M1 segment. Additional multifocal luminal irregularity of the bilateral carotid termini and proximal M1 vessels initially raised concern for Moya-Moya disease in a young patient.
A repeat CTA performed in the ED after foley catheter placement demonstrated thin recanalization of the right M1 segment.

Conventional angiography revealed extensive luminal irregularities of the intracranial arteries in the anterior circulation more suggestive of atherosclerotic disease.

Discussion

Spontaneous recanalization of large-vessel occlusion is rare. This case illustrates an exceptional instance of M1segment recanalization triggered by an acute hypertensive response during Foley catheter placement. The temporal association between catheter insertion, blood pressure elevation, and radiographic recanalization suggests a hemodynamic mechanism—likely shear stress–mediated thrombus dislodgement or compression due to transient hyperperfusion.

Teaching Point

Spontaneous recanalization of large-vessel occlusion can occur in the hyperacute phase, though very rare. Acute blood pressure surges can trigger recanalization. This case supports the need for cautions blood pressure management in acute strokes with large vessel occlusion, balancing perfusion against hemorrhage risk.

References

Kassem-Moussa H, Graffagnino C. Nonocclusion and Spontaneous Recanalization Rates in Acute Ischemic Stroke: A Review of Cerebral Angiography Studies. Arch Neurol. 2002;59(12):1870–1873. doi:10.1001/archneur.59.12.1870

Images/Tables

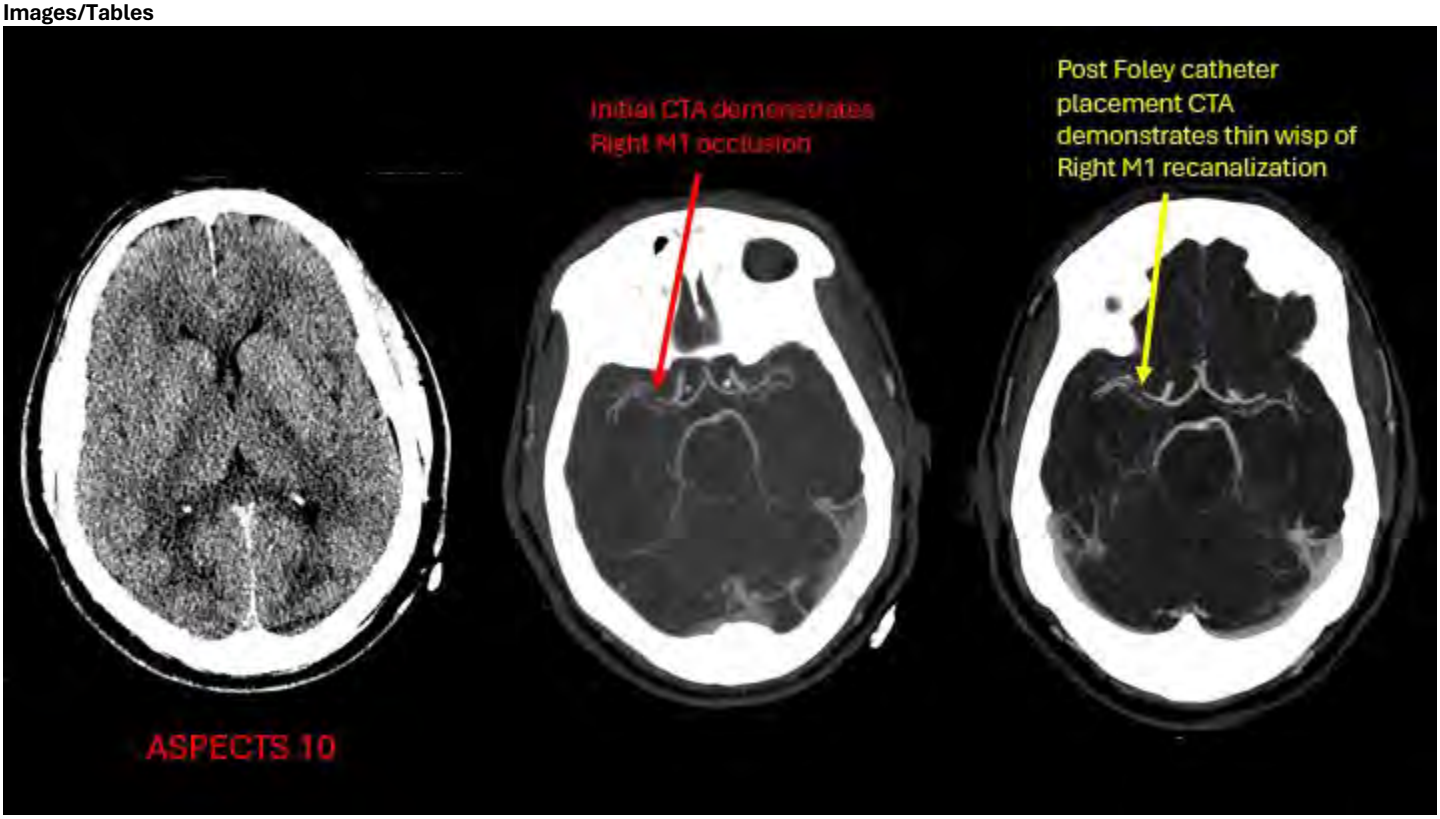

1084 " Interesting Case of Extensive Intra and Extracranial IgG-4 Related Disease with Incomplete Improvement After Pulse Steroids and Rituximab"

Mohammad S Alahmadi MD, Maria Lucia Brun-Vergara MD, Paulo Puac-Polanco MD, Carlos Torres MD
University of Ottawa, Ottawa, Ontario, Canada

Clinical History

24-year-old female with IgG4-related intra- and extracranial mass causing reduced right visual acuity, with incomplete improvement after pulse steroids and rituximab.

She was well until she presented with left ear sensorineural hearing loss. MRI showed opacification of left mastoid air cells. She was diagnosed with tympanometry dysfunction.

In November 2024, she developed headaches that persisted until March 2025, when she was admitted to hospital after right eye blurring and abduction palsy. MRI showed a lesion involving the left nasopharynx, clivus, jugular foramen, mastoid air cells, dura, Meckel's cave, pituitary, tentorium, and leptomeninges.

Right mastoidectomy and biopsy during the admission confirmed IgG4-related disease.

At outpatient follow-up, she had persistent right eye abduction palsy and blurriness. Prednisone was started with a plan for rituximab.

Despite therapy, she developed progressive right eye visual loss, reaching blackness. She received outpatient pulse steroids.

After this, vision improved, despite receiving her first rituximab dose. She was later sent to ED for reassessment due to lack of further improvement and to consider pulse steroids.

Imaging Findings

Infiltrative lesion of the left nasopharynx and left clivus, extends to the left jugular foramen with diffuse dural thickening involving tentorium and leptomeningeal, extending anteriorly to the right cavernous sinus, Meckel's cave and pituitary gland.

Enhancement noted in bilateral mastoid air cells.

The follow up showed improvement of the prior findings , however there is new nodular area of enhancement with T2/FLAIR hyperintensity , above the right anterior clinoid process, inseparable to the cisternal segment of the right optic nerve, extending to the optic canal with Increased T2 signal of the right intracanalicular optic nerve and extending up to the right side of the optic chiasm.

Discussion

IgG4-related disease is a systemic, fibroinflammatory condition that often presents as infiltrative or mass-like lesions affecting multiple organs. Diagnosis is based on histopathology, requiring an IgG4-positive plasma cell infiltrate comprising ≥40% of IgG-positive cells or >50 cells per high-power field.

Head and neck involvement of IgG4-related disease is frequent where orbit and salivary glands are the most affected sites, where orbital involvements present as painless proptosis, diplopia and restricted ocular motility.

IgG4 related disease can be intracranially with pachymeningitis and hypophysitis and affecting cranial nerves III, IV and VI within the cavernous sinus as wells as the optic nerves in the optic canal or suprasellar region, causing ophthalmoplegia or compressive optic neuropathy.

In our case, the disease began as typical mastoid involvement mimicking chronic mastoiditis, then progressed to the left nasopharynx, dura, leptomeninges, pituitary, and cavernous sinus. Steroids and rituximab improved the extensive disease; however, a new lesion later developed in the optic nerve and chiasm, impairing vision.

Teaching Point

IgG-4 related disease can start affecting the mastoid and middle ear cavity and mimic mastoid effusion or mastoiditis.

The disease can spread intracranially with leptomeningeal and pituitary involvement , also extracranially within the nasopharynx like in this case.

This case shows that despite treatment by steroids and Rituximab it showed mixed response with improvement of the initial lesion presentation with interval development of new lesion affecting the optic nerve and chiasm.

References

Thompson A, Whyte A. Imaging of IgG4-related disease of the head and neck. Clin Radiol. 2018 Jan;73(1):106-120. doi: 10.1016/j.crad.2017.04.004. Epub 2017 May 10. PMID: 28501095.

Sirvisetty H, Bockhorst S, Hamidi R. Perineural Spread of Orbital Immunoglobulin G4-Related Disease: A Case Report. Cureus. 2025 Jan 21;17(1):e77790. doi: 10.7759/cureus.77790. PMID: 39981439; PMCID: PMC11841963.

Goulam-Houssein S, Grenville JL, Mastrocostas K, Munoz DG, Lin A, Bharatha A, Vlachou PA. IgG4-related intracranial disease. Neuroradiol J. 2019 Feb;32(1):29-35. doi: 10.1177/1971400918806323. Epub 2018 Oct 15. PMID: 30320530; PMCID: PMC6327361.

Hofmeyr L, Herbst G, Pretorius E, Sarembock B, Taylor K, Roytowski D. Case Report: Diagnosis of Petrous Apex IgG4-Related Disease by Middle Cranial Fossa Craniotomy and Temporal Bone Biopsy. Front Neurol. 2022 Jun 9;13:874451. doi: 10.3389/fneur.2022.874451. PMID: 35756934; PMCID: PMC9218261.

Schiffenbauer AI, Wahl C, Pittaluga S, Jaffe ES, Hoffman R, Khosroshahi A, Stone JH, Deshpande V, Gahl WA, Gill F. IgG4-related disease presenting as recurrent mastoiditis. Laryngoscope. 2012 Mar;122(3):681-4. doi: 10.1002/lary.22486. Epub 2012 Jan 17. PMID: 22252885; PMCID: PMC3547986.

Images/Tables

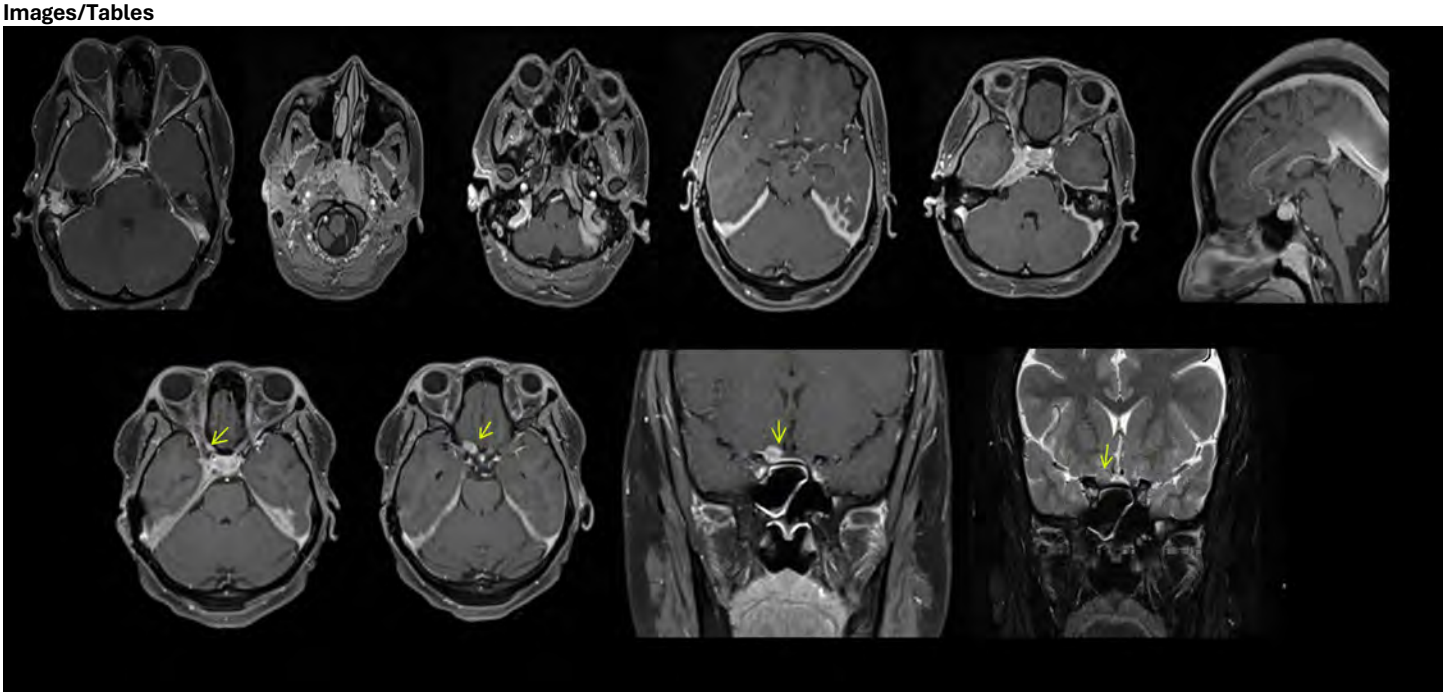

1091 Axonal Shear Injury After Low-Mechanism Trauma in Vanishing White Matter Disease

Christopher E Roberts MD, Jeffrey R Sachs MD

Wake Forest University School of Medicine, Winston-Salem, NC, USA

Clinical History

A young adult male presented to the ED via EMS as an unknown trauma due to unwitnessed MVC. He was found by EMS with a GCS of 4 and the car airbags deployed. En route, he remained hemodynamically stable and was given naloxone without improvement in mentation. On arrival to the ED, he remained stable but with persistent low GCS. Physical exam revealed mild frontal scalp and periorbital ecchymosis with a small eyelid laceration, but no other traumatic injuries. Initial trauma imaging was negative except for the CT head.

Imaging Findings

Non-contrast CT head demonstrated cerebral atrophy with diffuse white matter hypoattenuation, concerning for leukodystrophy. Additionally, there was indeterminate periventricular hyperattenuation concerning for posttraumatic hemorrhage or mineralization. Short term follow up dual energy CT head was recommended. Creation of a virtual non-calcium map demonstrated persistent periventricular hyperattenuation, concerning for hemorrhage in the setting of axonal shear injury. Brain MR was recommended with susceptibility weighted imaging showing extensive periventricular susceptibility artifact confirming microhemorrhage in the setting of axonal shear injury. Of note, many of the hemorrhages were linear in morphology extending from the corpus callosum into the adjacent white matter. Abnormal FLAIR hyperintensity was throughout the white matter with periventricular cystic changes and age advanced atrophy, in keeping with history of vanishing white matter disease after the patient's identify was confirmed.

Discussion

Vanishing white matter (VWM), also known as childhood ataxia with central nervous system hypomyelination (CACH), is a rare type of leukoencephalopathy broadly presenting with ataxia, spasticity, and optic atrophy with neurologic deterioration. Pathologic characteristics include white matter rarefaction, cystic degeneration, and loss of oligodendrocytes by apoptosis. Diagnosis is typically based upon clinical features, imaging, and genetic testing for pathogenic variants involving genes encoding the subunits of the eukaryotic translation initiation factor 2b which are inherited in an autosomal recessive pattern. Additionally, minor intracranial trauma, infection or even fright are thought to precipitate a more rapid neurologic decline in patients with VWM. This case shows intracranial trauma resulting in extensive axonal shear injury. While the details of the MVC in this case are incomplete, the absence of other signs of trauma elsewhere in the body suggests that the intracranial injury was disproportionate to the mechanism of trauma experienced by this patient; this also raises the possibility that axonal shear injury could be the, or amongst several, potential underlying mechanisms accounting for relatively minor trauma precipitating rapid neurologic decline. Unfortunately for this patient, the injury resulted in rapid neurologic decline without a return to a previously high functioning neurologic baseline.

Teaching Point

This case highlights the imaging findings of VWM disease, a rare leukodystrophy affecting the white matter with a broad clinical spectrum. It is hypothesized that patients with VWM disease may be more susceptible to axonal shear injuries, potentially accounting for the observation of minor trauma contributing to rapid neurologic decline. Additionally, it demonstrates the utility of dual energy CT to help differentiate hemorrhage from calcification.

References

van der Knaap MS, Pronk JC, Scheper GC. Vanishing white matter disease. *The Lancet Neurology*. 2006. 5:413-423. doi.org/10.1016/S1474-4422(06)70440-9

Mathew D, Mahomed N. Vanishing white matter disease imaged over 3 years. *SA JRadiol*. 2019. 23:1661.doi: 10.4102/sajr.v23i1.1661.

Images/Tables

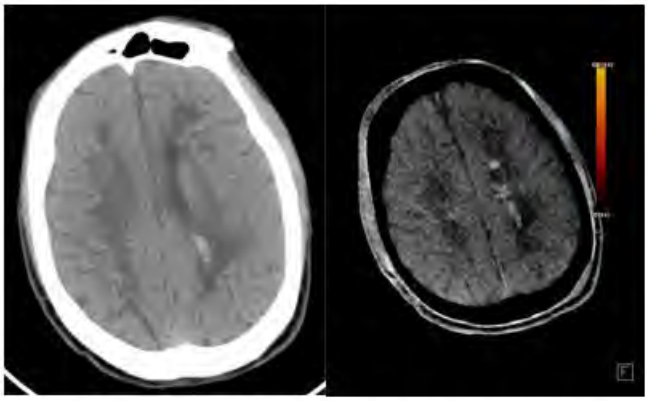

Figure 1. Axial noncontrast CT head with follow up dual energy virtual non-calcium map showing periventricular hemorrhage on a background of abnormal white matter.

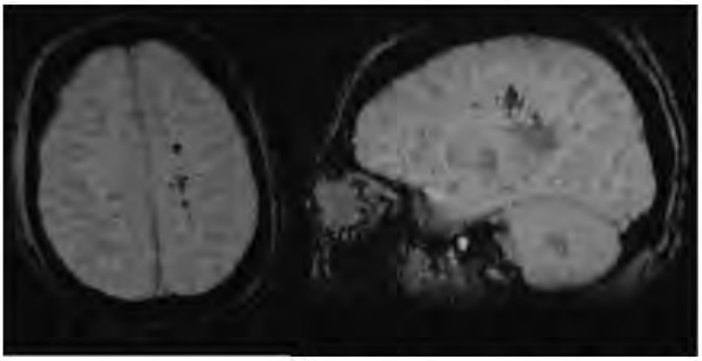

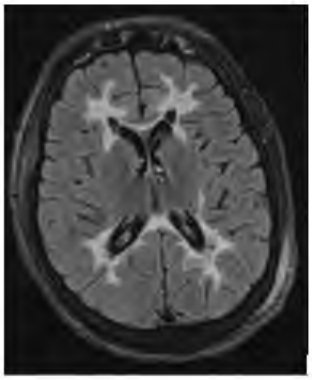

Figure 2. Subsequent brain MR. SWI showing extensive periventricular microhemorrhage, consistent with axonal shear injury. FLAIR showing abnormal white matter hyperintensity, periventricular cystic changes, and atrophy, in keeping with history of vanishing white matter disease.

1104 When Fungus Mimics Malignancy: Hyperplastic Candidiasis of the Tongue

Sushmitha Puttappa Shivagange MD, Eduardo Portela De Oliveira MD, Isabelle Filion MD
University of Ottawa, Ottawa, Ontario, Canada

Clinical History

89-year-old male was referred to ENT for a left anterior tongue lesion associated with pain and progressive growth. Medical history includes lung nodule concerning for adenocarcinoma spectrum lesion. History was negative for weight loss, dysphagia, restricted tongue movement and immunocompromised status. On physical exam by an ENT specialist, an exophytic anterolateral lesion within the dorsum of tongue with an overlying white plaque was visualised. The patient underwent punch biopsy of the lesion and was referred for CT Neck.

Imaging Findings

CT neck: Homogenously enhancing lesion involving the left anterior aspect of the mobile tongue crossing the midline towards the right along the mucosa. No extension to the base of tongue. No cervical lymphadenopathy. Imaging findings raised concern for malignant neoplasm of tongue. (Figure 1a, 1b and 1c)

Discussion

Chronic hyperplastic candidiasis (CHC) is a distinct clinical subtype of oral candidiasis, presenting as slightly raised, well-circumscribed whitish plaques, most commonly at the labial commissures, but also on the tongue and buccal mucosa. CHC can be challenging to diagnose and manage because it clinically mimics oral neoplasms and carries a risk of progression to severe dysplasia or malignancy, particularly in immunocompromised patients[1,2].

No definitive imaging features of CHC have been described in the literature, highlighting the significance of this case report. On CT and MRI, it may appear as either an exophytic or nonexophytic enhancing soft tissue mass mimicking oropharyngeal carcinoma, as reported in a case report of invasive candidiasis with fungal osteomyelitis by Tan HY et al[3]. Imaging cannot distinguish CHC from oral malignancy and the histopathologic evaluation remains the definitive diagnostic method.

Histopathological examination from punch biopsy revealed acanthotic squamous mucosa with acute mucositis and reactive atypia with fungal elements consistent with Candida species, suggestive of hyperplastic candidiasis. Negative for high-grade dysplasia or invasive carcinoma.
Our patient was treated with fluconazole for three weeks, which led to marked resolution of the candidiasis and tongue hypertrophy.

Teaching Point

Radiologists should be familiar with the imaging appearance of oral CHC, as it is indistinguishable from oropharyngeal malignancies on imaging, creating significant diagnostic and management challenges. Misdiagnosis may not only cause undue patient anxiety but also lead to unnecessary invasive or radical interventions. Given the risk of malignant transformation, early recognition and early diagnosis and prompt treatment are essential.

References

References:

1. Basile J, Younis R, Salter R, Brown R. Oral Nodular Chronic Hyperplastic Candidiasis of the Tongue: A Case Report. Cureus. 2023;15(7):e42195. Published 2023 Jul 20. doi:10.7759/cureus.42195.
2. Taylor M, Brizuela M, Raja A. Oral Candidiasis. [Updated 2023 Jul 4]. In: StatPearls [Internet]. Treasure Island (FL): StatPearls Publishing; 2025 Jan. Available from: https://www.ncbi.nlm.nih.gov/books/NBK545282/.
3. Tan HY, Low JG, Roche E, Tan HK. A case report of invasive candidiasis and fungal osteomyelitis mimicking oropharyngeal carcinoma recurrence in an immunocompetent patient following transoral robotic surgery. Int J Surg Case Rep. 2017;35:33-36. doi:10.1016/j.ijscr.2017.04.005.

Images/Tables

1115 Extramedullary Glottic Plasmacytoma: Rare Presentation as a Laryngeal Mass

Sushmitha Puttappa Shivagange MD, Eduardo Portela De Oliveira MD, Augusto Lio Da Mota Goncalves Filho MD, Isabelle Filion MMus, BSc, BMus
University of Ottawa, Ottawa, Ontario, Canada

Clinical History

Extramedullary Glottic Plasmacytoma: Rare Presentation as a Laryngeal Mass

Imaging Findings

CT Neck:

Enhancing mass involving posterior and both lateral infraglottic region involving the vocal cords, posterior and lateral walls of upper trachea causing significant narrowing of airway. The mass is also involving the cricoid cartilage with diffuse demineralization. (Fig 1a and 1b)
Expansile lytic lesion with soft tissue mass seen within the body of mandible on the right with erosion of inner cortex and extending into the buccal mucosa and also in the manubrium (not shown).

MRI Neck:

T2 hyperintense homogeneously enhancing infraglottic lesion involving and replacing the cricoid cartilage causing narrowing of the infraglottic airway more posteriorly.
Multiple expansile lytic lesions with cortical erosions and enhancing soft tissue component in the right mandibular body, manubrium and along the floor of right maxillary sinus. (Fig 2-3).
Imaging differential considered was primary glottic/infraglottic malignancy, likely squamous cell carcinoma with osseous lytic metastasis. Other differentials included chondroma, chondrosarcoma and metastasis.

Discussion

Multiple myeloma, the most common plasma cell neoplasm, primarily affects the skeletal system. Extramedullary plasmacytoma (EMP) refers to soft-tissue plasmacytoma or plasma cell infiltration occurring at an anatomical site distant from the bone marrow, typically resulting from hematogenous spread. The most frequently involved sites include the nasal cavity, paranasal sinuses, nasopharynx, gingiva, tonsils, thyroid, larynx, lymph nodes, and orbital cavity, cricoid involvement is exceedingly rare [1,2]. What makes this case particularly interesting is that the patient's primary presentation of plasma cell myeloma as a laryngeal mass causing upper airway obstructive symptoms.

In addition to the imaging findings described above, multiple smaller enhancing lesions were seen in the left mandibular body, left inferior maxillary sinus floor, clivus, left occipital condyle, left C2 articular mass and ischium.

Our patient's blood work demonstrated marked rouleaux formation and the presence of IgA monoclonal protein. Bone marrow aspiration revealed extensive marrow infiltration by plasma cell myeloma, comprising 70–80% of the total cellularity. She was initiated on 6 cycles of chemotherapy, followed by autologous hematopoietic stem cell transplantation (HSCT) with good response to the treatment and improvement in her upper airway symptoms.

Follow up CT imaging demonstrated the significant interval resolution of soft tissue mass involving the cricoid cartilage with development of diffuse sclerosis of the cricoid (Fig d). The mandibular lesion and other other lytic lesions remain grossly stable.

Teaching Point

Cricoid and laryngeal involvement by plasma cell neoplasms is exceedingly rare, and imaging features mimic more common laryngeal malignancies. Most reported cases are anecdotal, highlighting the value of documenting such rare presentations. Radiologists should consider plasma cell neoplasm in the differential diagnosis of atypical laryngeal masses, as early recognition can prompt appropriate systemic evaluation.

References

1. Oztürk M, Mavili E, Gorkem SB, Cagli S, Yüce I. An unusual cause of dyspnea: myelomatous involvement of cricoid cartilage. A case report. Neuroradiol J. 2008;21(4):584-586. doi:10.1177/197140090802100419.
2. Raghuram S, Faizal B, Sanjeevan KV, et al. Recurrent extramedullary plasmacytomas without multiple myeloma: A case report with review of the literature. Cancer Treat Res Commun. 2022;31:100550. doi:10.1016/j.ctarc.2022.100550.
3. Floré B, Hermans R. Multiple myeloma involving the cricoid cartilage. JBR-BTR. 2013;96(2):87-88. doi:10.5334/jbr-btr.217.

Images/Tables

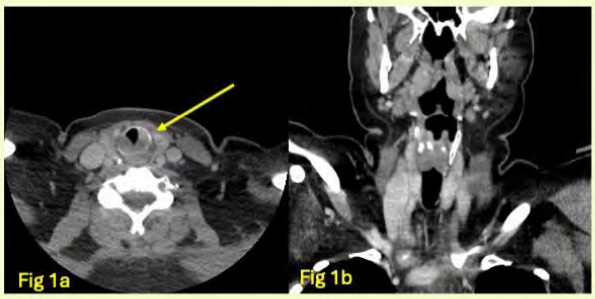

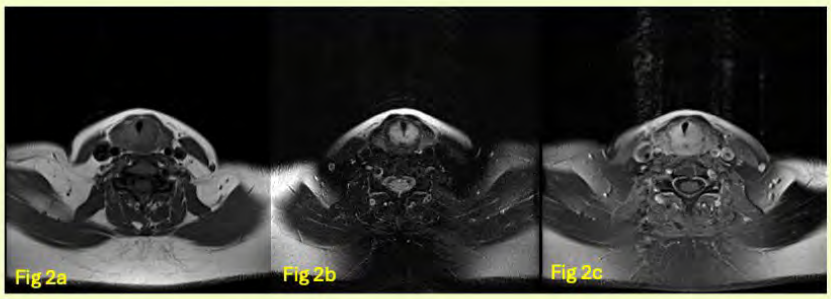

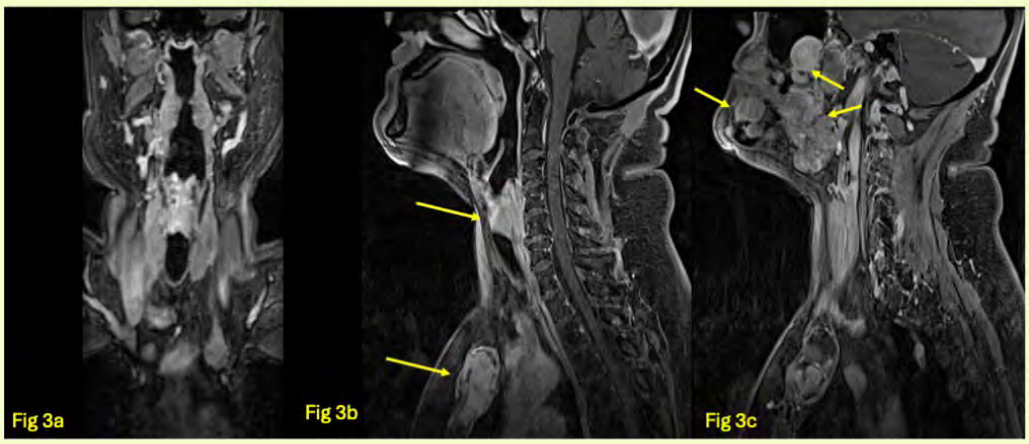

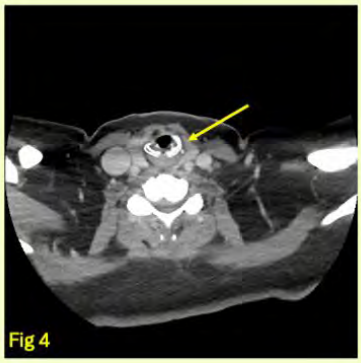

1136 Currarino Syndrome: Magnetic Resonance Imaging of the Neuroaxis in Caudal Malformations

Hanna Daniela Hernandez medical doctor[1], Karla Angelica Hernandez Medical Doctor[2], Sofia Zanabria Medical Doctor[1], Hector Marquez Medical Doctor[1]

[1]Centro Medico Nacional "20 de Noviembre", Ciudad de México, Ciudad de México, Mexico. [2]Hospital Escandon, Ciudad de México, Ciudad de México, Mexico

Clinical History

We present the case of a pediatric patient with a complex anorectal malformation, including rectal stenosis, funnel anus, and fistula. The initial surgical approach consisted of rectal biopsy, sigmoidostomy, lymph node biopsy, and colostomy. Hirschsprung's disease was suspected, although the biopsy was inconclusive. The infant was the product of the third pregnancy, born at term (40 weeks gestation). Magnetic resonance imaging (MRI) of the neuroaxis was requested as part of the planning for posterior sagittal rectoplasty and to rule out tethered spinal cord.

Imaging Findings

The MRI shows cervical and thoracolumbar vertebral bodies with preserved height and signal intensity, without alterations in posterior elements or intervertebral discs. In the sacral region, three incomplete vertebral bodies are identified due to the absence of the left lateral portion, forming a hemisacrum. The coccyx is absent. The spinal cord shows homogeneous intensity, with the conus medullaris located at the L1 level. No intramedullary abnormalities are observed. A sac containing cerebrospinal fluid is evident, extending through the sacral bone defect into the lumbosacral prevertebral space, with approximate dimensions of 62 × 36 × 39 mm (longitudinal × transverse × anteroposterior). This anterior meningocele causes superior displacement of the urinary bladder and anterior compression of the rectum. Stenosis of the anal canal and rectosigmoid segment is confirmed. No other neuroaxis abnormalities are identified.

Discussion

Currarino syndrome is a congenital condition characterized by the triad of anorectal malformation, sacral bone defect, and presacral mass. In this case, the imaging findings meet the diagnostic criteria: hemisacrum (scimitar sacrum), anorectal stenosis, and anterior meningocele. MRI is the study of choice for evaluating this condition, as it allows simultaneous characterization of the bone abnormalities, the spinal canal, and the presacral masses. Identifying tethered spinal cord is essential for surgical planning, as it may require prior neurosurgical intervention.

The anterior meningocele is the most frequent presacral mass, although teratomas, rectal duplication cysts, lipomas, or combinations thereof may also be found. MRI allows differentiation of these based on their signal characteristics and anatomical relationships. Anorectal reconstruction and resection of the presacral mass are essential to prevent complications such as rupture or malignant transformation.

Teaching Point

Currarino's triad should be considered when a hemisacrum, anorectal malformation, and presacral mass coexist, with anterior meningocele being the most common finding. Magnetic resonance imaging (MRI) is essential for characterizing the bony anatomy, spinal canal, and presacral structures, as well as for ruling out tethered spinal cord, a condition that alters the surgical approach. Furthermore, it allows differentiation between types of presacral masses, evaluation of their relationship to adjacent structures, and anticipation of complications. Its systematic use in the context of congenital caudal malformations improves diagnostic accuracy, optimizes multidisciplinary surgical planning, and contributes to better clinical outcomes.

References

1. Ghabili K, Badawy M , Dai R, et al. Currarino Triad. Radiographics. 2025; 45(9):e250124. Doi: 10.1148/rg.250124.
2. Currarino Syndrome in a Fetus, Infant, Child, and Adolescent: Spectrum of Clinical Presentations and Imaging Findings. Canadian Association of Radiologist Journal 2017; 68(1):90-95. Doi: 10.1016/j.carj.2016.05.007.

Images/Tables

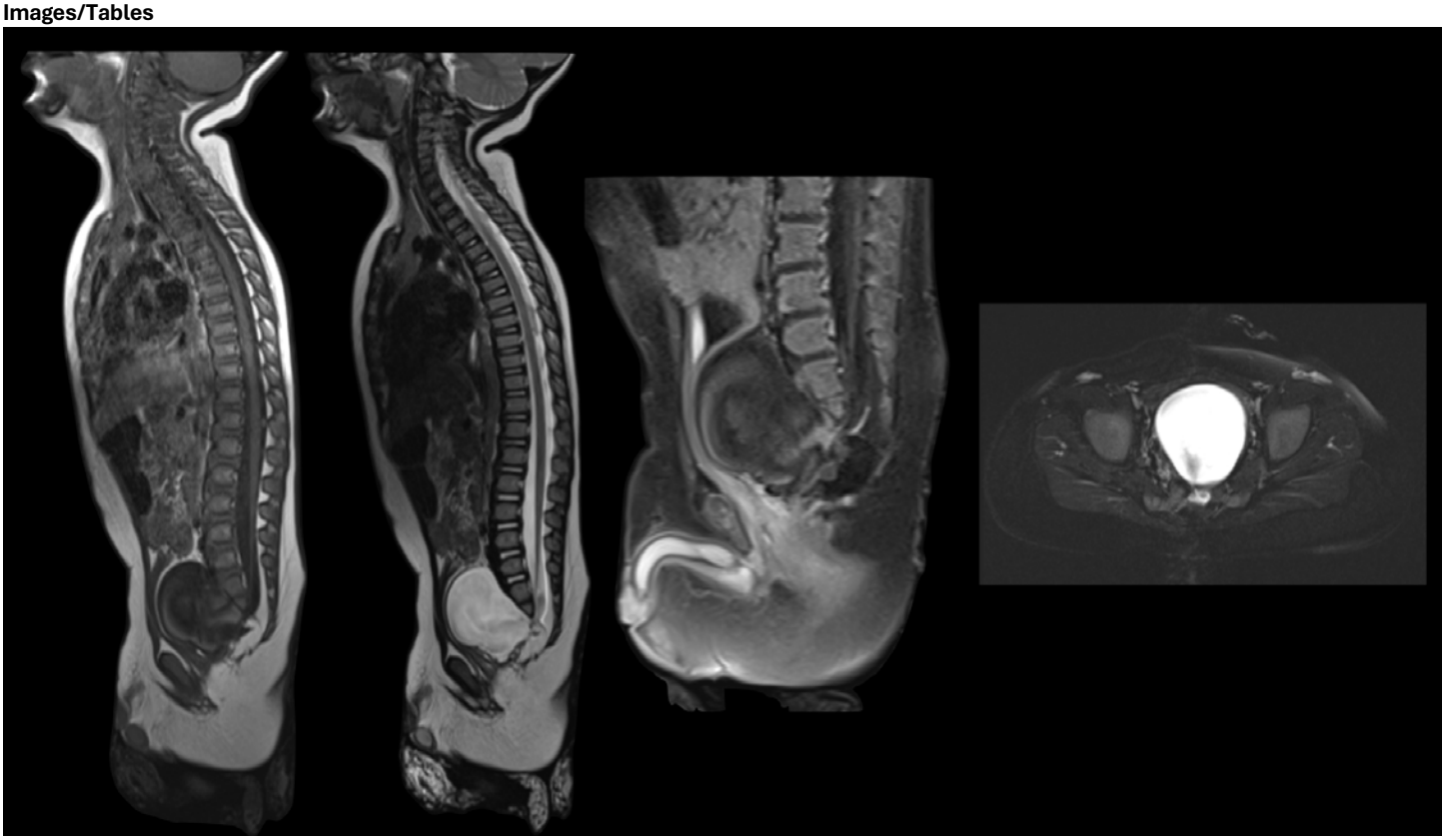

1142 Neuro-Behçet's Disease with Optic Involvement: An Imaging Perspective

Sofia Zanabria MD[1], Hanna Daniela Hernandez MD[1], Karla Angelica Hernandez MD[2]
[1]Centro Medico Nacional "20 de Noviembre", Ciudad de Mexico, Ciudad de Mexico, Mexico. [2]Hospital Escandon, Ciudad de Mexico, Ciudad de Mexico, Mexico

Clinical History

A 52-year-old female patient with no history of chronic degenerative diseases presented with right facial paralysis in February 2025, followed by progressive weakness in the right side of her body, stumbling, and falls. In June, she experienced syncope, disorientation, blurred vision, visual and auditory hallucinations, and urinary incontinence. She was admitted to the neurology service for incomplete right-sided pyramidal syndrome. Her condition did not improve despite empirical treatment. HLA-B51 positive.

Imaging Findings

Brain CT and MRI revealed multiple abnormalities consistent with neuro-Behçet's disease. Deepened sulci and fissures, supratentorial ventricular dilation, and hypointense lesions on T1 and hyperintense lesions on T2/FLAIR were observed in the left internal capsule, basal ganglia, thalamus, midbrain, pons, and corpus callosum. These lesions showed moderate and irregular post-contrast enhancement, as well as diffusion restriction. On FLAIR and T2 FS images, bilateral optic nerve involvement was evident, with increased caliber and signal intensity, predominantly on the left side and extending toward the optic chiasm, which also showed enhancement. Single-voxel spectroscopy showed loss of the choline/creatine ratio, an increased choline peak, decreased NAA, and the presence of lactate, suggesting active inflammation. Neuroaxis studies ruled out intramedullary abnormalities. Generalized cortico-subcortical volume loss was identified.

Discussion

Neuro-Behçet's disease is a parenchymal form of Behçet's disease, characterized by perivascular inflammatory infiltration with demyelination and edema. Clinical manifestations can be acute or progressive, and sometimes mimic neoplastic processes, complicating diagnosis in the absence of systemic flares. Optic nerve and chiasm involvement, although less frequent, can occur during active phases. The differential diagnosis includes multiple sclerosis, lymphoma, brain abscess, and vasculitis. The integration of clinical, immunological, and imaging findings is essential for establishing a diagnosis and guiding immunosuppressive treatment. Furthermore, longitudinal follow-up using neuroimaging allows for the evaluation of therapeutic response, the detection of early relapses, and the adjustment of immunological management in a personalized and dynamic manner.

Teaching Point

This case highlights the value of advanced neuroimaging in the diagnosis of inflammatory diseases of the central nervous system. Magnetic resonance imaging (MRI) identified a topographic pattern characteristic of neuro-Behçet's disease, with involvement of the brainstem, basal ganglia, internal capsule, and corpus callosum. Post-contrast enhancement and diffusion restriction were key to distinguishing inflammatory activity. Optic nerve and chiasm involvement, evidenced in FLAIR and T2 FS sequences, underscores the importance of including orbital studies in patients with visual symptoms. Cerebral spectroscopy complemented the structural analysis by revealing metabolic alterations consistent with active inflammation. These findings reinforce the need to integrate functional and structural imaging techniques to improve diagnostic accuracy in atypical neurological presentations.

References

1.Chae E, Do K, Beom Joon et al. Radiologic and Clinical Findings of Behcet Disease: Comprehensive Review of Multisystemic Involvement. Radiographics.2008; 28 (5):e31. Doi: 10.1148/rg.e31.

2.Borhani-Haghighi A, Kardeh B, Banerjee S, et al. Neuro Behcet´s disease: An update of diagnosis, differential diagnoses, and treatment. Mult Scler Relat Disord. 2020(39):101906. Doi: 10.1016/j.msard.2019.101906.

Images/Tables

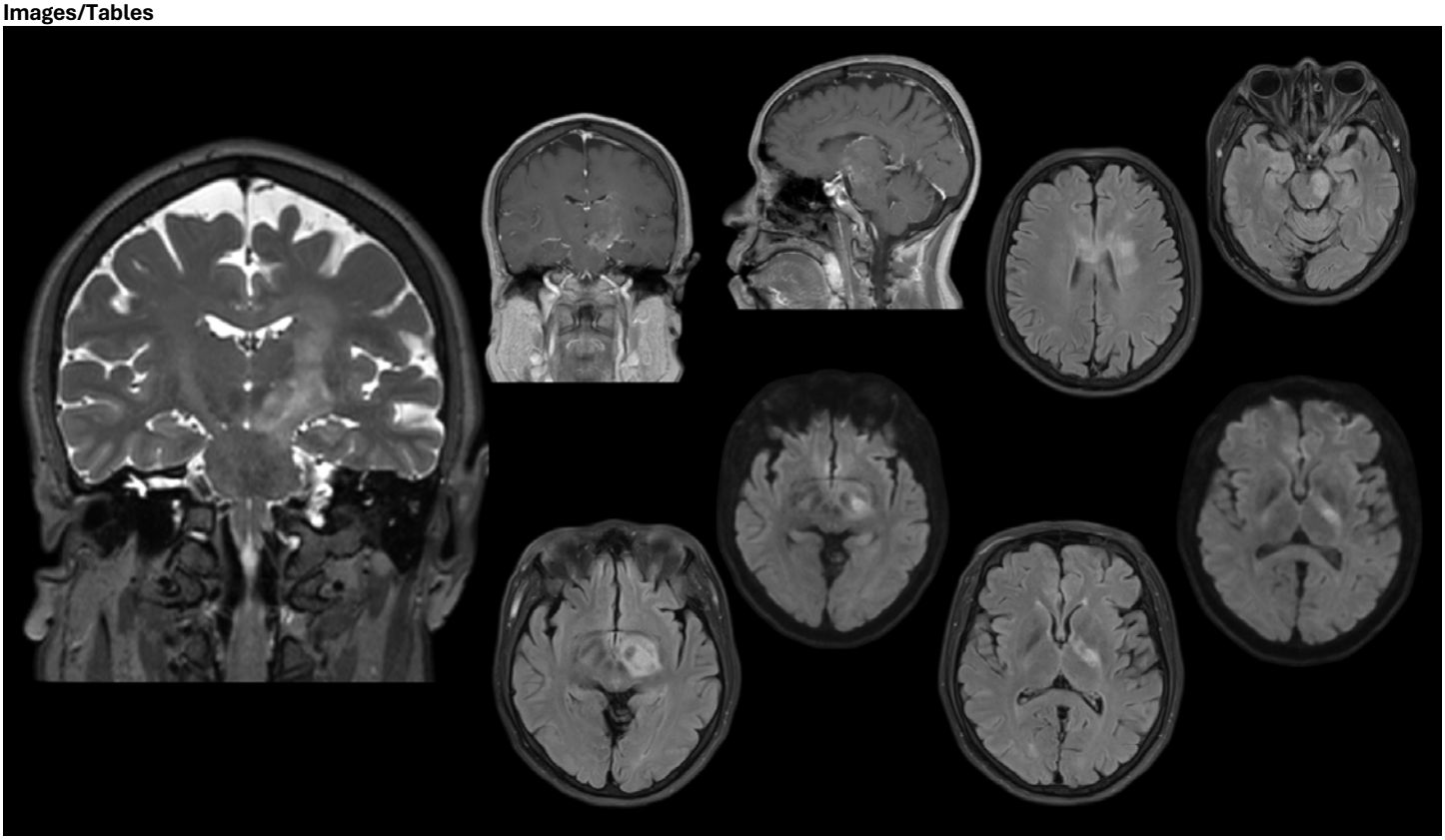

1147 "Black Vertebra" - Extensive Emphysematous Osteomyelitis of L5-S1- an Illustrative Report

GOGULDEEP VELUSWAMY MD[1], Rudy L. Van Hemert, Jr. MD[2], Luis Nunez MD[1], Prashanth Reddy Damalcheruvu MD[2], Shobhit Sharma MD[2], Venkatram Krishnan MD[2], Nivedita Radder MD[2]

[1]UAMS, Little Rock, Arkansas, USA. [2]University of Arkansas for Medical Sciences, Little Rock, Arkansas, USA

Clinical History

The patient, a 53-year-old female, presented with worsening low back pain, fever, abdominal pain and fatigue for 5 days. She was diagnosed with a new onset diabetes with hyperosmolar state, ketoacidosis and sepsis. The blood cultures grew anaerobic E coli. The patient developed

emphysematous osteomyelitis of L5-S1 with epidural phlegmon and abscess formation for which she was treated with antibiotics, L5-S1 posterior decompression, epidural abscess drainage and L5-S1 discectomy. Surgery and pathology confirmed the imaging findings of osteomyelitis and epidural abscess. Post surgery she had rapid improvement of the symptoms with mild residual back ache for which she is treated conservatively.

Imaging Findings

The initial CT of lumbar spine showed emphysematous osteomyelitis with extensive intra-osseous air foci in the L5, S1 vertebral bodies and in the disc space. The same day MRI corroborated with the findings in CT and showed an associated epidural soft tissue component with air foci. The follow up MRI after 3 days showed increasing epidural soft tissue with development of epidural abscess causing severe spinal canal narrowing at L4-5 and L5-S1 levels. Post surgery, the follow-up imaging after few weeks showed extensive cortical destruction of the L5, S1 vertebrae and 30% reduction in height. Near complete resolution of the air foci with persistent enhancement of the L5, S1 vertebral bodies and residual epidural soft tissue component was noted. There was osteolysis causing separation of the pedicles from the L5 vertebral body and resultant instability at L4-5 level which caused an acquired arachnoid cyst formation with clumping of nerve roots at L4-5 level.

Discussion

Emphysematous osteomyelitis is a rare, rapidly progressing infection characterized by gas formation within bones, leading to severe morbidity if untreated[2]. In the spine, it can cause significant bone destruction and instability, requiring urgent surgical and medical intervention. Early diagnosis and a multidisciplinary approach are crucial for effective management and improved patient outcomes. Over the past 40 years, there have been very few cases of EO; for instance, between 1981 and 2020, only 45 cases were identified. Vertebral bodies were involved in about 48% of the cases. About 27% of the cases were polymicrobial, and the rest were monomicrobial, with the most common organism being Escherichia coli (14 cases)[1]. Our patient had blood cultures that grew anaerobic E coli. Most of the case reports we reviewed showed only focal involvement in the lumbar vertebrae. Such extensive involvement as in our case and the complication of segmental motion instability secondary to bony destruction causing separation of pedicles from the vertebral body with resultant acquired arachnoid cyst formation seen in our case has not been documented in the prior published studies.

Teaching Point

Intra-osseous air foci in emphysematous osteomyelitis can cause signal void with absence of enhancement in the postcontrast T1 MRI images giving rise to the “Black Vertebra sign”. Aggressive nature of the emphysematous osteomyelitis can cause widespread bone destruction with rapid epidural abscess formation and vertebral instability. Imaging plays a vital role in assessment of the potential complications and the post treatment changes.

References

1.Sung S, Lee B.H, Kim J.H, Park Y, Ha J.W, Moon S.H, et al. Emphysematous osteomyelitis of the spine: a rare case report. *Medicine.* 2020;99 DOI: 10.1097/MD.0000000000021113.

2.*Ram P.C, Martinez S, Korobkin M, Breiman R.S, Gallis H.R, Harrelson J.M. CT detection of intraosseous gas: a new sign of osteomyelitis. AJR Am J Roentgenol. 1981;137:721–723. DOI: 10.2214/ajr.137.4.721*.

Images/Tables

Fig 1

Fig 2

Fig 1. Initial sagittal CT showing L5-S1 emphysematous discitis-osteomyelitis with intra-osseous air foci (asterisk) in L5, S1 vertebrae, disc space and in anterior epidural soft tissue soft tissue component.

Fig 2. Initial post contrast sagittal T1 weighted fat suppressed MRI Prominent signal void (asterisk) with absent enhancement in L5 and S1 vertebrae in MRI image secondary to air foci with "black vertebra" sign and epidural phlegmon.

Fig 3

Fig 3. Follow up post contrast sagittal T1 MRI image 3 days after the initial MRI showing progressive increase with anterior epidural abscess formation showing rim enhancement (asterisk).

Fig 4

Fig 4. Sagittal CT image a few weeks following L5-S1 posterior decompression, drainage of epidural abscess and antibiotic therapy showing interval resolution of the vertebral air foci and prominent cortical destruction of the L5 vertebral body with relative sparing along the endplates.

Fig 5

Fig 6

Figs 5 and 6. Follow up post treatment coronal and sagittal CT images with arrows pointing at the bilateral pedicles separated from the L5 vertebral body due to extensive end plate destruction causing potential instability.

Fig 7

Fig 7. Postcontrast sagittal T1 weighted MRI image, a few weeks following posterior decompression at L5-S1 showing residual enhancing intravertebral and epidural soft tissue components (asterisk) with no abscess.

Fig 8

Fig 8. Post treatment sagittal T2 MRI image showing loculated T2 hyperintense intrathecal acquired arachnoid cyst (asterisk) formation at L5 level secondary to segmental motion instability at L4-5 level causing prominent anterior displacement of the traversing nerve roots (arrow).

Fig 9

Fig 9. Axial T2 MRI image showing longer arrow pointing at the loculated intrathecal collection at L4-5 level. Shorter arrow pointing at the fat in the epidural space confirming the intrathecal location of the collection which is seen causing prominent clumping of the traversing nerve roots.

1154 A Spinal Incidentaloma with a Diagnostic Twist: The Rare Desmoid-Type Fibromatosis

Mohanad S Alhumayed MD, Karen C Chen MD, Taylor Robinson MD, James Y Chen MD
University of California San Diego, San Diego, CA, USA

Clinical History

A 49-year-old woman presented with a primary complaint of left arm radiculopathy and weakness.

Imaging Findings

A. Imaging Findings:

MRI of the cervical spine and dedicated brachial plexus MRI revealed a 5.5 cm left paraspinal mass at the C7-T1 level. The mass extended into the neural foramen, invaded the trunks of the left brachial plexus, and encased the left subclavian vein. PET-CT confirmed the mass to be hypermetabolic with an SUVmax of 5.7. The imaging characteristics were classic for a Pancoast tumor.

B. Pathologic Findings:

Core biopsy demonstrated a moderately cellular proliferation of bland spindle cells in a myxocollagenous matrix. Immunohistochemistry showed definitive nuclear reactivity for beta-catenin, confirming the diagnosis of desmoid-type fibromatosis.

Discussion

This case illustrates a critical diagnostic pathway for a spine-incidentaloma. What began as a radiological differential of nerve sheath tumor versus pancoast tumor culminated in the histopathological diagnosis of a rare, locally aggressive desmoid-type fibromatosis. This sequence underscores the vital role of the spine imager in initiating the diagnostic cascade and highlights a profound pitfall: a benign entity can perfectly mimic both a common neurogenic tumor and a lethal carcinoma on imaging. The case reinforces the indispensable role of biopsy in guiding management, especially when a lesion bridges anatomical compartments from the spine to the thoracic inlet.

Teaching Point

For paraspinal masses at the thoracic inlet, the differential diagnosis must extend beyond schwannoma and pancoast tumor to include rare benign entities like desmoid-type fibromatosis. Histopathological confirmation is critical, as the correct diagnosis can be a revelation, preventing misdirected, aggressive treatment and appropriately guiding therapy.

References

Bektas M, Bell T, Khan S, et al. Desmoid tumors: a comprehensive review. Adv Ther. 2023;40(9):3697-3722. doi: 10.1007/12325-023-02592-0.

Images/Tables

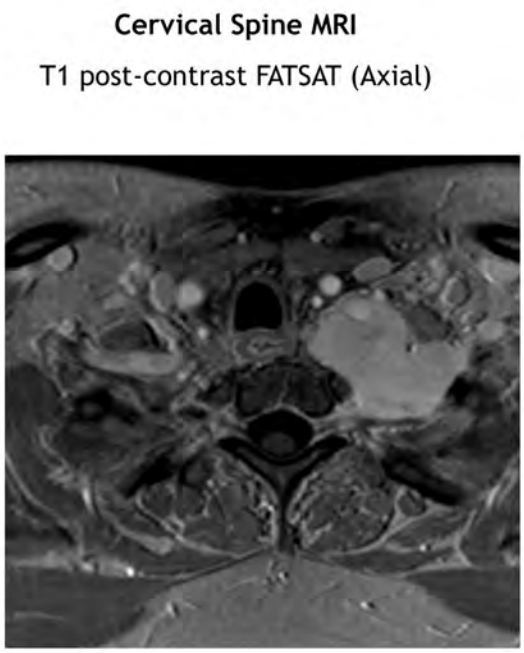

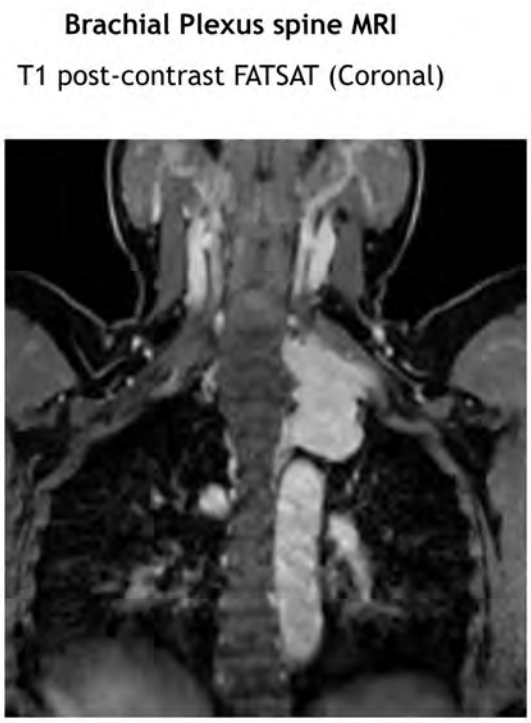

1155 Strangulation, Stroke, and a Mimicker: Vessel Wall MRI Reclassifies a "Floating Thrombus" as an Unstable Atheroma

Kamand Khalaj MD MPH[1], Kasra Rahbar MD[2]
[1]UTHealth Houston, Houston, Texas, USA. [2]Baylor College of Medicine, Houston, Texas, USA

Clinical History

A 65-year-old man with a prior right carotid endarterectomy (CEA) presented with acute right hemispheric stroke symptoms immediately after a physical altercation where he was strangled by his necklace.

Imaging Findings

Initial CTA revealed a filling defect in the right cervical internal carotid artery (ICA), presumed to be a floating thrombus adherent to an atherosclerotic plaque. Brain MRI confirmed multiple acute right cortical border zone embolic infarcts. Subsequent vessel wall MRI performed several days later demonstrated a vulnerable atheromatous plaque with lipid-rich necrotic core and thin fibrous cap. T1-hyperintensity of the plaque and the adherent filling defect was absent, which argues against the presence of thrombus or intraplaque hemorrhage.

Discussion

The patient was initially anticoagulated, which is often first-line management for a carotid floating thrombus. However, vessel wall MRI findings prompted a pivotal change to revascularization. Medical therapy alone would be insufficient, given the absence of thrombus and the risk of further embolic stroke from the unstable, floating atheroma, necessitating definitive surgical intervention. Given the history of prior CEA, Transcarotid Artery Revascularization (TCAR) was selected to minimize the risks of re-operation. This procedure utilizes flow reversal to capture fragile plaque material that can be dislodged during stent deployment and protect against distal embolization. The procedure was successful and uncomplicated. There was immediate resolution of the filling defect on the post-stent angiographic run and capture of soft plaque material in the TCAR filter. This case highlights that carotid floating filling defects can sometimes represent unstable plaque rather than thrombus, a distinction with critical therapeutic implications.

Teaching Point

Vessel wall MRI is a crucial problem-solving tool that can distinguish between carotid thrombus and unstable atheroma when findings on CTA are equivocal. This distinction, particularly the absence of T1 hyperintensity, directly guides the critical management decision between medical management and prompt revascularization.

References

Saba L, Yuan C, Hatsukami TS, Balu N, Qiao Y, DeMarco JK, Saam T, Moody AR, Li D, Matouk CC, Johnson MH, Jäger HR, Mossa-Basha M, Kooi ME, Fan Z, Saloner D, Wintermark M, Mikulis DJ, Wasserman BA; Vessel Wall Imaging Study Group of the American Society of Neuroradiology. Carotid Artery Wall Imaging: Perspective and Guidelines from the ASNR Vessel Wall Imaging Study Group and Expert Consensus Recommendations of the American Society of Neuroradiology. AJNR Am J Neuroradiol. 2018 Feb;39(2):E9-E31. doi: 10.3174/ajnr.A5488. Epub 2018 Jan 11. PMID: 29326139; PMCID: PMC7410574.

Images/Tables

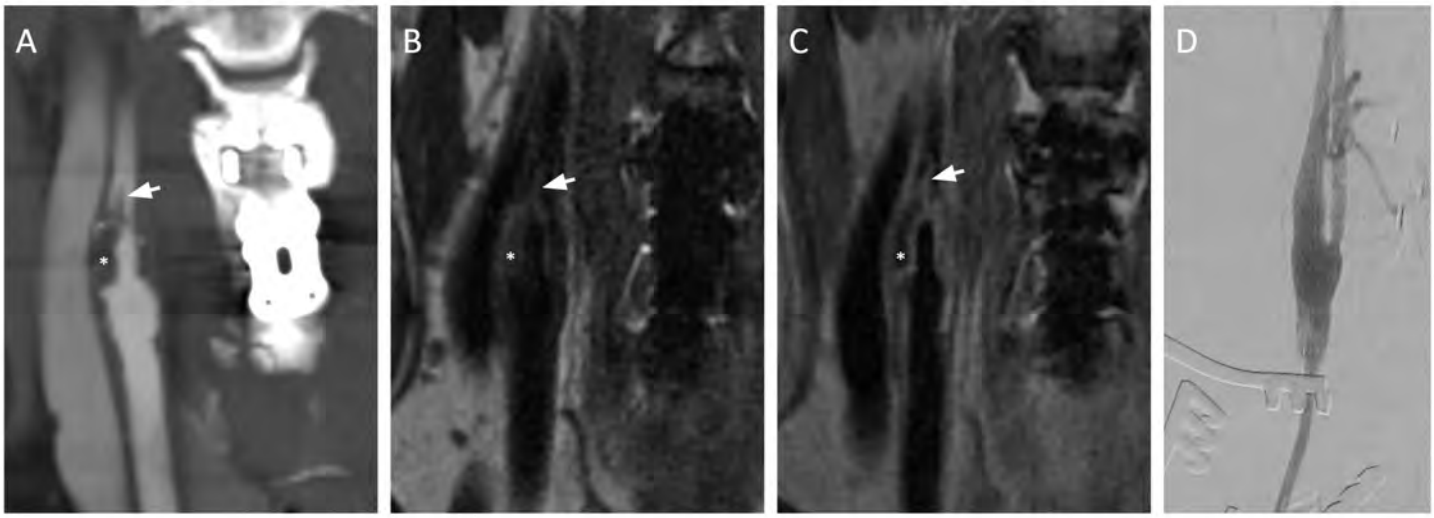

Imaging and procedural findings of a traumatized, unstable carotid plaque. (A) Coronal CTA reformat demonstrates a floating filling defect in the right cervical ICA (arrow) adherent to a non-calcified atherosclerotic plaque (*). (B) Coronal pre-contrast 3D T1 Cube Vessel Wall MRI shows T1 hypointensity of the filling defect (arrow) and plaque (*), arguing against thrombus or intraplaque hemorrhage, which are typically T1 hyperintense due to the presence of methemoglobin. (C) Coronal post-contrast 3D T1 Cube image reveals a thin enhancing fibrous cap (arrow) overlying the lipid-rich necrotic core (*), consistent with a vulnerable plaque. (D) Final angiographic run following TCAR stenting shows a patent stent with resolution of the filling defect. Soft plaque material was captured in the TCAR filter (not shown).

1159 Pleomorphic Adenoma of the Soft Palate Extending into the Parapharyngeal Space

Grace Yoon MD, Alexander Ree MD
Cook County Hospital, Chicago, IL, USA

Clinical History

A 46-year-old man presented with progressive nasal obstruction over one month, which had worsened to the point of making nasal breathing difficult. He denied nasal drainage, postnasal drip, or epistaxis and had no relief from nasal stents, strips, or intermittent intranasal fluticasone use. Previously, he had mild snoring but recently developed excessive daytime sleepiness and fatigue due to difficulty breathing at night.

Fiberoptic laryngoscopy demonstrated a submucosal mass centered in the right soft palate, abutting and displacing the right torus tubarius, and extending medially toward the midline and posteriorly into the retromolar trigone region. The mucosal surface was intact, and no cervical lymphadenopathy was identified.

Imaging Findings

Contrast-enhanced CT of the neck revealed a large, well-circumscribed hypodense mass located along the lateral margin of the right oropharynx. The lesion demonstrated internal attenuation higher than that of simple fluid. The parapharyngeal fat plane was partially effaced, but adjacent osseous structures and major vessels remained distinct.

Discussion

Pleomorphic adenoma, the most common benign salivary gland tumor, typically arises from the parotid gland but can also originate from the minor salivary glands of the oral cavity, particularly the palate. Palatal pleomorphic adenomas are usually submucosal, slow-growing, and painless, but when large, may cause nasal obstruction or dysphagia.

In this case, the lesion's location and imaging appearance prompted consideration of several cystic or mixed-density entities, including a type IV second branchial cleft cyst and, importantly, a cystic metastatic lymph node from papillary thyroid carcinoma. Cystic nerve sheath tumor and lymphatic malformation were considered less likely.
Core-needle biopsy confirmed pleomorphic adenoma of the soft palate. The patient subsequently underwent transoral resection of the right palatal mass, which extended into the parapharyngeal space with attachment to the styloid process and abutment of the skull base at the middle cranial fossa floor. Postoperative recovery was uneventful.

Teaching Point

Pleomorphic adenoma of the soft palate, though rare, should be included in the differential diagnosis of well-circumscribed, hypodense palatal or parapharyngeal masses. Imaging can help guide appropriate surgical planning for complete excision with preservation of surrounding structures.

References

- Som PM, Curtin HD, Mancuso AA. Imaging-based approach to salivary gland masses. *Radiology* 2000;216(1):19–30.
- Olsen KD. Tumors and surgery of the parapharyngeal space. *Laryngoscope* 1994;104(5 Pt 2 Suppl 63):1–28.
- Sigal R, Monnet O, de Baere T, Micheau C, Vanel D, Luboinski B, Lacourreye L, Schwaab G, Bosq J, Marsault C. Adenomas of the salivary glands: CT and MR imaging features. *Radiology* 1988;168(2):465–468.
- Som PM, Brandwein M. Salivary glands: anatomy and pathology. In: Som PM, Curtin HD, eds. *Head and Neck Imaging*, 5th ed. St. Louis: Mosby; 2011:2054–2126.
- Takimoto T, Hara M, Yamada T, et al. Pleomorphic adenoma arising from the soft palate extending into the parapharyngeal space: CT and MR findings. *Dentomaxillofac Radiol* 2006;35(5):384–387.

Images/Tables

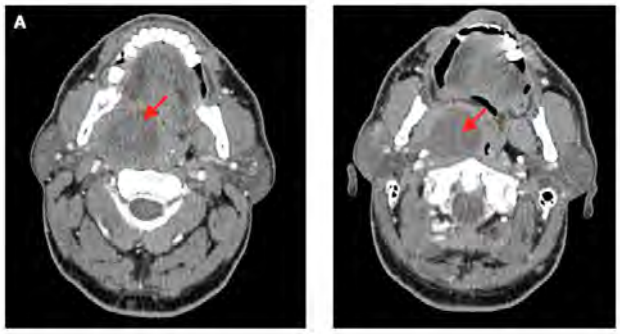

(A) Axial contrast-enhanced CT of the neck demonstrates a large, well-circumscribed, hypodense mass (arrow) centered in the right soft palate, extending laterally into the parapharyngeal space and medially toward the oropharyngeal airway. The lesion causes effacement of the parapharyngeal fat plane.

(B) Sagittal and (C) coronal reformatted CT image shows superior extension of the mass.

1168 From Silent Lesion to Neurosurgical Emergency: Pineal Cyst Apoplexy with Hydrocephalus

Hussein Alsadi MD[1], Motaz Daraghma MD[2], Kyle Werth MD[1]

[1]University of Kansas Medical Center, Kansas City, KS, USA. [2]University of Missouri-Kansas City, Kansas City, MO, USA

Clinical History

A 21-year-old female with a known benign pineal cyst presented with a one-week history of worsening headaches. The cyst was first identified incidentally at age 10, measuring approximately 1 cm, and had been clinically stable for several years without symptoms. On current presentation, she described dull, progressive headaches rated 4/5 in intensity without visual changes, nausea, or focal neurological deficits. Physical examination revealed normal cranial nerves, symmetric and reactive pupils, preserved upward gaze, and no signs of Parinaud's syndrome. Vital signs and laboratory studies were normal. She was admitted to the neurologic intensive care unit for close monitoring and started on acetazolamide to reduce intracranial pressure. Given persistent symptoms and ventricular enlargement, she underwent endoscopic third ventriculostomy the next day. Her postoperative course was uneventful, and she was discharged home in stable condition. At two-week follow-up, she reported significant headache improvement without new neurological symptoms.

Imaging Findings

MRI of the brain demonstrated enlargement of the pineal region cyst to 2 cm in maximal diameter, previously 1 cm at age 10 (not shown). Axial T2-weighted image (A) shows the pineal cystic lesion with fluid–fluid levels. Sagittal T2-weighted image (B) shows mass effect from the enlarging cyst on the midbrain, resulting in cerebral aqueduct obstruction. Axial FLAIR image (C) demonstrates associated supratentorial hydrocephalus with mild transependymal periventricular edema. Susceptibility-weighted image (D) demonstrates layering hematocrit level and susceptibility signal consistent with hemorrhage. Axial T1-weighted image (E) shows isointense signal within the cyst, again consistent with blood products. Axial postcontrast T1-weighted image (F) shows no nodular or thick enhancement.

Discussion

Pineal cysts are common incidental findings, observed in up to 10% of brain MRIs and as many as 40% of autopsies. Most remain small and asymptomatic, but larger cysts may compress adjacent structures, causing headache, visual disturbance, or hydrocephalus. Pineal cyst apoplexy, defined as hemorrhage within a benign pineal cyst is a rare but critical complication that can lead to acute obstructive hydrocephalus. Risk factors include larger cyst size, trauma, anticoagulation, hypertension, and vascular malformations, although many cases occur spontaneously. Clinically, pineal cyst apoplexy often presents with sudden headache, nausea, or signs of increased intracranial pressure and, occasionally, dorsal midbrain findings such as vertical gaze palsy. On imaging, hemorrhagic cysts exhibit internal blood products and fluid–fluid levels without a solid enhancing mass. MRI provides superior sensitivity to blood products and mass effect. Management depends on clinical stability: conservative therapy may be appropriate for stable patients, whereas acute hydrocephalus necessitates prompt surgical decompression; most effectively achieved with endoscopic third ventriculostomy or cyst fenestration. Prognosis is excellent with timely recognition and intervention.

Teaching Point

Pineal cyst apoplexy is a rare but potentially life-threatening complication that can rapidly progress to obstructive hydrocephalus. This case highlights the importance of early radiologic recognition and timely neurosurgical intervention. Endoscopic third ventriculostomy provided effective management with excellent short-term recovery. Prompt diagnosis and treatment are essential to prevent permanent neurological deficits and optimize patient outcomes.

References

1. Atallah O, Chaurasia B, Badary A, et al. Pineal apoplexy: Highlighting the causes, treatment, and outcome. J Neurol Surg Cent Eur Neurosurg 2025; 86(1):85–98. PMID: 38788759.
2. Kim E, Kwon SM. Pineal cyst apoplexy: A rare complication of a common entity. Brain Tumor Res Treat 2020; 8(1):66–70. PMID: 32390357.
3. Barboriak DP, Lee L, Provenzale JM. Serial MR imaging of pineal cysts: Implications for natural history and follow-up. AJR Am J Roentgenol 2001; 176(3):737–743. PMID: 11222216.
4. Starke RM, Cappuzzo JM, Erickson NJ, Sherman JH. Pineal cysts and other pineal region malignancies: Determining factors predictive of hydrocephalus and malignancy. J Neurosurg 2017; 127(2):249–254. PMID: 27767399.
5. Tamura Y, Yamada Y, Tucker A, et al. Endoscopic surgery for hemorrhagic pineal cyst following antiplatelet therapy: Case report. Neurol Med Chir (Tokyo) 2013; 53(9):625–629. PMID: 24067776.

Images/Tables

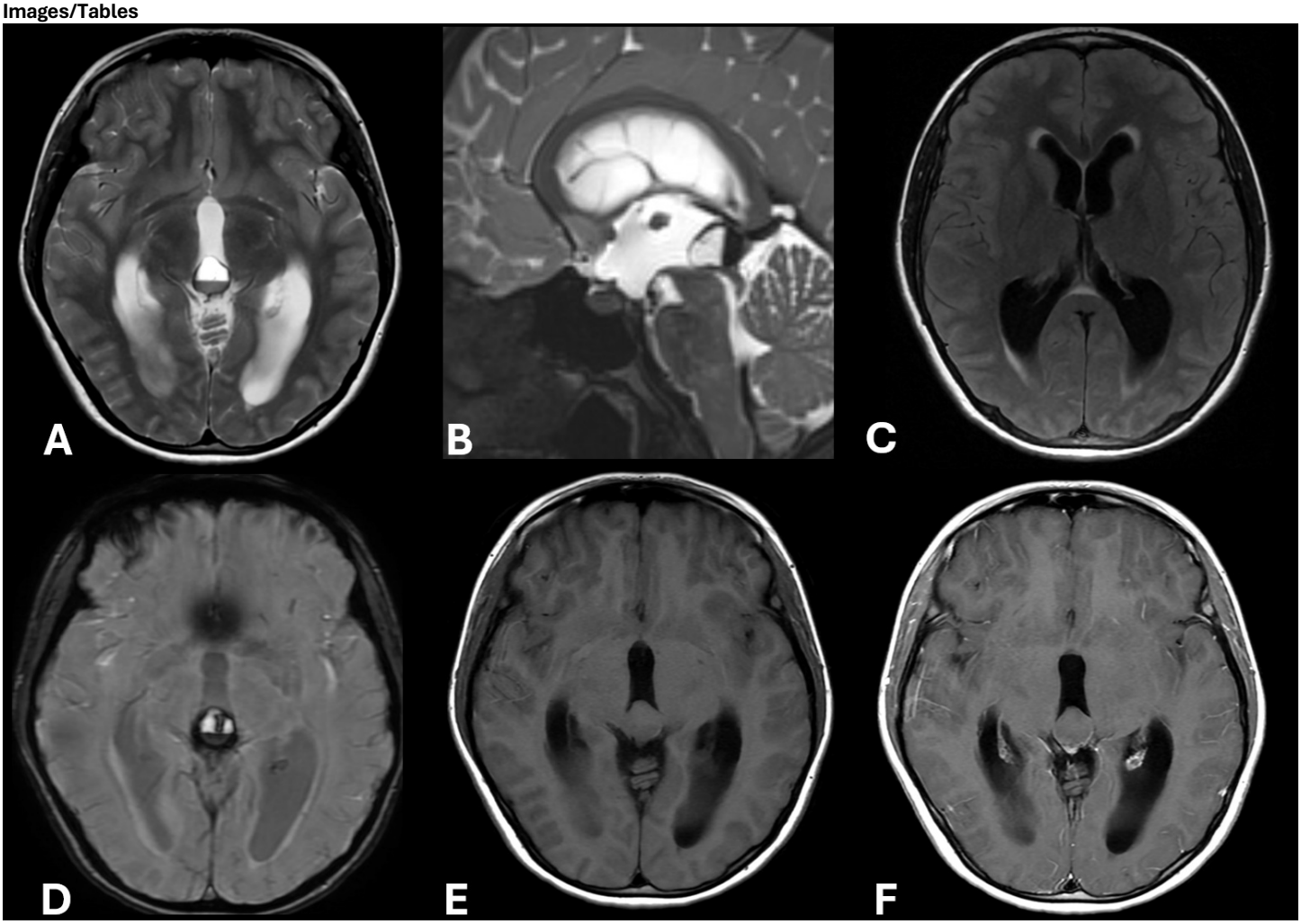

1182 Stretch Injury of the Posterior Communicating Artery during Transsphenoidal Pituitary Surgery

Kamand Khalaj MD MPH[1], Kasra Rahbar MD[2]

[1]UTHealth Houston, Houston, Texas, USA. [2]Baylor College of Medicine, Houston, Texas, USA

Clinical History

A 71-year-old man with progressive bitemporal hemianopsia from a nonfunctioning pituitary macroadenoma underwent elective transsphenoidal resection. The initial resection was uneventful, with the surgeon noting the tumor was soft and easily aspirated. However, during a period of no active manipulation, the patient developed sudden severe bradycardia that progressed to a 6-second asystole, resolving spontaneously. The remainder of the surgery was completed uneventfully. Immediate postoperative neurological exam revealed a new right hemiplegia and left oculomotor nerve palsy.

Imaging Findings

Preoperative MRI demonstrated a pituitary macroadenoma with chiasmatic compression. Emergent postoperative CT revealed thick subarachnoid hemorrhage (SAH) centered in the premesencephalic cistern. CTA and subsequent cerebral angiography identified an abnormal, sharply angulated course of the left posterior communicating artery (PComA) through the sella turcica, anterior and medial to the posterior clinoid process; this aberrant course was new compared to preoperative studies. Follow-up MRI confirmed an acute ischemic infarct in the left anterior thalamus and posterior limb of the internal capsule.

Discussion

The triad of intraoperative asystole (a trigeminocardiac reflex), subarachnoid hemorrhage, and a thalamocapsular infarct indicates an iatrogenic vascular injury. The trigeminocardiac reflex occurring during a time of no active surgical manipulation and the absence of violation of the tumor capsule or hemorrhage visualized intraoperatively argue against direct transection as the mechanism of injury, particularly since the PComA's course was normal on preoperative imaging. We hypothesize the PComA was adherent to the tumor capsule and sustained a stretch injury during decompression and descent of the suprasellar tumor capsule, leading to SAH. The immediate right hemiplegia is due to ischemic infarct caused by avulsion of the thalamoperforator arteries arising from the PComA. The oculomotor nerve palsy likely resulted from either ischemia of its vasa nervorum (supplied by the PComA) or injury from SAH. The patient's hemiparesis partially improved over time, but the oculomotor palsy was permanent.

Teaching Point

This case illustrates a rare mechanism of vascular injury during transsphenoidal surgery: stretch and avulsion of an artery adherent to the tumor capsule, which can occur despite a normal preoperative vascular appearance. This distinct mechanism of iatrogenic vascular injury differs from direct arterial transection or pseudoaneurysm, which are a well-recognized complications of transsphenoidal surgery.

References

1. Babgi M, Alsaleh S, Babgi Y, Baeesa S, Ajlan A. Intracranial Intradural Vascular Injury during Endoscopic Endonasal Transsphenoidal Surgery: A Case Report and Literature Review. J Neurol Surg Rep. 2020 Jul;81(3):e52-e58. doi: 10.1055/s-0040-1717056. Epub 2020 Sep 24. PMID: 32983828; PMCID: PMC7515681.

Images/Tables

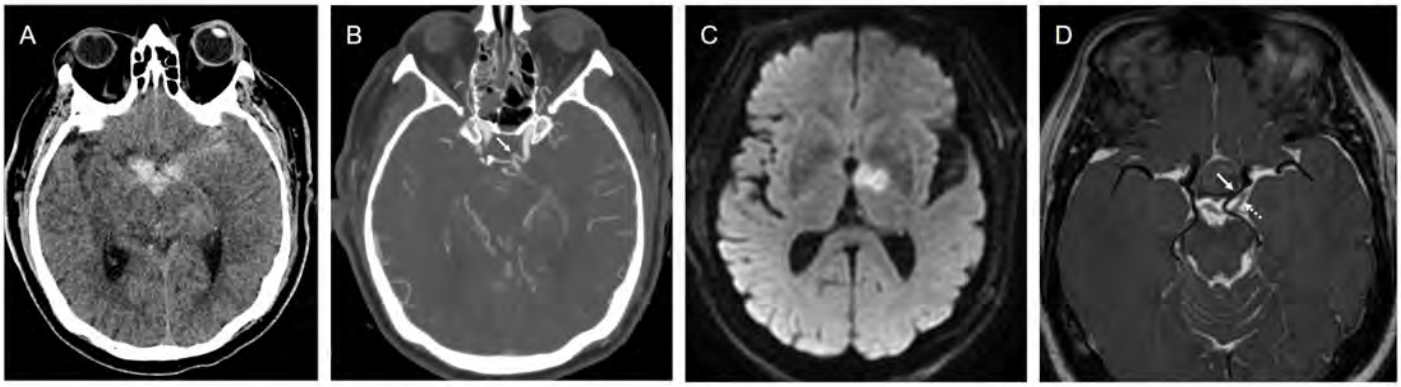

Imaging findings of iatrogenic posterior communicating artery (PComA) stretch injury during transsphenoidal pituitary surgery. (A) Immediate postoperative non-contrast head CT demonstrates acute subarachnoid hemorrhage in the perimesencephalic cistern. (B) Axial CTA maximum intensity projection reveals the abnormal, sharply angulated course of the left PComA traversing the sella turcica. (C) Axial diffusion-weighted image (DWI) shows restricted diffusion in the left anterior thalamus and posterior limb of the internal capsule, consistent with acute ischemic infarct in the territory of thalamoperforating arteries arising from the PComA. (D) Axial 3D T2 Cube minimum intensity projection from preoperative MRI demonstrates the normal preoperative course of the PComA in relation to both the pituitary macroadenoma capsule (solid arrow) and the left oculomotor nerve (dashed arrow).

1184 Diffuse Leptomeningeal Myelomatosis, an Unusual Presentation of CNS Multiple Myeloma

GOGULDEEP VELUSWAMY MD[1], Rudy L. Van Hemert, Jr. MD[2], Luis Nunez MD[1], Dhruba Dasgupta MD[1], Prashanth Reddy Damalcheruvu MD[2], Shobhit Sharma MD[2], Venkatram Krishnan MD[1], Nivedita Radder MD[1]

[1]UAMS, Little Rock, Arkansas, USA. [2]University of Arkansas for Medical Sciences, Little Rock, Arkansas, USA

Clinical History

The patient was a 70 year old male with history IgG lambda multiple myeloma on teclistamab. Presented to UAMS for 1 and half week history of nausea, vomiting, malaise, and worsening peripheral vision accompanied with gait abnormalities and auditory deficits. The family reported that the symptoms have been progressively getting worse, with symptoms of tunnel vision, complete deafness, and vertigo/inability to walk. In view of the above clinical scenario with a history of multiple myeloma, CSF analysis with flow cytometry showed myeloma cells confirming the findings of leptomeningeal myelomatosis. The patient had worsening mentation in view of advanced disease and was transferred to hospice care.

Imaging Findings

Axial T2/ FLAIR and susceptibility weighted images from MRI done a week apart showed rapidly increasing cerebellar edema and microhemorrhages with effacement of fourth ventricle. There was rapid interval development of moderate acute hydrocephalus under pressure and development of sulcal FLAIR hyperintensities. Post contrast images showed prominent nodular leptomeningeal enhancement along the sulci, cerebellar folia and along multiple cranial nerves with multiple microbleeds prominently along the cerebellar foliae.There were no calvarial lesions to suggest a direct spread. These imaging findings were consistent with leptomeningeal myelomatosis secondary to hematogenous spread.

Discussion

The etiology of LMM is still unknown, although several theories have been suggested. A possibility is the direct continuous spread from eroded lytic lesions of the skull. The most accepted mechanism of leptomeningeal involvement is the hematogenous spread of plasma cells: myeloma cells may invade the central nervous system (CNS) through the choroid plexuses and then spread via cerebrospinal fluid[1] (CSF). Typically, the neoplastic involvement of subarachnoid space (also called “carcinomatous meningitis”) produces a thicker, lumpy, or nodular enhancement but can appear also thin and linear; in addition, enhancement of the intra-cisternal tracts of the cranial nerves can be shown, indicating pathological involvement of the nerves[2,3].The main differential diagnosis of LE in patient with MM is infective meningitis as treatment for hematological malignancies typically involves systemic therapies with the associated risk of immunosuppression and opportunistic infections[4]. Our patient had associated subarachnoid hemorrhages in the sulcal spaces and in the cerebellar foliae which appears to be a rare presentation.

Teaching Point

Nodular diffuse leptomeningeal enhancement along the sulcal spaces, cranial nerves with rapidly increasing hydrocephalus in a patient with long standing multiple myeloma should raise the suspicion of rare but a highly possible cause of leptomeningeal myelomatosis.

References

1.Miki Y, Kamata K, Akemoto Y, et al. Leptomeningeal and intraventricular myelomatosis manifesting an aggressive form of communicating hydrocephalus. *Neuropathology* 2021; 41(3): 243–249. DOI: 10.1111/neup.12728

2.Smirniotopoulos JG, Murphy FM, Rushing EJ, et al. Patterns of contrast enhancement in the brain and meninges. *Radiographics* 2007; 27(2): 525–551. DOI: 10.1148/rg.272065155

3.Lasocki A, Gangatharan S, Gaillard F, et al. Intracranial involvement by multiple myeloma. *Clin Radiol* 2015; 70(8): 890–897. DOI: 10.1016/j.crad.2015.03.014

4.Lasocki A, Seymour JF. Central nervous system manifestations of systemic haematological malignancies and key differentials. *Clin Radiol* 2022; 77(5): 328–336. DOI: 10.1016/j.crad.2022.01.043

Images/Tables

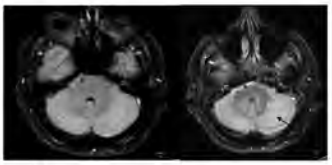

Fig 1 Fig 2

Axial FLAIR images in the upper row from MRI done a week apart showing worsening of FLAIR hyperintensities in bilateral cerebellum.

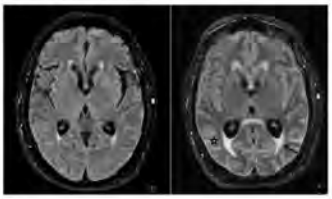

Fig 3 Fig 4

Development of moderate acute hydrocephalus under pressure as noted by increasing periventricular CSF flow in the FLAIR images done a week apart. Also noted is the sulcal hyperintensities in the FLAIR images as noted by the asterisk.

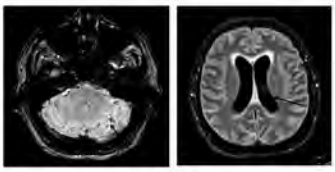

Fig 5 Fig 6

Fig5. Axial susceptibility weighted image showing prominent cerebellar edema with microhemorrhages(arrow). Fig 6. Axial FLAIR image showing development of moderate hydrocephalus(arrow).

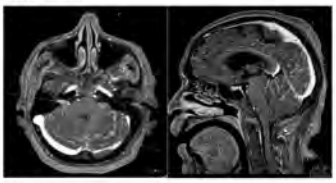

Fig 7 Fig 8

Post contrast axial and sagittal T1 weighted images showing arrows pointing to nodular leptomeningeal enhancement along the sulci and the cerebellar folliae, enhancement along right 7-8th nerve complex.

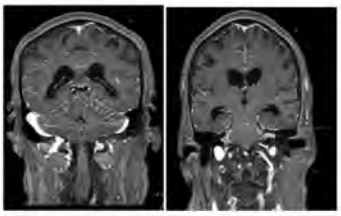

Fig 9 Fig 10

Coronal postcontrast T1 MRI showing extensive supra and infratentorial leptomeningeal enhancement with arrows pointing showing enhancement of bilateral 5th, 7-8 th nerve complexes.